
**Influence of the Glucocorticoid-Induced Leucine
Zipper (GILZ) on Macrophage-Associated
Inflammation and Statin-Mediated Effects**

Dissertation zur Erlangung des Grades des Doktors der
Naturwissenschaften der Naturwissenschaftlich-Technischen
Fakultät der Universität des Saarlandes

von

Rebecca Linnenberger

Saarbrücken

2022

Tag des Kolloquiums: 20. Juli 2023
Dekan: Univ.-Prof. Dr. Ludger Santen
Berichterstatter: Univ.-Prof. Dr. Alexandra K. Kiemer
Univ.-Prof. Dr. Christian Ducho
Vorsitz: Univ.-Prof. Dr. Andriy Luzhetskyy
Akad. Mitarbeiter: PD Dr. Martin Frotscher

Die Inhalte der vorliegenden Arbeit wurden an der Universität des Saarlandes an der Naturwissenschaftlich-Technischen Fakultät in der Fachrichtung Pharmazie im Zeitraum von November 2017 bis August 2021 angefertigt.

Erstgutachter: Prof. Dr. Alexandra K. Kiemer

Zweitgutachter: Prof. Dr. Christian Ducho

“Sapere aude”

[Immanuel Kant]

Summary

The glucocorticoid-induced leucine zipper (GILZ) is an immunomodulatory protein playing a pivotal role in macrophages' immune response. The aim of the present studies was the investigation and role of GILZ in different settings: The first part of this study focused on the function and regulation of GILZ in aging and macrophage activation. The term “inflammaging” describes the acquired state of low-term chronic inflammation contributing to an age-related imbalanced immune system. The elucidation of impaired glucocorticoid metabolism and reduced levels of glucocorticoids (GC) in the myeloid compartment of aged mice resulting in a dysregulated immune network was part of this study.

Second, this study focused on statins' effects on GILZ. Statins represent the most prescribed class of drugs for the treatment of hypercholesterolemia as the underlying condition in cardiovascular diseases (CVDs). Besides lipid-lowering actions, statins exert muscle-related side effects and are postulated to mediate anti-inflammatory actions by mechanisms not fully elucidated. Statins can induce GILZ in skeletal muscle and macrophages. The study revealed mechanistic aspects of *Gilz*-upregulation and the involvement of the mevalonate pathway in macrophages *in vitro* and *ex vivo* as well as the mediating role of GILZ in statin-induced muscle damage *in vitro* and *in vivo*.

Zusammenfassung

Der Glucocorticoid-induzierte Leucin Zipper (GILZ) ist ein Protein mit immunmodulierenden Eigenschaften, welches eine wichtige Rolle in der Immunantwort von Makrophagen spielt. Ziel der vorliegenden Studien war die Untersuchung von GILZ in unterschiedlichen Ansätzen: Die Rolle und Funktion von GILZ während des Alterungsprozesses und bei Makrophagenaktivierung war Bestandteil des ersten Studienteils. Mit zunehmendem Lebensalter verändert sich das Immunsystem hin zu einem entzündungsähnlichen Zustand. Die Untersuchung im myeloiden Kompartiment von gealterten Mäusen zeigte, dass reduzierte Glucocorticoid (GC) Spiegel und ein veränderter Glucocorticoidmetabolismus Teil dieses fehlregulierten Immunnetzwerkes sind.

Ein weiteres Ziel dieser Studie war die Untersuchung des Einflusses von Statinen auf GILZ. Bei Statinen handelt es sich um die meistverordnete Gruppe von Arzneimitteln, die bei Hypercholesterinämie eingesetzt werden. Neben ihrer lipidsenkenden Wirkung werden Statine auch muskelschädigende und anti-entzündliche Eigenschaften, deren Mechanismen nicht vollständig geklärt sind, zugeschrieben. Zunächst wurde gezeigt, dass Statine *Gilz* in Muskelzellen und Makrophagen induzieren kann. Es konnten mechanistische Aspekte der *Gilz* Induktion unter Beteiligung des Cholesterolsyntheseweges in Makrophagen *in vitro* und *ex vivo*, sowie die Beteiligung von GILZ an muskelschädigenden Eigenschaften *in vivo* und *in vitro*, gezeigt werden.

Abbreviations

11 β -HSD.....	11 β -hydroxysteroid dehydrogenase
aa.....	amino acid
ACLY.....	ATP citrate lyase
ACTH.....	adrenocorticotrophic hormone
AP-1.....	activator protein-1
ARG1.....	arginase 1
ATP.....	adenosine triphosphate
CK.....	creatine kinase
CREB.....	cyclic AMP response element-binding protein
CRH.....	corticotropin-releasing hormone
CSF.....	colony-stimulating factor
CVD.....	cardiovascular disease
DHEA.....	dehydroepiandrosterone
eNOS.....	endothelial nitric oxide synthase
FHRE.....	Forkhead responsive element, forkhead responsive element
FoxO3.....	Forkhead box class 3
FPP.....	farnesylpyrophosphate
GC.....	glucocorticoid
GGPP.....	geranylgeranylpyrophosphate
GILZ.....	glucocorticoid-induced leucine zipper
GM.....	granulocyte-macrophage
GR.....	glucocorticoid receptor
GRE.....	glucocorticoid response element

GTP.....	guanosine triphosphate
HMG-CoA.....	hydroxy-methyl-glutaryl-CoA
HPA.....	hypothalamic-pituitary-axis
I κ B.....	inhibitor of κ B
IFN.....	interferon
IL.....	interleukin
JAK.....	janus kinase
kDa.....	kilo Dalton
KLF2.....	Kruppel-like factor 2
LDL.....	low-density lipoprotein
LPS.....	lipopolysaccharide
M.....	macrophage
MHC II.....	major histocompatibility complex class II
MRC1.....	mannose receptor C-type 1
mRNA.....	messenger ribonucleic acid
mTOR/PGC-1 α	mammalian target of rapamycin/peroxisome proliferation-activated receptor- γ complex 1 α
MyD88.....	myeloid differentiation factor 88
NF- κ B.....	nuclear factor 'kappa-light-chain-enhancer' of activated B-cells
NFAT.....	nuclear factor of activated T cells
NLR.....	nucleotide-binding oligomerization domain receptor
NO.....	nitric oxide
PAMP.....	pathogen-associated molecular pattern
POMC.....	proopiomelanocortin
PRR.....	pattern-recognition receptor
Raf.....	rapidly growing fibrosarcoma
Ras.....	rat sarcoma

RNA	ribonucleic acid
ROS	reactive oxygen species
SAMS.....	statin-associated muscle symptoms
SLC27A2	very-long-chain acyl-CoA synthetase 1
STAT	signal transducers and activators of transcription
TGF- β	transforming growth factor beta 1
TLR	toll-like receptor
TNF.....	tumor necrosis factor
TSC22D3.....	transforming growth factor- β -stimulated clone 22 domain family member 3
TTP	tristetraprolin

Table of Content

Summary	VI
Zusammenfassung	VII
Abbreviations	VIII
1. Introduction	1
<i>1.1. Innate Immune Response</i>	<i>1</i>
1.1.1. Macrophages, Inflammation, and Cardiovascular Diseases.....	1
1.1.2. Macrophage Polarization	4
1.1.3. Inflammaging and Immunometabolism.....	6
<i>1.2. Glucocorticoid Metabolism</i>	<i>7</i>
1.2.1. Physiological Function and Regulation of Glucocorticoids	7
1.2.2. Glucocorticoid-Induced Leucine Zipper	10
<i>1.3. Cholesterol Metabolism</i>	<i>12</i>
1.3.1. Statins	12
1.3.1.1. General Aspects	12
1.3.1.2. Adverse Effects of Statins.....	14
1.3.1.3. Pleiotropic Effects of Statins	15
1.3.2. Bempedoic Acid	17
2. Objective	18
3. Results	20
<i>3.1. Amplified Host Defense by Toll-Like Receptor-Mediated Downregulation of the Glucocorticoid-Induced Leucine Zipper (GILZ) in Macrophages</i>	<i>20</i>
<i>3.2. Altered Glucocorticoid Metabolism Represents a Feature of Macroph-aging</i>	<i>41</i>
<i>3.3. The Glucocorticoid-Induced Leucine Zipper (GILZ) Mediates Statin-Induced Muscle Damage</i>	<i>66</i>

3.4. <i>Statins and Bempedoic Acid: Different Actions of Cholesterol Inhibitors on Macrophage Activation</i>	91
4. Summary and Conclusion	125
5. References	127
Appendix	XIII
<i>General Methods</i>	<i>XIII</i>
Reagents	XIII
Cell Culture.....	XIII
Mice	XIV
Cytotoxicity Measurement	XIV
RNA Isolation, Reverse Transcription, and Quantitative PCR (RT-qPCR)	XV
Luciferase Assay	XVI
<i>Introduction</i>	<i>XVIII</i>
<i>Results</i>	<i>XIX</i>
Effect of Bempedoic Acid on Cell Viability and <i>Gilz</i> expression	XIX
Involvement of the Mevalonate Pathway in Simvastatin-Induced <i>Gilz</i> and <i>Klf2</i> Expression	XXI
Involvement of FOXO3 in Simvastatin-Induced <i>Gilz</i> Expression	XXII
Involvement of <i>Gilz</i> Promoter Region in Statin-Induced <i>Gilz</i> Expression.....	XXIII
Effect of Simvastatin on <i>Gilz</i> and <i>Hmox</i> Expression <i>in vivo</i>	XXV
<i>Discussion</i>	<i>XXVI</i>
Curriculum Vitae	XXVIII
Acknowledgment	XXXI

1. Introduction

1.1. Innate Immune Response

1.1.1. Macrophages, Inflammation, and Cardiovascular Diseases

Macrophages were first described based on their phagocytotic nature by Metchnikoff in 1883 and are a milestone in the discovery of the immune system (Metchnikoff, 1883). Later on, they were classified as part of the mononuclear system as phagocytotic cells of the innate immune system (van Furth, R. & Cohn, Z. A., 1968). Macrophages belong to the first-line response of the immune system and are tissue-resident or recruited to the tissue. They are able to detect, engulf, and destroy foreign invaders as well as remove cell debris and maintain cell homeostasis (Lavin et al., 2015).

Macrophages recognize microbial invaders by pattern-recognition receptors (PRRs) detecting viral or bacterial pathogen-associated molecular patterns (PAMPs) such as the gram-negative cell wall component lipopolysaccharide (LPS). Recognized structures comprise toll-like receptor (TLR) families, nucleotide-binding oligomerization domain receptor (NLR) families which are expressed on the plasma membrane and/or on endosomes as well as nucleus-associated receptors (Brubaker et al., 2015). The first *Toll* protein was found in *Drosophila melanogaster* and was characterized by its genetic similarity to the interleukin (IL)-1 receptor as well as its actions *via* similar signaling pathways hinting towards the involvement of TLRs in innate immunity (Gay & Keith, 1991; K. V. Anderson et al., 1985). To date, the TLR family belongs to the most conserved receptor family mediating innate immune responses.

Macrophages can be activated by various TLRs: Representatives are TLR1/TLR2 heterodimers for recognition of peptidoglycans and lipoproteins, TLR3 activation by double-stranded ribonucleic acid (RNA), as well as TLR4 homodimers activation by LPS. TLR4 activation occurs either in a MyD88 (myeloid differentiation factor 88)-dependent or -independent manner (Leifer & Medvedev, 2016).

Macrophages have multiple functions: antigen-presentation, phagocytosis, and immunomodulation during acute inflammation but macrophages are also important mediators of the inflammatory resolution (Fujiwara & Kobayashi, 2005). Beyond their function as part of the innate immunity, macrophages are critical for physiological functions such as homeostasis, remodeling, and tissue repair (Zhang et al., 2021). They mediate their functions by secretion of different cytokines, interferons, growth factors, and messenger substances. Due to their involvement in many physiological functions, they are also pivotal players in the pathogenesis of all major diseases, e.g., chronic inflammatory diseases, cardiovascular diseases (CVDs), and cancer (Ardura et al., 2019).

Figure 1 shows the pathogenesis of atherosclerosis, describing the accumulation of low-density lipoprotein (LDL) in cells of the intima of blood vessels (Gisterå & Hansson, 2017). During progression, the LDL retention attracts monocytes - precursors of the macrophages in the circulation - resulting in their transmigration in the intima of the vessel wall. The release of growth factors, such as granulocyte-macrophage (GM) and macrophage (M) colony-stimulating factors (CSF) results in the transformation to macrophages and uptake of chemically modified LDL finally fuelling the maturation of dysfunctional, non-resolving macrophages, namely foam cells (Moore et al., 2013). In response, macrophages release inflammatory cytokines such as interleukin IL-1 β and tumor necrosis factor (TNF), thus, driving inflammation (Beuscher et al., 1990; Moyer et al., 1991). The progression of atherosclerosis leads to the formation of plaques characterized by a lipid core, fibrous cap, and infiltrated immune cells (Bentzon et al., 2014). The thickening of the vessel wall results in the narrowing of the lumen and with increased severity to sudden ruptures. Atherosclerotic events affect the entire cardiovascular system, causing cardiovascular diseases and might even result in

deadly myocardial infarctions or strokes, and, thus, are the leading cause of deaths worldwide (<https://www.who.int/news-room/fact-sheets/detail/the-top-10-causes-of-death>, 2021).

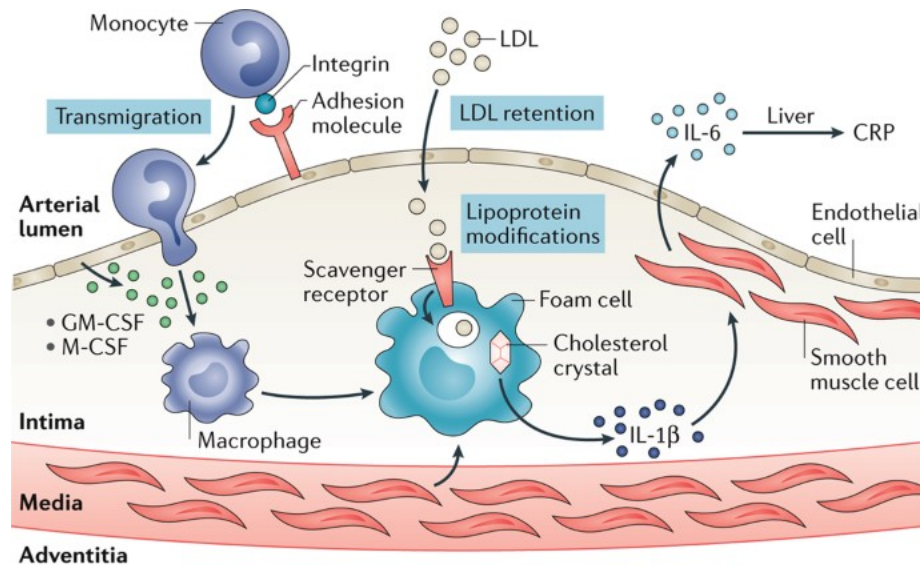


Figure 1: Overview of the immunological actions within an atherosclerotic vessel and the formation of an atherosclerotic plaque. LDL, low-density lipoprotein; GM-CSF, granulocyte-macrophage colony-stimulating factor; M-CSF, macrophage colony-stimulating factor; IL1- β , interleukin 1 β ; IL-6, interleukin 6; CRP, C-reactive protein (Gisterå & Hansson, 2017).

1.1.2. Macrophage Polarization

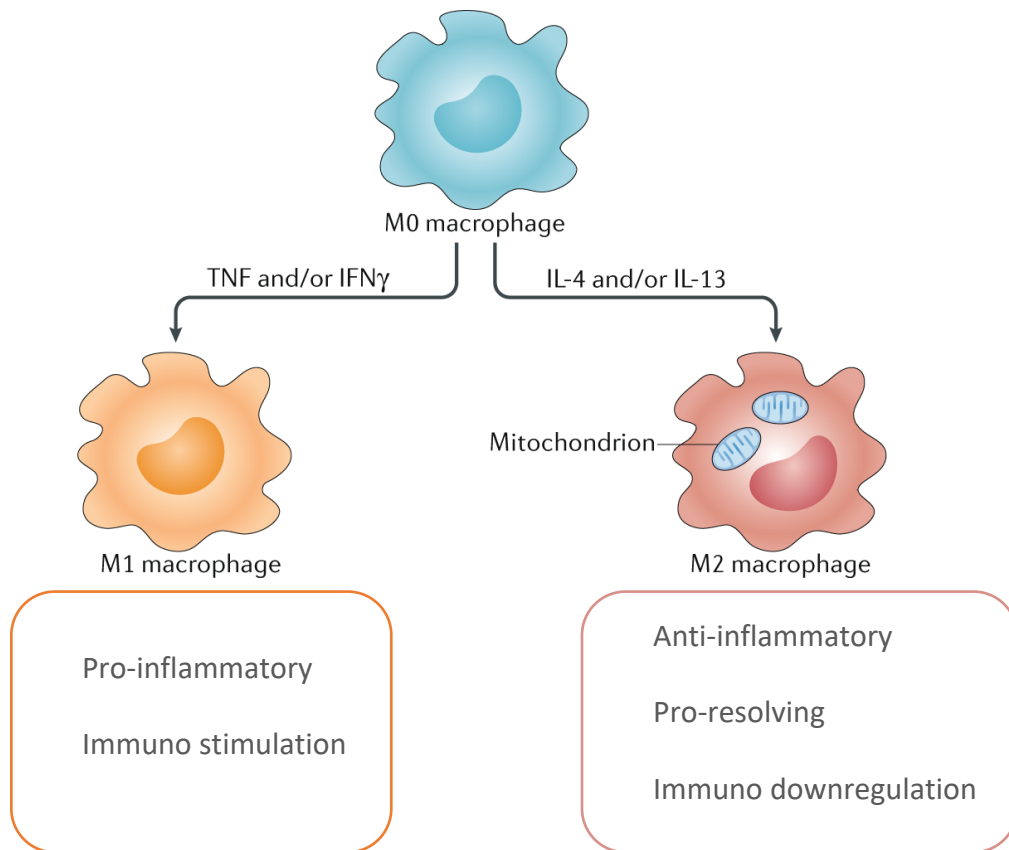


Figure 2: The dichotomy of macrophage polarization states and their mediated main effects. TNF, tumor-necrosis factor; IFN γ , interferon γ ; IL-4, interleukin 4; IL-13, interleukin 13. Adapted from (Russell et al., 2019; Solinas et al., 2009).

The paradigm regarding macrophages as a single cell population was outdated within the last decades and replaced by a dichotomy which described macrophage populations according to their original activity as pro-inflammatory M1 and anti-inflammatory M2 macrophages (Figure 2) (Italiani & Boraschi, 2014; Russell et al., 2019). However, this describes the two extreme populations not representing the plasticity and wide range of subsets implied. Macrophage subsets are characterized by different genetic makeups, expression of receptors, cytokine expression patterns, and distinct morphologies. Consequently, macrophage phenotypes are resident in very different environments and are involved in different conditions of disease (Biswas et al., 2012).

Thus, macrophages can respond to different stimuli showing temporally different phenotypes and allowing a tailored response according to their microenvironment. M1 macrophages are called “classically activated” since they respond to LPS and interferon (IFN) γ . However, in atherosclerotic lesions, it is unlikely that bacterial compounds activate an M1 phenotype. Particularly, endogenous TLR2 and 4 ligands such as fatty acids, oxidized lipids, and IFN γ activate this phenotype and the transcription factor nuclear factor ‘kappa-light-chain-enhancer’ of activated B-cells (NF- κ B) mediates the up-regulation of pro-inflammatory genes resulting in the expression of TNF, IL1 β , IL6, and different types of chemokines and chemokine receptors as well as reactive oxygen species (ROS) and nitric oxide (NO), thus, regarded as plaque-destabilizing and pro-atherogenic (Jinnouchi et al., 2020; Leitinger & Schulman, 2013). In contrast, M2 macrophages are activated by Th2 interleukins (IL4/IL13) as well as different lipid products and are supposed to promote the anti-atherogenic phenotype (Adamson & Leitinger, 2011; Barrett, 2020). The expression of their phenotypic markers like arginase 1 (ARG1), transforming growth factor-beta 1 (TGF- β), and mannose receptor C-type 1 (MRC1) are activated mainly *via* janus kinase (JAK)/signal transducers and activators of transcription (STAT) pathways (Colin et al., 2014).

However, the described M1/M2 paradigm is oversimplified and the rapid progress in the development of new technologies within the last years implied new macrophage subsets distinguishing them in the expression of surface markers, signaling pathways, and gene expression patterns (Vallejo et al., 2021; Willemsen & Winther, 2020).

1.1.3. Inflammaging and Immunometabolism

Aging is characterized by the deterioration of many physiological functions including the immune system. Cellular senescence as part of the aging process was first described in 1961 while observing cell cycle arrests in fibroblasts *in vitro* (Hayflick & Moorhead, 1961). The accumulation of senescent cells and a proinflammatory phenotype - termed “inflammaging” - describes one of the hallmarks of aging (Lopez-Otin et al., 2013). Aging of the innate immune system is triggered by many factors, such as ROS and elevated secretion of pro-inflammatory markers such as TNF, IL1, IL6, and IL8, inducing metabolic changes and skewing macrophages towards M1 representing a state of low-grade inflammation which is termed “inflammaging” (Franceschi et al., 2000; Fulop et al., 2016; Kulman et al., 2010; Yarbro et al., 2020). Consequently, inflammaging is associated with numerous diseases of the elderly such as cancer, immune disorders, or chronic inflammatory diseases (Olivieri et al., 2018). However, inflammaging describes two sides of a coin: Besides its detrimental effects, the changes within the immune function are supposed to be necessary adaptations for longevity and should rather be regarded as the coping strategy to combat a dysbalanced immune system, especially in centenarians; aging is accompanied by the expression of IL10 and TGF β as anti-inflammatory mediators (Fulop et al., 2016; Minciullo et al., 2016; Monti et al., 2017). Further, and in consequence of aging and hypothalamic feedback regulation, an imbalanced glucocorticoid (GC) metabolism characterized by elevated cortisol and decreased dehydroepiandrosterone (DHEA) levels are described (Baylis et al., 2013; Genedani et al., 2008).

1.2. Glucocorticoid Metabolism

1.2.1. Physiological Function and Regulation of Glucocorticoids

The hypothalamic-pituitary-axis (HPA) as part of the neuroendocrine system orchestrates the release and regulation of GCs. Endogenous GCs belong to the class of steroid hormones and are key players and regulators in a wide range of physiological functions in the body. They mediate versatile immune and metabolic functions, such as cell differentiation, cell growth, and tissue repair, and are involved in cell homeostasis (Strehl et al., 2019).

The ubiquitous expression of glucocorticoid receptors (GRs) and the genomic and rapid non-genomic expression of GCs underline their importance and versatile functions (Stahn & Buttgereit, 2008). The loop of GC release is regulated by hypothalamus stimulation and release of corticotropin-releasing hormone (CRH) stimulating the anterior pituitary gland to secrete adrenocorticotrophic hormone (ACTH). The circulating ACTH and its binding to the respective receptor at cells of the adrenal cortex results in the synthesis of GCs and, concurrently, initiates a negative feedback loop (Figure 3) (Bellavance & Rivest, 2014).

Besides the systemic release of GCs, the enzymatic activity of 11 β -hydroxysteroid dehydrogenase 1 (11 β -HSD1) is responsible for the regulation of GCs at the cellular level. They catalyze the conversion of inactive cortisone to active cortisol in humans, inactive 11-dehydrocorticosterone to active corticosterone in rodents, respectively, thus, determining the bioactivity of the glucocorticoid (Draper & Stewart, 2005).

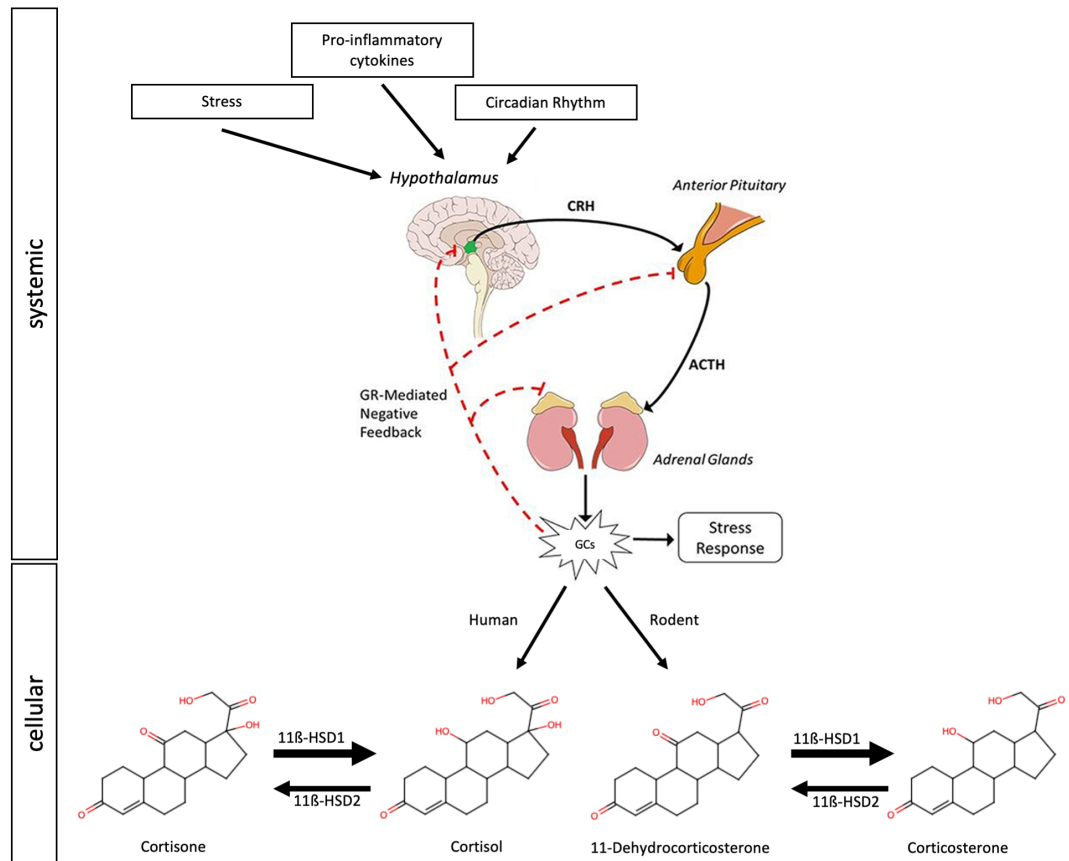


Figure 3: The hypothalamic-pituitary-axis, its hormone release, and glucocorticoid regulation on a cellular level. CRH, corticotropin-releasing hormone; ACTH, adrenocorticotropic hormone; GC, glucocorticoid; GR, glucocorticoid receptor; 11β-HSD, 11β-hydroxysteroid dehydrogenase. Adapted from (Tapp et al., 2019).

GCs have been exploited for immunosuppressive therapy for decades representing a powerful and cost-effective agent for the treatment of inflammatory diseases like rheumatoid arthritis, inflammatory bowel disease, multiple sclerosis, and allergic diseases (Strehl et al., 2019). Their genomic molecular mechanism of action includes trans-activation of proteins like I κ B (inhibitor of κ B) and glucocorticoid-induced leucine zipper (GILZ) as well as suppression of pro-inflammatory cytokines *via* trans-repression of the transcription factors NF- κ B and AP-1 (activator protein-1) exhibiting GCs main actions. However, the repression of proopiomelanocortin (POMC) and osteocalcin *via* cis-repression results mainly in GCs side effects (Figure 4) (Coutinho & Chapman, 2011; Reichardt et al., 2021).

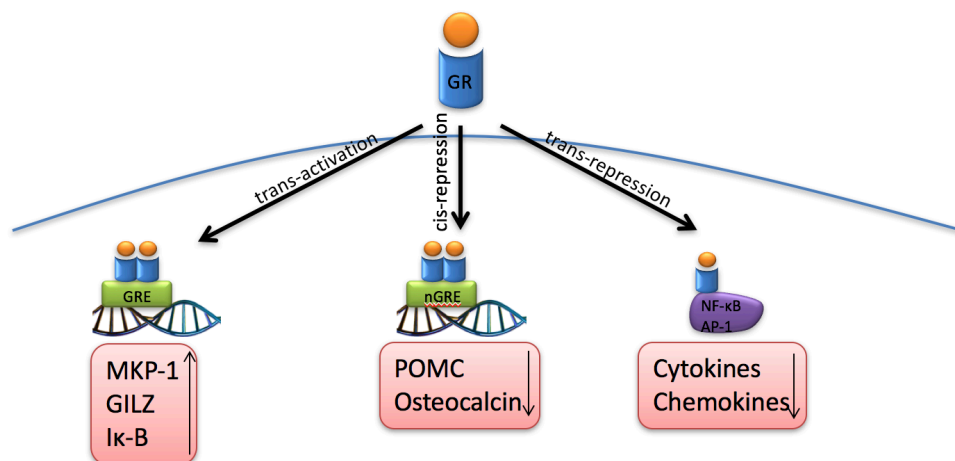


Figure 4: Mode of action of glucocorticoids. AP-1, activator protein 1; GR, glucocorticoid receptor; GRE, glucocorticoid response element; I κ B, inhibitor of NF- κ B; MKP-1, MAP kinase phosphatase 1; nGRE, negative glucocorticoid response element; POMC, proopiomelanocortin.

1.2.2. Glucocorticoid-Induced Leucine Zipper

D'Adamio et al. described the dexamethasone-inducible gene GILZ (*TSC22D3*) in murine thymocytes encoded by a 137 amino acid (aa) protein with a molecular mass of 17 kilo Dalton (kDa) (D'Adamio et al., 1997). Later, murine GILZ was identified in different other cell types, such as monocytes, macrophages, myoblasts, and B cells in splice variants of 201 aa, 43 aa, 80 aa length, and the 234 aa splice variant termed L-GILZ (Bruscoli et al., 2010; Hoppstädter & Kiemer, 2015; Soundararajan et al., 2007). The human analogue was complemented in 2001 characterizing hGILZ as a high homolog of mGILZ (97% homology in the coding region, 89% in the entire mRNA) with a protein length of 135 aa and a molecular mass of 15 kDa located on the X chromosome (Cannarile et al., 2001).

The human GILZ promoter was characterized by transcription factor binding sites for its transcriptional regulation, including six GREs (glucocorticoid response elements) for binding of STAT6, nuclear factor of activated T cells (NFAT), Oct-1, *c-myc*, Forkhead responsive elements (FHREs), cyclic AMP response element-binding protein (CREB), and estrogen-responsive sequence and might require further interaction of the transcription factor FoxO3 (Forkhead box class 3) (Asselin-Labat et al., 2004; Tynan et al., 2004).

Besides the transcriptional regulation, there are post-transcriptional regulations such as RNA binding proteins tristetraprolin (TTP) or HuR, by miRNA binding or epigenetically (Bruscoli et al, 2010; Das et al., 2006; Healy et al., 2020; Hoppstädter et al., 2016; Kuipers et al., 2005; Kumar & Reynolds, 2005; Lee et al., 2012; Massaro et al., 2010; Matsumoto et al., 2004; Mroz et al., 2015; Tuomisto et al., 2019; Wong et al., 2001).

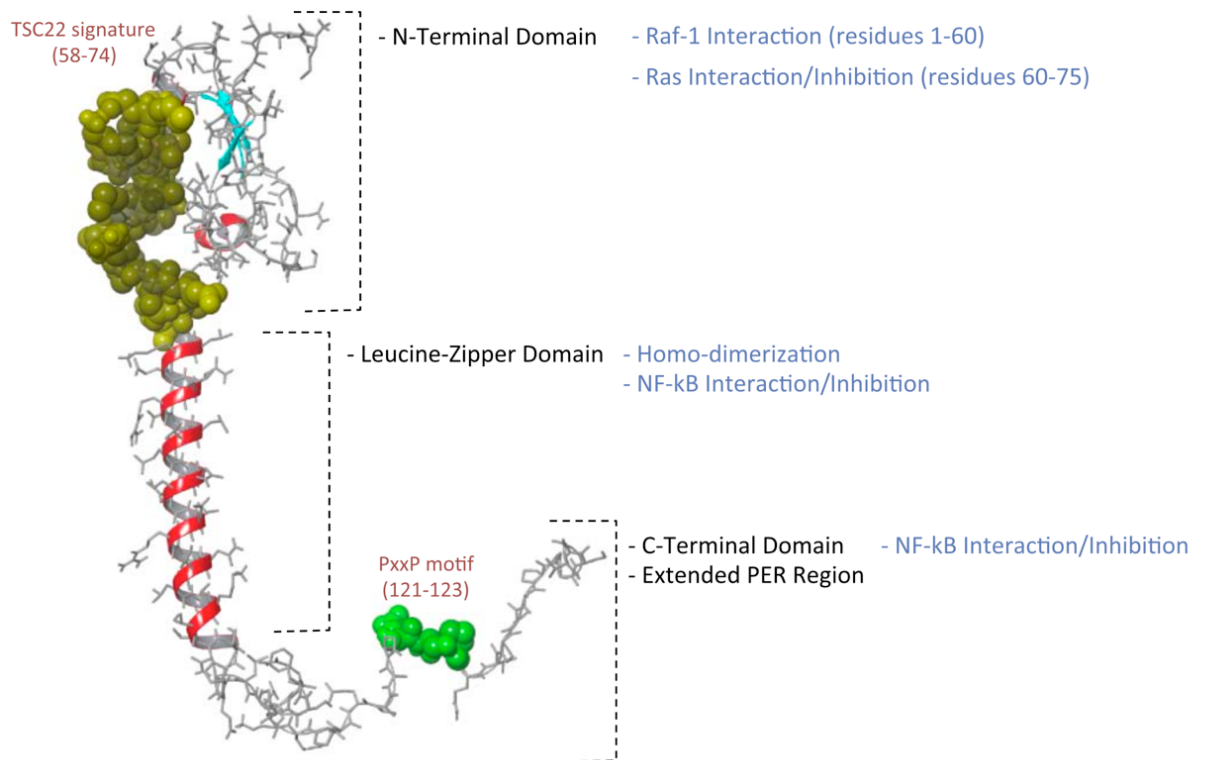


Figure 5: GILZ structure and its main domains for its binding activity and anti-inflammatory actions. Raf, rapidly growing fibrosarcoma; Ras, rat sarcoma; NF-κB; nuclear factor 'kappa-light-chain-enhancer' of activated B-cells. Adapted from (Ayroldi et al., 2014).

GILZ is regarded as a key mediator of anti-inflammatory effects of GCs. As shown in Figure 5 GILZ has three domains contributing to its anti-inflammatory actions (Ayroldi et al., 2014). Mainly, the C- and N-terminal domains interact with the transcription factors NF-κB and AP-1 or small proteins such as Raf (rapidly growing fibrosarcoma) or Ras (rat sarcoma) mediating their immunosuppressive activity (Bereshchenko et al., 2019; Mittelstadt & Ashwell, 2001).

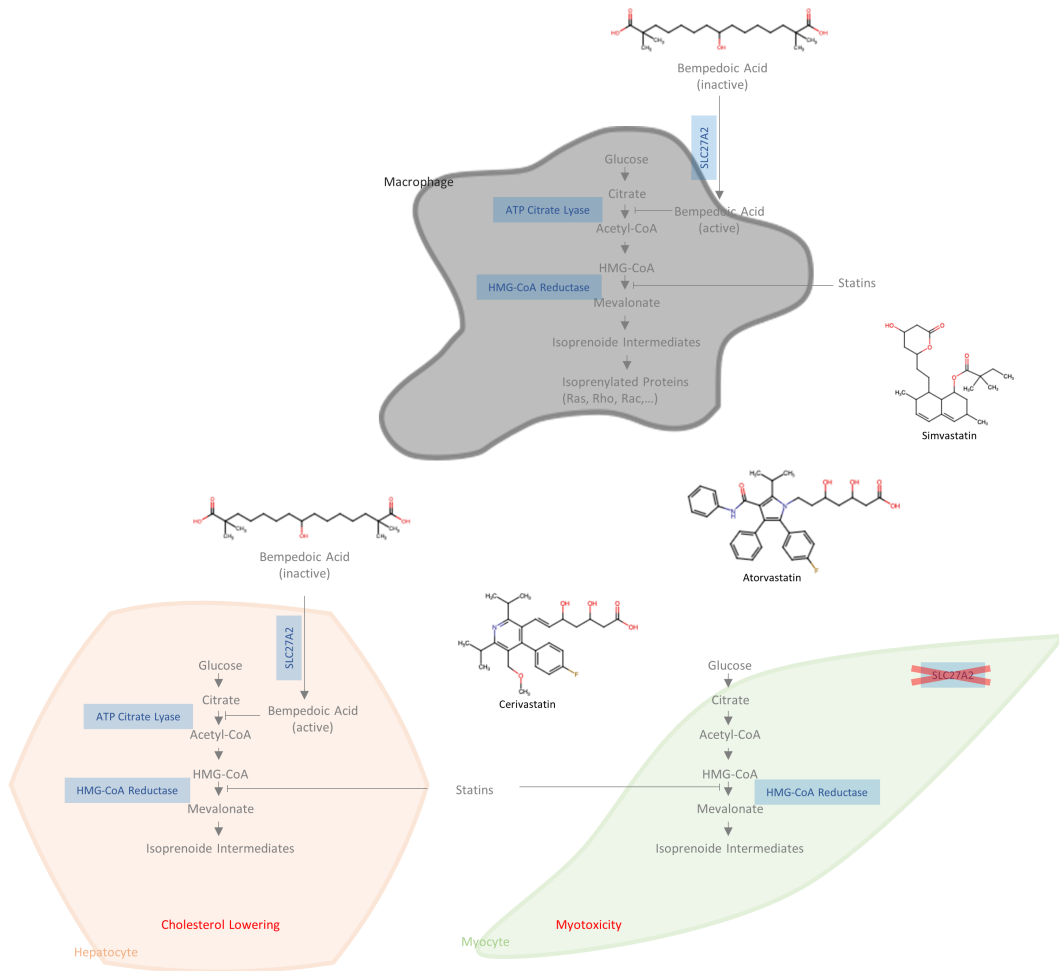
1.3. Cholesterol Metabolism

1.3.1. Statins

1.3.1.1. General Aspects

Statins, i.e., hydroxy-methyl-glutaryl-CoA (HMG-CoA) reductase inhibitors, belong to the first-line treatment of CVDs as the leading cause of death worldwide (<https://www.who.int/News-Room/Fact-Sheets/Detail/the-Top-10-Causes-of-Death>, 2021; Mach et al., 2020). Statins are therapeutic agents for the treatment of hypercholesterolemia and atherosclerotic diseases as underlying conditions for CVDs. Thus, statin prescriptions have been rising within the last years and statins are nowadays the most prescribed class of drugs (<https://clincalc.com/DrugStats/Top300Drugs.aspx>, 2021). The first compounds with hypocholesterolemic activity were discovered in 1976 as fungal metabolites from *Penicillium citrinum* (Endo et al., 1976). Amongst all representatives in this class of drugs the mode of action is the same: Statins interfere with the rate-limiting step of cholesterol synthesis in the liver by competitively inhibiting HMG-CoA reductase, resulting in a decreased hepatic cholesterol production, increased LDL receptor density, and enhanced LDL clearance from the circulation (Figure 6 A) (Sirtori, 2014). To date, there are two groups of statins known: Type I statins are natural or semi-synthetic statins namely lovastatin, simvastatin, pravastatin, and the first discovered mevastatin (also known as compactin). Type II statins compile the group of synthetic statins: Atorvastatin, rosuvastatin, cerivastatin, pitavastatin, and fluvastatin (Figure 6 B). Statins have a high affinity to their target with a K_i in a nanomolar range and the HMG-CoA-like structure either in an inactive lactone form or in its active hydroxy-acid form. *In vivo*, the inactive form is enzymatically hydrolyzed (Ward et al., 2019). Branched moieties determine statins' hydrophilicity/lipophilicity and thus are responsible for their pharmacokinetics and solubility (Murphy et al., 2020).

A



B

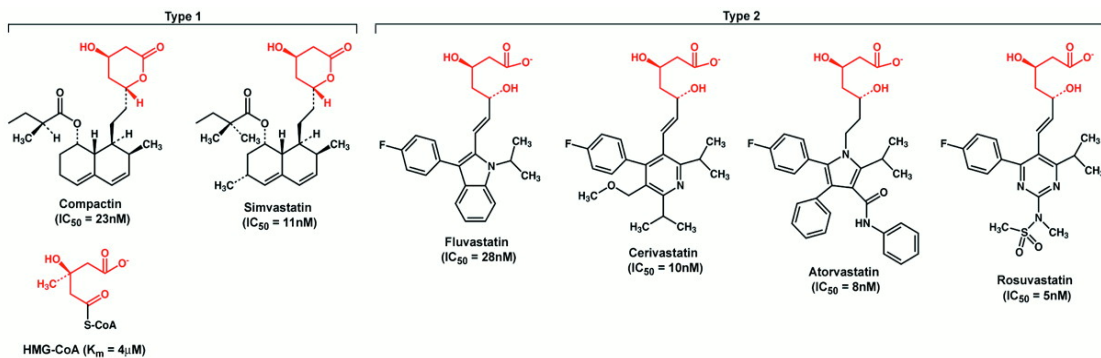


Figure 6: (A) Overview of the mevalonate pathway and the mode of action of statins and bempedoic acid. The potential pleiotropic effects of statins are highlighted in red. (B) Chemical structure of statins. Their HMG-CoA-like moiety is highlighted in red. IC_{50} values are indicated. Adapted from (Istvan & Deisenhofer). SLC27A2, very-long-chain acyl-CoA synthetase 1; CoA, coenzyme A; HMG, hydroxy-methyl-glutaryl.

1.3.1.2. Adverse Effects of Statins

Statins are effective agents for reducing blood cholesterol levels and show a sufficient safety-risk profile (Grundy et al., 2019). However, they can exert adverse effects ranging from peripheral neuropathy to renal and hepatic disorders as well as statin-associated muscle symptoms (SAMS) and might be the reason for an alarmingly high number of non-adherent therapy amongst high-risk patients (Macedo et al., 2014; Taylor et al., 2013; Toth et al., 2019). SAMS are the most described side effects of statins in the clinic and can be manifested as myalgia, myopathy, myositis with or without elevated creatine kinase (CK) levels, or in rare cases as a severe rhabdomyolysis (Stroes et al., 2015). SAMS are dependent on the class and dose of statin but are not related to their cholesterol-lowering action. They were also the reason for the withdrawal of cerivastatin from the market (Kobayashi et al., 2008). The mechanisms of statins' myotoxic action have not been elucidated in detail. There are several HMG-CoA-dependent and -independent hypotheses contributing to their explanation. These include the disruption of the mitochondrial respiratory chain, increased ROS production, impaired isoprenylated proteins involved in the RhoA/AKT/mTOR/PGC-1 α (mammalian target of rapamycin/peroxisome proliferation-activated receptor- γ complex 1 α) pathway as well as a genetic impact (reviewed by (Vinci et al., 2021)). Several different genetic polymorphisms regarding statins' metabolism, pharmacokinetics, and pharmacodynamics have been proposed but still need to be further investigated regarding their causality. These include polymorphisms in the metabolizing CYP enzymes as well as ABC transporters resulting in an affected hepatobiliary clearance (Sirtori et al., 2012; Wilke et al., 2005).

1.3.1.3. Pleiotropic Effects of Statins

Besides statins' undesired adverse effects early clinical studies and observations revealed that statins exert beneficial cardiovascular effects beyond their cholesterol-lowering actions known as "pleiotropic" effects (reviewed by (Yu & Liao, 2022)). The effects are mainly attributed to endothelial cells, vascular smooth muscle cells, platelets, and monocytes/macrophages and are supposed to be mevalonate-pathway-independent and -dependent.

Clinical and basic research studies found that statins stabilize the atherosclerotic plaque *via* impaired collagen content, increased plaque calcification, and reduced matrix metalloproteinase production as well as increased expression of the atheroprotective transcription factor Kruppel-like factor 2 (KLF2), which is also involved in GR network (Aikawa et al., 2001; Fukumoto et al., 2001; Healy et al., 2020; Nicholls et al., 2011; Tuomisto et al., 2019). Other studies showed an increased expression and activity of endothelial nitric oxide synthase (eNOS), reduced ROS generation, and antioxidant effects. Furthermore, decreased pro-inflammatory cytokine secretion, such as IL1 β , IL6, and TNF secretion were observed as well as altered major histocompatibility complex class II (MHC II) expression and impaired NF- κ B activity (Ikeda & Shimada, 1999; Kuipers et al., 2005; Laufs et al., 2000; Wassmann et al., 2001).

There are different molecular and cellular mechanisms proposed for statins' pleiotropic effects. On the one hand, the literature describes physico-chemical interactions of statins with cell membranes and thus, altered lipid rafts and membrane fluidity exerting different effects according to the lipophilicity of statins (Murphy et al., 2020). On the other hand, there are studies proposing interference in cellular trafficking and signaling of small GTPases (guanosine triphosphate) as the main mechanism. Inhibiting the synthesis of mevalonate, statins also prevents the synthesis of isoprenoid intermediates, such as farnesylpyrophosphate (FPP) and geranylgeranyl pyrophosphate (GGPP) (Liao, 2002; Nohria et al., 2009). FPP and GGPP serve as lipid attachments for the posttranslational modification of small GTPases, such as Ras and

Rho GTPases, thus influencing important cell functions (Goldstein & Brown, 1990; Van Aelst & D'Souza-Schorey, 1997).

1.3.2. Bempedoic Acid

The cholesterol-lowering agent was recently approved for the treatment of hypercholesterolemia. Bempedoic acid, a small synthetic fatty-acid-like prodrug, requires a liver-specific enzyme, the very-long-chain acyl-CoA synthetase 1 (SLC27A2), for transformation into its active -CoA derivative and halting cholesterol-synthesis by inhibition of the ATP (adenosine triphosphate) citrate lyase (ACLY) upstream of HMG-CoA reductase (Figure 6 A) (Filippov et al., 2014; Pinkosky et al., 2016). Administration of bempedoic acid represents a promising alternative treatment for patients with statin intolerance or muscle-related side effects since the converting enzyme SLC27A2 is not expressed in the skeletal muscle (Honigberg & Natarajan, 2019; Laufs et al., 2022). Notably, it has been reported that bempedoic acid has atheroprotective and anti-inflammatory effects by stabilizing atherosclerotic plaques and reduction of CRP as a clinical outcome (Baardman et al., 2020; Nguyen et al., 2021; Pinkosky et al., 2016; Samsundar et al., 2017). The proposed mechanism shows an inhibition of macrophage AMPK (adenosine monophosphate-activated protein kinase) by its inactive form thus decreasing a pro-inflammatory cytokine storm (Filippov et al., 2013).

2. Objective

GILZ is an immunomodulatory protein playing a pivotal role in macrophages' immune response. Its regulation mechanisms occur on transcriptionally and post-transcriptionally levels either by altered mRNA stability, miRNA binding, or epigenetically mechanisms (Bruscoli et al, 2010; Das et al., 2006; Healy et al., 2020; Hoppstädter et al., 2016; Kuipers et al., 2005; Kumar & Reynolds, 2005; Lee et al., 2012; Massaro et al., 2010; Matsumoto et al., 2004; Mroz et al., 2015; Tuomisto et al., 2019; Wong et al., 2001). However, gene regulation is dependent on different aspects such as cell type, cell microenvironment, and pathophysiological state. Thus, this work was concerned with the contribution to a better understanding of GILZ regulation in aging and macrophage activation. The two projects and their respective results were published in manuscript 3.1. "Amplified Host Defense by Toll-Like Receptor-Mediated Downregulation of the Glucocorticoid-Induced Leucine Zipper (GILZ) in Macrophages" and manuscript 3.2. "Altered Glucocorticoid Metabolism Represents a Feature of Macroph-aging".

Second, this study focused on statins' effects on GILZ. To date, the literature shows controversial results regarding potential pleiotropic effects of statins and bempedoic acid, such as anti-inflammation and myotoxicity (reviewed by Liao & Laufs, 2005). Bruscoli et al. identified GILZ as a mediator of the anti-myogenic effects of glucocorticoids (Bruscoli et al., 2010). Thus, this work focused on the effects of cholesterol-lowering agents on macrophages and muscle cells linking GILZ to potential pleiotropic effects of statins (Figure 7). The projects and their respective results were published in manuscript 3.3. "The Glucocorticoid-Induced Leucine Zipper (GILZ) Mediates Statin-Induced Muscle Damage", in manuscript 3.4. "Statins and Bempedoic Acid: Different Actions of Cholesterol Inhibitors on Macrophage Activation", and in the appendix of this thesis.

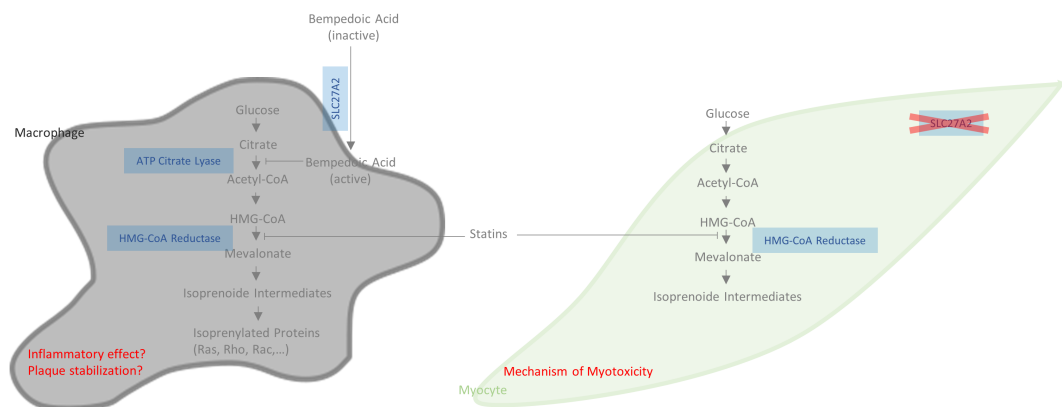


Figure 7: Graphical summary of the aims defined for this doctoral thesis regarding cholesterol-lowering drugs in macrophages and muscle cells.

In summary, the aims of this thesis comprise aspects of macrophage signaling pathways focusing on the role of GILZ in the context of metabolic and age-related factors as well as mechanistic insights of myogenic and anti-inflammatory statin effects:

- I. The impact of TLR agonists on GILZ regulation and identification of GILZ-targeting miRNAs in macrophages.
- II. Age-related changes in glucocorticoid metabolism and involvement of GILZ during aging in the myeloid compartment of mice.
- III. Mechanisms of GILZ-mediated myotoxic actions of statins.
- IV. Characterization of the impact of statins and bempedoic acid on macrophage polarization.
- V. The effect of statins on GILZ *in vitro*, *ex vivo*, and *in vivo* and statins' potential anti-inflammatory effect in macrophages.

3. Results

3.1. Amplified Host Defense by Toll-Like Receptor-Mediated Downregulation of the Glucocorticoid-Induced Leucine Zipper (GILZ) in Macrophages

Front Immunol. **2019**, doi: 10.3389/fimmu.2018.03111

J. Hoppstädter, B. Diesel, R. Linnenberger, N. Hachenthal, S. Flamini, M. Minet, P. Leidinger, and C. Backes designed, performed, and analyzed experiments. J. Hoppstädter wrote the paper. All authors contributed to the drafting the manuscript. S. Bruscoli, C. Riccardi, F. Grässer, E. Meese, and H. Huwer provided materials and discussed data. A. K. Kiemer initiated the study and participated in data interpretation and manuscript preparation. All authors read and approved the final manuscript.

Rebecca Linnenberger was involved in the design, performance, and analysis of miRNA and TAT-GILZ NF- κ B/AP-1 reporter gene assays and the respective cell culture. She prepared the corresponding figures, description of methods, and was involved in the drafting process of the manuscript, as well as the critical review of the manuscript.

© Hoppstädter, Diesel, Linnenberger, Hachenthal, Flamini, Minet, Leidinger, Backes, Grässer, Meese, Bruscoli, Riccardi, Huwer and Kiemer. This is an open-access article distributed under the terms of the Creative Commons Attribution Licence (CC BY).



Amplified Host Defense by Toll-Like Receptor-Mediated Downregulation of the Glucocorticoid-Induced Leucine Zipper (GILZ) in Macrophages

Jessica Hoppstädter^{1*}, Britta Diesel¹, Rebecca Linnenberger¹, Nina Hachenthal¹, Sara Flamini², Marie Minet¹, Petra Leidinger³, Christina Backes⁴, Friedrich Grässer⁵, Eckart Meese³, Stefano Bruscoli², Carlo Riccardi², Hanno Huwer⁶ and Alexandra K. Kiemer¹

OPEN ACCESS

Edited by:

Alexandre Corthay,
Oslo University Hospital, Norway

Reviewed by:

Kishore Kumar Jella,
Emory University, United States
Philippe Georgel,
Université de Strasbourg, France
Esmail Mortaz,
National Research Institute of
Tuberculosis and Lung Diseases, Iran

*Correspondence:

Jessica Hoppstädter
j.hoppstaedter@mx.uni-saarland.de

Specialty section:

This article was submitted to
Molecular Innate Immunity,
a section of the journal
Frontiers in Immunology

Received: 23 August 2018

Accepted: 17 December 2018

Published: 22 January 2019

Citation:

Hoppstädter J, Diesel B,
Linnenberger R, Hachenthal N,
Flamini S, Minet M, Leidinger P,
Backes C, Grässer F, Meese E,
Bruscoli S, Riccardi C, Huwer H and
Kiemer AK (2019) Amplified Host
Defense by Toll-Like
Receptor-Mediated Downregulation of
the Glucocorticoid-Induced Leucine
Zipper (GILZ) in Macrophages.
Front. Immunol. 9:3111.
doi: 10.3389/fimmu.2018.03111

¹ Pharmaceutical Biology, Department of Pharmacy, Saarland University, Saarbrücken, Germany, ² Pharmacology, Department of Medicine, Perugia University, Perugia, Italy, ³ Human Genetics, Department of Medicine, Saarland University, Homburg, Germany, ⁴ Chair for Clinical Bioinformatics, Saarland University, Saarbrücken, Germany, ⁵ Virology, Department of Medicine, Saarland University, Homburg, Germany, ⁶ Cardiothoracic Surgery, Völklingen Heart Centre, Völklingen, Germany

Activation of toll-like receptors (TLRs) plays a pivotal role in the host defense against bacteria and results in the activation of NF- κ B-mediated transcription of proinflammatory mediators. Glucocorticoid-induced leucine zipper (GILZ) is an anti-inflammatory mediator, which inhibits NF- κ B activity in macrophages. Thus, we aimed to investigate the regulation and role of GILZ expression in primary human and murine macrophages upon TLR activation. Treatment with TLR agonists, e.g., Pam₃CSK₄ (TLR1/2) or LPS (TLR4) rapidly decreased GILZ mRNA and protein levels. In consequence, GILZ downregulation led to enhanced induction of pro-inflammatory mediators, increased phagocytic activity, and a higher capacity to kill intracellular bacteria (*Salmonella enterica* serovar *typhimurium*), as shown in GILZ knockout macrophages. Treatment with the TLR3 ligand polyinosinic: polycytidylic acid [Poly(I:C)] did not affect GILZ mRNA levels, although GILZ protein expression was decreased. This effect was paralleled by sensitization toward TLR1/2- and TLR4-agonists. A bioinformatics approach implicated more than 250 miRNAs as potential GILZ regulators. Microarray analysis revealed that the expression of several potentially GILZ-targeting miRNAs was increased after Poly(I:C) treatment in primary human macrophages. We tested the ability of 11 of these miRNAs to target GILZ by luciferase reporter gene assays. Within this small set, four miRNAs (hsa-miR-34b*, -222, -320d, -484) were confirmed as GILZ regulators, suggesting that GILZ downregulation upon TLR3 activation is a consequence of the synergistic actions of multiple miRNAs. In summary, our data show that GILZ downregulation promotes macrophage activation. GILZ downregulation occurs both via MyD88-dependent and -independent mechanisms and can involve decreased mRNA or protein stability and an attenuated translation.

Keywords: inflammation, MyD88, TRIF, NF- κ B, cytokine, nitric oxide, phagocytosis, microRNA

INTRODUCTION

Macrophages are strategically distributed all over the body and represent the first line of defense to invading pathogens. In response to bacterial or viral infections, these phagocytic cells engulf and destroy the infectious agent. Macrophages recognize a variety of microbial products, such as bacterial cell wall components and nucleic acids, via pathogen recognition receptors (PRRs). These receptors include Toll-like receptors (TLRs), as well as cytosolic NOD-like receptors, RIG-I-like receptors, and DNA sensors (1, 2).

Once a pathogen is recognized and phagocytosed, macrophages generate a wide range of biologically active molecules, e.g., pro-inflammatory cytokines, chemokines, and growth factors. Cytokines released by macrophages, such as interferons (IFNs), tumor necrosis factor (TNF)- α , and interleukin (IL)-1 α/β , stimulate the activity of both the innate and adaptive immune response. Pathogen uptake usually also results in antimicrobial responses such as reactive oxygen species (ROS) and nitric oxide (NO) production, thus enabling a rapid response to infection (3, 4).

Activated macrophages can be deactivated by various mediators, including IL-10, prostaglandins, G-protein coupled receptor ligands, or glucocorticoids (GCs) (3, 4). Anti-inflammatory factors such as IL-10 are also released by macrophages themselves, and failure to produce these mediators can lead to non-resolving inflammation (3, 4).

The Glucocorticoid-induced leucine zipper (GILZ) is an endogenous inhibitor of immune responses. GILZ exerts its anti-inflammatory activity mainly by inhibition of the pro-inflammatory transcription factors nuclear factor (NF)- κ B and activator protein (AP)-1 (5–8). In addition, GILZ has been implicated in the negative regulation of mitogen-activated protein kinase (MAPK) signaling (9–11).

Early studies on GILZ focused on its effects on thymocytes and T lymphocytes because of its strong induction by GCs in the thymus (12). Several reports indicated that the pro-apoptotic effects of GILZ overexpression in T lymphocytes mimic GC treatment (5, 8, 12–14). Moreover, GILZ depletion attenuates GC-induced apoptosis in B lymphocytes (15, 16).

In monocytes and macrophages, GILZ can be upregulated by various anti-inflammatory factors, such as GCs, IL-4 or IL-10, and the natural compound curcumin (6, 17–20). In accordance with the GC-like actions of GILZ in lymphocytes, GILZ overexpression in macrophage-like THP-1 cells results in decreased expression of chemokines and macrophage activation markers, as well as NF- κ B activity upon treatment with the TLR4 ligand lipopolysaccharide (LPS) (6).

We previously reported that primary human *in vitro* differentiated and *ex vivo* pulmonary macrophages express high constitutive levels of GILZ (11, 21). Both siRNA-mediated GILZ knockdown in human macrophages and GILZ knockout in murine bone marrow-derived macrophages (BMMs) increased the responsiveness toward LPS, suggesting that repression of endogenous GILZ expression represents a positive feedback loop in macrophage activation.

Little is known about the role and regulation of GILZ after stimulation with other TLR ligands, e.g., activators of TLR1/2 or TLR3. The extracellular TLR1/2 heterodimer recognizes bacterial triacetylated lipopeptides and their mimic, the synthetic compound Pam₃CSK₄. In contrast, intracellular TLR3 detects double-stranded RNA, i.e., an intermediate in viral replication, as well as its synthetic analogon polyinosinic:polycytidylic acid [Poly(I:C)]. TLRs differentially activate transcription factors due to the varying involvement of the adapter molecules MyD88 (myeloid differentiation primary response gene 88) and TRIF (TIR domain-containing adapter inducing IFN- β). All TLRs except TLR3 can initiate MyD88-dependent signaling, and MyD88-independent signaling via TLR3 or TLR4 utilizes TRIF for signal transduction (1, 2).

In the present study, we provide evidence for dual regulation of GILZ upon MyD88- and TRIF-dependent TLR activation and link GILZ expression levels with pivotal macrophage defense mechanisms, such as phagocytosis and bactericidal activity.

MATERIALS AND METHODS

Materials

Cell media (RPMI1640, #R0883; DMEM, #D6546), fetal calf serum (FCS, #F7524), penicillin/streptomycin (#P433), and glutamine (#G7513) were from Sigma-Aldrich. Anti-GILZ antibodies were obtained from either Santa Cruz Biotechnology (polyclonal goat anti-GILZ Ab, #sc-26518) or eBioscience (CFMKG15, #14-4033-82). The anti-tubulin antibody (#T9026) was obtained from Sigma-Aldrich. Anti-rabbit IRDye 680- and anti-mouse IRDye 800-conjugated secondary antibodies were from LI-COR Biosciences (#926-68071, #926-32210). The anti-rabbit IRDye 800-conjugated secondary antibody was from Rockland (#612-132-120). Anti-p44/42 (ERK1/2) mouse antibody (L34F12, #4696S) and anti-phospho-p44/42 MAPK (Thr202/Tyr204) rabbit mAbs (20G11, #4376S) were obtained from Cell Signaling Technology. TLR ligands, i.e., ultrapure LPS from *Escherichia coli* K12 (#tlrl-pek1ps), Pam₃CSK₄ (#tlrl-pms), lipoteichoic acid (LTA, #tlrl-pslta), and Poly(I:C) (#tlrl-pic) were purchased from Invivogen. Phorbol 12-myristate 13-acetate (PMA, #524400) and BAY 11-7082 (Cay10010266-10) were from Cayman Chemical. BAY 11-7085 (#196872) was

Abbreviations: AMS, alveolar macrophages; AP-1, activator protein-1; ATA, aurointricarboxylic acid; BMMs, bone marrow-derived macrophages; CFU, colony-forming units; CXCL, C-X-C motif ligand; DMEM, Dulbecco's modified Eagle medium; ERK, extracellular signal regulated kinase; FCS, fetal calf serum; GC, glucocorticoid; GILZ, glucocorticoid-induced leucine zipper; HEK, human embryonic kidney; HMDMs, human monocyte-derived macrophages; GM-CSF, granulocyte macrophage colony stimulating factor; IL, interleukin; INF, interferon; iNOS, inducible NO synthase; KO, knockout; LPS, lipopolysaccharide; LTA, lipoteichoic acid; MOI, multiplicity of infection; NF- κ B, nuclear factor- κ B; MAPK, mitogen-activated protein kinase; M-CSF, macrophage colony stimulating factor; MPI, Max Planck Institute; MyD88, myeloid differentiation primary response gene 88; NO, nitric oxide; NOD, nucleotide-binding oligomerization domain; PMA, phorbol 12-myristate 13-acetate; Poly(I:C), polyinosinic:polycytidylic acid; PRR, pattern recognition receptor; RPMI, Roswell Park Memorial Institute; ROS, reactive oxygen species; RIG-I, retinoic acid-inducible gene-I; STAT, signal transducer and activator of transcription; TAT, trans-activator of transcription; TNE, tumor necrosis factor; TLR, toll-like receptor; TRIF, TIR domain-containing adapter inducing IFN- β ; TTP, tristetraprolin; UTR, untranslated region; WT, wild-type.

obtained from Calbiochem. Human M-CSF (#M6518), MTT (#M5655), actinomycin D (#A9415), and aurointricarboxylic acid (ATA, #A1895) were obtained from Sigma-Aldrich. Murine GM-CSF (#130-095-735), M-CSF (#130-101-704), IFN- γ (#130-105-782), IL-4 (#130-097-761), and TNF- α (#130-101-689) were obtained from Miltenyi Biotec. Primers and dual-labeled probes were from Eurofins MWG Operon. Taq polymerase (5 U/ μ L, #E00007), Taq buffer (#B0005) and the dNTP mix (#D0056) were from Genscript. D-luciferin was obtained from Applchem (#A1029,0050). Coelenterazine was from Biotium (#10110). Restriction enzymes (BamHI, #R3136S; EcoRI, #R0101S; SacI, #R0156S; SpeI, #R0133L) were purchased from New England Biolabs. Other chemicals were obtained from either Sigma-Aldrich or Carl Roth unless stated otherwise.

Mice

Mice were housed in a 12:12 h light-dark cycle with food and water *ad libitum*. Mice expressing Cre recombinase under the control of endogenous *Lyz2* (lysozyme 2) promoter/enhancer elements (LysMcre mice, The Jackson Laboratory, #B6.129P2-*Lyz2*^{tm1(cre)lfo/j}) were crossed with C57BL/6J mice bearing *LoxP* sites upstream and downstream of *Gilz* exon 6 (11, 22) to obtain myeloid-specific GILZ KO mice. Genotyping was performed according to protocols provided by The Jackson Laboratory and as described by Bruscoli et al. (22).

Cell Culture

Cell Lines

THP-1 (#TIB202), U937 (#CRL-1593.2), and L929 cells (#CRL-6364) were obtained from ATCC and grown in standard medium (RPMI 1640, 10% FCS, 100 U/mL penicillin G, 100 μ g/mL streptomycin, 2 mM glutamine). THP-1 and U937 were differentiated into macrophage-like cells by treatment with PMA (100 nM) for 48 h. HEK293T cells (ATCC, #CRL-3216) were cultured in high glucose DMEM medium with supplements (10% FCS, 100 U/mL penicillin G, 100 μ g/mL streptomycin, 2 mM glutamine). HEK-BlueTM Null1 cells (Invivogen, #hkb-null1) were grown in high glucose DMEM medium supplemented with 10% FCS, 2 mM glutamine, 50 U/mL penicillin G, 50 μ g/mL streptomycin, 100 μ g/mL Normocin (Invivogen, #ant-nr-1), and 100 μ g/mL Zeocin (Invivogen, #ant-zn-1).

Human Alveolar Macrophages (AMs)

AMs were isolated from human non-tumor lung tissue obtained from patients undergoing lung resection. The use of human material for isolation of primary cells was reviewed and approved by the local Ethics Committees (permission no. 213/06; State Medical Board of Registration, Saarland, Germany). The informed consent of all participating subjects was obtained. Isolation was performed according to a previously described method (23) with minor modifications. After visible bronchi were removed, the lung tissue was cut into pieces (~1 cm³) and washed at least three times with BSS (balanced salt solution; 137 mM NaCl, 5 mM KCl, 0.7 mM Na₂HPO₄, 10 mM HEPES, 5.5 mM glucose, pH 7.4). The washing buffer was collected and centrifuged (15 min, 350 x g). Erythrocytes were lysed by incubation with hypotonic buffer (155 mM NH₄Cl, 10 mM

KHCO₃, 1 mM Na₂EDTA) for 2–5 min at 37°C, and the cell suspension was washed with PBS (137 mM NaCl, 2.7 mM KCl, 10.1 mM Na₂HPO₄, 1.8 mM KH₂PO₄, pH 7.4). Cells were resuspended in AM medium (RPMI 1640, 5% FCS, 100 U/mL penicillin G, 100 μ g/mL streptomycin, 2 mM glutamine), seeded at a density of 0.5–1 \times 10⁶ cells/well into a 12- or 6-well plate and incubated at 37°C for 2 h. Adherent cells were washed at least 5 times with PBS, and cells were cultured in AM medium overnight before further use. AM preparations were 95% pure as assessed by flow-cytometric analysis of intracellular CD68 expression (23, 24).

Human Monocyte-Derived Macrophages

Monocytes were isolated from healthy adult blood donors (Blood Donation Center, Saarbrücken, Germany) and differentiated with M-CSF as described in Dembek et al. (25). The use of the human material was reviewed and approved by the local Ethics Committees (permission no. 130/08; State Medical Board of Registration, Saarland, Germany). Peripheral blood mononuclear cells (PBMCs) were isolated by density gradient centrifugation using Lymphocyte Separation Medium 1077 (Promocell, #C-44010) and Leucosep tubes (Greiner Bio-One, #227290) as recommended by the suppliers. After washing with PBS, monocytes were purified from PBMCs by magnetic cell sorting using anti-CD14 microbeads (Miltenyi, #130-050-201) according to the manufacturer's instructions, except that 10% of the recommended bead amount was used (25). Monocyte purity was > 95% as indicated by CD14 expression (data not shown). Monocytes were seeded into 12 well plates (5 \times 10⁵ cells/well) and differentiated into macrophages in RPMI 1640 supplemented with 10% FCS, 100 U/mL penicillin G, 100 mg/mL streptomycin, 2 mM glutamine, and 20 ng/mL M-CSF at 37°C and 5% CO₂ for 7 d. The medium was changed every other day.

Murine Bone Marrow-Derived Macrophages (BMMs)

BMMs were obtained from 8 to 12-week-old male wild-type (WT, LysMCre^{+/+}/floxed GILZ^{-/-}) or GILZ knockout (KO, LysMCre^{+/+}/floxed GILZ^{+/-}) mice as described previously with minor modifications (11). Femurs and tibias were flushed with standard medium (RPMI 1640, 10% FCS, 100 U/mL penicillin G, 100 μ g/mL streptomycin, 2 mM glutamine). After centrifugation (10 min, 250 x g), erythrocytes were lysed by incubation in hypotonic buffer (155 mM NH₄Cl, 10 mM KHCO₃, 1 mM Na₂EDTA) for 2 min at 37°C. Cells were washed with PBS, resuspended in standard medium containing M-CSF (50 ng/mL, 30 mL per preparation), transferred into a 75 cm² culture flask and allowed to adhere overnight. Non-adherent cells were collected and cultured in a 150 cm² culture flask for another 5 d in M-CSF-containing medium. Differentiated cells were detached with accutase (Sigma-Aldrich, #A6964), suspended in standard medium supplemented with 10 ng/mL M-CSF, and seeded into 96-well plates (7.5 \times 10⁴ cells/well) for TNF measurements or into 12-well plates (5 \times 10⁵ cells per well) for all other applications unless indicated otherwise. BMMs were > 95% pure as indicated by flow cytometric analysis using an antibody against F4/80 (data not shown).

MPI Cells

MPI cells, i.e., non-transformed self-renewing primary murine macrophages, were obtained from WT or GILZ KO mice based on a previously described method (26). MPI cells were prepared from fetal livers of 15-d-old mouse embryos by pushing the tissue through 70 μ m cell strainers while washing with PBS. Cells were washed once with PBS and then resuspended in standard medium (RPMI 1640, 10% FCS, 100 U/mL penicillin G, 100 μ g/mL streptomycin, 2 mM glutamine) supplemented with 30 ng/mL GM-CSF. Proliferating cells were subcultured by splitting them 1:5 after 6–8 d. Cell preparations were > 95% positive for macrophage markers F4/80 and CD68, as indicated by flow cytometric analysis (data not shown). Cells were seeded into 96-well plates (4×10^4 cells/well) for determination of NO release or into 12 well plates (2×10^5 cells/well) for phagocytosis assays.

Determination of Cell Viability

The MTT colorimetric assay was performed to ensure that non-toxic concentrations of U0126, BAY-11-7082, BAY-11-7085, and ATA were used. Cells were incubated for 24 h with the test compounds diluted in a cell-type specific medium. After that, cells were incubated with MTT solution (5 mg/mL in medium) for 2 h. The supernatant was discarded, and cells were lysed in 100 μ L DMSO. Absorbance measurements were carried out at 550 nm with 630 nm as the reference wavelength using a microplate reader (Tecan Sunrise). The cell viability obtained from at least two independent experiments was calculated relative to untreated and solvent controls (data not shown).

Cytokine Quantification

Cytokines were quantified in AM supernatants using a Milliplex MAP Human Cytokine Kit (Millipore, #HCYTOMAG-60K) as detailed in Hoppstädter et al. (23). AMs were kept at a density of 1×10^5 cells per well in 96 well plates in a total volume of 100 μ L medium in the presence or absence of Pam₃CSK₄ (100 ng/mL) or Poly(I:C) (10 μ g/mL) for 6 h. The supernatants were collected and stored at -80°C until they were used in the multiplex cytokine assay. The immunoassay procedure was performed using a serial dilution of the 10,000 pg/mL human cytokine standard according to the manufacturer's instructions, and the plate was read at the Luminex 200 System (Millipore).

Murine TNF- α was quantified by bioassay as previously described (11). L929 cells were seeded at a density of 3×10^4 cells per well into a 96-well plate. After 24 h, the medium was replaced by 100 μ L of actinomycin D solution (1 μ g/mL in standard medium) and cells were incubated for 1 h at 37°C . Subsequently, BMM supernatants (100 μ L per well) were added. Dilution series of recombinant murine TNF- α (100–2,500 pg/mL) were run alongside the samples to generate a standard curve. The plates were incubated for an additional 24 h at 37°C . The MTT assay (see Determination of Cell Viability) was used to assess cell viability.

RNA Isolation, Reverse Transcription, and Quantitative RT-PCR

Total RNA was isolated using the RNeasy Plus Mini Kit (Qiagen, #74134), and 200 ng RNA were reverse transcribed using the High-Capacity cDNA Reverse Transcription Kit (Applied Biosystems, #4368813) according to the manufacturer's recommendations. The cDNA was diluted with 80 μ L TE buffer (Applichem, #A0386) before use. The CFX96 TouchTM Real-Time PCR Detection System (Bio-Rad) was used for real-time RT-PCR. For *TNF*, *IL6*, *CXCL8*, *GILZ*, and *ACTB*, one 25 μ L reaction mix contained 2.5 U Taq polymerase, 500 nM sense and antisense primers, 60–100 nM probe, 200 μ M dNTPs, 3–4 mM MgCl₂, 2.5 μ L 10x Taq buffer, 3 μ L Template, and molecular biology grade water (Applichem, #A7398). The reaction conditions were 95°C for 8 min followed by 40 cycles of 15 s at 95°C , 15 s at a reaction dependent temperature varying from 57 to 60°C , and 15 s at 72°C . For *ZFP36* detection, the 5x HOT FIREPol[®] EvaGreen[®] qPCR Mix Plus (Solis Biodyne, #08-25) was used according to the manufacturer's recommendations. Primer and probe sequences as well as specific reaction conditions are given in **Supplementary Table 1**. Standard curves were generated by serial dilution of the PCR product cloned into pGEMTeasy (Promega, #A1360). All samples and standards were analyzed in triplicate.

Western Blotting

Cells were lysed in lysis buffer [50 mM Tris-HCl, 1% (m/v) SDS, 10% (v/v) glycerol, 5% (v/v) 2-mercaptoethanol, 0.004% (m/v) bromphenol blue] supplemented with a protease inhibitor mix (cOmplete; Roche Diagnostics, #04693124001) and stored at -80°C until further use. After sonication, lysates were boiled for 5 min at 95°C . Proteins were separated by SDS-PAGE on 12–15% gels using the Mini-Protean Tetra Cell system (BioRad) and transferred onto Immobilon FL-PVDF membranes (Millipore, #IPFL00010) using the Tetra Blotting Module (BioRad). The membranes were blocked in blocking buffer for near-infrared Western Blotting (Rockland, MB070) for 1 h, incubated with primary antibody dilutions (1:500–1:2,000 in Rockland blocking buffer) for 3 h at room temperature or at 4°C overnight and with IRDye 680 or IRDye 800 conjugated secondary antibodies (1:5,000–1:10,000) for 1.5 h at room temperature. Blots were scanned with an Odyssey Infrared Imaging System (LI-COR Bioscience), and relative protein amounts were determined using either Odyssey or ImageJ software.

Griess Assay

MPI cells were cultured in 96-well plates (4×10^4 cells per well) and treated as indicated. After 20 h, the concentration of nitrite was measured in the supernatants by Griess assay as previously described (20). In brief, 90 μ L 1% sulfanilamide in 5% H₃PO₄ and 90 μ L 0.1% N-(1-naphthyl)ethylenediamine dihydrochloride in H₂O were added to 100 μ L of the cell culture supernatant, followed by absorbance measurement at 550 nm and the reference wavelength 630 nm using a Tecan Sunrise microplate reader. A standard curve of sodium nitrite dissolved in the medium was run alongside the samples. Total cellular protein concentrations used for data normalization

were determined by Pierce BCA protein assay (ThermoFisher Scientific, #23225) according to the manufacturer's instructions.

Phagocytosis Assay

Particle uptake was quantified after incubation of macrophages with 1.75 μm latex beads (Fluoresbrite Carboxylated YG microspheres; Polysciences, #17687) at a 50:1 bead/cell ratio in full medium. Subsequently, cells were washed 5 times with ice-cold PBS to remove remaining fluorospheres and detached from plates using ice-cold TEN buffer (40 mM Tris, 1 mM EDTA, 150 mM NaCl). Cells were resuspended in ice-cold PBS (137 mM NaCl, 2.7 mM KCl, 10.1 mM Na_2HPO_4 , 1.8 mM KH_2PO_4 , pH 7.4) and particle-associated fluorescence was determined using an LSR Fortessa flow cytometer (BD Biosciences). Particle uptake was verified by quenching the fluorescence of particles that were merely attached with trypan blue solution (1 mg/mL in PBS, data not shown).

Salmonella Infection and Determination of Colony Forming Units (CFU)

The *Salmonella enterica* serovar *typhimurium* (*S. typhimurium*) wild-type strain 12023 (resp. 14028s) was a gift from D. Monack (Stanford University). *S. typhimurium* was grown to stationary phase overnight in LB medium (Carl Roth, #X968.1) at 37°C with aeration. 2×10^5 BMMs per well were seeded into a 24-well plate, followed by infection at an MOI of 100:1. 30 min post-infection, gentamycin (100 $\mu\text{g}/\text{mL}$, Sigma-Aldrich, #G1397) was added to kill extracellular bacteria. One hundred and twenty minutes post-infection, fresh medium containing 10 $\mu\text{g}/\text{mL}$ gentamycin was added to the cells. Eight hours post-infection, cells were lysed in 200 μL 1% Triton X-100 (Sigma-Aldrich, #T8787) in water and 1:10 serial dilutions of bacteria suspensions were plated on LB plates. Colony-forming units (CFU) were determined the following day in 1:10 and 1:100 dilutions and the dilution factor was included in CFU calculations.

miRNA Detection

Total RNA for miRNA detection was isolated from AMs using the miRNEasy Kit (Qiagen, #217004). The RNA quality was assessed using the Agilent Bioanalyzer 2100 and RNA 6000 Pico Chips (Agilent Technologies, #5067-1513) as recommended by the supplier. For miRNA expression analysis, the Agilent microarray platform and Human miRNA 8x60K microarrays (Release 16.0, Agilent Technologies, #G4870A) were used according to manufacturer's instructions. In brief, 100 ng total RNA and the miRNA Complete Labeling and Hyb Kit (Agilent Technologies, #5190-0456) were used to generate fluorescently labeled miRNA. The microarrays were loaded and incubated for 20 h at 55°C and 20 rpm. After several washing steps, the microarrays were scanned with the Agilent Microarray Scanner at 3 microns in double path mode. The Total Gene Signal provided by the Agilent Feature Extraction software was used for quantitative data analysis. Normalization between arrays was carried out using quantile normalization. The data have been deposited in NCBI's Gene Expression Omnibus (27) and are accessible through GEO Series accession number GSE123756.

Luciferase Reporter Gene Assay

miRNA overexpression vectors were generated by cloning the miRNA precursor sequences into the BamHI/EcoRI sites of pSG5 (Agilent Technologies, #216201) using the primers given in **Supplementary Table 2** or as previously described (28–30). GILZ 3'UTR-luciferase reporter constructs were generated by coupling the GILZ 3'UTR sequence to a firefly luciferase reporter gene (21). Human GILZ 3'UTR cDNA was amplified using the Expand High fidelity PCR System (Sigma-Aldrich, #11732641001) and the following primers: 5'-GCC TAC TAG TGC AGA GCC ACT AAA CTT G-3' and 5'-AAT AGA GCT CAC TCT CAC AAA ACC CGC TAC-3'. The SacI/SpeI digested PCR product was inserted into the respective cloning site of pMIR-REPORT (Ambion, #AM5795). Plasmid DNA was purified from overnight cultures with the Genopure Plasmid Midi Kit (Roche, #3143414001). Reporter gene assays were performed by transfecting HEK293T cells with the pMIR-REPORT reporter construct, a pre-miRNA vector, and phRG-TK Renilla (Promega, #E6291). HEK 293T cells were seeded at a density of 2×10^4 cells per well into a 96-well-plate, grown for 24 h and transfected using PolyFect (Qiagen, #301105) according to the manufacturer's recommendations. Twenty-four hours after transfection, cells were lysed with 5x Passive Lysis Buffer (Promega, #E1941). Luciferase activity was determined after the addition of firefly luciferase substrate (470 μM D-luciferin, 530 μM ATP, 270 μM coenzyme A, 33 mM DTT, 20 mM Tricine, 2.67 mM MgSO_4 , and 0.1 mM EDTA, pH 7.8) or renilla substrate (0.1 M NaCl, 25 mM Tris-HCl, pH 7.5, 1 mM CaCl_2 , 1 μM coelenterazine) by luminescence measurement using a Glomax Discover multiplate reader (Promega). Firefly luciferase activity was normalized to renilla luciferase activity to correct for variations in transfection efficiency, and relative luminescence was calculated relative to PSG5 control transfected cells. Data were also normalized to the impact of each miRNA on the luciferase mRNA without GILZ 3'UTR to adjust for GILZ 3'UTR-specific effects.

miRNA Mimic Transfection

miRNA mimics (hsa-miR-34b*, -222, -320d, -484, and scrambled control; MISSION miRNA, Sigma-Aldrich, #HMI0510, #HMI0400, #HMI0475, #HMI0593, #HMC0002) were reverse transfected into HEK293T cells (2.5×10^5 cells in a 6-well plate) using the Lipofectamine RNAiMAX transfection reagent (ThermoFisher Scientific, #13778075) as recommended by the supplier. Mimics were used at a final concentration of 50 nM. To examine potential synergistic effects, a combination of all four miRNA mimics (12.5 nM each) was compared with scrambled controls (50 nM) or miR-34b* mimic (12.5 nM) only. The latter was co-transfected with scrambled control mimics (37.5 nM) to ensure comparable transfection conditions.

NF- κ B/AP-1 Reporter Gene Assay

HEK-Blue cells (HEK-Blue BlueTM Null1, Invivogen, #hkb-null1) expressing secreted embryonic alkaline phosphatase (SEAP) under the control of the IFN- β minimal promoter fused to five NF- κ B and AP-1 binding sites were used to determine NF- κ B/AP-1 activity. Cells were seeded into 96-well plates (5×10^5 cells/well) and treated immediately as indicated. After 24 h,

supernatants were collected, and SEAP activity was determined using the QuantiBlue reagent (Invivogen, #REP-QB2) according to the supplier's instructions. For miRNA mimic experiments, HEK-Blue cells (2×10^5 cells/well in 96-well plates) were reverse transfected with single miRNA mimics (50 nM), scrambled control (50 nM), or a mix of miR-34b*, -222, -320d, and -484 mimics (12.5 nM, each) using the Lipofectamine RNAiMAX transfection reagent as recommended by the supplier (see miRNA Mimic Transfection for details). Twenty-four hours later, cells were treated as indicated and incubated for another 24 h. Subsequently, SEAP activity was determined as described above.

TAT-Fusion Proteins

The cell-permeable trans-activator of transcription peptide (TAT)-GILZ fusion protein and the respective control protein (TAT-Co) were generated and purified as previously (13, 31). In brief, TAT and TAT-GILZ sequences were inserted into the pGEX-4T2 plasmid (GE Healthcare, #28-9545-50) to produce an in-frame fusion protein. The GST fusion protein expression was induced in *E. coli* BL21 (GE Healthcare, #27-1542-01) with 0.1 mM isopropyl β -D-thiogalactopyranoside (Sigma-Aldrich, #I5502). After lysis by sonication, proteins were purified with glutathione-sepharose 4B beads (GE Healthcare, #17-0756-01) according to the manufacturer's instructions. Protein purity was evaluated by SDS-PAGE and Coomassie blue staining.

Statistics

All experiments were performed at least three times, and at least two biological replicates were analyzed for all *in vitro* experiments unless stated otherwise. Data distribution was determined by the Shapiro-Wilk test. For normally distributed data, means of two groups were compared with non-paired two-tailed Student's *t*-test. For data that were not normally distributed, means of two groups were compared using the Mann-Whitney test. Means of more than two groups were compared by one-way ANOVA with Bonferroni's *post hoc* test (normal distribution) or Kruskal-Wallis ANOVA followed by Mann-Whitney test (no normal distribution). Statistical significance was set at $p < 0.05$, $p < 0.01$, or $p < 0.001$. Data analysis was performed using Origin software (OriginPro 8.6G; OriginLab).

RESULTS

Downregulation of GILZ by TLR Agonists

Because most studies on GILZ focused on its pharmacological induction, there are only limited data on the regulation of endogenous GILZ during the immune response. To investigate macrophage responses toward TLR1/2 and TLR3 ligands, we treated human AMs, human monocyte-derived macrophages, as well as non-differentiated and PMA-differentiated U937 and THP-1 cells with Pam₃CSK₄ and Poly(I:C). Out of these human macrophages and macrophage-like cells, AMs were the only cell type that showed a robust activation by Poly(I:C) regarding cytokine production (Figure 1A, Supplementary Figure 1). Thus, we used these cells to further examine GILZ expression. As reported previously (21), GILZ mRNA levels were highly

reduced upon TLR1/2 and TLR4, but not TLR3 stimulation (Figure 1B). In contrast, GILZ protein levels decreased both after MyD88-dependent stimulation by Pam₃CSK₄ and TRIF-dependent activation by Poly(I:C) (Figures 1C–E), implicating a dual regulation of GILZ.

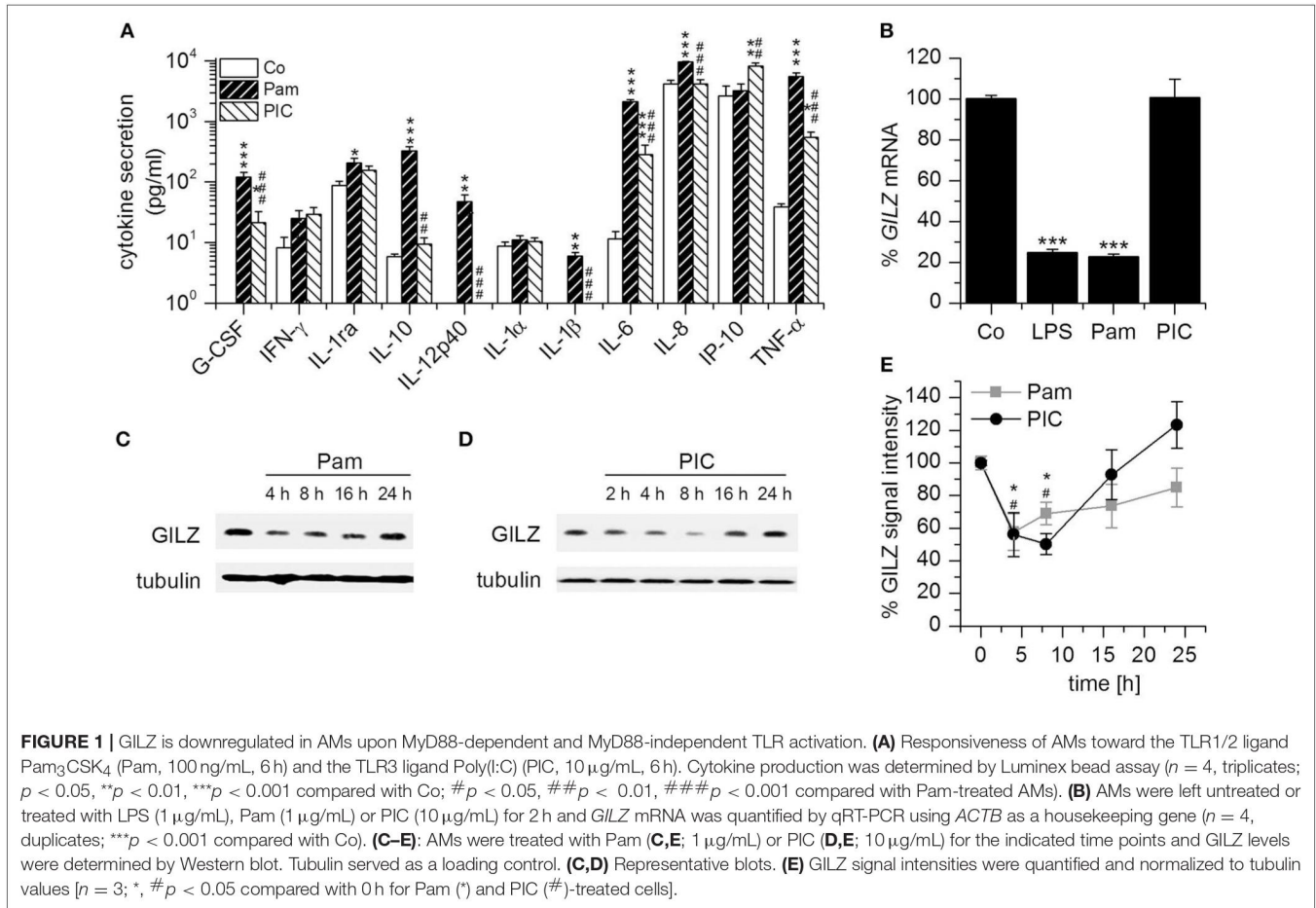
During the late stages of sepsis, macrophages adjust to the prolonged stimulation by LPS or other TLR ligands and enter a hyporesponsive state termed endotoxin or LPS tolerance. LPS-tolerant macrophages are characterized by reduced secretion of pro-inflammatory cytokines and upregulation of anti-inflammatory genes. We previously showed that GILZ represents a key mediator of LPS tolerance (11). In contrast, pretreatment of AMs with low-dose Poly(I:C) for 24 h resulted in reduced GILZ levels (Figures 2A,B) and an enhanced LPS- or Pam₃CSK₄-induced pro-inflammatory response, as shown by qPCR analysis of *TNF*, *IL6*, and *CXCL8* expression (Figures 2C,D). This observation is in line with a recent report showing that macrophages generate a type of innate immune memory by activating the TLR3 pathway, thereby enhancing the immune response to a subsequent PAMP exposure (32). Our data suggest that this might, at least in part, be due to GILZ downregulation.

Functional Implications of Gilz Downregulation

We then sought to characterize the functional implications of GILZ downregulation. To examine whether lack of GILZ modulates macrophage activation after Pam₃CSK₄ and Poly(I:C), we treated murine WT and GILZ KO macrophages with increasing dosages of both stimuli, and TNF- α secretion was quantified. Compared with their WT counterparts, GILZ KO cells released higher levels of TNF- α after stimulation with either TLR ligand (Figures 3A,B). Loss of GILZ has been shown to enhance LPS-induced ERK-signaling in macrophages and thereby promote inflammatory actions, including TNF- α production (11). Therefore, we investigated Pam₃CSK₄- and Poly(I:C)-mediated ERK phosphorylation. We detected ERK activation after treatment with both TLR ligands, and GILZ KO BMMs showed higher levels of pERK after 15 min for Pam₃CSK₄ and after 30 min for Poly(I:C) when compared with equally treated WT cells (Figures 3C–F).

Since ERK activity might play a role in increased cytokine expression concomitant with GILZ KO, we blocked ERK activation with the inhibitor U0126 and quantified TNF- α after Pam₃CSK₄ or Poly(I:C) treatment. Inhibition of ERK signaling abolished the increased responsiveness of GILZ KO cells toward both ligands, indicating that loss of GILZ enhances the inflammatory response by modulating ERK activity (Figures 3G,H).

Apart from the production of inflammatory cytokines, macrophage-dependent host defense involves the release of nitric oxide (NO) and phagocytosis of the invading pathogen. Thus, we examined the influence of GILZ expression on these parameters. NO production was elevated in GILZ KO cells when compared with equally treated WT cells upon TLR4 activation by LPS alone or in combination with IFN- γ (Figure 4A). TLR2 ligands, i.e., Pam₃CSK₄ or lipoteichoic acid (LTA), induced NO only when



combined with IFN- γ . As seen for LPS, the response was higher in GILZ KO macrophages (**Figure 4B**).

To assess their phagocytic capacity, WT and GILZ KO macrophages were incubated with fluorescent latex particles. The total percentage of cells with particle-associated fluorescence and the percentage of cells that engulfed 0, 1, 2, or more than 2 particles was determined by flow cytometry after 15 and 30 min (**Figures 4C–E**). GILZ KO macrophages phagocytosed more particles than WT cells, which was especially evident in the fraction that took up more than two particles.

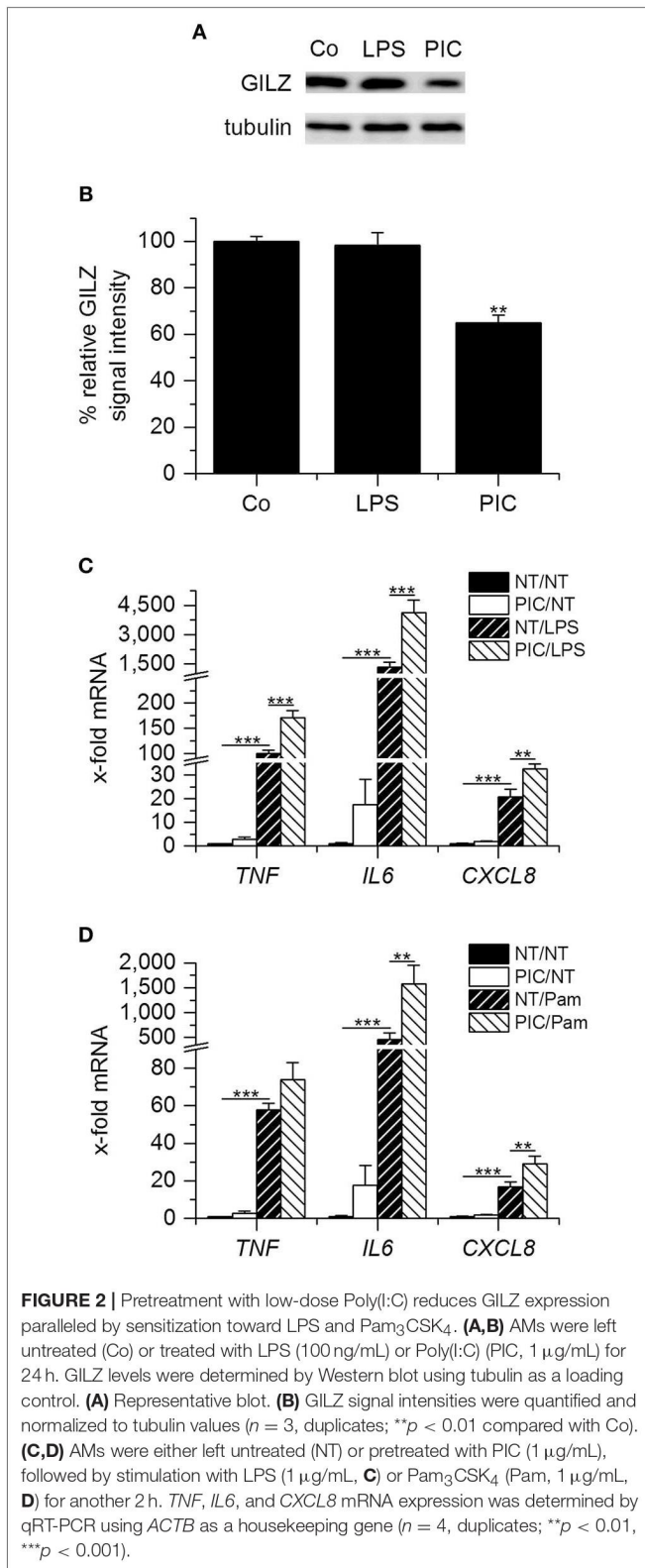
To determine the influence of GILZ expression on the phagocytic activity of differentially polarized macrophages, WT, and GILZ KO macrophages were either left untreated or pretreated with LPS/IFN- γ , IL-4, or dexamethasone for 20 h. Subsequently, latex beads were added, and uptake was quantified by flow cytometry. Phagocytosis was enhanced by LPS/IFN- γ and impaired by dexamethasone treatment. Regardless of the treatment scheme, GILZ KO macrophages had a higher uptake efficiency than equally treated WT cells (**Figures 4F,G** and **Supplementary Figure 2**).

Next, we investigated whether the loss of GILZ modulated the bactericidal capacity. WT and GILZ KO BMMs were exposed to *Salmonella typhimurium*, and extracellular bacteria were removed after 30 min. After 8 h the number of viable bacteria

within the cells was determined. GILZ KO macrophages were more efficient regarding the killing of intracellular bacteria, as indicated by lower CFU counts when compared with WT macrophages (**Figure 4H**).

Mechanisms of GILZ Downregulation

We then aimed to address the mechanisms underlying GILZ downregulation in activated macrophages. Both the MyD88- and TRIF-dependent pathways can lead to the activation of the pro-inflammatory transcription factor NF- κ B. Thus, we blocked NF- κ B signaling in AMs by pretreatment with the inhibitors BAY-11-7082 or BAY-11-7085, followed by treatment with the TLR ligands LPS, Pam₃CSK₄, and Poly(I:C), and found that GILZ downregulation was abrogated in inhibitor-treated cells (**Figures 5A,B**). The efficiency of the inhibitor treatment was verified by the impairment of LPS-induced *TNF* production (**Supplementary Figure 3**). As seen previously, LPS treatment also resulted in downregulation of *GILZ* on the mRNA level. The effect was reversible by inhibition of NF- κ B (**Figure 5C**), suggesting an involvement of an NF- κ B-inducible factor in *GILZ* mRNA regulation. We previously reported that downregulation of GILZ upon MyD88-dependent TLR activation required the presence of the RNA-binding protein tristetrin (TTP, encoded by *ZFP36*) (11, 21). Therefore, we speculated that TTP



might be, at least in part, regulated via NF- κ B. We found indeed that *ZFP36* mRNA was induced upon LPS treatment in an NF- κ B-dependent fashion (Figure 5D).

In line with the finding that Poly(I:C) was unable to reduce *GILZ* mRNA levels, we observed no induction of TTP after Poly(I:C) treatment (Figure 5E), suggesting an entirely different mode of action.

miRNAs are endogenous small noncoding RNAs that can facilitate translational repression (33). A bioinformatics approach implicated more than 250 miRNAs as potential GILZ regulators. Interestingly, there were more predictions for GILZ than for well-characterized miRNA targets, such as *CXCL8*, *IL6*, and *TNF* (34) (Figure 5F). To evaluate whether miRNAs are involved in Poly(I:C)-induced GILZ repression, AMs were either left untreated or treated with Poly(I:C), aurintricarboxylic acid (ATA), an inhibitor of ribonuclease activities which also affects miRNA processing (35), or a combination of both for 8 h, followed by quantification of GILZ protein levels. We observed that ATA treatment was able to prevent Poly(I:C)-mediated GILZ downregulation, suggesting that miRNAs indeed affect GILZ expression (Figure 5G).

Microarray analysis revealed that the expression of several potentially GILZ-targeting miRNAs was increased in Poly(I:C) treated AMs, although these effects were in some cases rather donor-dependent (Figure 6A). We tested the ability of 11 of these miRNAs predicted to target GILZ and expressed by Poly(I:C)-treated AMs to regulate GILZ by luciferase reporter gene assays. Within this small set, four miRNAs decreased the activity of the luciferase reporter encoded by a gene fused to the *GILZ* 3'UTR (Figure 6B). To determine the influence of these miRNAs on endogenous GILZ expression, we transfected HEK293T cells with mimics of the four candidate miRNAs, i.e., miR-34b*, -222, -320d, and -484, and observed that all mimics were able to reduce GILZ expression, although to a different extent (Figures 6C,D). To examine whether these miRNAs exert synergistic effects, HEK293T cells were transfected with the most potent mimic, i.e., miR-34b*, or a mix of all four miRNA mimics. As shown in Figures 6E,F, repression of GILZ expression was more efficient when using the miRNA mimic mix, suggesting that GILZ downregulation upon TLR3 activation is a consequence of the synergistic actions of multiple miRNAs.

We then wondered whether reduced GILZ expression upon miRNA mimic treatment might affect downstream effectors. To this end, HEK-Blue cells expressing a reporter gene under the control of the transcription factors NF- κ B and AP-1 were used. Since HEK-Blue cells express endogenous TLR3, reporter gene activity was inducible by Poly(I:C). This effect was profoundly impaired by co-treatment with a cell-permeable GILZ peptide, indicating that GILZ can inhibit NF- κ B/AP-1 activation in this system (Figure 6G). In line with these findings, Poly(I:C)-induced NF- κ B/AP-1 activity was enhanced in HEK Blue cells transfected with the miR-34b* mimic or a mix of all four mimics, i.e., under conditions that resulted in the highest degree of GILZ repression (Figure 6H).

DISCUSSION

To date, only a few studies have addressed the regulation of endogenous GILZ during the immune response in the

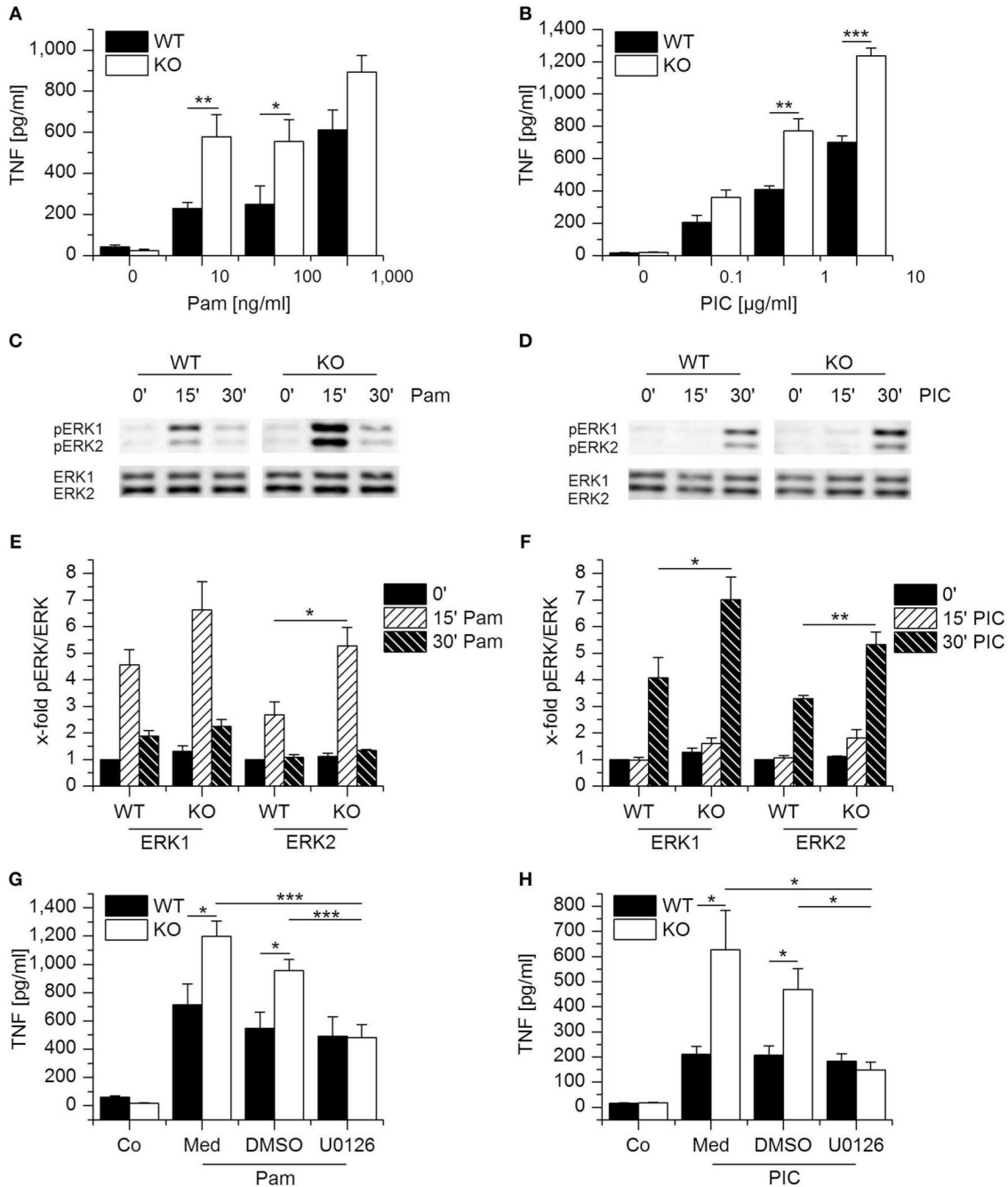


FIGURE 3 | Loss of GILZ increases the responsiveness of macrophages toward Pam₃CSK₄ and Poly(I:C). **(A,B)** Wildtype- (WT) and GILZ Knockout-(KO) BMMs were treated with Pam₃CSK₄ (4 h, **A**) or Poly(I:C) (6 h, **B**) at the indicated concentrations. TNF secretion was quantified by bioassay ($n = 4$, triplicates). **(C–F)** WT and GILZ KO BMMs were treated with Pam₃CSK₄ (100 ng/mL, **C** and **E**) or Poly(I:C) (10 µg/mL, **D,F**) for the indicated periods of time. ERK activation was determined by Western blot. **(C,D)** Representative blots. **(E,F)** pERK signal intensities were quantified and normalized to total ERK signals. Values for untreated WT cells (0') were set as 1 ($n \geq 3$). **(G, H)**: WT and GILZ KO BMMs were pretreated with medium only (Med), the solvent control DMSO (0.1%), or U0126 (10 µM) for 2 h, followed by activation with Pam₃CSK₄ (100 ng/mL, 4 h; **G**) or Poly(I:C) (10 µg/mL, 6 h). TNF production was assessed by bioassay (Co: untreated cells; $n = 4$, triplicates). * $p < 0.05$, ** $p < 0.01$, *** $p < 0.001$.

absence of glucocorticoids. In both epithelial (36) and endothelial cells (37), inflammatory cytokines have been demonstrated to attenuate GILZ levels. GILZ expression has also been shown

to be decreased in activated macrophages from patients with Crohn's disease or tuberculosis (6), and nasal explants from patients suffering from chronic rhinosinusitis lack GILZ (38).

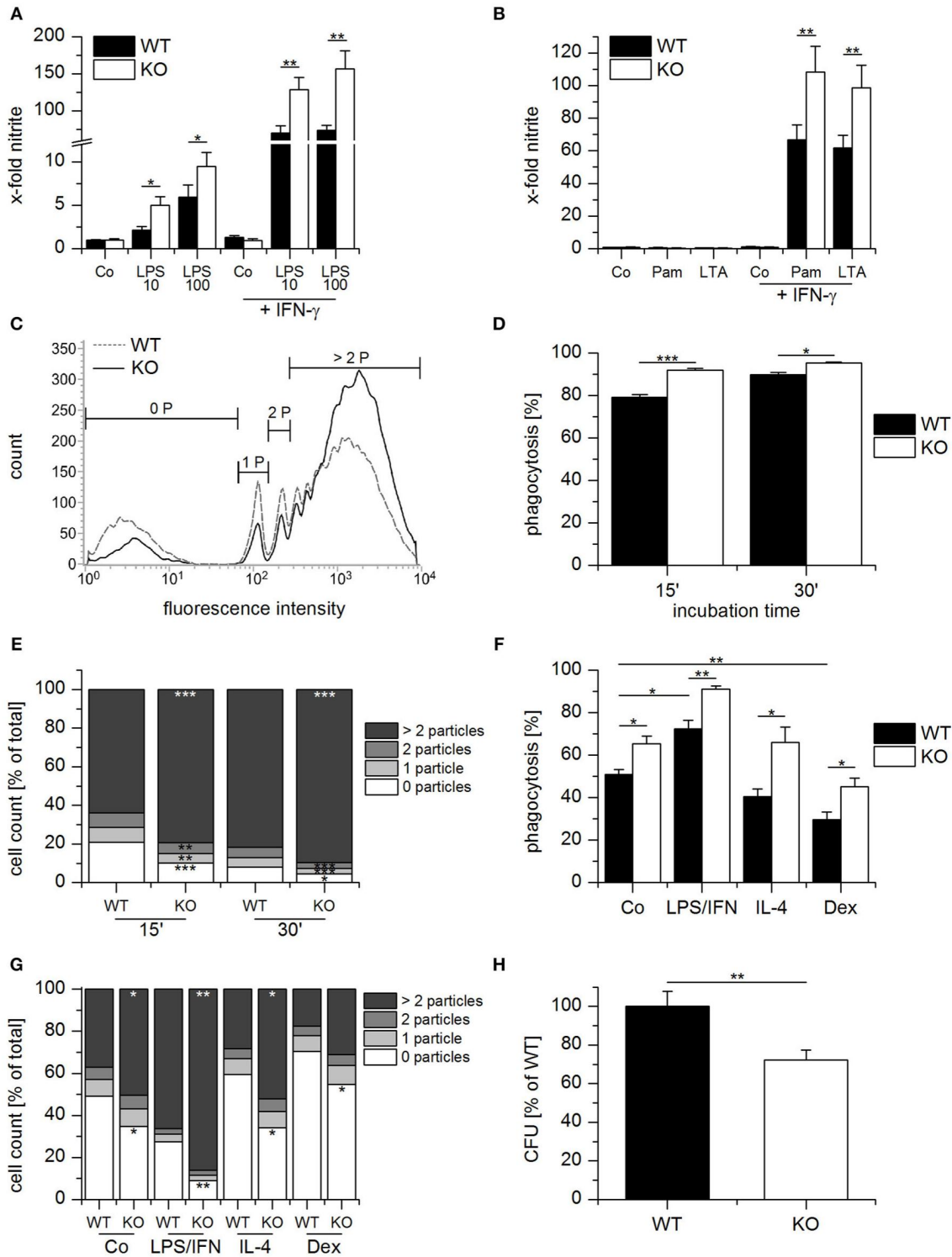


FIGURE 4 | Anti-bacterial host defense is enhanced in GILZ knockout macrophages. **(A,B)** Wildtype- (WT) and GILZ Knockout- (KO) MPI macrophages were treated with LPS (10 or 100 ng/mL) Pam₃CSK₄ (Pam, 1 μg/mL, **B**), or lipoteichoic acid (LTA, 5 μg/mL, **B**) with or without co-stimulation by IFN-γ (20 ng/mL) for 20 h. NO-production was measured by Griess assay. Data were normalized to total protein concentration and expressed as x-fold of untreated cells (n = 4, triplicates). **(C-E)** Phagocytic activity of WT and GILZ KO MPI cells. MPI cells were incubated with fluorescent latex particles (diameter 1.75 μm, 50 particles per cell) for 15 or 30 min and particle-associated fluorescence was quantified by flow cytometry (15 min: n = 2, 30 min: n = 6, triplicates). **(C)** Representative histogram for 15 min. 0 P, cells without particles; 1 P, 1 particle; 2 P, 2 particles; > 2 P, more than 2 particles. **(G)** Phagocytic activity as a total percentage of cells with particles. **(E)** The *(Continued)*

FIGURE 4 | percentage of cells that engulfed 0, 1, 2 or more than 2 particles was quantified as shown in (C), (F,G) WT and GILZ KO BMMs were left untreated (Co) or treated with LPS (1 μ g/mL) and INF- γ (IFN, 20 ng/mL), IL-4 (20 ng/mL) or dexamethasone (Dex, 1 μ M) for 20 h, followed by incubation with fluorescent latex particles (diameter 1.75 μ m, 50 particles per cell) for 1 h. Particle uptake was quantified by flow cytometry. (F) Total percentage of cells with particle-associated fluorescence. (D) Percentage of cells with 0, 1, 2 or more than 2 particles. (H) Relative number of viable bacteria in *Salmonella typhimurium*-infected WT and GILZ KO BMMs. Extracellular bacteria were removed after 30 min, and the remaining bacteria were killed using gentamicin. Eight hours following infection, monolayers were lysed, and the number of intracellular bacteria was determined as Colony Forming Units (CFU) ($n = 8$, triplicates). * $p < 0.05$, ** $p < 0.01$, *** $p < 0.001$ as indicated or compared with equally treated WT cells (E,G).

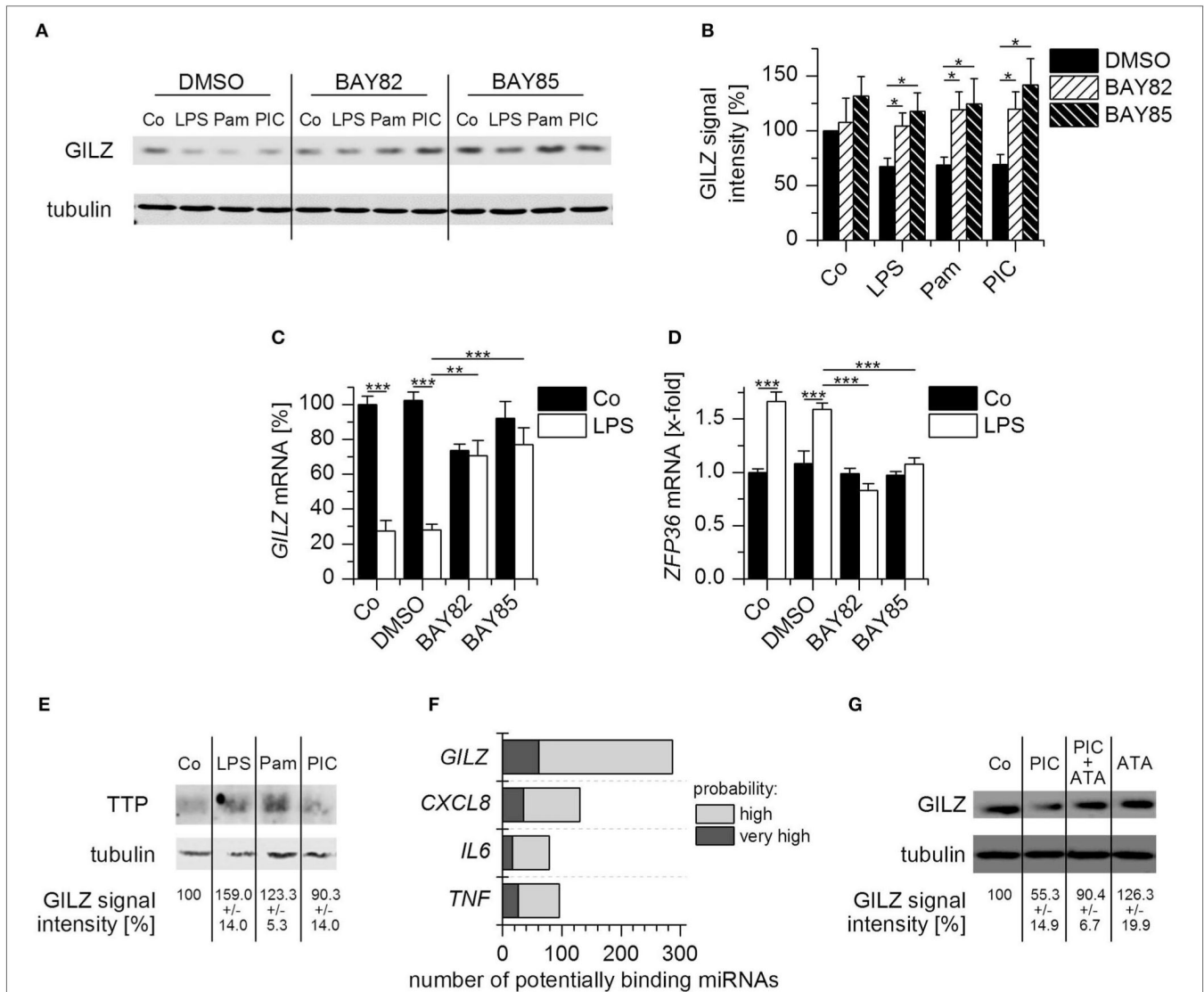


FIGURE 5 | Mechanisms of GILZ downregulation upon TLR activation. (A,B) AMs pretreated with BAY-11-7082 (BAY82, 5 μ M), BAY-11-7085 (BAY85, 5 μ M), or the solvent control DMSO (0.1%) for 1 h, followed by treatment with LPS (100 ng/mL), Pam₃CSK₄ (Pam, 1 μ g/mL), Poly(I:C) (PIC, 10 μ g/mL), or medium (Co) for 4 h. GILZ expression was determined by Western blot. Tubulin served as a loading control. (A) Representative blot. (B) GILZ signal intensities were quantified and normalized to tubulin values ($n = 7$). Values for unstimulated DMSO controls were set as 100%. (C,D) After preincubation with BAY-11-7082 or BAY-11-7085 (5 μ M, 1 h), solvent (0.1% DMSO) or medium only (Co), AMs were treated with LPS (100 ng/mL) for 2 h. GILZ and ZFP36 mRNA expression was determined by qRT-PCR using ACTB as a housekeeping gene ($n = 3$, duplicates). (E) AMs were either left untreated (Co) or treated with LPS (100 ng/mL), Pam₃CSK₄ (Pam, 1 μ g/mL), or Poly(I:C) (PIC, 10 μ g/mL) for 4 h. TTP levels were determined by Western blot using tubulin as a loading control. GILZ signal intensities were normalized to tubulin and are shown as a percentage of untreated cells ($n = 2$, triplicates). (F) The number of miRNAs predicted to target GILZ, CXCL8, IL6, and TNF was assessed via the microRNA Data Integration Portal (mirDIP, accession date 02/02/2018). (G) AMs were either left untreated (Co) or treated with Poly(I:C) (PIC, 10 μ g/mL), aurintricarboxylic acid (ATA, 25 μ M), or a combination of both for 8 h. GILZ expression was quantified by Western blot. Signal intensities were normalized to tubulin and expressed as a percentage of untreated cells ($n = 3$). * $p < 0.05$, ** $p < 0.01$, *** $p < 0.001$.

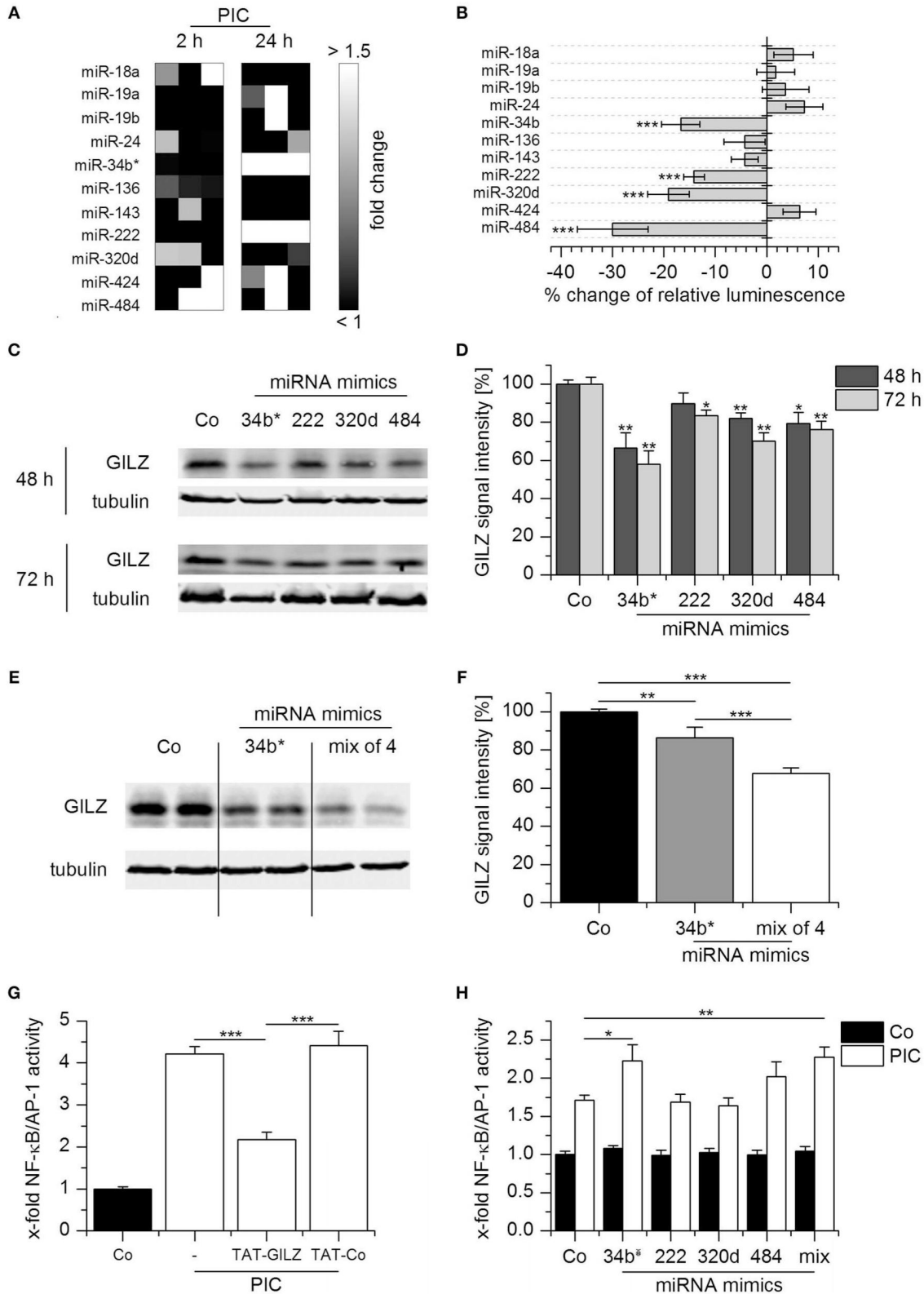


FIGURE 6 | miRNA-mediated GILZ downregulation. **(A)** miRNA induction in Poly(I:C)-treated AMs (10 μg/mL for 2 h or 1 μg/mL for 24 h) was assessed by microarray analysis. Data are presented as fold change compared with untreated cells from the same donor. Individual changes per donor (n = 3) are shown. **(B)** The interaction (Continued)

FIGURE 6 | of individual miRNAs with GILZ was determined by miRNA overexpression in HEK293 cells co-transfected with a luciferase reporter construct containing the GILZ 3'UTR. Luminescence was measured 24 h after transfection and is shown as percent change compared with control vector-transfected cells lacking miRNA overexpression ($n = 3-8$, quintuplicates or sextuplicates). Significances were calculated in comparison with control vector-transfected cells. **(C,D)** HEK293T cells were transfected with miRNA mimics or scrambled controls (50 nM). GILZ expression was determined by Western blot at the indicated time points. **(C)** Representative blots. **(D)** GILZ signal intensities were quantified and normalized to tubulin values ($n = 3$, duplicates; Co: cells transfected with scrambled controls, set as 100%). **(E,F)** HEK293T cells were transfected with scrambled controls (50 nM, Co), miR-34b* (12.5 nM miR-34b* mimic + 37.5 nM scrambled controls), or a mix of miR-34b*, -222, -320d, and -484 mimics (12.5 nM each). GILZ expression was quantified after 48 h by Western blot. **(E)** Representative blot. **(F)** GILZ signal intensities were normalized to tubulin values ($n = 3$, duplicates or triplicates). Co values were set as 100%. **(G)** NF- κ B/AP-1 activity was measured in untreated HEK-Blue reporter cells (Co) or after activation with PIC (1 μ g/mL, 24 h) in the presence or absence of a cell-permeable GILZ peptide (TAT-GILZ, 2 μ g/mL) or the respective control peptide (TAT-Co, 2 μ g/mL; $n = 3$, triplicates). **(H)** HEK-Blue reporter cells were transfected with scrambled control (Co) or the indicated miRNA mimic. Twenty hours after transfection, cells were either left untreated or treated with PIC (1 μ g/mL, 24 h), and NF- κ B/AP-1 activity was determined ($n = 3$, triplicates). * $p < 0.05$, ** $p < 0.01$, *** $p < 0.001$ vs. Co or as indicated.

Furthermore, reduced *GILZ* mRNA levels were observed in liver tissue from patients with alcoholic hepatitis (17).

Besides the high abundance of GILZ in endothelial cells (21, 37), we previously demonstrated high GILZ levels in primary human monocyte-derived and pulmonary macrophages (21). GILZ expression was diminished in human alveolar macrophages as well as *in vivo* in mouse lungs upon TLR4 activation.

Further investigations indicated that *GILZ* mRNA was destabilized upon MyD88-mediated TLR activation, since LPS and Pam₃CSK₄, but not Poly(I:C), the activator of MyD88-independent TLR3, reduced *GILZ* mRNA expression. Downregulation of *GILZ* on the mRNA level required the presence of both the RNA-binding protein TTP and the *GILZ* 3'-untranslated region (21).

Our results presented within this study suggest that NF- κ B activation is also required, which might at least in part be due to NF- κ B-mediated TTP induction. Indeed, NF- κ B has been previously shown to regulate TTP on the transcriptional level in LPS-stimulated RAW264.7 macrophages (39). However, the composition of the entire RNA-protein complex rather than the binding of TTP alone might dictate the fate of *GILZ* mRNA. The regulatory networks driving mRNA decay are considered to consist of multiple RNA-binding proteins, whose binding activity may be further modulated by miRNAs (40, 41). Thus, we cannot rule out the possibility that TTP-mediated *GILZ* mRNA destabilization requires accessory factors that may also be regulated by NF- κ B.

Although Poly(I:C) did not decrease *GILZ* mRNA levels in macrophages, GILZ protein expression was reduced. Furthermore, Poly(I:C)-induced GILZ downregulation was dependent on both NF- κ B activation and the presence of miRNAs. Our investigations revealed that multiple miRNAs act as GILZ regulators, suggesting that GILZ downregulation upon TLR3 activation is instead a consequence of synergistic miRNA actions. Promoter analysis using the miRGen v3.0 database (42) revealed that only miR-222 might be a direct target of NF- κ B, whereas the promoters of miR-34b, miR-320d-1, and miR-484 lack NF- κ B binding sites. NF- κ B activation might influence miRNA expression indirectly, e.g., by modulation of miRNA processing via induction of the RNase Dicer (43). Finally, it is also possible that additional miRNAs are induced that were not identified by our approach.

Investigations on the functional significance of GILZ downregulation revealed an enhanced sensitivity toward LPS in

human macrophages after siRNA-mediated GILZ knockdown, as indicated by increased cytokine expression and NF- κ B activity (21). Within a follow-up study (11) we observed an increased response toward LPS in GILZ KO BMMs, such as enhanced NF- κ B and AP-1 activity, suggesting repression of GILZ expression as a regulatory mechanism that amplifies macrophage activation. These findings are in line with our observation that treatment with a cell-permeable GILZ fusion protein can prevent PIC-induced NF- κ B/AP-1-dependent activation in HEK-Blue cells.

In addition to its direct interaction with pro-inflammatory transcription factors, GILZ has also been reported to attenuate MAPK signaling in general and ERK signaling in particular (9–11). In the present study, we showed that the absence of GILZ increased both TLR1/2 and TLR3 activation, as indicated by augmented ERK activity, and, as a consequence, increased production of TNF- α . These findings suggest a role for GILZ repression in innate immune memory/trained immunity. Both terms describe an adaptation of innate immune cell functions due to previous pathogen exposure, resulting in cross-protection between infections with different pathogens (32, 44).

The increased production of cytokines, such as TNF- α , promotes an acute inflammatory response that helps to clear invading organisms but also contributes to tissue damage. Another factor that plays a similarly ambivalent role in response to infections is nitric oxide (NO), a molecule with antimicrobial and proinflammatory functions. NO is generated from arginine in a reaction catalyzed by the enzyme nitric oxide synthase (NOS). Due to its inducible expression the principal isoform expressed in macrophages, i.e., NOS2, is also known as iNOS. iNOS expression can be elevated by activating cytokines, such as IFN- γ , and repressed by anti-inflammatory mediators, e.g., IL-4 or IL-10. Various PAMPs of bacterial, viral, or fungal origin have also been reported to enhance iNOS expression and function, with LPS as the most prominent example. LPS usually synergizes with IFN- γ to activate both NF- κ B and STAT1, thereby inducing high levels of iNOS (45). Our data show that LPS- as well as LPS/IFN- γ -induced NO production can be increased by GILZ depletion. This finding is in line with the observation that LPS-induced NF- κ B activity is increased in GILZ KO macrophages (11). In addition, we showed that treatment with TLR2 ligands, i.e., Pam₃CSK₄ and LTA, results in similar effects when co-administered with IFN- γ . TLR2 ligands did not, however, induce NO on their own, which might be attributed to the lack

of TRIF-dependent IFN- β production and subsequent STAT1 activation upon TLR2 activation (46).

The ability to engulf particles, including pathogens and apoptotic cells, is a significant characteristic of macrophages. The phagocytic capacity is not necessarily associated with a specific macrophage phenotype, but rather constitutes a general attribute of these cells (24, 47). In this study, we show that lack of GILZ promotes phagocytosis in untreated as well as differentially polarized macrophages, including GC-treated cells. GCs have only recently been shown to impair phagocytosis by inhibiting the expression of genes that are required for phagosome formation (48). Whether or not these genes, such as *CD14*, *CD48*, and *MARCKS* are regulated in a GILZ-dependent manner presently remains elusive.

Although GILZ knockout macrophages showed a higher phagocytic activity, the number of viable bacteria in *S. typhimurium*-infected cells was reduced. This finding suggests that GILZ depletion enhances the bactericidal activity of macrophages, which is also supported by the observation that NO production is increased in GILZ knockout macrophages.

In conclusion, our data show that GILZ expression can be downregulated on different levels depending on the nature of the stimulus. In return, GILZ downregulation can promote essential macrophage functions, such as cytokine production, phagocytosis, and bactericidal activity. Thus, GILZ repression can help to clear pathogens, but might also be detrimental to the host by promoting excessive inflammatory disorders. Therefore, GILZ might represent a potential target for therapeutic

interventions, both in order to restrict or to stimulate innate immune responses depending on the nature of the disease.

AUTHOR CONTRIBUTIONS

JH, BD, RL, NH, SF, MM, PL, and CB designed, performed, and analyzed the experiments. JH wrote the paper. All authors contributed to drafting the manuscript. SB, CR, FG, EM, and HH provided materials and discussed the data. AK initiated the study and participated in data interpretation and manuscript preparation. All authors read and approved the final manuscript.

FUNDING

This work was funded, in part, by the Deutsche Forschungsgemeinschaft, Bonn, Germany (KI702).

ACKNOWLEDGMENTS

The authors thank Theresa Stadter, Katharina Sauer, Anke Guckeisen, and Sarah Bender for support in generating murine macrophage data, and Eva Dilly for support in animal maintenance.

SUPPLEMENTARY MATERIAL

The Supplementary Material for this article can be found online at: <https://www.frontiersin.org/articles/10.3389/fimmu.2018.03111/full#supplementary-material>

REFERENCES

1. Leifer CA, Medvedev AE. Molecular mechanisms of regulation of Toll-like receptor signaling. *J Leukocyte Biol.* (2016) 100:927–41. doi: 10.1189/jlb.2MR0316-117RR
2. Brubaker SW, Bonham KS, Zanoni I, Kagan JC. Innate immune pattern recognition: a cell biological perspective. *Ann Rev Immunol.* (2015) 33:257–90. doi: 10.1146/annurev-immunol-032414-112240
3. Zhou D, Huang C, Lin Z, Zhan S, Kong L, Fang C, et al. Macrophage polarization and function with emphasis on the evolving roles of coordinated regulation of cellular signaling pathways. *Cell Signal.* (2014) 26:192–7. doi: 10.1016/j.celsig.2013.11.004
4. Mosser DM, Edwards JP. Exploring the full spectrum of macrophage activation. *Nat Rev Immunol.* (2008) 8:958–69. doi: 10.1038/nri2448
5. Ayroldi E, Migliorati G, Bruscoli S, Marchetti C, Zollo O, Cannarile L, et al. Modulation of T-cell activation by the glucocorticoid-induced leucine zipper factor via inhibition of nuclear factor kappaB. *Blood* (2001) 98:743–53. doi: 10.1182/blood.V98.3.743
6. Berrebi D, Bruscoli S, Cohen N, Foussat A, Migliorati G, Bouchet-Delbos L, et al. Synthesis of glucocorticoid-induced leucine zipper (GILZ) by macrophages: an anti-inflammatory and immunosuppressive mechanism shared by glucocorticoids and IL-10. *Blood* (2003) 101:729–38. doi: 10.1182/blood-2002-02-0538
7. Di Marco B, Massetti M, Bruscoli S, Macchiarulo A, Di Virgilio R, Velardi E, et al. Glucocorticoid-induced leucine zipper (GILZ)/NF-kappaB interaction: role of GILZ homo-dimerization and C-terminal domain. *Nucleic Acids Res.* (2007) 35:517–28. doi: 10.1093/nar/gkl1080
8. Mittelstadt PR, Ashwell JD. Inhibition of AP-1 by the glucocorticoid-inducible protein GILZ. *J Biol Chem.* (2001) 276:29603–10. doi: 10.1074/jbc.M101522200
9. Ayroldi E, Zollo O, Macchiarulo A, Di Marco B, Marchetti C, Riccardi C. Glucocorticoid-induced leucine zipper inhibits the Raf-extracellular signal-regulated kinase pathway by binding to Raf-1. *Mol Cell Biol.* (2002) 22:7929–41. doi: 10.1128/MCB.22.22.7929-7941.2002
10. Ayroldi E, Zollo O, Bastianelli A, Marchetti C, Agostini M, Di Virgilio R, et al. GILZ mediates the antiproliferative activity of glucocorticoids by negative regulation of Ras signaling. *J Clin Investig.* (2007) 117:1605–15. doi: 10.1172/JCI30724
11. Hoppstädter J, Kessler SM, Bruscoli S, Huwer H, Riccardi C, Kiemer AK. Glucocorticoid-induced leucine zipper: a critical factor in macrophage endotoxin tolerance. *J Immunol.* (2015) 194:6057–67. doi: 10.4049/jimmunol.1403207
12. D'Adamio F, Zollo O, Moraca R, Ayroldi E, Bruscoli S, Bartoli A, et al. A new dexamethasone-induced gene of the leucine zipper family protects T lymphocytes from TCR/CD3-activated cell death. *Immunity* (1997) 7:803–12.
13. Delfino DV, Agostini M, Spinicelli S, Vito P, Riccardi C. Decrease of Bcl-xL and augmentation of thymocyte apoptosis in GILZ overexpressing transgenic mice. *Blood* (2004) 104:4134–41. doi: 10.1182/blood-2004-03-0920
14. Delfino DV, Agostini M, Spinicelli S, Vacca C, Riccardi C. Inhibited cell death, NF-kappaB activity and increased IL-10 in TCR-triggered thymocytes of transgenic mice overexpressing the glucocorticoid-induced protein GILZ. *Int Immunopharmacol.* (2006) 6:1126–34. doi: 10.1016/j.intimp.2006.02.001
15. Bruscoli S, Biagioli M, Sorcini D, Frammartino T, Cimino M, Sportoletti P, et al. Lack of Glucocorticoid-induced leucine zipper (GILZ) deregulates B cell survival and results in B cell lymphocytosis in mice. *Blood* (2015). 126:1790–801. doi: 10.1182/blood-2015-03-631580
16. Bruscoli S, Sorcini D, Flamini S, Gagliardi A, Adamo F, Ronchetti S, et al. Glucocorticoid-induced leucine zipper inhibits interferon-gamma production in B cells and suppresses colitis in mice. *Front Immunol.* (2018) 9:1720. doi: 10.3389/fimmu.2018.01720

17. Hamdi H, Bigorgne A, Naveau S, Balian A, Bouchet-Delbos L, Cassard-Douclier AM, et al. Glucocorticoid-induced leucine zipper: a key protein in the sensitization of monocytes to lipopolysaccharide in alcoholic hepatitis. *Hepatology* (2007) 46:1986–92. doi: 10.1002/hep.21880
18. Vago JP, Tavares LP, Garcia CC, Lima KM, Perucci LO, Vieira EL, et al. The role and effects of glucocorticoid-induced leucine zipper in the context of inflammation resolution. *J Immunol.* (2015) 194:4940–50. doi: 10.4049/jimmunol.1401722
19. Hoppstädter J, Kiemer AK. Glucocorticoid-induced leucine zipper (GILZ) in immunosuppression: master regulator or bystander? *Oncotarget* (2015) 6:38446–57. doi: 10.18632/oncotarget.6197
20. Hoppstädter J, Hachenthal N, Valbuena-Perez JV, Lampe S, Astanina K, Kunze MM, et al. Induction of glucocorticoid-induced leucine zipper (GILZ) contributes to anti-inflammatory effects of the natural product curcumin in macrophages. *J Biol Chem.* (2016) 291:22949–60. doi: 10.1074/jbc.M116.733253
21. Hoppstädter J, Diesel B, Eifler LK, Schmid T, Brüne B, Kiemer AK. Glucocorticoid-induced leucine zipper is downregulated in human alveolar macrophages upon Toll-like receptor activation. *Eur J Immunol.* (2012) 42:1282–93. doi: 10.1002/eji.201142081
22. Bruscoli S, Velardi E, Di Sante M, Bereshchenko O, Venanzi A, Coppo M, et al. Long glucocorticoid-induced leucine zipper (L-GILZ) protein interacts with ras protein pathway and contributes to spermatogenesis control. *J Biol Chem.* (2012) 287:1242–51. doi: 10.1074/jbc.M111.316372
23. Hoppstädter J, Diesel B, Zarbock R, Breinig T, Monz D, Koch M, et al. Differential cell reaction upon Toll-like receptor 4 and 9 activation in human alveolar and lung interstitial macrophages. *Respir Res.* (2010) 11:124. doi: 10.1186/1465-9921-11-124
24. Hoppstädter J, Seif M, Dembek A, Cavalius C, Huwer H, Kraegeloh A, et al. M2 polarization enhances silica nanoparticle uptake by macrophages. *Front Pharmacol.* (2015) 6:55. doi: 10.3389/fphar.2015.00055
25. Dembek A, Laggai S, Kessler SM, Czepukojc B, Simon Y, Kiemer AK, et al. Hepatic interleukin-6 production is maintained during endotoxin tolerance and facilitates lipid accumulation. *Immunobiology* (2017) 222:786–96. doi: 10.1016/j.imbio.2017.01.003
26. Fejer G, Sharma S, Gyory I. Self-renewing macrophages—a new line of enquiries in mononuclear phagocytes. *Immunobiology* (2015) 220:169–74. doi: 10.1016/j.imbio.2014.11.005
27. Edgar R, Domrachev M, Lash AE. Gene expression omnibus: NCBI gene expression and hybridization array data repository. *Nucleic Acids Res.* (2002) 30:207–10. doi: 10.1093/nar/30.1.207
28. Szczyrba J, Nolte E, Hart M, Doll C, Wach S, Taubert H, et al. Identification of ZNF217, hnRNP-K, VEGF-A and IPO7 as targets for microRNAs that are downregulated in prostate carcinoma. *Int J Cancer* (2013) 132:775–84. doi: 10.1002/ijc.27731
29. Imig J, Motsch N, Zhu JY, Barth S, Okoniewski M, Reineke T, et al. microRNA profiling in Epstein-Barr virus-associated B-cell lymphoma. *Nucleic Acids Res.* (2011) 39:1880–93. doi: 10.1093/nar/gkq1043
30. Szczyrba J, Loprich E, Wach S, Jung V, Unteregger G, Barth S, et al. The microRNA profile of prostate carcinoma obtained by deep sequencing. *Mol Cancer Res.* (2010) 8:529–38. doi: 10.1158/1541-7786.MCR-09-0443
31. Cannarile L, Cuzzocrea S, Santucci L, Agostini M, Mazzon E, Esposito E, et al. Glucocorticoid-induced leucine zipper is protective in Th1-mediated models of colitis. *Gastroenterology* (2009) 136:530–41. doi: 10.1053/j.gastro.2008.09.024
32. Liu B, Liu Q, Yang L, Palaniappan SK, Bahar I, Thiagarajan PS, et al. Innate immune memory and homeostasis may be conferred through crosstalk between the TLR3 and TLR7 pathways. *Sci Signal.* (2016) 9:ra70. doi: 10.1126/scisignal.aac9340
33. Iwakawa HO, Tomari Y. The functions of MicroRNAs: mRNA decay and translational repression. *Trends Cell Biol.* (2015) 25:651–65. doi: 10.1016/j.tcb.2015.07.011
34. Rebane A, Akdis CA. MicroRNAs: Essential players in the regulation of inflammation. *J Allergy Clin Immunol.* (2013) 132:15–26. doi: 10.1016/j.jaci.2013.04.011
35. Tan GS, Chiu CH, Garchow BG, Metzler D, Diamond SL, Kiriakidou M. Small molecule inhibition of RISC loading. *ACS Chem Biol.* (2012) 7:403–10. doi: 10.1021/cb200253h
36. Eddleston J, Herschbach J, Wagelie-Steffen AL, Christiansen SC, Zuraw BL. The anti-inflammatory effect of glucocorticoids is mediated by glucocorticoid-induced leucine zipper in epithelial cells. *J Allergy Clin Immunol.* (2007) 119:115–22. doi: 10.1016/j.jaci.2006.08.027
37. Hahn RT, Hoppstädter J, Hirschfelder K, Hachenthal N, Diesel B, Kessler SM, et al. Downregulation of the glucocorticoid-induced leucine zipper (GILZ) promotes vascular inflammation. *Atherosclerosis* (2014) 234:391–400. doi: 10.1016/j.atherosclerosis.2014.03.028
38. Zhang XH, Lu X, Long XB, You XJ, Gao QX, Cui YH, et al. Chronic rhinosinusitis with and without nasal polyps is associated with decreased expression of glucocorticoid-induced leucine zipper. *Clin Exp Allergy* (2009) 39:647–54. doi: 10.1111/j.1365-2222.2008.03198.x
39. Chen YL, Jiang YW, Su YL, Lee SC, Chang MS, Chang CJ. Transcriptional regulation of tristetraprolin by NF-kappaB signaling in LPS-stimulated macrophages. *Molecular biology reports* (2013) 40:2867–77. doi: 10.1007/s11033-012-2302-8
40. Doyle F, Tenenbaum SA. Trans-regulation of RNA-binding protein motifs by microRNA. *Front Genet.* (2014) 5:79. doi: 10.3389/fgene.2014.00079
41. Wu X, Brewer G. The regulation of mRNA stability in mammalian cells: 2.0. *Gene* (2012) 500:10–21. doi: 10.1016/j.gene.2012.03.021
42. Georgakilas G, Vlachos IS, Zagganas K, Vergoulis T, Paraskevopoulou MD, Kanellos I, et al. DIANA-miRGen v3.0: accurate characterization of microRNA promoters and their regulators. *Nucleic Acids Res.* (2016) 44:D190–5. doi: 10.1093/nar/gkv1254
43. Guan Y, Yao H, Wang J, Sun K, Cao L, Wang Y. NF-kappaB-DICER-miRs axis regulates TNF-alpha expression in responses to endotoxin stress. *Int J Biol Sci.* (2015) 11:1257–68. doi: 10.7150/ijbs.12611
44. Netea MG, Joosten LA, Latz E, Mills KH, Natoli G, Stunnenberg HG, et al. Trained immunity: a program of innate immune memory in health and disease. *Science* (2016) 352:aaf1098. doi: 10.1126/science.aaf1098
45. Bogdan C. Nitric oxide synthase in innate and adaptive immunity: an update. *Trends Immunol.* (2015) 36:161–78. doi: 10.1016/j.it.2015.01.003
46. Toshchakov V, Jones BW, Perera PY, Thomas K, Cody MJ, Zhang S, et al. TLR4, but not TLR2, mediates IFN-beta-induced STAT1alpha/beta-dependent gene expression in macrophages. *Nat Immunol.* (2002) 3:392–8. doi: 10.1038/ni774
47. Mills CD, Ley K. M1 and M2 macrophages: the chicken and the egg of immunity. *J Innate Immunity* (2014) 6:716–26. doi: 10.1159/000364945
48. Olivares-Morales MJ, De La Fuente MK, Dubois-Camacho K, Parada D, Diaz-Jimenez D, Torres-Riquelme A, et al. Glucocorticoids impair phagocytosis and inflammatory response against crohn's disease-associated adherent-invasive *Escherichia coli*. *Front Immunol.* (2018) 9:1026. doi: 10.3389/fimmu.2018.01026

Conflict of Interest Statement: The authors declare that the research was conducted in the absence of any commercial or financial relationships that could be construed as a potential conflict of interest.

Copyright © 2019 Hoppstädter, Diesel, Linnenberger, Hachenthal, Flamini, Minet, Leidinger, Backes, Grässer, Meese, Bruscoli, Riccardi, Huwer and Kiemer. This is an open-access article distributed under the terms of the Creative Commons Attribution License (CC BY). The use, distribution or reproduction in other forums is permitted, provided the original author(s) and the copyright owner(s) are credited and that the original publication in this journal is cited, in accordance with accepted academic practice. No use, distribution or reproduction is permitted which does not comply with these terms.



Supplementary Material

Amplified host defense by Toll-like receptor-mediated downregulation of the glucocorticoid-induced leucine zipper (GILZ) in macrophages

Jessica Hoppstädter^{1*}, Britta Diesel¹, Rebecca Linnenberger¹, Nina Hachenthal¹, Sara Flamini², Marie Minet¹, Petra Leidinger³, Christina Backes⁴, Friedrich Grässer⁵, Eckart Meese³, Stefano Bruscoli², Carlo Riccardi², Hanno Huwer⁶, Alexandra K. Kiemer¹

¹ Pharmaceutical Biology, Department of Pharmacy, Saarland University, Saarbrücken, Germany

² Pharmacology, Department of Medicine, Perugia University, Perugia, Italy

³ Human Genetics, Department of Medicine, Saarland University, Homburg, Germany

⁴ Chair for Clinical Bioinformatics, Saarland University, Saarbrücken, Germany

⁵ Virology, Department of Medicine, Saarland University, Homburg, Germany

⁶ Cardiothoracic Surgery, Völklingen Heart Centre, Völklingen, Germany

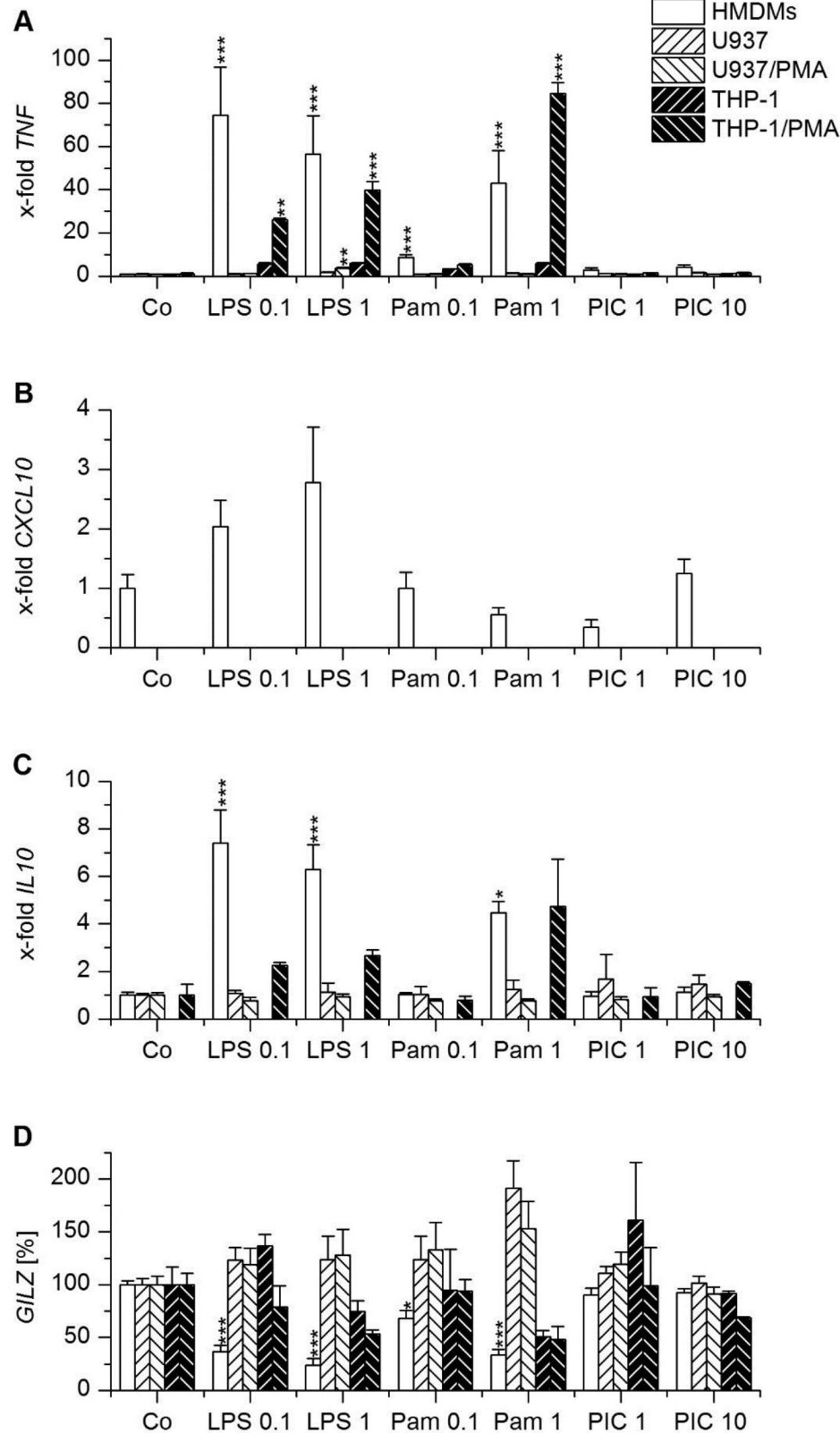
*** Correspondence:**

Jessica Hoppstädter, Ph.D.

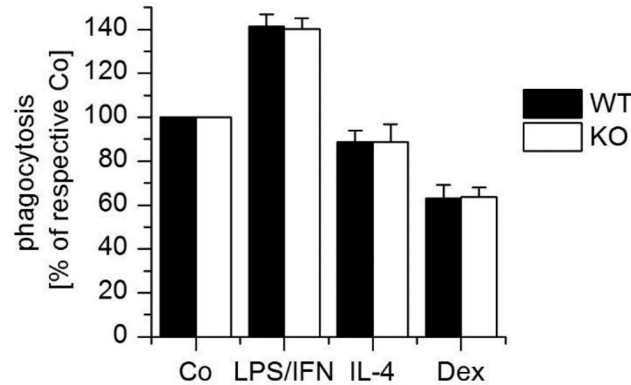
j.hoppstaedter@mx.uni-saarland.de

Supplementary Material

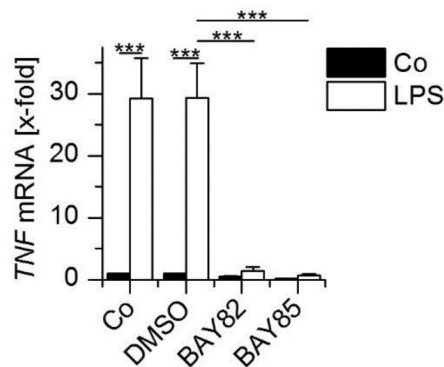
Supplementary Figures



Supplementary Figure 1. Responsiveness of human macrophages and macrophage-like cells towards the TLR1/2 ligand Pam₃CSK₄ and the TLR3 ligand Poly(I:C). Human monocyte-derived macrophages (HMDMs), as well as undifferentiated or PMA-differentiated U937 and THP-1 cells were left untreated (Co) or treated with LPS (0.1 or 1 µg/ml), Pam₃CSK₄ (Pam, 0.1 and 1 µg/ml), or PIC (PIC, 1 and 10 µg/ml) for 2 h. and mRNA was quantified by qRT-PCR using *ACTB* as a housekeeping gene (n = 2-3, triplicates). *p < 0.05, **p < 0.01, ***p < 0.001 vs. Co.



Supplementary Figure 2. Different treatment schemes do not alter the effect of GILZ depletion on phagocytosis. WT and GILZ KO BMMs were left untreated (Co) or treated with LPS (1 $\mu\text{g/ml}$) and $\text{INF-}\gamma$ (IFN, 20 ng/ml), IL-4 (20 ng/ml) or dexamethasone (Dex, 1 μM) for 20 h, followed by incubation with fluorescent latex particles (diameter 1.75 μm , 50 particles per cell) for 1 h. Particle uptake was quantified by flow cytometry. The total percentage of cells with particle-associated fluorescence in LPS/IFN, IL-4, or Dex-treated cells was normalized to the respective value for cells that were not treated otherwise prior to particle exposure.



Supplementary Figure 3. *NF- κ B* inhibition. After preincubation with BAY-11-7082 or BAY-11-7085 (5 μM , 1 h), solvent (0.1% DMSO) or medium only (Co), AMs were treated with LPS (100 ng/ml) for 2 h. *TNF* mRNA expression was determined by qRT-PCR using ACTB as a housekeeping gene (n = 3, duplicates).

Supplementary Material

Supplementary Tables

Supplementary Table 1: PCR conditions.

Gene	Sequence (5'→3') forward primer	Sequence (5'→3') reverse primer	Probe sequence (5'FAM→3'BHQ)	Probe [nM]	MgCl ₂ [mM]	Annealing [°C]
<i>IL6</i>	AAT AAT AAT GGA AAG TGG CTA TGC	AAT GCC ATT TAT TGG TAT AAA AAC	TCC TTT GTT TCA GAG CCA GAT CAT TTC T	100	4	57
IL8 (CXCL8)	TGC CAG TGA AAC TTC AAG CA	ATT GCA TCT GGC AAC CCT AC	CAG ACC CAC ACA ATA CAT GAA GTG TTG A	100	4	59
<i>TNF</i>	CTC CAC CCA TGT GCT CCT CA	CTC TGG CAG GGG CTC TTG AT	CAC CAT CAG CCG CAT CGC CGT CTC	100	3	60
GILZ (TSC22D3)	TCC TGT CTG AGC CCT GAA GAG	AGC CAC TTA CAC CGC AGA AC	TCC CGA ATC CCC ACA AGT GCC CGA	100	4	60
β-actin (ACTB)	TGC GTG ACA TTA AGG AGA AG	GTC AGG CAG CTC GTA GCT CT	CAC GGC TGC TTC CAG CTC CTC	60	4	60
<i>CXCL10</i>	GAG CCT ACA GCA GAG GAA CC	AAG GCA GCA AAT CAG AAT CG	TCC AGT CTC AGC ACC ATG AAT CAA A	60	4	60
<i>IL10</i>	CAA CAG AAG CTT CCA TTC CA	AGC AGT TAG GAA GCC CCA AG	AGC CTG ACC ACG CTT TCT AGC TGT TGA G	100	4	60
TTP (ZFP36)	TCG CCA CCC CAA ATA CAA	TTC GCT AGG GTT GTG GAT	no probe	N/A	N/A	60

Supplementary Table 2: Primers used to clone miRNA overexpression vectors.

miRNA	forward primer (plus EcoR1 site)	reverse primer (plus BamH1 or BglII site)
hsa-miR-18a	GC GAA TTC ATG GGA AGC CAA GTT GGG CTT TAA	GA GGA TCC CAC CTA TAT ACT TGC TTG GCT
hsa-miR-19a	GC GAA TTC ATG ATC CAA TAA TTC AAG CCA AGC	GA GGA TCC GCA GAT TCT ACA TCG ACA CAA
hsa-miR-19b	GC GAA TTC ATG TAG CTG TAG AAC TCC AGC TTC	GA GGA TCC GGG TTT GAG TTT CCC TTA CTT
hsa-miR-34b	GC GAA TTC ATG TAC GCG TGT TGT GCG CTG CGA	GA GGA TCC AAC CGC GGG TTT CCT CGC ACT
hsa-miR-136	GC GAA TTC ATG AGC TCT TCC ATT TCC TGG AGT	GA GGA TCC TCT GCT CTG ATT AGT TGG GCA
hsa-miR-222	GC GAA TTC ATG GAA AAT ATG TGG CAC TTT ATT	GA GGA TCC CTT AAC ACC CTA GAA CTT GAC
hsa-miR-320d1	GC GAA TTC ATG CCT TCA AAT GAC AAA ACA CAC	GA GGA TCC TTC CTT TCC TAT TTC TTT CCT
hsa-miR-484	GC GAA TTC ATG AAA ACC GAC GCC CTT CTC TCC	GA GGA TCC GTC CAC GTC ACG AGC TCA TTC

3.2. Altered Glucocorticoid Metabolism Represents a Feature of Macroph-aging

Aging Cell **2020**, doi: 10.1111/accel.13156

J. V. Valbuena Perez, R. Linnenberger, A. Dembek, M. H. Schulz, M. R. Meyer, J. Hoppstädter conducted experiments and acquired and analyzed data. J. V. Valbuena-Perez and J. Hoppstädter wrote the manuscript. S. Bruscoli, C. Riccardi, M. R. Meyer, A. K. Kiemer, and J. Hoppstädter supervised and designed research studies and revised the manuscript.

Rebecca Linnenberger carried out, analyzed, and validated the following experimental work described in this publication. In detail, she performed parts of the quantitative real-time PCR, Western blotting, and the homovanillic acid assay. She participated in the cell culture for the determination of steroid levels, the determination of 11 β -HSD1 activity in peritoneal macrophages, and the isolation of murine peritoneal macrophages, murine peripheral blood leukocytes, and their respective cell culture. Finally, she critically reviewed the manuscript.

© Valbuena Perez, Linnenberger, Dembek, Bruscoli, Riccardi, Meyer, Kiemer, Hoppstädter. This is an open-access article distributed under the terms of the Creative Commons Attribution Licence (CC BY).

Received: 4 November 2019 | Revised: 20 March 2020 | Accepted: 5 April 2020

DOI: 10.1111/ace.13156

ORIGINAL PAPER

Aging Cell



WILEY

Altered glucocorticoid metabolism represents a feature of macroph-aging

Jenny Vanessa Valbuena Perez¹ | Rebecca Linnenberger¹ | Anna Dembek¹ |
Stefano Bruscoli² | Carlo Riccardi² | Marcel H. Schulz^{3,4} | Markus R. Meyer⁵ |
Alexandra K. Kiemer¹ | Jessica Hoppstädter¹

¹Pharmaceutical Biology, Department of Pharmacy, Saarland University, Saarbrücken, Germany

²Pharmacology, Department of Medicine, Perugia University, Perugia, Italy

³Institute for Cardiovascular Regeneration, Goethe University, Frankfurt am Main, Germany

⁴German Center for Cardiovascular Research (DZHK), Partner Site RheinMain, Frankfurt am Main, Germany

⁵Department of Experimental and Clinical Toxicology, Institute of Experimental and Clinical Pharmacology and Toxicology, Center for Molecular Signaling (PZMS), Saarland University, Homburg, Germany

Correspondence

Jessica Hoppstädter, Ph.D., Pharmaceutical Biology, Department of Pharmacy, Saarland University, 66123 Saarbrücken, Germany. Email: j.hoppstaedter@mx.uni-saarland.de

Funding information

Deutsche Forschungsgemeinschaft, Grant/Award Number: KI702; Studienstiftung des deutschen Volkes

Abstract

The aging process is characterized by a chronic, low-grade inflammatory state, termed “inflammaging.” It has been suggested that macrophage activation plays a key role in the induction and maintenance of this state. In the present study, we aimed to elucidate the mechanisms responsible for aging-associated changes in the myeloid compartment of mice. The aging phenotype, characterized by elevated cytokine production, was associated with a dysfunction of the hypothalamic–pituitary–adrenal (HPA) axis and diminished serum corticosteroid levels. In particular, the concentration of corticosterone, the major active glucocorticoid in rodents, was decreased. This could be explained by an impaired expression and activity of 11 β -hydroxysteroid dehydrogenase type 1 (11 β -HSD1), an enzyme that determines the extent of cellular glucocorticoid responses by reducing the corticosteroids cortisone/11-dehydrocorticosterone to their active forms cortisol/corticosterone, in aged macrophages and peripheral leukocytes. These changes were accompanied by a downregulation of the glucocorticoid receptor target gene glucocorticoid-induced leucine zipper (GILZ) in vitro and in vivo. Since GILZ plays a central role in macrophage activation, we hypothesized that the loss of GILZ contributed to the process of macroph-aging. The phenotype of macrophages from aged mice was indeed mimicked in young GILZ knockout mice. In summary, the current study provides insight into the role of glucocorticoid metabolism and GILZ regulation during aging.

KEYWORDS

cellular immunology, cytokines, inflammation, mononuclear cell, mouse models, reactive oxygen species, steroid control of aging, TSC22D3

Valbuena Perez and Linnenberger contributed equally to this work.

This is an open access article under the terms of the Creative Commons Attribution License, which permits use, distribution and reproduction in any medium, provided the original work is properly cited.

© 2020 The Authors. *Aging Cell* published by the Anatomical Society and John Wiley & Sons Ltd.

1 | INTRODUCTION

While the adaptive immune system usually deteriorates with age, innate immune cells can cause a chronic, low-grade systemic inflammatory state, termed “inflammaging” (Franceschi et al., 2000). This chronic inflammation, fueled by continuous exposure to exogenous and endogenous stimuli during the lifespan, is considered by geroscience as one of the seven pillars of aging, and largely determines the onset of age-related diseases (Franceschi, Garagnani, Parini, Giuliani, & Santoro, 2018). Different factors, such as cellular senescence, altered metabolic activity, and endocrine disorders contribute to sustaining inflammaging (Bandaranayake & Shaw, 2016).

The macrophage is a key driver of age-related inflammation. The theory of inflammaging has been intertwined with “macroph-aging,” that is, the chronic activation of macrophages, since it was first described (Franceschi et al., 2000; Prattichizzo, Bonafe, Olivieri, & Franceschi, 2016). Macrophages are a widely distributed, heterogeneous, plastic cell population, with central roles as effectors and mediators of the innate and adaptive immune response (Mosser & Edwards, 2008; Wynn, Chawla, & Pollard, 2013; Zhou et al., 2014). Several studies in humans and animals have reported age-related alterations in different macrophage functions, such as phagocytic activity, pro-inflammatory cytokine secretion, and antigen presentation (Jackaman et al., 2017; Sebastian, Espia, Serra, Celada, & Lloberas, 2005). Furthermore, a loss of macrophages has been associated with an improved inflammation-induced pathology and survival after systemic immunostimulation (Bouchlaka et al., 2013), and with reduced neurodegeneration (Yuan et al., 2018) in murine models of aging.

Endogenous glucocorticoids (GCs) are central regulators of immune functions. They can exert their action by binding to the widely expressed glucocorticoid receptor (GR) through genomic mechanisms (transactivation, transrepression, and composite glucocorticoid response element-binding), or nongenomic effects (Cain & Cidlowski, 2017). GC secretion is regulated in a circadian manner and in response to stress by the hypothalamic–pituitary–adrenal (HPA) axis, whose function is dysregulated with advancing age (Gupta & Morley, 2014). However, the role of systemic and local GC production during aging processes is largely unknown.

Due to the importance of macrophage activation and GC responses in the aged immune system, we aimed to evaluate the age-associated changes in GC metabolism in the myeloid compartment of mice in order to improve the current understanding of “macroph-aging.”

2 | RESULTS

2.1 | Inflammation in aged mice is associated with decreased serum GC levels

Previous studies demonstrated that levels of circulating pro-inflammatory mediators, such as tumor necrosis factor (TNF)- α ,

interleukin (IL)-6, and C-reactive protein (CRP), are elevated in aged individuals, a circumstance which correlates with increased risk of morbidity and mortality (Bandaranayake & Shaw, 2016; Minciullo et al., 2016). In line with these findings, we observed a pro-inflammatory phenotype in aged C57BL/6 mice when compared with their young counterparts. This phenotype was characterized by increased basal TNF- α and LPS-induced IL-6 and TNF- α serum levels (Figure 1a,b). In peritoneal macrophages (PMs) isolated from aged animals, a higher production of LPS-induced TNF and H₂O₂ was found. In addition, extracellular-signal-regulated kinase (ERK) 1/2 activation, which is critically involved in cytokine production in macrophages (Hoppstädter et al., 2015, 2016), was increased (Figure 1c–f).

Senescent cells (SCs) are characterized by elevated cytokine production, upregulation of the cyclin-dependent kinase inhibitors p16 (*Cdkn2a*) and p21 (*Cdkn1a*), and downregulation of the senescence suppressor sirtuin-1 (*Sirt1*) (Lee, Lee, Lee, & Min, 2019; Tchkonja, Zhu, van Deursen, Campisi, & Kirkland, 2013; van Deursen, 2014). None of these effects were observed in PMs obtained from aged mice, indicating that these macrophages do not resemble SCs (Figure 1g).

Serum analyses by ELISA showed significantly reduced corticosteroid levels in aged mice (Figure 2a). Due to known cross-reactivities, however, conventional antibody-based detection methods for corticosteroids do not allow to distinguish between inactive cortisone/11-dehydrocorticosterone (11-DHC) and active cortisol/corticosterone. Thus, we developed an LC-HRMS/MS-based method to quantify the serum levels of the main GCs in rodents (Gong et al., 2015), that is, active corticosterone and inactive 11-DHC, in sera from young and aged mice. Aged mice displayed decreased serum levels of both corticosteroids compared with young animals. While the mean of total GC and 11-DHC levels was reduced by half, levels of active corticosterone decreased by two-thirds (Figure 2b,c).

The synthesis of GCs within the adrenal cortex is regulated via the release of corticotropin-releasing hormone (CRH) from the hypothalamus, which stimulates the secretion of adrenocorticotrophic hormone (ACTH) from the anterior pituitary gland (Gupta & Morley, 2014). Serum levels of both CRH and ACTH were reduced in aged animals (Figure 2d,e). The expression of genes involved in the cholesterol homeostasis or corticosteroid synthesis within the adrenal gland remained unchanged, except that the cholesterol efflux mediator ATP-binding cassette transporter G1 (*Abcg1*) was upregulated (Figure 2f). Taken together, these findings suggest an HPA axis dysfunction in aged mice.

2.2 | GC homeostasis in aged cells and tissues

Irrespective of serum GC levels, the cellular GC responsiveness is ultimately determined by the intracellular availability of active GCs, as well as the expression of the GR (*Nr3c1*) (Cain & Cidlowski, 2017; Oakley & Cidlowski, 2013). However, GR levels

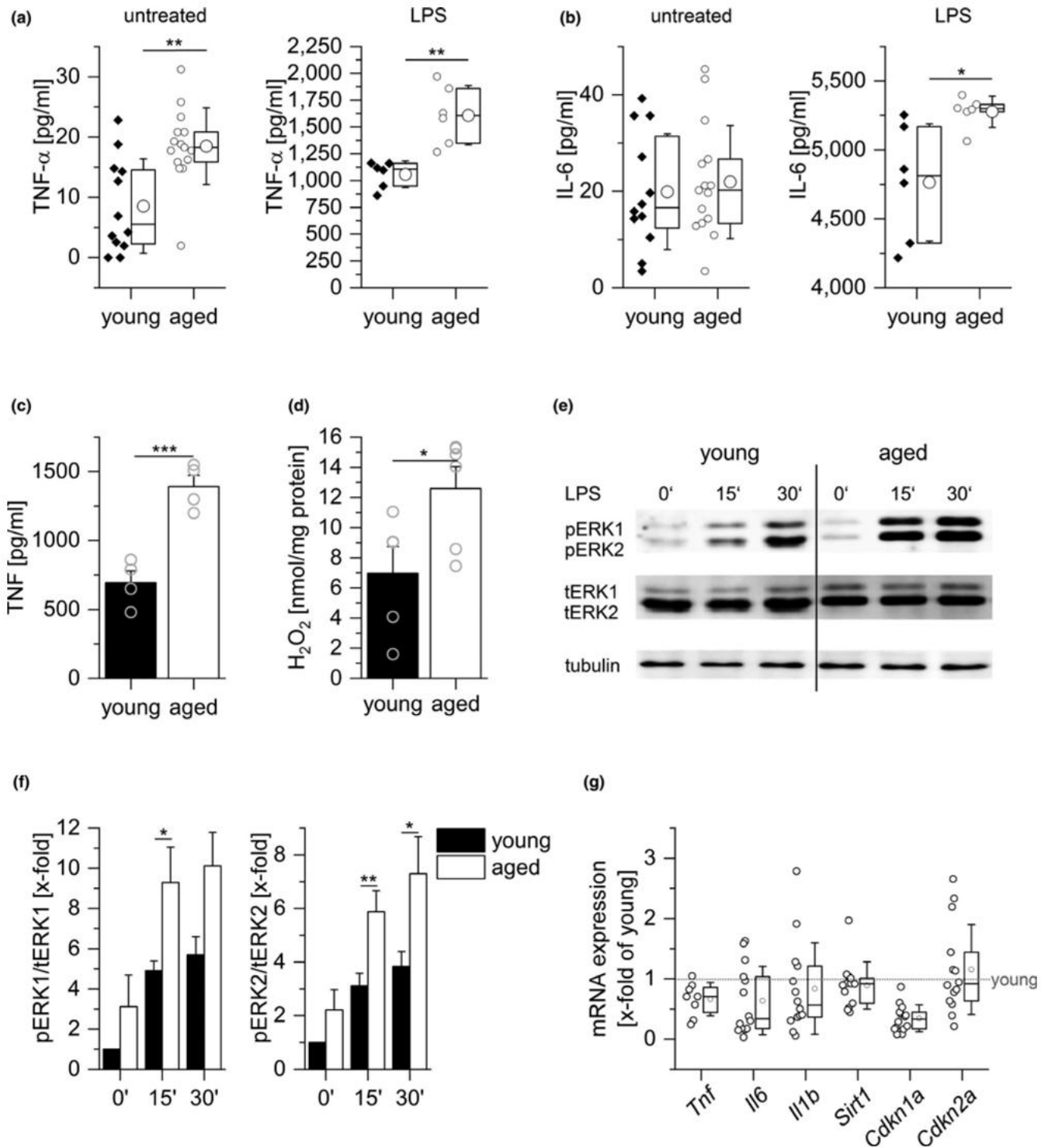


FIGURE 1 Inflammation in aged mice. Levels of TNF- α (a) and IL-6 (b) in sera from young (10 weeks) and aged (20–22 months) C57BL/6 mice as determined by ELISA; untreated: $n = 12$ (young) or $n = 15$ (aged), LPS (5 mg/kg BW, 4 hr): $n = 6$. (c) PMs obtained from young and aged mice were stimulated with LPS (100 ng/ml, 4 hr), and TNF was quantified in the supernatants by bioassay ($n = 4$, triplicates). (d) H_2O_2 production was measured in PM supernatants by homovanillic acid assay (young: $n = 5$, aged: $n = 6$). (e) ERK phosphorylation after LPS treatment (100 ng/ml) was examined by Western blot. Total ERK (tERK) and tubulin served as loading controls. (e) One representative blot out of six is shown. (f) pERK1/2 signal intensities were normalized to total ERK1/2. Values for untreated cells from young mice were set as 1 ($n = 6$ in replicates). (g) Gene expression in PMs from young and aged mice was determined by qPCR and normalized against the housekeeping gene (*Ppia*). Values for PMs from young mice were set as 1 ($n = 14$). Box plots show the 25–75th percentiles (box), mean (square), median (line), and SD (whiskers). Bars show the mean \pm SEM, and circles within bars indicate the mean of each individual experiment. * $p < .05$, ** $p < .01$, *** $p < .001$ by two-tailed t test (a–c), Mann–Whitney U test (d, g), or ANOVA with Bonferroni's post hoc test (f)

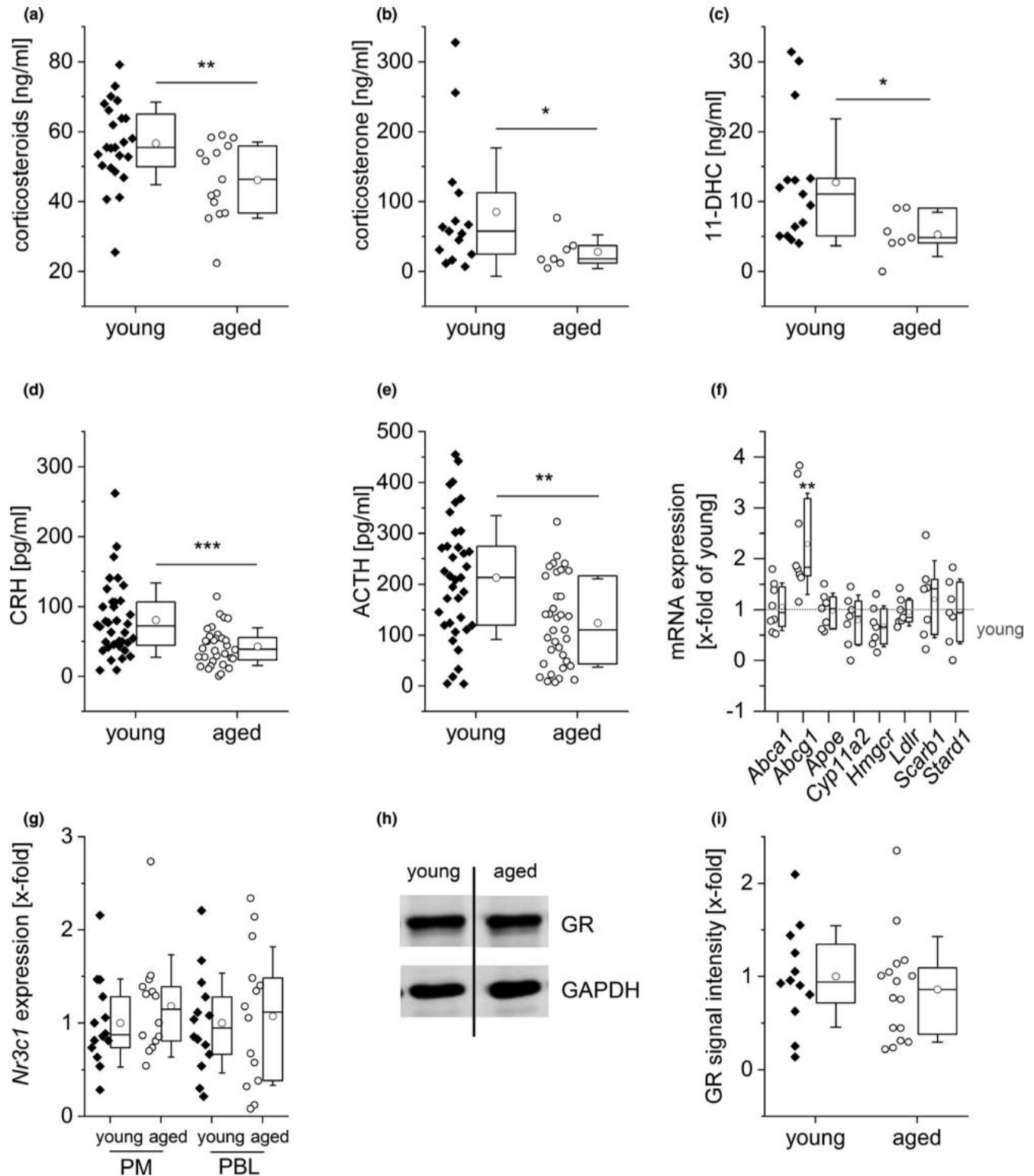


FIGURE 2 Decreased GC levels in aged mice. (a) Total serum corticosteroid levels were quantified in sera of young ($n = 24$) and aged ($n = 15$) mice by ELISA. (b, c) Corticosterone (b) and 11-dehydrocorticosterone (11-DHC, c) concentrations were determined in sera of young ($n = 15$) and aged ($n = 7$) mice by LC-HRMS/MS. (d, e) CRH (d) and ACTH (e) levels were determined in sera of young ($n = 34$) and aged ($n = 33$) mice by ELISA. (f) Expression levels of genes involved in cholesterol homeostasis and corticosteroid biosynthesis were measured in adrenal glands from young ($n = 12$) and aged ($n = 8$) mice by qPCR, normalized against the housekeeping gene (*Csnk2a2*), and expressed as x-fold of samples from young mice. (g) Expression of GR mRNA (*Nr3c1*) in PMs and PBLs from young and aged mice ($n = 14$). Data were normalized against the housekeeping gene (*Ppia*) and are expressed as fold change of young. (h, i) GR protein levels were measured by Western blot in PMs obtained from young ($n = 12$) and aged ($n = 16$) mice. (h) Representative blot. (i) GR signal intensities were normalized to the loading control GAPDH and are expressed as x-fold of young. Box plots show the 25–75th percentiles (box), mean (circle), median (line), and SD (whiskers). * $p < .05$, ** $p < .01$, *** $p < .001$ by two-tailed t test (a, d, e) or Mann–Whitney *U* test (b, c, f)

remained unchanged with aging in PMs, peripheral blood leukocytes (PBLs), liver, lung, and lymphoid tissues (Figure 2g-i and Figure S1).

It is well established that macrophages and other cells and tissues can generate active cortisol from inactive cortisone to locally amplify steroid action (Gilmour et al., 2006). We, therefore, determined gene expression levels of the enzyme 11 β -hydroxysteroid dehydrogenase type 1 (11 β -HSD1, *Hsd11b1*), which locally converts GCs to their active form. We found a significantly lower *Hsd11b1* gene expression in PM and PBLs from aged mice (Figure 3a), and also in the liver, where the enzyme is most abundant (Figure S2A). Accordingly, 11 β -HSD1 protein levels were reduced in aged PMs (Figure 3b,c). On the other hand, the gene expression of *Hsd11b2*, the isozyme that exerts dehydrogenase (cortisol/corticosterone to cortisone/11-DHC) activity, remained unchanged in PMs and PBLs from aged mice compared with young controls (Figure S2b).

Transcription of *Hsd11b1* is regulated by members of the CCAAT/enhancer-binding protein (C/EBP) family of transcription factors (Chapman, Holmes, & Seckl, 2013). To determine whether these upstream regulators of 11 β -HSD1 were altered in aged PM and PBL, mRNA levels of C/EBP α and C/EBP β were measured. Both genes were significantly downregulated in PMs from aged animals. In PBLs, a similar tendency for *Cebpa* expression was observed, while the expression of *Cebpb* remained unchanged (Figure S2c,d).

Since 11 β -HSD1 regulates the intracellular availability of active GCs, age-related changes in 11 β -HSD1 reductase activity were evaluated by measuring the conversion rate of deuterated cortisone to cortisol in isolated young and aged PMs by LC-HRMS/MS. The downregulation of the enzyme was indeed paralleled by lower levels of intracellular conversion of cortisone to cortisol (Figure 3d,e). These findings suggested that reduced 11 β -HSD1 expression translates into less corticosterone available to activate the GR in aging macrophages in the in vivo setting.

To assess the functional consequences of the loss of 11 β -HSD1, THP-1 macrophages were pretreated with the 11 β -HSD1 inhibitor PF915275, followed by an analysis of GR translocation upon cortisone treatment. 11 β -HSD1 inhibition abrogated GR translocation (Figure 3f) and reduced the cortisone-induced expression of GR-responsive genes, particularly the anti-inflammatory mediator glucocorticoid-induced leucine zipper (GILZ, *Tsc22d3*) (Figure 3g). Similar results were obtained when using PMs from young mice instead of THP-1 cells (Figure 3h).

2.3 | GILZ downregulation as a feature of inflammaging

Our data suggested GILZ expression as an indicator of altered GC homeostasis. Thus, we analyzed its expression in human blood samples from the publicly available GTEx database (version 8). GILZ tended to be downregulated in human blood samples from aged individuals, although the expression levels showed high inter-individual variability (Figure 4a).

To further elucidate whether GILZ expression was affected by the aging process, we measured its expression in various murine cells and tissues. Based on a multi-color flow cytometric analysis (Figure 4b,c and Figure S3), we found that GILZ was highly expressed in myeloid peripheral blood cells from young animals (Figure 4d), and was significantly downregulated in monocytes from aged mice (Figure 4e).

Furthermore, flow cytometric quantification of GILZ expression in PMs obtained from aged mice showed reduced GILZ levels when compared with cells derived from young animals (Figure 5a,b). GILZ was highly expressed in myeloid cells in livers, spleens, and mesenteric lymph nodes from young mice (Figure 5c, Figures S4 and S5). In tissues from aged animals, we observed a downregulation of GILZ, which was particularly evident in the monocyte and macrophage compartment (Figure 5d, Figures S4 and S5).

GILZ represents a potent endogenous suppressor of inflammatory responses (Bereshchenko, Migliorati, Bruscoli, & Riccardi, 2019; Hoppstädter & Kiemer, 2015; Ronchetti, Migliorati, Bruscoli, & Riccardi, 2018). Thus, we hypothesized that the loss of GILZ in aging macrophages might contribute to inflammaging. To test this hypothesis, we compared young mice bearing a myeloid-specific GILZ knockout (KO) with young and aged wild-type (WT) mice. The phenotype of aged mice was mimicked in young GILZ KO mice: Both baseline and LPS-induced serum TNF- α levels were elevated in both groups (Figure 6a). Furthermore, we analyzed aspects of cell activation in PMs from young WT, old WT, and young KO mice (Figure 6b-e). TNF production, generation of reactive oxygen species, and ERK phosphorylation were increased both in macrophages from aged WT as well as young KO animals, indicating that the downregulation of GILZ might be a central feature of inflammaging.

3 | DISCUSSION

Aging, defined as the functional decline that occurs during the lifespan of an organism, constitutes a risk factor for several human pathologies (Lopez-Otin, Blasco, Partridge, Serrano, & Kroemer, 2013). For instance, the prevalence and mortality associated with CVD are expected to grow exponentially, as the world population continues to age (Costantino, Paneni, & Cosentino, 2016). Inflammation is known to promote aging processes (Franceschi et al., 2018; Kennedy et al., 2014). Indeed, longitudinal studies have shown a correlation between inflammation and longevity, capability, and cognition in the aged population (Arai et al., 2015). The changes in the immune system associated with aging, globally known as immunosenescence, affect both innate and adaptive immunity. Rather than solely detrimental, such changes represent an adaptive/remodeling response that results in dysregulated homeostasis not only of immunity, but also of other systems that influence and are influenced by the immune system, such as the nervous and endocrine systems (Fulop et al., 2017). The chronic, low-grade systemic inflammatory state observed with advancing age, termed inflammaging (Franceschi et al., 2000),

involves functional alterations of immune cells as a consequence of different mechanisms, including cellular senescence, oxidative stress, mitochondrial dysfunction, defective autophagy and mitophagy, inflammasome activation, and dysbiosis (Franceschi et al., 2018). Population studies have demonstrated that aged individuals show elevated circulating levels of pro-inflammatory mediators/markers, such as TNF- α , IL-6, and CRP, which correlate

with increased risk of morbidity and mortality (Bandaranayake & Shaw, 2016; Minciuolo et al., 2016).

While the mechanisms responsible for the initiation of inflammaging are still widely unknown, an increasing body of evidence suggests that the accumulation of SCs is critically involved in this process. Factors secreted by cells with a senescence-associated secretory phenotype (SASP), that is, pro-inflammatory cytokines

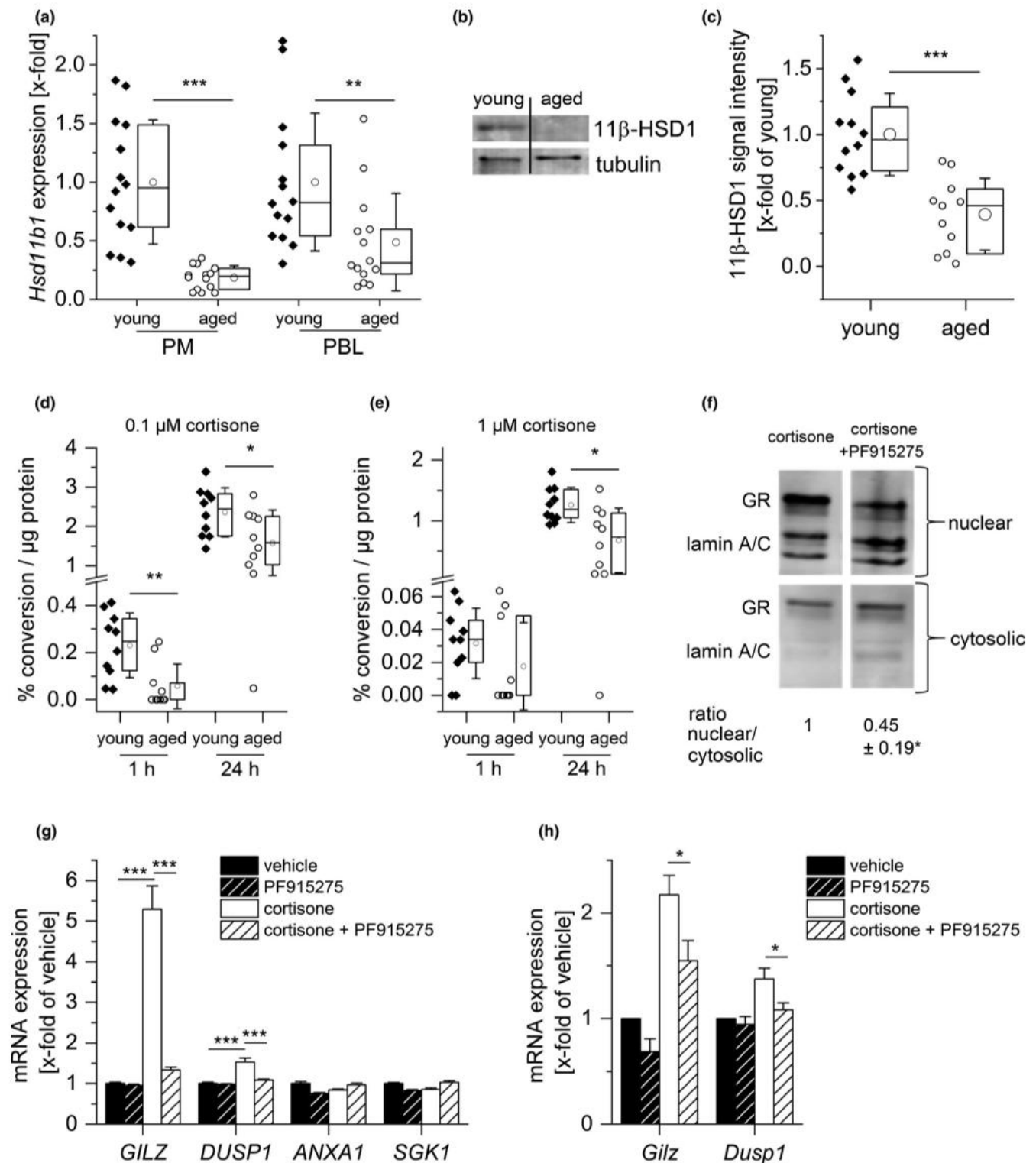


FIGURE 3 Alterations in GC metabolism in aged immune cells. (a) *Hsd11b1* expression in PMs and PBLs from young and aged mice ($n = 14$) was measured by RT-qPCR, normalized to *Ppia*, and expressed as x-fold of young. (b, c) 11β -HSD1 protein expression was measured in PMs (young: $n = 12$, aged: $n = 11$). (b) Representative blot. (c) Densitometric analysis, normalized to the housekeeping protein tubulin. Values for young mice were set as 1. (d, e) PMs isolated from young and aged animals ($n = 10$) were incubated for 1 or 24 hr with 0.1 μ M (d) or 1 μ M (e) cortisone-D8, and the conversion to cortisol-D8 was measured in supernatants by LC-HRMS/MS. Conversion percentages were normalized to total protein content. (f, g) THP-1 macrophages were treated with either vehicle (0.1% DMSO) or the 11β -HSD1 inhibitor PF915275 (100 nM) for 1 hr, followed by cortisone treatment (100 nM) for 4 hr. (f) GR content in nuclear and cytosolic fractions was analyzed by Western blot. Lamin (A/C) was used as an indicator for the presence or absence of nuclear proteins. One representative blot is shown. Densitometric quantification data are presented as x-fold of the nuclear/cytosolic GR ratio in cortisone-treated cells ($n = 4$, $*p < .05$ versus cortisone-treated cells). (g) GR-dependent gene expression was analyzed by qPCR and normalized to the housekeeping gene *ACTB*. Data are presented as x-fold of vehicle-treated cells ($n = 3$, triplicates). (h) PMs obtained from young mice were treated with either vehicle (0.1% DMSO) or PF915275 (100 nM) for 1 hr, followed by cortisone treatment (100 nM) for 4 hr. *Gilz* and *Dusp1* expression were analyzed by qPCR, normalized to the housekeeping gene *Ppia*, and expressed as x-fold of vehicle control ($n = 8$). Box plots show the 25–75th percentiles (box), mean (circle), median (line), and SD (whiskers). Bars show the mean \pm SEM. $*p < .05$, $**p < .01$, $***p < .001$ by two-tailed *t* test (a, c), one-sample *t* test (f), Mann-Whitney *U* test (d, e), or ANOVA with Bonferroni's post hoc test (g, h)

and chemokines, matrix metalloproteinases, and growth factors, have been shown to contribute to age-related diseases. This pro-inflammatory program is thought to be activated in order to initiate the immune-mediated clearance of SCs (Tchkonja et al., 2013; van Deursen, 2014). Noticeably, macrophage depletion by clodronate treatment has been reported to induce a drastic reduction of age-associated inflammatory responses to systemic immunostimulation in aged mice (Bouchlaka et al., 2013). These findings strongly support the hypothesis that macrophages play a vital role in aging processes, a phenomenon previously termed "macroph-aging" (Franceschi et al., 2000). In line with these assumptions, our data show an inflammatory phenotype in old versus young adult mice, as indicated by elevated TNF- α and IL-6 serum levels, increased TNF- α and reactive oxygen species production in macrophages from aged animals, and increased ERK phosphorylation upon LPS stimulation.

The global pro-inflammatory state, however, is not the only determinant of successful/unsuccessful aging, as a compensatory, anti-inflammatory response, is observed in parallel to inflammaging, particularly in very long-lived individuals (centenarians). The mediators associated with anti-inflammaging include transforming growth factor (TGF)- β , IL-10, dehydroepiandrosterone (DHEA), and cortisol (Baylis, Bartlett, Patel, Roberts, 2013; Minciuolo et al., 2016). It is considered that, ultimately, the ability of the anti-inflammatory network to cope with and modulate chronic inflammation is determinant either to attain healthy aging and longevity or for the onset of chronic inflammatory diseases.

The synthesis of GCs within the adrenal cortex is regulated by the HPA axis via the release of CRH and arginine vasopressin (AVP) from the hypothalamus. Subsequently, CRH and AVP stimulate the secretion of ACTH from the anterior pituitary gland (Gupta & Morley, 2014). Serum levels of both CRH and ACTH were reduced in aged animals. The expression of genes involved in the regulation of intracellular cholesterol levels or corticosteroid synthesis within the adrenal gland remained unchanged, except that the ATP-binding cassette transporter G1 (*Abcg1*) was upregulated. Although *Abcg1* is mainly described to mediate cholesterol efflux, there might be additional functions within the adrenal cortex, as suggested by a mild glucocorticoid insufficiency observed in *Abcg1* knockout mice

(Hoekstra et al., 2019). In summary, these observations suggest a dysfunction of the HPA axis with advanced age.

The involvement of GC signaling and metabolism in chronic inflammation and stress-related disorders, two phenomena that occur with aging, has been a topic of interest for the last decades (Herriot, Wrosch, Gouin, & Miller, 2017). Literature reports indicate associations between both higher and lower GC levels and negative health outcomes (Gaffey, Bergeman, Clark, & Wirth, 2016; Raison & Miller, 2003). In rodents, an increase (Kizaki et al., 2002), no differences (Morano, Vazquez, & Akil, 1994) and, more recently, a decrease (Zambrano, Reyes-Castro, & Nathanielsz, 2015) in serum corticosteroids with age have been reported. However, investigations on total corticosteroid concentrations in blood or urine do not consider that aging might affect the glucocorticoid metabolism.

Cellular GC responsiveness is determined by the intracellular availability of active GCs, as well as the expression of GRs. Although a previous study reported elevated GR mRNA expression in peritoneal exudate cells from aged mice (Kizaki et al., 1998), our findings suggest that alterations in GC homeostasis from PMs are not associated with altered GR expression but with reduced intracellular activation of 11-DHC by 11β -HSD1.

Transcription of *Hsd11b1* is controlled by members of the C/EBP family of transcription factors. Interestingly, C/EBP α and C/EBP β themselves are GC-inducible (Ayala-Sumano et al., 2013; Chapman et al., 2013), suggesting a feed-forward loop to further amplify local glucocorticoid signaling. In our setting, both *Cebpa* and *Cebpb* were downregulated in aged macrophages, implying that this regulatory circuit might be disrupted in aged mice.

There might be different functional implications of blunted 11β -HSD1 signaling in aged macrophages: It has been shown that 11β -HSD1-deficient mice are more susceptible to endotoxemia, and macrophages derived from these mice are hyperresponsive to LPS stimulation (Zhang & Daynes, 2007). Loss of 11β -HSD1 in macrophages has also been associated with delayed phagocytic capacity (Gilmour et al., 2006).

In our hands, pharmacological inhibition of 11β -HSD1 resulted in a decreased expression of GC-responsive genes, particularly *GILZ*. *GILZ* was first identified as a dexamethasone-inducible gene in murine thymocytes (D'Adamio et al., 1997) and has been suggested to play

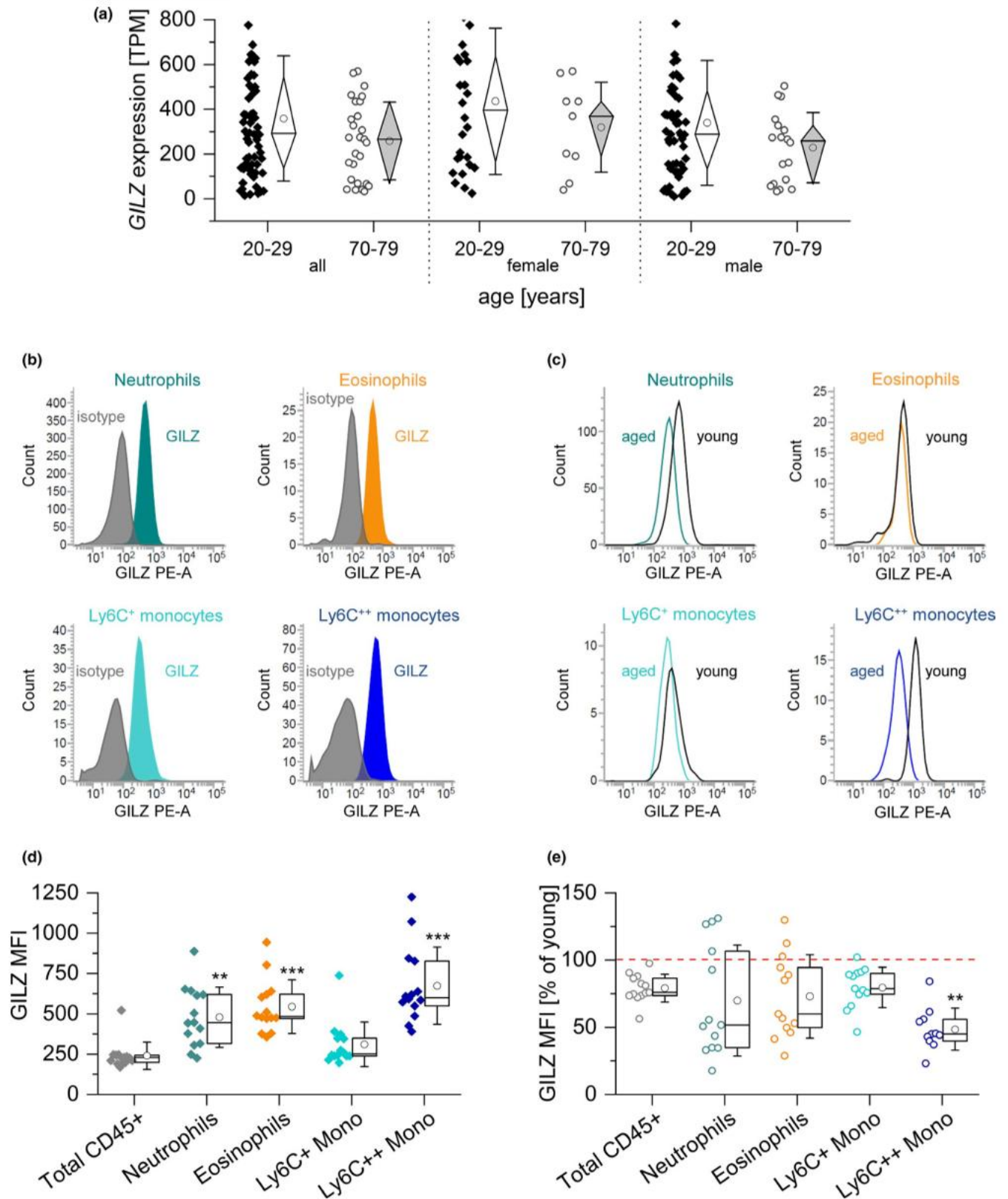


FIGURE 4 GILZ expression in human and murine blood samples from young and aged individuals. (a) GILZ expression in human blood samples. Expression data were retrieved from the GTEx database and are shown as TPM (transcripts per million) (20–29 years: 27 ♀, 57 ♂; 70–79 years: 9 ♀, 18 ♂). (b) Representative histograms showing GILZ expression in myeloid subsets in young mice. Colored: GILZ signal; gray: isotype control. (c) Representative histograms showing GILZ signals in cells from aged and young mice. Gray line: young; colored line: aged. (d) Background-subtracted GILZ median fluorescence intensity (MFI) in myeloid blood cells from young mice ($n = 14$). ** $p < .01$, *** $p < .001$ compared with MFI values for total CD45⁺ cells by ANOVA with Bonferroni's post hoc test. (e) GILZ expression in myeloid subsets of aged mice ($n = 13$). The GILZ MFI of young cells was set as 100% for each subset. Box plots show the 25–75th percentile (box), mean (circle), median (line), and SD (whiskers). * $p < .05$, ** $p < .01$ compared with the same subset in young animals by Mann–Whitney U test. Mono: monocytes

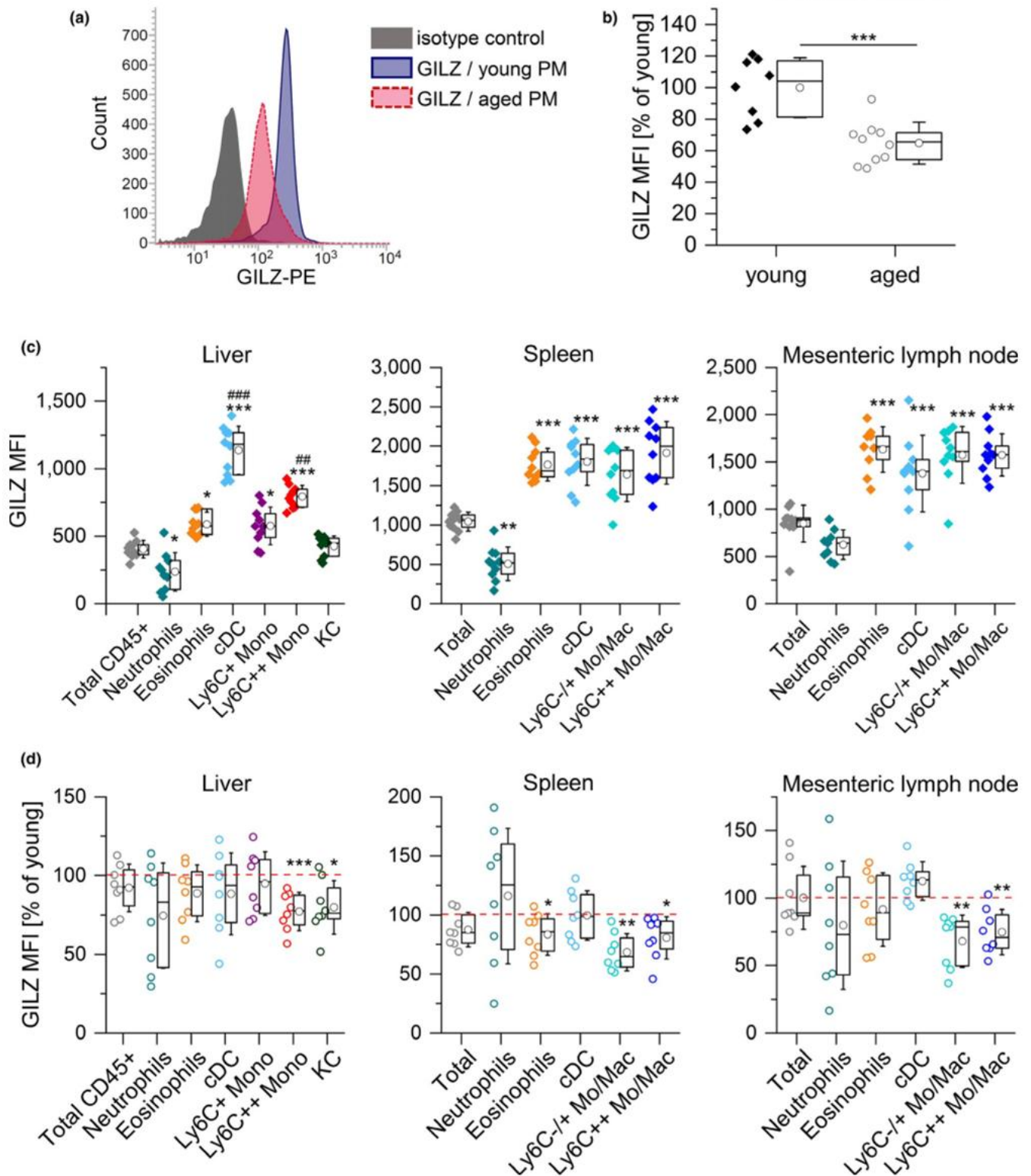


FIGURE 5 GILZ expression in myeloid cells from young and aged mice. (a, b) GILZ expression in PMs from young and aged mice was determined by flow cytometry. (a) Representative histogram. (b) Background-subtracted GILZ median fluorescence intensity (MFI) (young: $n = 8$, aged: $n = 10$). (c) GILZ MFI in myeloid cells in the liver and lymphoid tissues of young mice ($n = 10$). *** $p < .001$ compared with MFI values for total CD45⁺ (liver) or total cells (spleen and lymph node), ** $p < .01$, ### $p < .001$ compared with all other subsets (ANOVA with Bonferroni's post hoc test). (d) GILZ expression in myeloid subsets of aged mice. The GILZ MFI of young cells was set as 100% for each subset ($n = 8$). * $p < .05$, ** $p < .01$, *** $p < .001$ compared with the same subset in young animals by Mann-Whitney U test. Box plots show the 25–75th percentiles (box), mean (circle), median (line), and SD (whiskers). Mono: monocytes; Mo/Mac: monocytes and macrophages; cDC: classical dendritic cells; KC: Kupffer cells

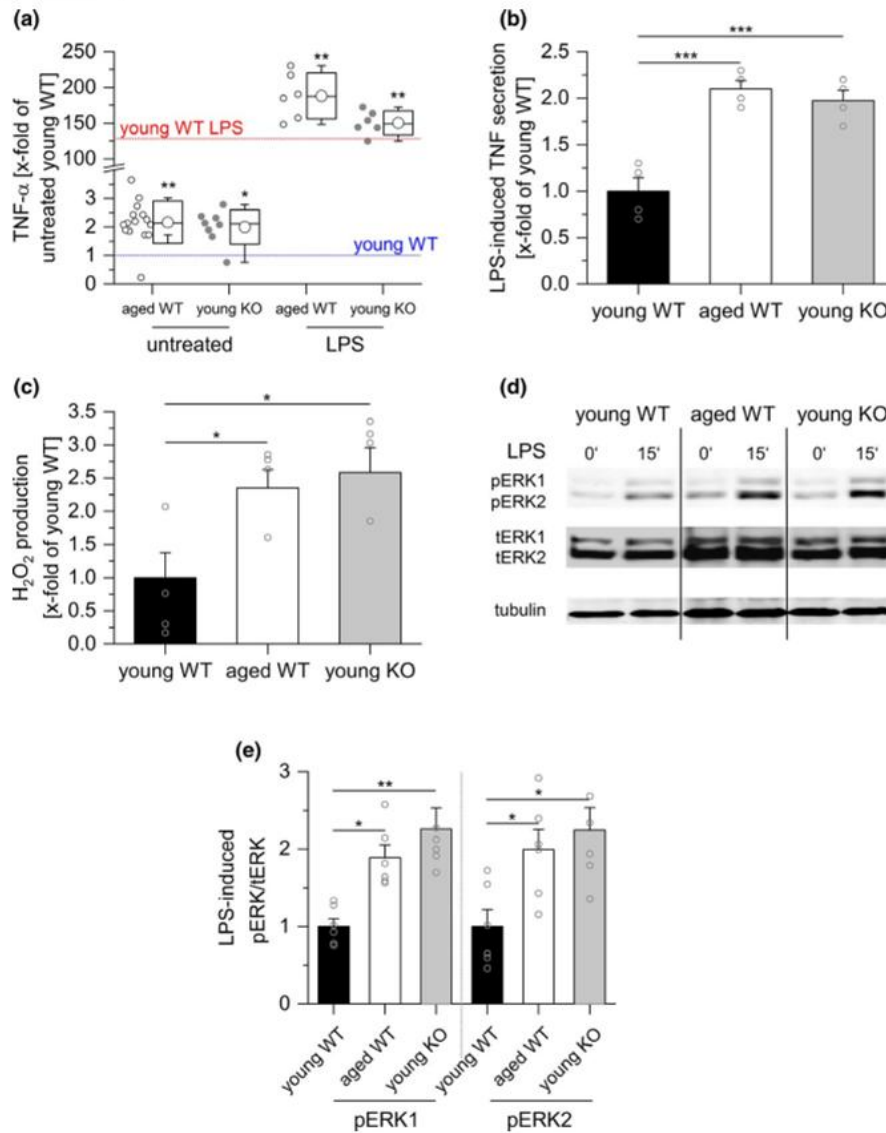


FIGURE 6 GILZ knockout mimics inflammaging. (a) Serum TNF- α levels in young GILZ knockout (KO) mice were determined by ELISA and compared with serum concentrations in young and aged wild-type (WT) mice (see Figure 1). The mean of the values for young untreated WT mice was set as 1 (blue line). The red line indicates the mean TNF- α level in LPS-treated young WT mice, expressed as x-fold of untreated young WT mice. Untreated young KO: $n = 12$, LPS-treated young KO (5 mg/kg BW, 4 hr): $n = 6$. * $p < .05$, ** $p < .01$ compared with equally treated young WT animals by ANOVA with Bonferroni's post hoc test. (b) PMs obtained from young and aged WT, as well as young KO mice, were stimulated with LPS (100 ng/ml, 4 hr), and TNF production was assessed by bioassay. Values for young WT mice were set as 1 ($n = 4$, triplicates). (c) H₂O₂ production was measured in PM supernatants by homovanillic acid assay (young WT and KO: $n = 5$, aged: $n = 6$). (d, e) ERK phosphorylation after LPS treatment (100 ng/ml, 15') was analyzed by Western blot. (d) One representative blot out of six is shown. Total ERK (tERK) and tubulin served as loading controls. (e) Densitometric analysis of LPS-induced ERK phosphorylation. pERK1/2 signal intensities were normalized to tERK1/2 and expressed as x-fold of young WT. Box plots show the 25–75th percentiles (box), mean (circle), median (line), and SD (whiskers). Bars show the mean \pm SEM, and circles within bars indicate the mean of each experiment. * $p < .05$, ** $p < .01$, *** $p < .001$ by ANOVA with Bonferroni's post hoc test

a critical role in the anti-inflammatory activity of GCs (Bereshchenko et al., 2019; Ronchetti et al., 2018). On the molecular level, GILZ facilitates its anti-inflammatory activity by binding to the pro-inflammatory transcription factors NF- κ B and activator protein (AP)-1, thereby preventing their nuclear translocation (Ayroldi et al., 2001; Bruscoli et al., 2018). GILZ also interferes with mitogen-activated protein kinase (MAPK) signaling, for example, by binding to Ras/Raf, resulting in the inhibition of downstream MAP kinases, such as ERK

(Hoppstädter et al., 2015; Ricci et al., 2019). In this manner, GILZ plays a vital role in macrophage activation (Hoppstädter et al., 2012, 2015; Hoppstädter, Diesel, et al., 2019; Hoppstädter & Kiemer, 2015). Under inflammatory conditions, repression of GILZ expression represents a regulatory mechanism that prolongs and/or increases pro-inflammatory responses in human and murine macrophages (Hoppstädter et al., 2012, 2015). In contrast, the immunosuppressive phenotype of macrophages differentiated in the presence of M-CSF and IL-10 is

associated with elevated *GILZ* expression (Seif, Hoppstädter, Breinig, & Kierner, 2017). Based on these observations and the findings on GC homeostasis in aged mice shown within the present study, we hypothesized that *GILZ* might be downregulated during inflammaging. We indeed observed reduced *GILZ* levels in blood monocytes, PMs, as well as monocytes and macrophages in various tissues, from aged mice. The analysis of publicly available GTEx datasets showed that *GILZ* also tended to be downregulated in human blood samples from aged individuals, although the expression levels showed high inter-individual variability. This may be explained by the fact that *GILZ* expression follows a circadian rhythm (Ayyar, Almon, Jusko, & DuBois, 2015) and can also be influenced by medication, most notably GCs and statins (Bereshchenko et al., 2019; Hoppstädter et al., 2020).

To assess the functional implications of *GILZ* downregulation, we compared young WT, old WT, and young myeloid-specific *GILZ* KO mice, and found that *GILZ* KO mimicked the inflammaging phenotype. These data support the hypothesis that the loss of *GILZ* in aging macrophages fuels the process of tissue inflammaging. Of note, other effectors of GC responses, such as dual-specificity phosphatase 1 (*Dusp1*) (Hoppstädter & Ammit, 2019), may also contribute to the overall effect.

In summary, the present study suggests a link between GC metabolism and the age-related inflammatory status that was unknown to date. The reduced circulating corticosterone levels, together with a decreased availability of active GCs within cells as a consequence of diminished 11 β -HSD1 expression, might contribute to the imbalance between pro- and anti-inflammatory signaling in aged macrophages, thus promoting inflammaging.

4 | EXPERIMENTAL PROCEDURES

4.1 | Materials

Fetal bovine serum (FBS, #F7524), RPMI1640 (#R0883), trypsin/EDTA (#T3924), Accutase (#L11-007-1), penicillin/streptomycin (#P433), and glutamine (#G7513) were from Sigma-Aldrich. Anti-p44/42 (ERK1/2) mouse antibody (L34F12, #4696S) and anti-phospho-p44/42 MAPK (Thr202/Tyr204) rabbit mAbs (20G11, #4376S) were obtained from Cell Signaling Technology. The anti-tubulin antibody (#T9026) was obtained from Sigma-Aldrich. The anti-GAPDH antibody (OTI2D9, #TA802519) was from OriGene. Anti-rabbit IRDye 680- and anti-mouse/anti-goat IRDye 800-conjugated secondary antibodies were from LI-COR Biosciences (#926-68071, #926-32210, #926-32214). The anti-rabbit IRDye 800-conjugated secondary antibody was obtained from Rockland (#612-132-120). Antibodies for flow cytometry, that is, anti-CD16/CD32 (Fc γ III/II Receptor) (2.4G2, #553142), anti-CD45-FITC (104, #561874), anti-CD45R/B220-FITC (RA3-6B2, #553087), anti-NK-1.1-Brilliant Violet™ 510 (PK136, #563096), anti-CD11c-APC (HL3, #550261), anti-CD11b-APC-R700 (M1/70, #564985), anti-CD14 Brilliant Violet™ 510 (rmC5-3, #740125), anti-I-A/I-E-PerCP-Cy™ 5.5 (M5/114.15.2, #562363), anti-F4/80-Brilliant Violet™ 421 (T45-2342, #565411), anti-Ly6G-APC-H7 (1A8,

#565369), anti-Ly6C-Brilliant Violet™ 421 (AL-21, #562727), and Brilliant stain buffer (#563794) were obtained from BD Biosciences. Anti-*GILZ*-PE (CFMKG15, #12-4321-82) and PE-labeled rat IgG2a isotype control (eBR2a, #12-4033-82) were from eBioscience. Anti-CD68-Alexa594 (FA-11, #137020) and the Zombie Yellow viability stain (#423104) were from BioLegend. The anti-11 β -HSD1 polyclonal goat antibody (#AF3397-SP) was from Abcam. Anti-GR rabbit mAb (D8H2, #3660) and anti-Lamin A/C rabbit polyclonal Ab (#2032) were from Cell Signaling.

The TNF- α and IL-6 ELISA kits were purchased from Cayman Chemical (#500850, #583371), the corticosterone ELISA kit (#ADI-900-097) was from Enzo, and the CRH (#CEA835M) and ACTH (#CEA836Mu) ELISA kits were from Cloud Clone. Ultrapure LPS from *Escherichia coli* K12 (#tlrl-peklps) was obtained from InvivoGen. Phorbol 12-myristate 13-acetate (PMA, #524400) was from Cayman Chemical. MTT (# M5655), actinomycin D (#A9415), homovanillic acid (HVA, #H1252), and horseradish peroxidase (#P8250) were obtained from Sigma-Aldrich. Murine M-CSF (#130-101-704) and TNF- α (#130-101-689) were obtained from Miltenyi Biotec. The 11 β -HSD1 inhibitor PF 915275 was obtained from Santa Cruz (#sc-204182). DNA oligos were provided by Eurofins Genomics. The 5x HOT FIREPol® EvaGreen® qPCR Mix Plus was from Solis BioDyne (#08-25). Other chemicals were obtained from either Sigma-Aldrich or Carl Roth unless stated otherwise.

4.2 | Mice

Mice were housed in a 12/12-hr light/dark cycle with food and water ad libitum. Myeloid-specific *GILZ* knockout (KO) mice were generated as previously described (Bruscoli et al., 2012; Hoppstädter et al., 2015). For aging studies, young (10 weeks) and aged (20–22 months) C57BL/6J mice were either not treated or treated with one intraperitoneal injection of 5 mg/kg LPS (#tlrl-smlps; InvivoGen) or vehicle (endotoxin-free DPBS, #TMS-012-A; Sigma-Aldrich) for 4 hr before sacrifice (approval number GB 3-2.4.2.2-06/2016). Female mice were used for LPS injections. Groups of untreated mice comprised both male and female mice. No sex-dependent differences in any of the readout parameters were observed (data not shown).

4.3 | Cell culture

4.3.1 | Murine peritoneal macrophages

Peritoneal macrophages were isolated from young and aged C57BL/6J mice by washing the peritoneal cavity with cold PBS-EDTA (137 mM NaCl, 2.7 mM KCl, 10.1 mM Na₂HPO₄, 1.8 mM KH₂PO₄, 5 mM Na₂EDTA, pH 7.4). The fluid was collected and centrifuged for 10 min at 350 g and 4°C. Cells were resuspended in RPMI-1640 medium supplemented with 10% FCS (FBS Good Forte, #P40-47500; PAN-Biotech), 100 U/ml penicillin, 100 μ g/ml streptomycin, and 2 mM glutamine,

seeded into a 35 mm cell culture dish, and allowed to adhere for 2 hr. Nonadherent cells were removed by washing with PBS, and PMs were detached with Accutase. The cell suspension was centrifuged, and the pellets were frozen at -80°C . Alternatively, cells were resuspended and plated in RPMI-1640 medium without FCS and, after removing the non-adherent cells after 1 hr, treated as indicated. PMs were $>95\%$ pure as determined by flow cytometric analysis of F4/80 and CD68 expression (data not shown).

4.3.2 | Murine peripheral blood leukocytes

Whole blood from young and aged C57BL/6J mice was collected in PBS-EDTA (5 mM EDTA in PBS) containing tubes and centrifuged at 500 g and 4°C for 20 min. The cell pellet was resuspended in 1 ml erythrocyte lysis buffer (155 mM NH_4Cl , 10 mM KHCO_3 , 1 mM Na_2EDTA) and incubated on ice for 15 min. After 5 min of centrifugation at 500 g and 4°C , the supernatant was discarded and the PBL pellet was frozen at -80°C until further use.

4.3.3 | Cell lines

THP-1 (#TIB202) and L929 cells (#CRL-6364) were obtained from ATCC and grown in standard medium (RPMI 1640, 10% FCS, 100 U/ml penicillin G, 100 $\mu\text{g}/\text{ml}$ streptomycin, 2 mM glutamine). THP-1 cells were differentiated into macrophage-like cells by treatment with PMA (100 ng/ml) for 48 hr and kept in serum-free medium for cortisone treatment.

4.4 | Enzyme-linked immunosorbent assay

Serum TNF- α , IL-6, corticosteroid, CRH, and ACTH levels were quantified in murine serum samples by ELISA as recommended by the supplier.

4.5 | TNF bioassay

Murine TNF (TNF- α/β) levels in cell culture supernatants were quantified by bioassay as previously described (Hoppstädter, Diesel, et al., 2019; Hoppstädter et al., 2015).

4.6 | Homovanillic acid assay

H_2O_2 levels were measured using the homovanillic acid (HVA) assay, as described previously (Kessler et al., 2017). PMs were seeded at a density of approximately 2.5×10^5 cells per well into a 24-well plate. After 1 hr, cells were washed with PBS twice and 300 μl freshly prepared HVA solution (100 μM HVA, 4 U/ml horseradish peroxidase, dissolved in PBS containing Ca^{2+} and Mg^{2+} ;

Sigma-Aldrich) was added. Cells were then incubated at 37°C for 2 hr. 40 μl HVA stop buffer (0.1 M glycine, 0.1 M NaOH, 25 mM EDTA in water; Sigma-Aldrich) were added to each well of a black 96-well plate, and 260 μl of the extracellular HVA supernatant were added. The fluorescence (312 nm excitation, 420 nm emission) was determined using a SpectraMax M5e (Molecular Devices). A standard curve of H_2O_2 (0–5 μM) was run alongside the samples. Total cellular protein concentrations used for data normalization were determined by Pierce BCA protein assay (Thermo Fisher Scientific, #23225) according to the manufacturer's instructions.

4.7 | Quantitative RT-PCR

Quantitative RT-PCR (qPCR) was performed as described previously (Dembek et al., 2017; Hoppstädter, Dembek, et al., 2019; Hoppstädter, Diesel, et al., 2019; Hoppstädter et al., 2015, 2016; Kessler et al., 2017). Total RNA from cells was isolated using the High Pure RNA Isolation Kit (#11828665001; Roche), following the manufacturer's instructions. Total RNA from murine tissue was isolated using the QIAzol lysis reagent (#79306; Qiagen) as recommended by the supplier. Residual genomic (g) DNA contamination was removed using the DNA-free™ DNA Removal Kit (#AM1906; Thermo Fisher Scientific). To verify the absence of gDNA, a SINE-PCR was performed using the GenScript Taq DNA polymerase (#E00007; GenScript). The primer sequences were as follows: forward 5'-CTTCTGGAGTGTGTTGAAGAC-3', reverse 5'-CTGGAACACTCACTGAAGAC-3'. RNA was considered free of gDNA contamination when no product was detected by agarose gel electrophoresis.

RNA was reverse-transcribed using the High Capacity cDNA Reverse Transcription Kit (#4368813; Thermo Fisher Scientific) in the presence of an RNase inhibitor (RNaseOUT™, #10777019; Thermo Fisher Scientific) following the manufacturer's instructions.

qPCR was performed using the 5x HOT FIREPol EvaGreen qPCR Mix and a total volume of 20 μl . The primer sequences and annealing temperatures for each transcript are detailed in Table S1. The CFX96 touch™ Real-Time PCR detection system (Bio-Rad Laboratories) was used to quantify gene expression. Data were analyzed either by absolute quantification, using a standard curve of the PCR product cloned into the pGEM-T Easy vector (#A1360, Promega), or with the comparative $\Delta\Delta\text{Ct}$ method. Housekeeping genes were chosen based on the literature, or after evaluating the expression stability of at least three candidate genes under the experimental conditions, using the geNorm, NormFinder, and BestKeeper Software tools. Absolute amounts of the transcript were normalized to the corresponding housekeeping genes.

4.8 | Western Blotting

Protein lysates were prepared in either SB lysis buffer (50 mM Tris-HCl, 1% SDS, 10% glycerol, 5% β -mercaptoethanol, 0.004% bromophenol blue, in water) or RIPA buffer (50 mM Tris-HCl, 1%

Triton X-100, 0.1% SDS, 0.5% sodium deoxycholate, 150 mM NaCl, in water), supplemented with a protease inhibitor cocktail (cOmplete[®] Mini, #04693124001; Roche). Samples were sonicated for 5 s and stored at -80°C until further analysis. The protein concentration in RIPA lysates was measured using the Pierce[™] BCA Protein Assay Kit (#23225; Thermo Fisher Scientific) (Dembek et al., 2017; Hoppstädter, Diesel, et al., 2019).

The cell fractionation was performed based on a published method (Suzuki, Bose, Leong-Quong, Fujita, & Riabowol, 2010). Briefly, cells were washed with ice-cold PBS once and detached by scraping. After centrifugation (4°C , 12,000 g, 30 s) the supernatant was discarded, and the cell pellet was resuspended in 0.1% NP-40 in PBS. The supernatant obtained after centrifugation (4°C , 12,000 g, 30 s) represented the cytosolic fraction. The remaining pellet, that is, the nuclear fraction, was resuspended in 0.1% NP-40 in PBS. One volume of 2x Laemmli buffer with β -mercaptoethanol (100 mM Tris-HCl, pH 6.8, 2% SDS, 20% glycerol, 10% β -mercaptoethanol, 0.008% bromophenol blue), supplemented with a protease inhibitor cocktail (cOmplete[®] Mini, #04693124001; Roche), was added to one volume of sample. After sonication, samples were boiled at 95°C for 1 min and were stored at -80°C until further analysis.

SDS-polyacrylamide gel electrophoresis, blotting, and staining were performed as described previously. Signals were detected using an Odyssey[®] Near-Infrared Imaging System and software (LI-COR Biosciences) (Dembek et al., 2017; Hoppstädter, Dembek, et al., 2019; Hoppstädter, Diesel, et al., 2019; Hoppstädter et al., 2016).

4.9 | Flow cytometry

Murine spleens and mesenteric lymph nodes were disrupted manually by carefully pushing them through a 40- μm EASYstrainer (#542040; Greiner Bio-One) while washing with RPMI 1640 without additives. Peripheral blood samples (50 μl) were collected from the tail vein and diluted in 1 ml cold PBS-EDTA. Cells were centrifuged, resuspended in erythrocyte lysis buffer (155 mM NH_4Cl , 10 mM KHCO_3 , 1 mM Na_2EDTA) and incubated on ice for 10 min. Liver samples were generated by digestion of the left lateral liver lobe using the liver dissociation kit (#130-105-8807; Miltenyi Biotec) and the gentleMACS Octo Dissociator (Miltenyi Biotec) according to the manufacturer's instructions.

Cells were washed with PBS and stained with a viability dye (Zombie Yellow, #423101; BioLegend) at room temperature in the dark for 20 min, followed by a blocking step with mouse BD Fc Block[™] (#553142) at room temperature for another 10 min. Extracellular markers were stained by incubation with an antibody cocktail diluted in Brilliant stain buffer (#563794; BD Biosciences) on ice in the dark for 30 min. The composition of the antibody cocktails is given in Table S2. Cells were washed with FACSwash (PBS with 2.5% FCS and 0.05% sodium azide) and fixed for 30 min on ice in eBioscience[™] IC Fixation Buffer (1:1 in PBS, #00-8222-49; Thermo Fisher Scientific), followed by intracellular staining with either anti-GILZ-PE or the corresponding isotype control.

For intracellular staining, cells were permeabilized with saponin buffer (0.2% saponin in FACSwash) for 10 min at room temperature and blocked on ice in saponin blocking buffer (PBS with 20% FCS and 0.2% saponin) for 30 min. After centrifugation, cells were resuspended in 200 μl saponin buffer. 100 μl of the cell suspension were incubated with anti-GILZ-PE (5 $\mu\text{g}/\text{ml}$), and 100 μl were incubated on ice and in darkness with the appropriate isotype control (5 $\mu\text{g}/\text{ml}$) for another 30 min. Subsequently, samples were washed in saponin buffer and resuspended in eBioscience[™] IC Fixation Buffer. The specificity of the anti-GILZ antibody was validated by negative staining of GILZ knockout cells (Hoppstädter et al., 2016).

Sample analysis was performed on a BD LSRFortessa (BD Biosciences) using BD FACSDiva 8.0 software. The ArC amine-reactive compensation kit (Invitrogen, #A10346), anti-rat/hamster beads (BD Biosciences, #552845), or anti-mouse plus beads (BD, #560497) were used to generate compensation controls. All gates were set by using the appropriate fluorescence minus one (FMO) control (Kessler et al., 2019).

4.10 | Determination of steroid levels via LC-HRMS/MS

The determination of steroid levels was performed using liquid chromatography-high-resolution mass spectrometry (LC-HRMS/MS). Samples were mixed 1:1 with an internal standard (cortisol-D4, 100 $\mu\text{g}/\text{ml}$ in acetonitrile containing 0.1% formic acid), and centrifuged at 18,407 g and -10°C for 10 min. The supernatant was transferred into an MS vial, and a volume of 5 μl was used for analysis.

Chromatographic separation of the analytes was carried out on a Dionex UltiMate UHPLC System (Thermo Fisher Scientific) using an Accucore[™] Phenyl-Hexyl LC column (100 mm \times 2.1 mm, 2.6 μm) heated to 40°C . Mobile phase A was water with 0.1% formic acid and ammonium formate; mobile phase B was acetonitrile with 0.1% formic acid. The LC gradient was as follows: Starting with 2% solvent B over 0.1 min, the gradient was increased to 98% solvent B until 5 min, maintained at 98% until 7.5 min, and decreased to 2% until 10 min. The flow rate was set to 600 $\mu\text{l}/\text{min}$. Detection of analytes was achieved via high-resolution mass spectrometry on a Thermo Fisher Q-Exactive Plus equipped with heated electrospray ionization (HESI)-II source. The HESI-II source conditions were as follows: sheath gas, nitrogen, at 55 arbitrary units; auxiliary gas, nitrogen, at 15 arbitrary units; temperature, 450°C ; spray voltage, 3.50 kV; ion transfer capillary temperature, 275°C ; and S-lens RF level, 55.0. Mass spectrometry was done in positive polarity mode using targeted single ion monitoring (tSIM) mode. The settings for tSIM mode were as follows: resolution, 35,000; microscans, 1; AGC target, $5e4$; maximum IT, 200 ms; isolation window, 2.0 m/z; normalized collision energy (NCE), 35; scan range, m/z 150–900; spectrum data type, profile; and under-fill ratio, 0.5%. The peak areas of the analytes were normalized using the internal standard peak area ratio.

4.11 | Determination of 11 β -HSD1 activity in peritoneal macrophages

The activity of 11 β -HSD1 in PMs from young and aged mice was measured after incubating the cells with 0.1 μ M or 1 μ M cortisone-D8 for 1 or 24 hr. At the end of treatment, supernatants were collected and cortisone-D8 and cortisol-D8 levels were analyzed as described under 1.9. The conversion to cortisol-D8 was expressed as a percentage of the total steroid amount measured and is presented as a ratio to total cellular protein content within the well. Protein concentrations were determined after lysing the cells in RIPA buffer by using the Pierce™ BCA Protein Assay Kit (#23225; Thermo Fisher Scientific) as recommended by the supplier.

4.12 | GTEX data retrieval and expression analysis

The data used for the analyses described in this manuscript were downloaded from the GTEX Portal on 02/14/20, corresponding to GTEX Analysis data V8 (GTEX Consortium, 2017). Expression data (TPM values) in the file GTEX_Analysis_2017-06-05_v8_RNASeqCv1.1.9_gene_tpm.gct were linked to meta-information using GTEX_Analysis_v8_Annotations_SampleAttributesDS.xls and GTEX_Analysis_v8_Annotations_SubjectPhenotypesDS.txt files in the R programming language.

4.13 | Statistics

Box plots show the 25–75th percentiles (box), mean (circle), median (line), and SD (whiskers). Results within bar graphs are expressed as mean \pm SEM. Statistically significant differences between means were determined using the GraphPad Prism 6.0 or Origin 2019 software. Outliers were determined using the Grubbs' test or Dixon's Q test. Unless stated otherwise, an unpaired Welch's t test was performed for the comparison of two groups, and the comparison of three or more groups was carried out by one- or two-way analysis of variance (ANOVA) followed by Bonferroni's post hoc analysis for individual differences. Where specified, median comparison of two groups was performed using Mann-Whitney U test. Results were considered significant at $p < .05$.

ACKNOWLEDGMENTS

This study was funded by the DFG (Deutsche Forschungsgemeinschaft, #KI702 to AKK). RL was supported by the Studienstiftung des deutschen Volkes.

CONFLICT OF INTEREST

The authors declare no conflict of interest.

AUTHOR CONTRIBUTIONS

JVVP, RL, AD, MHS, MRM, and JH conducted experiments and acquired and analyzed the data. JVVP and JH wrote the manuscript.

SB, CR, MRM, AKK, and JH supervised and designed research studies and revised the manuscript.

DATA AVAILABILITY STATEMENT

The data used for the analyses described in this manuscript were downloaded from the GTEX Portal on 02/14/20, corresponding to GTEX Analysis data V8 (GTEX Consortium et al., 2017).

ORCID

Alexandra K. Kiemer  <https://orcid.org/0000-0002-7224-9900>

Jessica Hoppstädter  <https://orcid.org/0000-0001-8758-1554>

REFERENCES

- Arai, Y., Martin-Ruiz, C. M., Takayama, M., Abe, Y., Takebayashi, T., Koyasu, S., ... von Zglinicki, T. (2015). Inflammation, but not telomere length, predicts successful ageing at extreme old age: A longitudinal study of semi-supercentenarians. *EBioMedicine*, 2(10), 1549–1558. <https://doi.org/10.1016/j.ebiom.2015.07.029>
- Ayala-Sumano, J. T., Velez-delValle, C., Beltran-Langarica, A., Marsch-Moreno, M., Hernandez-Mosqueira, C., & Kuri-Harcuch, W. (2013). Glucocorticoid paradoxically recruits adipose progenitors and impairs lipid homeostasis and glucose transport in mature adipocytes. *Scientific Reports*, 3, 2573. <https://doi.org/10.1038/srep02573>
- Ayrolidi, E., Migliorati, G., Bruscoli, S., Marchetti, C., Zollo, O., Cannarile, L., ... Riccardi, C. (2001). Modulation of T-cell activation by the glucocorticoid-induced leucine zipper factor via inhibition of nuclear factor kappaB. *Blood*, 98(3), 743–753. <https://doi.org/10.1182/blood.v98.3.743>
- Ayyar, V. S., Almon, R. R., Jusko, W. J., & DuBois, D. C. (2015). Quantitative tissue-specific dynamics of in vivo GILZ mRNA expression and regulation by endogenous and exogenous glucocorticoids. *Physiological Reports*, 3(6), e12382. <https://doi.org/10.14814/phy2.12382>
- Baylis, D., Bartlett, D. B., Patel, H. P., & Roberts, H. C. (2013). Understanding how we age: insights into inflammaging. *Longev Heal*, 2, 8. <https://doi.org/10.1186/20462395-2-8>
- Bandaranayake, T., & Shaw, A. C. (2016). Host resistance and immune aging. *Clinics in Geriatric Medicine*, 32(3), 415–432. <https://doi.org/10.1016/j.cger.2016.02.007>
- Bereshchenko, O., Migliorati, G., Bruscoli, S., & Riccardi, C. (2019). Glucocorticoid-induced leucine zipper: A novel anti-inflammatory molecule. *Frontiers in Pharmacology*, 10, 308. <https://doi.org/10.3389/fphar.2019.00308>
- Bouchlaka, M. N., Sckisel, G. D., Chen, M., Mirsoian, A., Zamora, A. E., Maverakis, E., ... Murphy, W. J. (2013). Aging predisposes to acute inflammatory induced pathology after tumor immunotherapy. *Journal of Experimental Medicine*, 210(11), 2223–2237. <https://doi.org/10.1084/jem.20131219>
- Bruscoli, S., Sorcini, D., Flamini, S., Gagliardi, A., Adamo, F., Ronchetti, S., ... Riccardi, C. (2018). Glucocorticoid-induced leucine zipper inhibits interferon-gamma production in B cells and suppresses colitis in mice. *Frontiers in Immunology*, 9, 1720. <https://doi.org/10.3389/fimmu.2018.01720>
- Bruscoli, S., Velardi, E., Di Sante, M., Bereshchenko, O., Venanzi, A., Coppo, M., ... Riccardi, C. (2012). Long glucocorticoid-induced leucine zipper (L-GILZ) protein interacts with ras protein pathway and contributes to spermatogenesis control. *Journal of Biological Chemistry*, 287(2), 1242–1251. <https://doi.org/10.1074/jbc.M111.316372>
- Cain, D. W., & Cidlowski, J. A. (2017). Immune regulation by glucocorticoids. *Nature Reviews Immunology*, 17(4), 233–247. <https://doi.org/10.1038/nri.2017.1>

- Chapman, K., Holmes, M., & Seckl, J. (2013). 11beta-hydroxysteroid dehydrogenases: Intracellular gate-keepers of tissue glucocorticoid action. *Physiological Reviews*, 93(3), 1139–1206. <https://doi.org/10.1152/physrev.00020.2012>
- Costantino, S., Paneni, F., & Cosentino, F. (2016). Ageing, metabolism and cardiovascular disease. *Journal of Physiology*, 594(8), 2061–2073. <https://doi.org/10.1113/JP270538>
- D'Adamo, F., Zollo, O., Moraca, R., Ayroldi, E., Bruscoli, S., Bartoli, A., ... Riccardi, C. (1997). A new dexamethasone-induced gene of the leucine zipper family protects T lymphocytes from TCR/CD3-activated cell death. *Immunity*, 7(6), 803–812. [https://doi.org/10.1016/s1074-7613\(00\)80398-2](https://doi.org/10.1016/s1074-7613(00)80398-2)
- Dembek, A., Laggai, S., Kessler, S. M., Czepukoic, B., Simon, Y., Kiemer, A. K., & Hoppstädter, J. (2017). Hepatic interleukin-6 production is maintained during endotoxin tolerance and facilitates lipid accumulation. *Immunobiology*, 222(6), 786–796. <https://doi.org/10.1016/j.imbio.2017.01.003>
- Franceschi, C., Bonafe, M., Valensin, S., Olivieri, F., De Luca, M., Ottaviani, E., & De Benedictis, G. (2000). Inflamm-aging. An evolutionary perspective on immunosenescence. *Annals of the New York Academy of Sciences*, 908, 244–254. <https://doi.org/10.1111/j.1749-6632.2000.tb06651.x>
- Franceschi, C., Garagnani, P., Parini, P., Giuliani, C., & Santoro, A. (2018). Inflammaging: A new immune-metabolic viewpoint for age-related diseases. *Nature Reviews Endocrinology*, 14(10), 576–590. <https://doi.org/10.1038/s41574-018-0059-4>
- Fulop, T., Larbi, A., Dupuis, G., Le Page, A., Frost, E. H., Cohen, A. A., ... Franceschi, C. (2017). Immunosenescence and inflamm-aging as two sides of the same coin: Friends or foes? *Frontiers in Immunology*, 8, 1960. <https://doi.org/10.3389/fimmu.2017.01960>
- Gaffey, A. E., Bergeman, C. S., Clark, L. A., & Wirth, M. M. (2016). Aging and the HPA axis: Stress and resilience in older adults. *Neuroscience and Biobehavioral Reviews*, 68, 928–945. <https://doi.org/10.1016/j.neubiorev.2016.05.036>
- Gilmour, J. S., Coutinho, A. E., Cailhier, J. F., Man, T. Y., Clay, M., Thomas, G., ... Chapman, K. E. (2006). Local amplification of glucocorticoids by 11 beta-hydroxysteroid dehydrogenase type 1 promotes macrophage phagocytosis of apoptotic leukocytes. *The Journal of Immunology*, 176(12), 7605–7611. <https://doi.org/10.4049/jimmunol.176.12.7605>
- Gong, S., Miao, Y. L., Jiao, G. Z., Sun, M. J., Li, H., Lin, J., ... Tan, J. H. (2015). Dynamics and correlation of serum cortisol and corticosterone under different physiological or stressful conditions in mice. *PLoS ONE*, 10(2), e0117503. <https://doi.org/10.1371/journal.pone.0117503>
- GTEX Consortium, Laboratory, Data Analysis & Coordinating Center (LDACC)—Analysis Working Group, Statistical Methods Groups—Analysis Working Group, Enhancing GTEX (eGTEX) Groups, NIH Common Fund, NIH/NCI, ... Montgomery, S. B. (2017). Genetic effects on gene expression across human tissues. *Nature*, 550(7675), 204–213. <https://doi.org/10.1038/nature24277>
- Gupta, D., & Morley, J. E. (2014). Hypothalamic-pituitary-adrenal (HPA) axis and aging. *Comprehensive Physiology*, 4(4), 1495–1510. <https://doi.org/10.1002/cphy.c130049>
- Herriot, H., Wrosch, C., Gouin, J. P., & Miller, G. E. (2017). Intra-individual cortisol variability and low-grade inflammation over 10 years in older adults. *Psychoneuroendocrinology*, 77, 141–149. <https://doi.org/10.1016/j.psyneuen.2016.12.010>
- Hoekstra, M., Ouweneel, A. B., Nahon, J. E., van der Geest, R., Kroner, M. J., van der Sluis, R. J., & Van Eck, M. (2019). ATP-binding cassette transporter G1 deficiency is associated with mild glucocorticoid insufficiency in mice. *Biochimica et Biophysica Acta (BBA) – Molecular and Cell Biology of Lipids*, 1864(4), 443–451. <https://doi.org/10.1016/j.bbalip.2019.01.003>
- Hoppstädter, J., & Ammit, A. J. (2019). Role of dual-specificity phosphatase 1 in glucocorticoid-driven anti-inflammatory responses. *Frontiers in Immunology*, 10, 1446. <https://doi.org/10.3389/fimmu.2019.01446>
- Hoppstädter, J., Dembek, A., Linnenberger, R., Dahlem, C., Barghash, A., Fecher-Trost, C., ... Kiemer, A. K. (2019). Toll-like receptor 2 release by macrophages: An anti-inflammatory program induced by glucocorticoids and lipopolysaccharide. *Frontiers in Immunology*, 10, 1634. <https://doi.org/10.3389/fimmu.2019.01634>
- Hoppstädter, J., Diesel, B., Eifler, L. K., Schmid, T., Brüne, B., & Kiemer, A. K. (2012). Glucocorticoid-induced leucine zipper is downregulated in human alveolar macrophages upon Toll-like receptor activation. *European Journal of Immunology*, 42(5), 1282–1293. <https://doi.org/10.1002/eji.201142081>
- Hoppstädter, J., Diesel, B., Linnenberger, R., Hachenthal, N., Flamini, S., Minet, M., ... Kiemer, A. K. (2019). Amplified host defense by Toll-like receptor-mediated downregulation of the glucocorticoid-induced leucine zipper (GILZ) in macrophages. *Frontiers in Immunology*, 9, 3111. <https://doi.org/10.3389/fimmu.2018.03111>
- Hoppstädter, J., Hachenthal, N., Valbuena-Perez, J. V., Lampe, S., Astanina, K., Kunze, M. M., ... Kiemer, A. K. (2016). Induction of glucocorticoid-induced leucine zipper (GILZ) contributes to anti-inflammatory effects of the natural product curcumin in macrophages. *Journal of Biological Chemistry*, 291(44), 22949–22960. <https://doi.org/10.1074/jbc.M116.733253>
- Hoppstädter, J., Kessler, S. M., Bruscoli, S., Huwer, H., Riccardi, C., & Kiemer, A. K. (2015). Glucocorticoid-induced leucine zipper: A critical factor in macrophage endotoxin tolerance. *The Journal of Immunology*, 194(12), 6057–6067. <https://doi.org/10.4049/jimmunol.1403207>
- Hoppstädter, J., & Kiemer, A. K. (2015). Glucocorticoid-induced leucine zipper (GILZ) in immunosuppression: Master regulator or bystander? *Oncotarget*, 6(36), 38446–38457. <https://doi.org/10.18632/oncotarget.6197>
- Hoppstädter, J., Valbuena Perez, J. V., Linnenberger, R., Dahlem, C., Legroux, T. M., Hecksteden, A., ... Kiemer, A. K. (2020). The glucocorticoid-induced leucine zipper mediates statin-induced muscle damage. *The FASEB Journal*, 34(3), 4684–4701. <https://doi.org/10.1096/fj.201902557RRR>
- Jackaman, C., Tomay, F., Duong, L., Abdol Razak, N. B., Pixley, F. J., Metharom, P., & Nelson, D. J. (2017). Aging and cancer: The role of macrophages and neutrophils. *Ageing Research Reviews*, 36, 105–116. <https://doi.org/10.1016/j.arr.2017.03.008>
- Kennedy, B. K., Berger, S. L., Brunet, A., Campisi, J., Cuervo, A. M., Epel, E. S., ... Sierra, F. (2014). Geroscience: Linking aging to chronic disease. *Cell*, 159(4), 709–713. <https://doi.org/10.1016/j.cell.2014.10.039>
- Kessler, S. M., Hoppstädter, J., Hosseini, K., Laggai, S., Haybaeck, J., & Kiemer, A. K. (2019). Lack of Kupffer cell depletion in diethylnitrosamine-induced hepatic inflammation. *Journal of Hepatology*, 70(4), 813–815. <https://doi.org/10.1016/j.jhep.2018.11.018>
- Kessler, S. M., Lederer, E., Laggai, S., Golob-Schwarzl, N., Hosseini, K., Petzold, J., ... Haybaeck, J. (2017). IMP2/IGF2BP2 expression, but not IMP1 and IMP3, predicts poor outcome in patients and high tumor growth rate in xenograft models of gallbladder cancer. *Oncotarget*, 8(52), 89736–89745. <https://doi.org/10.18632/oncotarget.21116>
- Kizaki, T., Ookawara, T., Oh-Ishi, S., Itoh, Y., Iwabuchi, K., Onoe, K., ... Ohno, H. (1998). An increase in basal glucocorticoid concentration with age induces suppressor macrophages with high-density Fc gamma RII/III. *Immunology*, 93(3), 409–414. <https://doi.org/10.1046/j.1365-2567.1998.00433.x>
- Kizaki, T., Suzuki, K., Ookawara, T., Izawa, T., Saitoh, D., Oh-Ishi, S., ... Ohno, H. (2002). Stress- and aging-associated modulation of macrophage functions. *Environmental Health and Preventive Medicine*, 6(4), 218–228. <https://doi.org/10.1007/BF02897973>
- Lee, S. H., Lee, J. H., Lee, H. Y., & Min, K. J. (2019). Sirtuin signaling in cellular senescence and aging. *BMB Reports*, 52(1), 24–34. <https://doi.org/10.5483/BMBRep.2019.52.1.290>

- Lopez-Otin, C., Blasco, M. A., Partridge, L., Serrano, M., & Kroemer, G. (2013). The hallmarks of aging. *Cell*, 153(6), 1194–1217. <https://doi.org/10.1016/j.cell.2013.05.039>
- Minciullo, P. L., Catalano, A., Mandraffino, G., Casciaro, M., Crucitti, A., Maltese, G., ... Basile, G. (2016). Inflammaging and anti-inflammaging: The role of cytokines in extreme longevity. *Archivum Immunologiae Et Therapiae Experimentalis*, 64(2), 111–126. <https://doi.org/10.1007/s00005-015-0377-3>
- Morano, M. I., Vazquez, D. M., & Akil, H. (1994). The role of the hippocampal mineralocorticoid and glucocorticoid receptors in the hypothalamo-pituitary-adrenal axis of the aged Fisher rat. *Molecular and Cellular Neurosciences*, 5(5), 400–412. <https://doi.org/10.1006/mcne.1994.1050>
- Mosser, D. M., & Edwards, J. P. (2008). Exploring the full spectrum of macrophage activation. *Nature Reviews Immunology*, 8(12), 958–969. <https://doi.org/10.1038/nri2448>
- Oakley, R. H., & Cidlowski, J. A. (2013). The biology of the glucocorticoid receptor: New signaling mechanisms in health and disease. *The Journal of Allergy and Clinical Immunology*, 132(5), 1033–1044. <https://doi.org/10.1016/j.jaci.2013.09.007>
- Prattichizzo, F., Bonafe, M., Olivieri, F., & Franceschi, C. (2016). Senescence associated macrophages and "macroph-aging": Are they pieces of the same puzzle? *Aging*, 8(12), 3159–3160. <https://doi.org/10.18632/aging.101133>
- Raison, C. L., & Miller, A. H. (2003). When not enough is too much: The role of insufficient glucocorticoid signaling in the pathophysiology of stress-related disorders. *American Journal of Psychiatry*, 160(9), 1554–1565. <https://doi.org/10.1176/appi.ajp.160.9.1554>
- Ricci, E., Ronchetti, S., Gabrielli, E., Pericolini, E., Gentili, M., Roselletti, E., ... Riccardi, C. (2019). GILZ restrains neutrophil activation by inhibiting the MAPK pathway. *Journal of Leukocyte Biology*, 105(1), 187–194. <https://doi.org/10.1002/JLB.3AB0718-255R>
- Ronchetti, S., Migliorati, G., Bruscoli, S., & Riccardi, C. (2018). Defining the role of glucocorticoids in inflammation. *Clinical Science (Lond)*, 132(14), 1529–1543. <https://doi.org/10.1042/CS20171505>
- Sebastian, C., Espia, M., Serra, M., Celada, A., & Lloberas, J. (2005). MacrophAging: A cellular and molecular review. *Immunobiology*, 210(2–4), 121–126. <https://doi.org/10.1016/j.imbio.2005.05.006>
- Seif, M., Hoppstädter, J., Breinig, F., & Kiemer, A. K. (2017). Yeast-mediated mRNA delivery polarizes immuno-suppressive macrophages towards an immuno-stimulatory phenotype. *European Journal of Pharmaceutics and Biopharmaceutics*, 117, 1–13. <https://doi.org/10.1016/j.ejpb.2017.03.008>
- Suzuki, K., Bose, P., Leong-Quong, R. Y., Fujita, D. J., & Riabowol, K. (2010). REAP: A two minute cell fractionation method. *BMC Research Notes*, 3, 294. <https://doi.org/10.1186/1756-0500-3-294>
- Tchkonia, T., Zhu, Y., van Deursen, J., Campisi, J., & Kirkland, J. L. (2013). Cellular senescence and the senescent secretory phenotype: Therapeutic opportunities. *J Clin Invest*, 123(3), 966–972. <https://doi.org/10.1172/JCI64098>
- van Deursen, J. M. (2014). The role of senescent cells in ageing. *Nature*, 509(7501), 439–446. <https://doi.org/10.1038/nature13193>
- Wynn, T. A., Chawla, A., & Pollard, J. W. (2013). Macrophage biology in development, homeostasis and disease. *Nature*, 496(7446), 445–455. <https://doi.org/10.1038/nature12034>
- Yuan, X., Klein, D., Kerscher, S., West, B. L., Weis, J., Katona, I., & Martini, R. (2018). Macrophage depletion ameliorates peripheral neuropathy in aging mice. *Journal of Neuroscience*, 38(19), 4610–4620. <https://doi.org/10.1523/JNEUROSCI.3030-17.2018>
- Zambrano, E., Reyes-Castro, L. A., & Nathanielsz, P. W. (2015). Aging, glucocorticoids and developmental programming. *Age*, 37(3), 9774. <https://doi.org/10.1007/s11357-015-9774-0>
- Zhang, T. Y., & Daynes, R. A. (2007). Macrophages from 11beta-hydroxysteroid dehydrogenase type 1-deficient mice exhibit an increased sensitivity to lipopolysaccharide stimulation due to TGF-beta-mediated up-regulation of SHIP1 expression. *The Journal of Immunology*, 179(9), 6325–6335. <https://doi.org/10.4049/jimmunol.179.9.6325>
- Zhou, D., Huang, C., Lin, Z., Zhan, S., Kong, L., Fang, C., & Li, J. (2014). Macrophage polarization and function with emphasis on the evolving roles of coordinated regulation of cellular signaling pathways. *Cellular Signalling*, 26(2), 192–197. <https://doi.org/10.1016/j.cellsig.2013.11.004>

SUPPORTING INFORMATION

Additional supporting information may be found online in the Supporting Information section.

How to cite this article: Valbuena Perez JV, Linnenberger R, Dembek A, et al. Altered glucocorticoid metabolism represents a feature of macroph-aging. *Aging Cell*. 2020;19:e13156. <https://doi.org/10.1111/acel.13156>

Supporting information

Altered glucocorticoid metabolism represents a feature of macroph-aging

Jenny Vanessa Valbuena Perez^{1*}, Rebecca Linnenberger^{1*}, Anna Dembek¹, Stefano Bruscoli², Carlo Riccardi², Marcel H. Schulz³, Markus R. Meyer⁴, Alexandra K. Kiemer¹, Jessica Hoppstädter^{1#}

¹Pharmaceutical Biology, Department of Pharmacy, Saarland University, Saarbrücken, Germany

²Pharmacology, Department of Medicine, Perugia University, Perugia, Italy

³Institute for Cardiovascular Regeneration, Goethe University Hospital, Frankfurt, Germany

⁴Department of Experimental and Clinical Toxicology, Institute of Experimental and Clinical Pharmacology and Toxicology, Center for Molecular Signaling (PZMS), Saarland University, Homburg, Germany

*Equal contribution.

#Correspondence:

Jessica Hoppstädter, Ph.D.

Pharmaceutical Biology

Department of Pharmacy

Saarland University

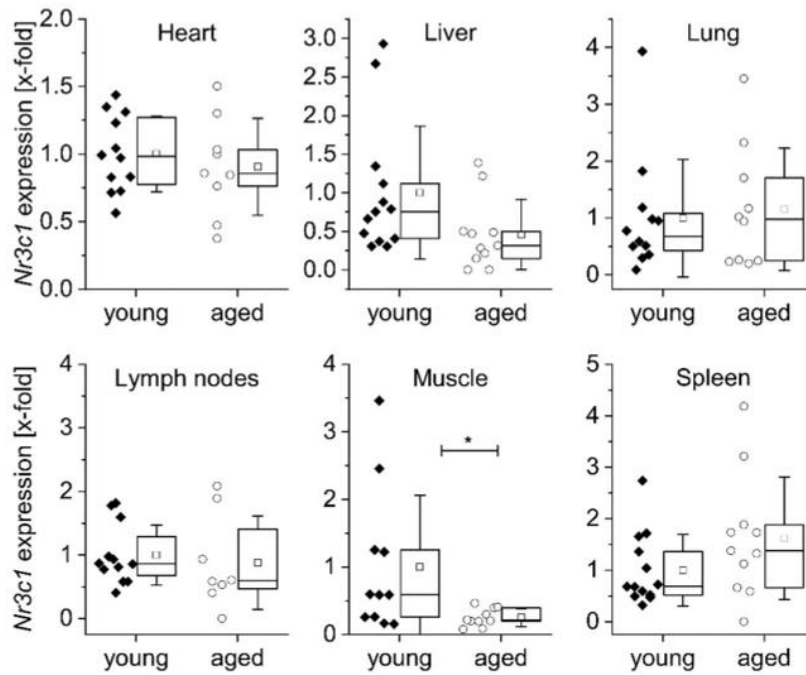
66123 Saarbrücken, Germany

Phone: +49 681 302 57304

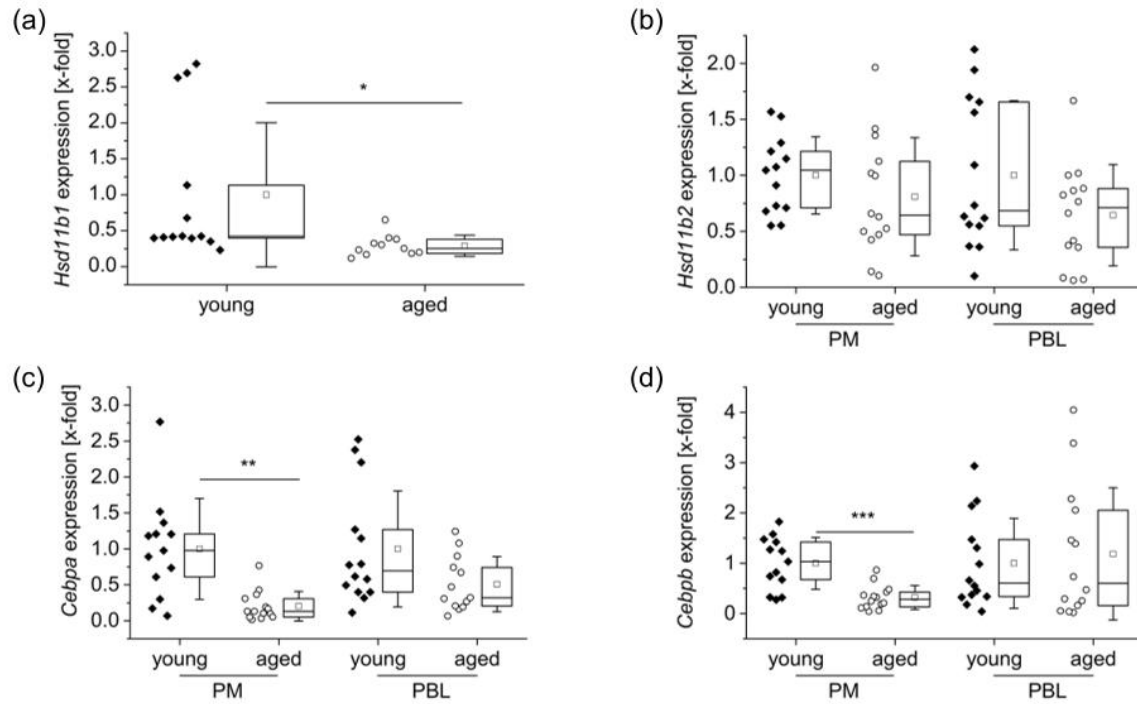
Fax: +49 681 302 57302

Email: j.hoppstaedter@mx.uni-saarland.de

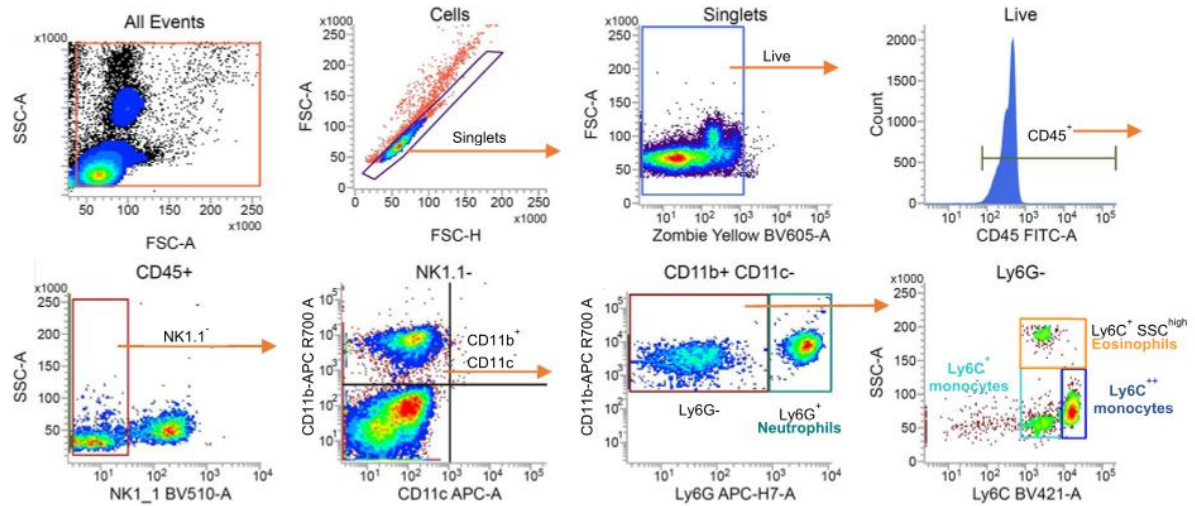
1. Supplementary figures



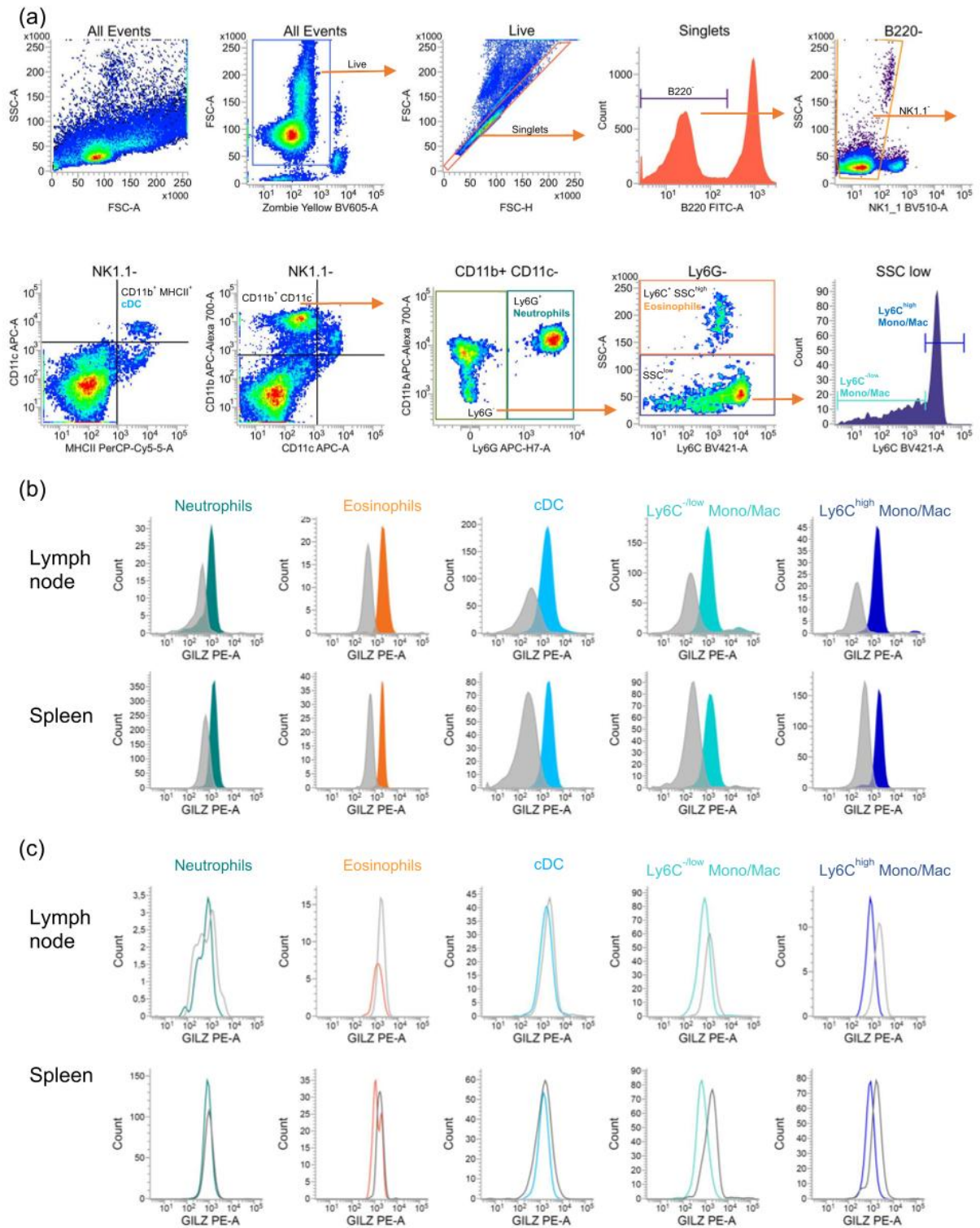
Supplementary figure S1. *GR* expression across tissues. *GR* (*Nr3c1*) expression in tissues from young and aged mice. mRNA expression levels were measured in heart, liver, lung, lymph nodes, skeletal muscle, and spleen tissues, normalized against the housekeeping gene *Ppia*, and expressed as x-fold of young (n=9-13). Box plots show the 25–75th percentiles (box), mean (square), median (line), and SD (whiskers). *p<0.05 relative to young mice, as determined by two-tailed t-test.



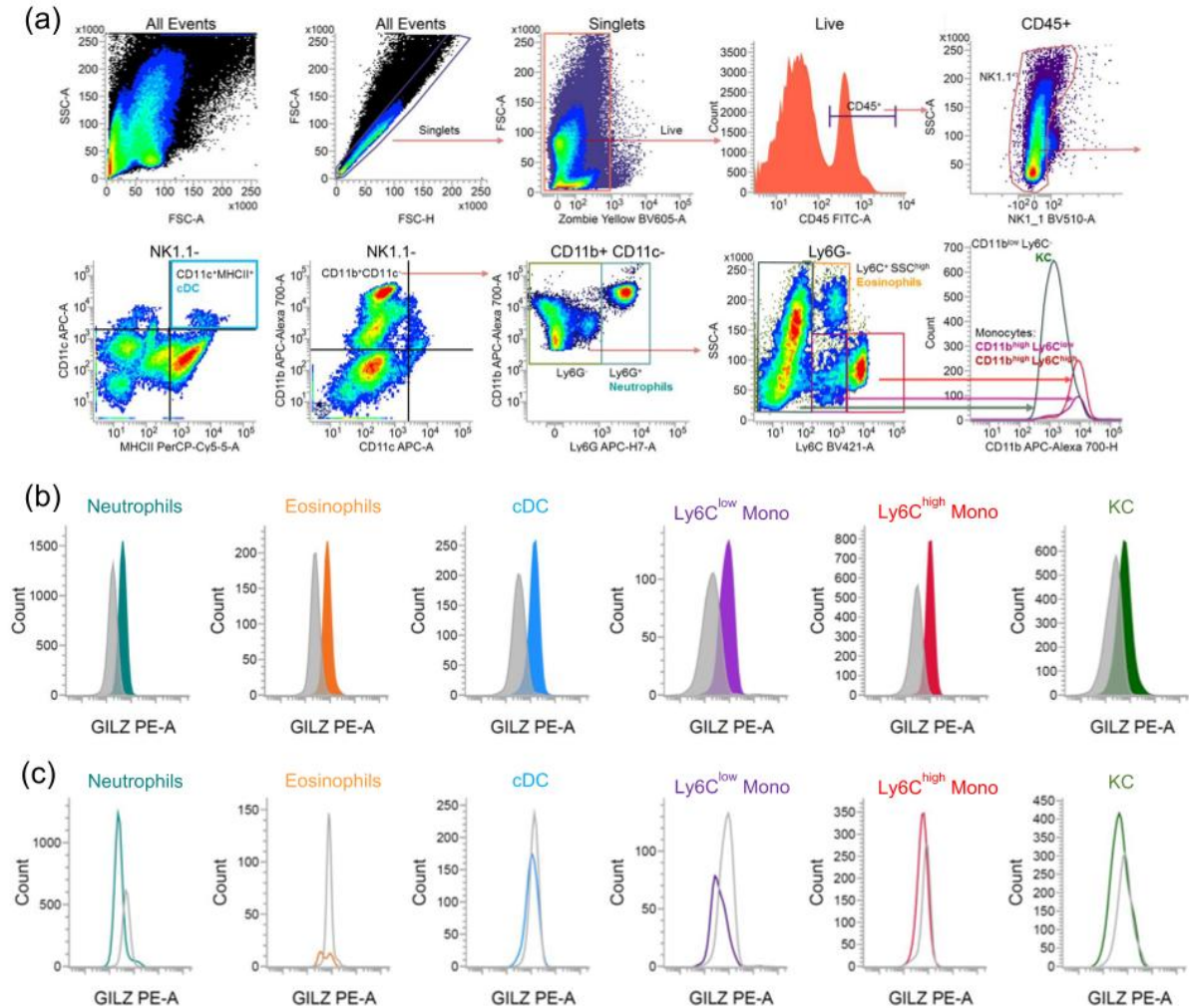
Supplementary figure S2. Alterations in the expression of genes involved in GC metabolism. (a) *Hsd11b1* expression in livers of young and aged mice (young: n=13, aged: n=11) was measured by qPCR, normalized to *Ppia*, and expressed as x-fold of young. (b-d): *Hsd11b2* (b), *Cebpa* (c), and *Cebpb* (d) expression levels were measured in PMs and PBLs (n=14), normalized to *Ppia*, and expressed as x-fold of young. Box plots show the 25–75th percentiles (box), mean (square), median (line), and SD (whiskers). * $p < 0.05$, ** $p < 0.01$, *** $p < 0.001$ by two-tailed t-test.



Supplementary figure S3. Determination of *GILZ* expression in myeloid cells in peripheral blood from young and aged mice. A: Gating strategy for the quantification of *GILZ* in myeloid cells from tail vein blood. Gates were set using fluorescence minus one (FMO) controls (not shown).



Supplementary figure S4. Determination of GILZ expression in myeloid cells in lymphoid tissues from young and aged mice. (a) Gating strategy for the quantification of GILZ in myeloid cells from lymphoid tissues. Gates were set using fluorescence minus one (FMO) controls (not shown). (b) Representative histograms showing GILZ expression in myeloid subsets in young mice. Colored: GILZ signal, gray: isotype control. (c) Representative histograms showing GILZ signals in cells from aged and young mice. Gray line: young; colored line: aged.



Supplementary figure S5. Determination of GILZ expression in myeloid cells in liver tissue from young and aged mice. (a) Gating strategy for the quantification of GILZ in myeloid cells from liver tissue. Gates were set using fluorescence minus one (FMO) controls (not shown). (b) Representative histograms showing GILZ expression in myeloid subsets in young mice. Coloured: GILZ signal, gray: isotype control. (c) Representative histograms showing GILZ signals in cells from aged and young mice. Gray line: young; colored line: aged.

2. Supplementary tables

Supplementary table S1: qPCR conditions.

Gene	NCBI Accession number	Forward primer sequence 5'-3'	Reverse primer sequence 5'-3'	µl primer [10 µM] / 20 µl reaction	Annealing T (°C)
<i>Human</i>					
<i>ACTB</i>	NM_001101.3	TGCGTGACATTAAGG AGAAG	GTCAGGCAGCTCGTA GCTCT	0.5	60
<i>ANXA1</i>	NM_000700.3	CTCACAGCTATCGTGA AGTGC	TGCCATTATGGCGAGTT CCAA	0.5	60
<i>DUSP1</i>	NM_004417.4	CAGCTGCTGCAGTTT GAGTC	AGGTAGCTCAGCGCA CTGTT	0.5	60
<i>SGK1</i>	NM_005627.4	GGAAGTCTGCAAGGAG AACATTG	GCTGCTTATGAAGCAC CTCAG	0.5	60
<i>TSC22D3 (GILZ)</i>	NM_004089.3	TCCTGTCTGAGCCCTG AAGAG	AGCCACTTACACCGCA GAAC	0.5	60
<i>Mouse</i>					
<i>Abca1</i>	NM_013454.3	ACAAGTCCATCGTGTC TCGC	GGGATGCTTGATCTGC CGTA	0.5	60
<i>Abcg1</i>	NM_009593.2	ACACCGATGTGAACC CGTTT	CAGATGTGTCAGGAC CGAGT	0.5	60
<i>ApoE</i>	NM_009696.3	CAGTGGCCCAGGAGA ATCAAT	TCACAGAGACTCAGA ATGTGC	0.5	60
<i>Cdkn1a</i>	NM_007669.5	GACCAGCCTGACAGA TTTCTA	TGGGCACTTCAGGGTT TTCT	0.5	60
<i>Cdkn2a</i>	NM_009877.2	CGGGGACATCAAGAC ATCGT	GCCGGATTTAGCTCTG CTCT	0.5	60
<i>Cebpa</i>	NM_0012875 23.1	TTCGGGTCGCTGGATC TCTA	TCAAGGAGAAACCAC CACGG	0.5	60
<i>Cebpb</i>	NM_0012877 39.1	GGAGACGCAGCACAA GGT	AGCTGCTTGAACAAG TTCCG	0.5	60
<i>Csnk2a2</i>	NM_009974.3	GTAAAGGACCCTGTGT CAAAGA	GTCAGGATCTGGTAG AGTTGCT	0.8	60
<i>Cyp11a2</i>	NM_019779.4	ATGAGATCCCTTCCCC TGGC	TGCCAGCTTCTCCCT GTAAA	0.5	60
<i>Hmgcr</i>	NM_008255.2	ATCCAGGAGCGAACC AAGAGAG	CAGAAGCCCCAAGCA CAAAC	0.5	60
<i>Hsd11b1</i>	NM_008288.2	GGAACCCAGGAAGGA AGATCA	CAGGCAGGACTGTTCT AAGAC	0.5	60
<i>Hsd11b2</i>	NM_008289.2	AACCTCTGGGAGAAA CGCAAG	GGCATCTACAAGTGG GCTAAGG	0.5	60
<i>I11b</i>	NM_008361.3	CCAAAAGATGAAGGG CTGCTT	GGAAGGTCCACGGGA AAGAC	0.5	60
<i>I16</i>	NM_031168.2	AAGAAATGATGGATG CTACCAAAGT	GTACTCCAGAAGACC AGAGGAAATT	0.4	60

<i>Ldlr</i>	NM_010700.3	TCAATGGGGGCAATC GGAAA	ACACTTTGTCCTCATA GATGGC	0.5	60
<i>Nr3c1</i>	NM_008173.3	AAAGAGCTAGGAAAA GCCATTGTC	TCAGCTAACATCTCTG GGAATTCA	0.5	61
<i>Ppia</i>	NM_008907.1	GGCCGATGACGAGCC C	TGTCTTTGGAAC TTG TCTGC	0.5	58
<i>Scarb1</i>	NM_016741.2	TCCTGAAGACACTATA AGCCCC	GTGCGGACAGGTGTG ACAT	0.5	60
<i>Sirt1</i>	NM_019812.3	TGGAGCAGGTTGCAG GAATC	GGCACCGAGGAACTA CCTGAT	0.5	60
<i>Stard1</i>	NM_011485.5	TGTACCAAGCGCAGA GGTTC	GGCCGTGTT CAGCTCT GATG	0.5	60
<i>Tnf</i>	NM_013693.2	CCATTCCTGAGTTCTG CAAAGG	AGGTAGGAAGGCCTG AGATCTTATC	0.5	60
<i>Tsc22d3</i> (<i>Gilt3</i>)	NM_010286.4	GCTGCTTGAGAAGAA CTCCCA	GAAC TTTCCAGTTGC TCGGG	0.5	60

Supplementary table S2: Antibody cocktails. All antibodies were used at a final concentration of 5 µg/ml.

Extracellular staining cocktail	
<i>Peripheral blood / Liver</i>	<i>Lymphoid tissues</i>
CD45-FITC	CD45R/B220-FITC
NK-1.1Brilliant Violet™ 510	NK-1.1Brilliant Violet™ 510
CD11c-APC	CD11c-APC
CD11b-APC-R700	CD11b-APC-R700
I-A/I-EPerCP-Cy™5.5	I-A/I-EPerCP-Cy™5.5
Ly-6G-APC-H7	Ly-6G-APC-H7
Ly-6C-Brilliant Violet™ 421	Ly-6C-Brilliant Violet™ 421

3.3. The Glucocorticoid-Induced Leucine Zipper (GILZ) Mediates Statin-Induced Muscle Damage

FASEBJ **2019**, doi: 10.1096/fj.201902557RRR

J. Hoppstädter, J. V. Valbuena Perez, R. Linnenberger, C. Dahlem, A. Hecksteden, W. K. F. Tse, S. Bruscoli, and S. Flamini conducted experiments. J. Hoppstädter, J. V. Valbuena Perez, R. Linnenberger, T. M. Legroux and C. Dahlem acquired and analyzed data. J. V. Valbuena Perez, J. Hoppstädter, A. K. Kiemer, and R. Linnenberger wrote the manuscript. A. Andreas, J. Herrmann, C. Herr, S. Bruscoli, and W. K. F. Tse supported the mouse and zebrafish experiments. S. Bruscoli, C. Riccardi, A. K. Kiemer, and J. Hoppstädter designed research studies. J. Herrmann, R. Müller, R. Bals, C. Riccardi, S. Bruscoli, A. K. Kiemer, A. Hecksteden, and J. Hoppstädter supervised the experiments, and all authors revised the manuscript. A. K. Kiemer initiated the study.

The author was involved in the design, performance, and analysis of the reporter gene assay and the respective cell culture. She performed crystal violet assays, analyzed muscle biopsies, and performed parts of the quantitative real-time PCR experiments. She prepared the corresponding figures, analyzed and prepared GEO datasets and wrote parts of the manuscript. Finally, she critically reviewed the manuscript and submitted the manuscript.

© Hoppstädter, Valbuena Perez, Linnenberger, Dahlem, Legroux, Hecksteden, Tse, Flamini, Andreas, Herrmann, Herr, Müller, Meyer, Bals, Riccardi, Bruscoli, Kiemer. This is an open-access article distributed under the terms of the Creative Commons Attribution Licence (CC BY).

Received: 8 October 2019 | Revised: 21 January 2020 | Accepted: 21 January 2020

DOI: 10.1096/fj.201902557RRR

RESEARCH ARTICLE



The glucocorticoid-induced leucine zipper mediates statin-induced muscle damage

Jessica Hoppstädter^{1,2} | Jenny Vanessa Valbuena Perez¹ | Rebecca Linnenberger¹ | Charlotte Dahlem¹ | Thierry M. Legroux¹ | Anne Hecksteden³ | William K. F. Tse⁴ | Sara Flamini² | Anastasia Andreas⁵ | Jennifer Herrmann⁵ | Christian Herr⁶ | Rolf Müller⁵ | Tim Meyer³ | Robert Bals⁶ | Carlo Riccardi² | Stefano Bruscoli² | Alexandra K. Kiemer¹

¹Department of Pharmacy, Pharmaceutical Biology, Saarland University, Saarbrücken, Germany

²Department of Medicine, Section of Pharmacology, University of Perugia, Perugia, Italy

³Institute of Sports and Preventive Medicine, Saarland University, Saarbrücken, Germany

⁴Center for Promotion of International Education and Research, Faculty of Agriculture, Kyushu University, Fukuoka, Japan

⁵Department of Microbial Natural Products, Helmholtz Institute for Pharmaceutical Research Saarland (HIPS), Saarbrücken, Germany

⁶Department of Internal Medicine V—Pulmonology, Allergology and Critical Care Medicine, Saarland University, Homburg, Germany

Correspondence

Alexandra K. Kiemer, Pharmaceutical Biology, Saarland University, Saarbrücken D-66123, Germany.
Email: pharm.bio.kiemer@mx.uni-saarland.de

Abstract

Statins, the most prescribed class of drugs for the treatment of hypercholesterolemia, can cause muscle-related adverse effects. It has been shown that the glucocorticoid-induced leucine zipper (GILZ) plays a key role in the anti-myogenic action of dexamethasone. In the present study, we aimed to evaluate the role of GILZ in statin-induced myopathy. Statins induced GILZ expression in C2C12 cells, primary murine myoblasts/myotubes, primary human myoblasts, and in vivo in zebrafish embryos and human quadriceps femoris muscle. *Gilz* induction was mediated by FOXO3 activation and binding to the *Gilz* promoter, and could be reversed by the addition of geranylgeranyl, but not farnesyl, pyrophosphate. Atorvastatin decreased Akt phosphorylation and increased cleaved caspase-3 levels in myoblasts. This effect was reversed in myoblasts from GILZ knockout mice. Similarly, myofibers isolated from knockout animals were more resistant toward statin-induced cell death than their wild-type counterparts. Statins also impaired myoblast differentiation, and this effect was accompanied by GILZ induction. The in vivo relevance of our findings was supported by the observation that *gilz* overexpression in zebrafish embryos led to impaired embryonic muscle development. Taken together, our data point toward GILZ as an essential mediator of the molecular mechanisms leading to statin-induced muscle damage.

Abbreviations: CVD, cardiovascular disease; DM, differentiation medium; FDB, *flexor digitorum brevis*; FHRE, forkhead-responsive element; FPP, farnesyl pyrophosphate; GGPP, geranylgeranyl pyrophosphate; GILZ, glucocorticoid-induced leucine zipper; HMG-CoA, 3-hydroxy-3-methylglutaryl coenzyme A; hpf, hours post fertilization; MHC, myosin heavy chain; MRF, muscle regulatory factor; MTT, 3-(4,5-dimethylthiazol-2-yl)-2,5-diphenyltetrazolium bromide; MVA, mevalonate; SAMS, statin-associated muscle symptoms.

Jessica Hoppstädter and Jenny Vanessa Valbuena Perez equally contributed to this work.

This is an open access article under the terms of the Creative Commons Attribution-NonCommercial-NoDerivs License, which permits use and distribution in any medium, provided the original work is properly cited, the use is non-commercial and no modifications or adaptations are made.

© 2020 The Authors. The FASEB Journal published by Wiley Periodicals, Inc. on behalf of Federation of American Societies for Experimental Biology

Funding information

Deutsche Forschungsgemeinschaft,
Grant/Award Number: KI702;
German Academic Exchange
Service; Studienstiftung

KEYWORDS

flexor digitorum brevis, HMG-CoA, muscle wasting, statin-associated muscle symptoms, *Tsc22d3*

1 | INTRODUCTION

Statins are the first line of treatment in the management of hyperlipidemia and the prevention of cardiovascular disease (CVD).^{1,2} These drugs are inhibitors of the 3-hydroxy-3-methylglutaryl coenzyme A (HMG-CoA) reductase enzyme, preventing the biosynthesis of cholesterol in the liver by blocking the mevalonate pathway and, as a consequence, enhancing clearance of circulating LDL-cholesterol.^{3,4} Since their introduction in 1987, statin prescription rates have risen, as shown by several studies in different populations,⁵⁻⁷ positioning them among the most prescribed drug classes worldwide. Given the high prevalence of CVD and the favorable data on CVD prevention by statins,^{8,9} this tendency seems to be maintained.

Statins have a satisfactory safety profile, their most relevant adverse effect being skeletal muscle toxicity.¹ Statin-associated muscle symptoms (SAMS) have an incidence of 5%-29% in clinical practice,^{1,10} can range from mild myalgia to, in rare cases, fatal rhabdomyolysis,¹¹ and are a frequent cause for nonadherence to treatment or its discontinuation.¹² Although several studies have been conducted, and a number of risk factors that contribute to the onset of SAMS have been described, such as sex, pharmacokinetic differences, or genetic factors,^{13,14} the molecular mechanisms leading to myopathy are still not fully understood.

The glucocorticoid-induced leucine zipper (GILZ) was first described as a dexamethasone-induced, immunomodulatory protein.¹⁵ Since then, it has been shown that GILZ basal expression is not restricted to immune cells but is extended to several tissues, including skeletal muscle.¹⁶ GILZ plays multiple roles in both glucocorticoid and non-glucocorticoid-mediated cellular processes¹⁷ beyond its immune-modulating function. For instance, studies demonstrated a role for GILZ in inhibition of adipocyte differentiation,¹⁸ in sodium homeostasis in the kidney,^{19,20} and in spermatogenesis.²¹ Of particular interest is the role described for GILZ in the regulation of skeletal muscle differentiation: GILZ is strongly induced by dexamethasone, mediating its antimyogenic effects *via* inhibition of the transcriptional activity of an early muscle regulatory factor (MRF), MyoD.²²

In the present study, we aimed to test the hypothesis that GILZ plays a role in the onset of SAMS, focusing on both myotoxic and antimyogenic effects.

2 | MATERIALS AND METHODS

2.1 | Reagents

Cell culture reagents, atorvastatin, simvastatin lactone, cerivastatin, and mevalonic acid lithium salt were obtained from Sigma-Aldrich (St. Louis, MO, USA). The simvastatin sodium salt, geranylgeranyl pyrophosphate (GGPP), and farnesyl pyrophosphate (FPP) were obtained from Cayman Chemicals (Ann Arbor, MI, USA). Statin stock solutions were prepared in DMSO.

2.2 | Cell line

C2C12 cells were maintained in high-glucose DMEM supplemented with 10% FBS, 100 U/mL penicillin, 100 µg/mL streptomycin, and 2 mM glutamine. For inducing differentiation, confluent cell layers were cultured in high-glucose DMEM supplemented with 2% horse serum, penicillin/streptomycin, and glutamine (differentiation medium, DM), with medium change every other day. All cells were cultured at 37°C in a humidified atmosphere with 5% CO₂. For experiments, cells were seeded at a density of 2.5×10^4 cells/cm² (or 5×10^4 cells/cm² for differentiation).

2.3 | Mice

C57BL/6J mice were housed in a 12/12-hour light/dark cycle with food and water *ad libitum*. GILZ knockout (KO) mice were generated as previously described.²¹ Animal care and maintenance were in compliance with regulations in Italy (DL 26/2014) and Europe (EU Directive 2010/63/EU).

2.4 | *Flexor digitorum brevis* (FDB) muscle fibers

FDB fibers were isolated from wild-type (WT) or GILZ KO mice following a protocol adapted from the literature.^{23,24} The FDB muscles were dissected under a stereomicroscope and digested in a 0.2% collagenase A solution in DMEM for 60 minutes. Then, the myofibers were carefully separated under a stereo dissecting microscope, dispersed in DMEM containing 10% horse serum by drawing through a series of

pipette tips with gradually decreasing diameter and purified by sedimentation steps. Pure fibers were plated in laminin-coated cell culture dishes and cultured in DMEM supplemented with 20% serum replacement 2, 1% horse serum, penicillin/streptomycin, and glutamine.

2.5 | Primary human myoblasts

Primary human myoblasts (#CC-2580) were obtained from Lonza (Basel, Switzerland) and grown in Skeletal Muscle Growth Medium-2 (SkGM-2 basal medium, Lonza) with supplements (Lonza, #CC-3244 containing human epidermal growth factor, dexamethasone, L-glutamine, FCS, and gentamicin/amphotericin-B) according to the manufacturer's instructions. For experiments, cells were seeded at a density of $1\text{--}1.5 \times 10^4$ cells/well in SkGM-2 with all supplements except for dexamethasone.

2.6 | Primary murine myoblasts

Primary myoblasts were isolated from hind limbs of male 3-day-old WT or GILZ KO mice. The hind limbs were dissected and shredded with scissors, washed in PBS, and digested with trypsin/EDTA for 60 minutes. After filtering through a 70- μm cell strainer, the cell suspension was diluted in DMEM supplemented with 10% FBS and centrifuged for 20 minutes at $200\times g$ and 4°C . The resuspended cells were preplated for 1 hour to allow fibroblast adhesion. Nonadherent cells were collected, centrifuged for 10 minutes at $200\times g$ and 4°C , resuspended in F-10-based primary myoblast growth medium (Ham's F-10 nutrient mixture supplemented with 20% FBS, penicillin/streptomycin, and glutamine), and plated onto collagen I-coated cell culture dishes (Sigma-Aldrich, St. Louis, MO, USA). Further enrichment of the myoblasts was achieved by dislodging and replating the cells onto collagen-coated dishes every fourth day for 1–2 weeks. Afterward, myoblasts were cultured in growth medium (40% DMEM, 40% Ham's F-10 nutrient mixture, 20% FBS), supplemented with penicillin/streptomycin and glutamine.

2.7 | Cytotoxicity measurement

For the 3-(4,5-dimethylthiazol-2-yl)-2,5-diphenyltetrazolium bromide (MTT) reduction assay, cells were seeded in 96-well plates at a density of 10^4 cells/well, allowed to adhere overnight, and treated with test compounds at the indicated concentrations. Cells incubated without any treatment were used as growth controls, cells incubated with solvent at the maximum concentration present in the assay (0.25%) served as negative

controls, and wells with treatment but without cells were used as blank. At the end of treatment, cells were incubated for 3 hours with MTT solution (0.5 mg/mL in medium) and lysed with DMSO. The absorbance was measured at 550 nm in a microplate reader (XFluor4 SunriseTM, TECAN, Männedorf, Switzerland), using a reference wavelength of 690 nm.

For the crystal violet assays, cells were seeded at a density of 10^4 cells/well into a 96-well plate. After overnight incubation, cells were treated with statins or vehicle control at the indicated concentrations. The cells were washed with PBS and incubated for 20 minutes with 50 μL /well of freshly prepared 0.5% crystal violet solution in water. After washing, the plate was air-dried for 24 hours. Cells were lysed in methanol by incubation for 20 minutes at room temperature. The optical density was measured at 570 nm. The background was determined by lysing cells with 50% DMSO before the staining procedure, and background-subtracted values were used to calculate the cell viability.

For evaluating the cell viability in FDBs, the number of living and nonliving myofibers was determined using the trypan blue exclusion method.

2.8 | RNA isolation, reverse transcription, and quantitative PCR (RT-qPCR)

Total RNA from cultured cells was isolated using the High Pure RNA Isolation Kit (Roche, Basel, Switzerland). RNA samples with an A260/A280 ratio higher than 1.8 were used for further analysis. Reverse transcription was done using the High-Capacity cDNA Reverse Transcription Kit (Thermo Fisher Scientific, Waltham, MA, USA) in the presence of RNase inhibitor (Thermo Fisher Scientific, Waltham, MA, USA). qPCR was performed on cDNA samples using the 5 \times HotFirePol EvaGreen qPCR Mix (Solis BioDyne, Tartu, Estonia) and the primer sequences detailed in Table 1. A CFX96 touch Real-Time PCR detection system, and the CFX Manager 2.1 software (Bio-Rad, Hercules, CA, USA) were used for qPCR analysis. Data were analyzed as previously described.²⁵ Housekeeping genes were chosen based on the literature, or after evaluating the expression stability of at least three candidate genes under the experimental conditions, using the geNorm, NormFinder, and BestKeeper software tools.²⁶

2.9 | Western blot

Cells were harvested either with RIPA buffer (50 mM Tris-HCl, 1% Triton X-100, 0.1% SDS, 0.5% sodium deoxycholate, 150 mM NaCl) supplemented with a protease/phosphatase inhibitor mix (P8340, P0044, Sigma-Aldrich,

TABLE 1 Primer sequences for qPCR analyses

Gene	Accession number	Forward primer sequence 5'-3'	Reverse primer sequence 5'-3'
Mouse			
<i>Csnk2a2</i>	NM_009974.3	GTAAAGGACCTGTGTCAAAGA	GTCAGGATCTGGTAGAGTTGCT
<i>Ppia</i>	NM_008907.1	GCGTCTCCTTCGAGCTGTTT	CACCCTGGCACATGAATCCT
<i>Hmgcr</i>	NM_008255.2	ATCCAGGAGCGAACCAAGAGAG	CAGAAGCCCCAAGCACAAAC
<i>Tsc22d3</i>	NM_010286.4	GCTGCTTGAGAAGAACTCCCA	GAACCTTTCCAGTTGCTCGGG
Human			
<i>RNA18S5</i>	NR_003278.3	AGGTCTGTGATGCCCTTAGA	GAATGGGGTTCAACGGGTTA
<i>TSC22D3</i>	NM_004089.3	CATGTGGTTTCCGTTAAGCTGG	AGGATCTCCACCTCCTCTCTC
Zebrafish			
<i>actb2</i>	NM_181601.4	AAATTGCCGCACTGGTT	ACGATGGATGGGAAGACA
<i>tsc22d3</i>	NM_200569.2	AACAACCAGCTGGAGCGCGAA	GCAGAGCCCGTGCTGCTGATT

St. Louis, MO, USA) or with SB lysis buffer (50 mM Tris-HCl, 1% SDS, 10% glycerol, 5% β -mercaptoethanol, 0.004% bromophenol blue, in water) supplemented with a protease inhibitor cocktail (cOmplete Mini, Roche, Basel, Switzerland). Western blots were performed as described previously, and signals were either detected by an HRP-based method²⁷ or with the LI-COR Odyssey imaging system (LI-COR Biosciences, Lincoln, NE, USA).^{28,29} Incubation with primary antibody dilutions was performed at 4°C overnight, and with secondary antibody dilutions at room temperature for 1-1.5 hours. The antibodies and dilutions used are listed in Table 2.

2.10 | Jenner-Giemsa staining

To measure the myogenic differentiation of C2C12 myotubes Jenner-Giemsa staining was performed following a previously published protocol.³⁰ In brief, cells were fixed in ice-cold methanol for 5 minutes, air-dried, and stored at 4°C until analysis. For staining, wells were incubated with Jenner's stain solution (diluted 1:3 in 1 mM sodium phosphate buffer pH 5.6) for 5 minutes at room temperature, washed with distilled water, and subsequently incubated with Giemsa solution (diluted 1:20 in the same buffer) for 10 minutes at room temperature. Wells were observed with a phase-contrast microscope equipped with a digital camera (ZEISS Axiovert 40 CFL with Canon EOS 400D, Oberkochen, Germany). Each well was photographed in 3-4 randomly selected regions. Images were analyzed using the free image-processing software Fiji (*Fiji is just ImageJ*).³¹

2.11 | Immunofluorescence

Myosin heavy chain (MHC) immunofluorescence (IF) was performed on C2C12 myotubes and whole zebrafish

embryos. Cells were cultured and differentiated on glass coverslips that were previously treated for 10 minutes in a 1:1 mixture of 70% ethanol and 0.1 N HCl.³² Cells were treated as indicated and prefixed by adding paraformaldehyde solution (4% in PBS) directly to the culture medium. After 2 minutes, the prefixation culture medium was replaced with a paraformaldehyde solution (4% in PBS), and cells were fixed for 15 minutes at room temperature. Cells were washed with PBS and permeabilized with a 0.2% Triton X-100 solution in PBS for 10 minutes at room temperature, washed, blocked in a 5% BSA solution in PBS for 1 hour at room temperature, and incubated with primary antibody (MF20, deposited by Donald A. Fischman in the Developmental Studies Hybridoma Bank, The University of Iowa, Department of Biology, Iowa City, IA, USA) diluted 1:50 in dilution buffer (1% BSA in PBS) at 4°C overnight. After washing, cells were incubated with secondary antibody diluted 1:800 in dilution buffer for 1 hour at room temperature. Cells were washed and counterstained with DAPI for 15 minutes at room temperature, mounted with FluorSave (Merck, Darmstadt, Germany), and observed with an Axio Observer Z1 epifluorescence microscope, equipped with an AxioCam Mr3 and AxioVision software (Zeiss, Oberkochen, Germany). Photographs from randomly selected regions were analyzed using the Fiji software.

Zebrafish embryos were fixed in paraformaldehyde solution at 4°C overnight, and then stored in methanol at -20°C for at least 4 hours. Embryos were permeabilized in acetone for 30 minutes at -20°C, washed, blocked in a 1% BSA solution in PBST for 2 hours at room temperature, and incubated with primary antibody (mouse anti-myosin F59, DSHB, Iowa City, IA) diluted 1:100 in blocking buffer at 4°C overnight. After washing in PBST, the embryos were incubated with secondary antibody (goat anti-mouse IgG (H+L), Alexa Fluor 597, Thermo Fisher Scientific, Waltham, MA, USA) 1:200 at room temperature for 4 hours, washed again, and observed on a Leica SP8 confocal microscope.

TABLE 2 Antibodies for Western blot analyses

Antibody	Dilution
Rat anti GILZ [CFMKG15] mAb (Thermo Fisher Scientific, Waltham, MA, USA)	For detection with HRP-labeled secondary antibodies: 1:1000 in 5% milk powder—TBST For detection with IR-labeled secondary antibodies: 1:1000 in Rockland blocking buffer (Rockland, Limerick, PA, USA)
Mouse anti GADPH [OTI2D9] (OriGene, Rockville, MA, USA)	1:2000 in 5% milk powder—TBST
Mouse anti Akt (pan) [40D4] mAb (New England Biolabs, Ipswich, MA, USA)	1:2000 in 5% milk powder—TBST
Rabbit anti phospho-Akt (Ser473) [D9E] XP® mAb (New England Biolabs, Ipswich, MA, USA)	1:2000 in 5% milk powder—TBST
Polyclonal rabbit anti phospho-FOXO3a (Ser253) (New England Biolabs, Ipswich, MA, USA)	1:2000 in 5% milk powder—TBST
Mouse anti FOXO3a [D12] mAb (Santa Cruz Biotechnology, Dallas, TX, USA)	1:1000 in gelatine buffer (0.75% gelatine A, 0.1% Tween-20, 20 mM Tris, 137 mM NaCl, pH 7.5)
Mouse anti myogenin [5FD] mAb (Santa Cruz Biotechnology, Dallas, TX, USA)	1:200 in 5% milk powder—TBST
Polyclonal rabbit anti cleaved Caspase-3 (Cell Signaling Technology, Beverly, MA, USA)	1:1000 in 5% milk powder—TBST
Goat anti-rat IgG (H+L), HRP (Thermo Fisher Scientific, Waltham, MA, USA)	1:5000 in 5% milk powder—TBST
Goat anti-mouse IgG (H+L), HRP (Thermo Fisher Scientific, Waltham, MA, USA)	1:5000 in 5% milk powder—TBST
Goat anti-rabbit IgG, HRP (Thermo Fisher Scientific, Waltham, MA, USA)	1:10 000 in 5% milk powder—TBST
Mouse anti- α -Tubulin [DM1A] (Sigma-Aldrich, St. Louis, MO, USA)	1:1000 in Rockland blocking buffer
IRDye 800CW Goat anti-Rat IgG (LI-COR Biosciences, Lincoln, NE, USA)	1:10 000 in Rockland blocking buffer

2.12 | Zebrafish treatment

Zebrafish embryos from the AB wild-type strain were used. The developmental stage was determined by embryo morphology in hours post fertilization (hpf).³³ To examine gene expression after statin treatment, embryos at 19–22 hpf were sorted, placed at a density of 2–3 embryos/cm² in 6-well plates, and incubated at 28°C in 0.3 × Danieau's solution (17 mM NaCl, 2 mM KCl, 1.5 mM HEPES, 1.8 mM Ca(NO₃)₂, 0.12 mM MgSO₄) containing 1 μ M statin or solvent control. 12 hours after treatment, 10–20 embryos were pooled, flash-frozen in liquid nitrogen, and stored at –80°C for RNA isolation and qPCR analysis. To analyze muscle development and movement of the embryos, *gilz* was overexpressed in zebrafish embryos by injecting 1200 pg RNA into 1–2 cell stage embryos.³⁴ RNA was generated using the pCS2+ construct. Statin treatment was performed by injection of 1-ng statin (equal to 1/2 of the daily human dose related to body weight) into the embryos in the 1–2 cell stage.

The morpholino antisense oligonucleotides (MO) were purchased from Gene Tools (Philomath, OR, USA). To knockdown *foxo3b*, a splicing MO (*foxo3b* MO 5'-TGGAGATGCACTGCGCTTACCTTCC-3') targeting exon 2 and intron 2 was used as previously described.³⁵ The Gene Tools random control oligo was used for comparison. MOs were dissolved in sterile water, and 1 nL containing 16 ng MO were injected into 1–2 cell stage embryos. The

knockdown was validated by detection of truncated PCR products in *foxo3b* morphants as described.³⁵ The used primers were: *foxo3b* forward GTGAGTTACTGCTGGTGATGC (exon 1) and *foxo3b* reverse CACCACGAGCTCTTTCCAGT (exon 3).

2.13 | In situ hybridization

Whole-mount *in situ* hybridization was used to analyze MyoD expression changes in zebrafish embryos. Embryos at 16 hpf were collected and fixed in 4% PFA solution at 4°C overnight. *In situ* hybridization was performed as previously described.³² In brief, dechorionated embryos were treated with 5 μ g/ μ L proteinase K in PBST for 5 minutes, washed and incubated for 1 hour in hybridization buffer (50% formamide, 5× SSC, 0.1% Tween 20, 1 mg/mL yeast torula RNA, 50 μ g/mL heparin) at 65°C. Subsequently, an antisense digoxigenin-labeled RNA probe was added, and the samples were incubated overnight. On the next day, embryos were washed, blocked for 1 hour (5% goat serum in PBST) and incubated with anti-DIG antibody (#11093274910, 1:5000, Roche, Basel, Switzerland) at 4°C overnight. Embryos were washed in AP buffer (100 mM Tris-HCl, 50 mM MgCl₂, 100 mM NaCl, 0.1% Tween20), and incubated with staining buffer (0.5% nitroblue tetrazolium, 0.375% 5-bromo-4-chloro-3-indolyl phosphate in AP buffer) in the dark for 30

minutes. Once the pattern appeared, embryos were washed, and 4% PFA was added for at least 20 minutes before embryos were analyzed under the microscope. Scoring was performed according to the following criteria: regular phenotype—parallel somites of same length, V-shaped, homogenous MyoD expression; mild phenotype—irregular somite formation, different lengths, line shaped, somites show less homogenous MyoD expression; severe phenotype: no clear somite formation, different lengths, line shaped, reduced and diffuse MyoD expression.

2.14 | Chromatin immunoprecipitation (ChIP)

The ChIP assay was performed using the EZ-ChIP Kit (Merck, Darmstadt, Germany) according to the manufacturer's instructions. Precleared lysates from 1×10^6 myoblasts in a volume of 100 μ L were incubated overnight at 4°C with 10 μ g monoclonal anti-FOXO3 antibody (D12, Santa Cruz Biotechnology, Dallas, TX, USA) or 10 μ g normal mouse IgG (Merck, Darmstadt, Germany). Immunocomplexes were purified, and qPCR analysis was performed using the SYBR Select Master Mix (Thermo Fisher Scientific, Waltham, MA, USA) and the Applied Biosystems 7300 qPCR system (Foster City, CA, USA). Primer sequences are given in Table 3.

2.15 | Luciferase gene reporter assay

Reporter gene assays were performed as previously described.²⁵ The proximal *Gilz* promoter (a fragment located between -1938 bp upstream and +206 bp downstream of the transcription start site) was cloned into the pGL3 luciferase reporter vector (Promega, Madison, WI, USA) using KpnI and SmaI according to the manufacturer's instructions. The FOXO3 reporter vector (FHRE-Luc) was a gift from Michael Greenberg (Addgene plasmid #1789).³⁶ The phRG-TK vector (Promega, Madison, WI, USA) provided constitutive expression of *Renilla* luciferase and served as an internal control value, to which expression of the firefly luciferase reporter gene was normalized. C2C12 cells were seeded at a density of 10^4 cells/well into 96-well plates, co-transfected in a 1:1

ratio with the luciferase vector using the Lipofectamine 3000 reagent (Thermo Fisher Scientific, Waltham, MA, USA) for 4 hours, treated as indicated, and harvested by the addition of 1 \times passive lysis buffer (Promega, Madison, WI, USA). Luciferase activity was determined by the addition of firefly luciferase substrate (470 μ M D-luciferin, 530 μ M ATP, 270 μ M coenzyme A, 33 μ M DTT, 20 μ M Tricine, 2.67 μ M MgSO₄, 1.07 μ M MgCO₃, and 0.1 μ M EDTA, pH 7.8) or renilla substrate solution (0.1 M NaCl, 25 mM Tris HCl pH 7.5, 1 mM CaCl₂, and 0.9 μ M coelenterazine) followed by luminescence measurement using the Glomax Discover multplate reader (Promega, Madison, WI, USA).

2.16 | Lentivirus preparation

Plasmids encoding lentiviral products were obtained from Addgene (Watertown, MA, USA). The packaging plasmid psPAX2 and the envelope plasmid pMD2.G were a gift from Didier Trono (Addgene plasmids #12260 and #12259). The pLKO.1-TRC cloning vector was a gift from David Root (Addgene plasmid #10878).³⁷ pLKO.1-scrambled shRNA was a gift from David Sabatini (Addgene plasmid #1864).³⁸

Two different sequences of short hairpin (sh) RNA targeting murine GILZ were used: shGILZ1 (5'-GGAGTACTGACTGGTCTCTTA-3'), and shGILZ2 (5'-ACAGCTTCACCTGACAATG-3'). shGILZ sequences were cloned into the pLKO.1-TRC cloning vector. In brief, the cloning vector was double digested with AgeI-HF and EcoRI-HF and purified from an agarose gel. The annealed oligos were then ligated into the vector using T4 DNA ligase overnight at room temperature. The ligation mix was transformed into GT116 *E. coli* (Invivogen, Toulouse, France), and ampicillin-resistant clones were screened for inserts by sequencing using the pLKO.1 sequencing primer.

Lentiviral particles were produced following Addgene's protocol. Briefly, 5×10^5 HEK-293T cells were plated into 6-cm cell culture dishes in medium without antibiotics and transfected at 50%-80% confluency with the transfer, packaging and envelope plasmids (1000:750:250) using the FuGENE 6 Transfection Reagent (Promega, Madison, WI, USA). Twelve to 15 hours after transfection, the medium was replaced with DMEM. The lentivirus-containing media were

TABLE 3 Primer sequences for ChIP experiments

	Forward primer sequence 5'-3'	Reverse primer sequence 5'-3'
FHRE1	TGGCCCAGTTAAACCACATCC	GCTGAAGTGTTCACAGTCCCTGA
FHRE2	TAACCGTGTAACAGGAGCCAG	GGAAGTCTGGGGAAATCCTA
FHRE3	AGCATGGGCAGAAAAAGGAATAAG	CTGGTTTGGTTGGTGTAACAGT
FHRE4 (IRE, insulin-responsive element)	AGAGCTTTCTTGGTCTGAGAGAAT	AATTTTGAGGTGAGTAGCAGTAGT
non-FHRE	GTATTCGGCCTTCTCTTGC	CTGCTGCGTGGTGAAAAACA

then harvested at 24 and 48 hours, pooled, centrifuged at $200\times g$ for 5 minutes, aliquoted, and stored at -20°C .

To determine the lentiviral titer, viral genomic RNA was purified from $200\mu\text{L}$ of freshly harvested lentivirus stock using the High Pure Viral RNA Kit (Roche, Basel, Switzerland). After digestion of residual DNA, 10-fold serial dilutions of the purified viral RNA were reverse transcribed and amplified *via* qPCR, using primers for the 5'LTR region (forward 5'-AGCTTGCCCTGAGTGCTTCA-3', reverse 5'-TGACTAAAAGGGTCTGAGGGA-3'), and the 5' end of the *gag* gene (forward 5'-GGAGCTAGAACGATTCGCAGTTA-3', reverse 5'-TGTAGCTGTCCCAGTATTTGTC-3'). The copy number (viral particles, VP) contained in the supernatant was calculated from comparison against a plasmid standard curve, and the titer calculated as viral particles per ml of supernatant (VP/mL). Biological titration of the vectors was performed *via* limiting dilution, and for each lentivirus, the ratio from biological to nonbiological titer was established and used for estimation of the functional titer (TU/mL) for all further preparations that were only titrated *via* the gRNA method. This titer was then used to determine the volume of viral supernatant needed for infecting cells at a given multiplicity of infection (MOI).

2.17 | Generation of C2C12^{shGILZ} stable cell lines

Stable, polyclonal C2C12 cell lines were generated by reverse transducing 7.5×10^4 cells in 6-well plates with scrambled shRNA, shGILZ1, or shGILZ2 lentiviral particles at an MOI of 10 in the presence of polybrene, following the protocol for the generation of stable cell lines available from Addgene (Watertown, MA, USA). Twenty-four hours after transduction, the medium was changed, and 48 hours after infection puromycin ($2\mu\text{g/mL}$) was added to select for transduced cells. The puromycin-resistant cells were expanded for 2-3 weeks, after which they were harvested for analysis of gene and protein expression. Further culture and experiments were done in $1\mu\text{g/mL}$ puromycin-containing medium. A nontransduced control was run in parallel to confirm that no viable cells were present after selection.

2.18 | Muscle biopsies and sample preparation

Two percutaneous muscle biopsies from the *musculus vastus lateralis* were obtained from a hypercholesteremic volunteer to determine GILZ baseline expression levels. After the onset of simvastatin treatment (40 mg/d), biopsies were obtained after 1-3 months. Semi-automatic needle biopsies were alternately performed on the right and left legs of the participant

using the Bard Magnum device with a 12-G disposable needle (C.R. Bard Gm bH, Karlsruhe, Germany). Local anesthesia of the skin and subcutaneous tissue was performed according to standard procedures using Lidocaine as an anesthetic. Muscle samples were immediately frozen in liquid nitrogen and stored at -80°C . Skeletal muscle biopsy samples were mechanically homogenized using a Precellys homogenizer (Bertin Corp., Rockville, MD, USA). RNA was isolated using the miRNeasy Micro Kit according to the manufacturer's instructions (Qiagen, Venlo, Netherlands). Reverse transcription and quantitative PCR was performed as described above.

2.19 | Statistics

Results are expressed as means of at least three independent experiments performed in replicates \pm SEM (standard error of the mean). Statistically significant differences between means were determined using the GraphPad Prism 6.0 or Origin 2018b software. An unpaired *t* test was performed for the comparison of two groups, and the comparison of three or more groups was carried out by one or two-way analysis of variance (ANOVA) followed by Bonferroni's post hoc analysis for individual differences. For MTT results F values and degrees of freedom were indicated. A comparison between medians was performed with Kruskal-Wallis test followed by Dunn's post hoc analysis. For categorical data, the chi-squared test was used. Results were considered significant at $P < .05$.

3 | RESULTS

3.1 | GILZ expression in human muscle biopsies

To investigate the potential effect of statin treatment on GILZ expression, we analyzed different publicly available gene expression profiling data sets. Gene Expression Omnibus (GEO) data sets GDS2987, GSE32547, and GSE4883 suggested that statins were able to induce GILZ in human endothelial cells, human pulmonary artery smooth muscle cells, human umbilical vein endothelial cells, and human peripheral blood monocytes (Supplemental Figure 1). Interestingly, statins also induced GILZ in a clinical setting: The analysis of a transcriptional profile of human quadriceps femoris muscle following statin treatment suggested a moderate increase in GILZ expression in biopsies from 12 patients receiving atorvastatin and simvastatin for 8 weeks, compared with those receiving placebo (ArrayExpress dataset E-TABM-116, Figure 1).³⁹ These results were in accordance with increased GILZ mRNA levels observed in muscle biopsies from a hypercholesteremic volunteer after simvastatin treatment (Supplemental Figure 2).

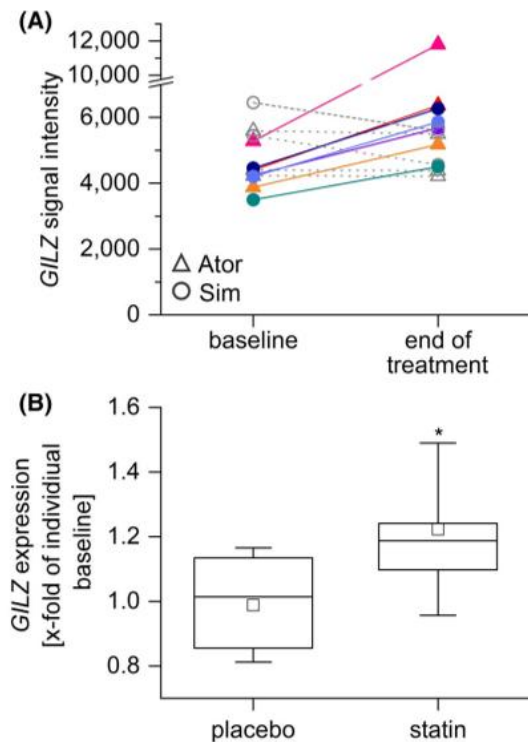


FIGURE 1 Analysis of the publicly available ArrayExpress dataset E-TABM-116: transcription profiling of human quadriceps femoris muscle following simvastatin (80 mg/d) and atorvastatin (40 mg/d) treatment. A, *GILZ* signal intensities (NCBI RefSeq NM_004089.3; scan REFs GI_37622900-A, GI_37622900-I) are shown. Connected data points represent patients before and after intervention for 8 weeks. B, *GILZ* expression after intervention is presented as \times -fold of individual baseline levels. Boxplots show the 25-75th percentiles, mean (square), median (line) and SD (whiskers). Placebo group: $n = 6$, statin group: $n = 12$. * $P < .05$

3.2 | Toxic concentrations of statin induce *GILZ* expression in muscle cells

To evaluate whether statins were able to induce *GILZ* in skeletal muscle cells, we treated C2C12 myoblasts and myotubes with 50 μ M atorvastatin, simvastatin, or cerivastatin. These relatively high statin concentrations are in accordance with the literature^{34,40-43} and were also chosen based on our observation that C2C12 myoblasts in cell culture express a 50-fold higher *Hmgcr* baseline level compared to muscle in vivo (Supplemental Figure 3). Statins were toxic after 24 hours—but not after 6 hours—at this concentration, as determined by MTT and crystal violet assay (Supplemental Figure 4). We detected an increase in *Gilz* mRNA expression in C2C12 myoblasts and primary human myoblasts after 6 hours of treatment with all statins, which was reversed by the addition of mevalonate (100 μ M) to the medium, indicating that the mechanism of *GILZ* induction relates to the inhibition of HMG-CoA reductase (Figure 2A). In C2C12 myotubes, the increase in *Gilz* expression was

less pronounced (Figure 2A). Western blot analysis showed an elevated expression of *GILZ* protein in C2C12 myoblasts as well as in primary murine and human myoblasts treated with toxic concentrations of statins (Figure 2B-D).

3.3 | *GILZ* induction can be reversed by geranylgeranyl pyrophosphate

The inhibition of HMG-CoA by statins does not only impair cholesterol biosynthesis, but also other biosynthetic pathways. Of main importance is the inhibition of protein prenylation resulting from the decreased synthesis of the isoprenoid derivatives GGPP and FPP. Thus, we evaluated whether *GILZ* induction could be reversed by the addition of any, or both, of these mediators to the medium. Co-treatment of C2C12 myoblasts with 10 μ M GGPP in addition to simvastatin completely reversed *Gilz* induction, while FPP had no effect (Figure 2E). GGPP treatment alone did not affect *Gilz* expression (data not shown).

3.4 | Statin-induced impairment of myogenesis is accompanied by *GILZ* induction

Myogenesis is a multistep, tightly regulated process that leads to the formation of skeletal muscle, both during embryonic development as well as in adult life, to maintain muscle homeostasis and repair after injury.⁴⁴ Statins are not only toxic toward skeletal muscle fibers but might also impair the muscle regeneration process.⁴⁵⁻⁴⁷ To examine these effects, we induced the differentiation of C2C12 myoblasts in the absence or presence of statins and evaluated myotube formation by Jenner-Giemsa staining and myosin heavy chain immunofluorescence. We observed that treatment of C2C12 cells with subtoxic concentrations of statins during differentiation resulted in less myotube formation and a significantly reduced fusion index after 6 days, where fully differentiated myotubes were visible in the control (Figure 3A-C). We analyzed *GILZ* expression levels in differentiating C2C12 and primary murine myotubes treated with statins and found that the impairment in myogenesis was accompanied by *GILZ* induction on both mRNA and protein level (Figure 3D,E). Since *GILZ* has been shown to mediate the antimyogenic effects of dexamethasone,²² we hypothesized that it might also be involved in the effects observed after statin treatment.

3.5 | *GILZ* knockout abolishes the cytotoxic effects of statins

To assess whether loss of *GILZ* could rescue statin-induced cytotoxicity, we isolated primary myoblasts from wildtype

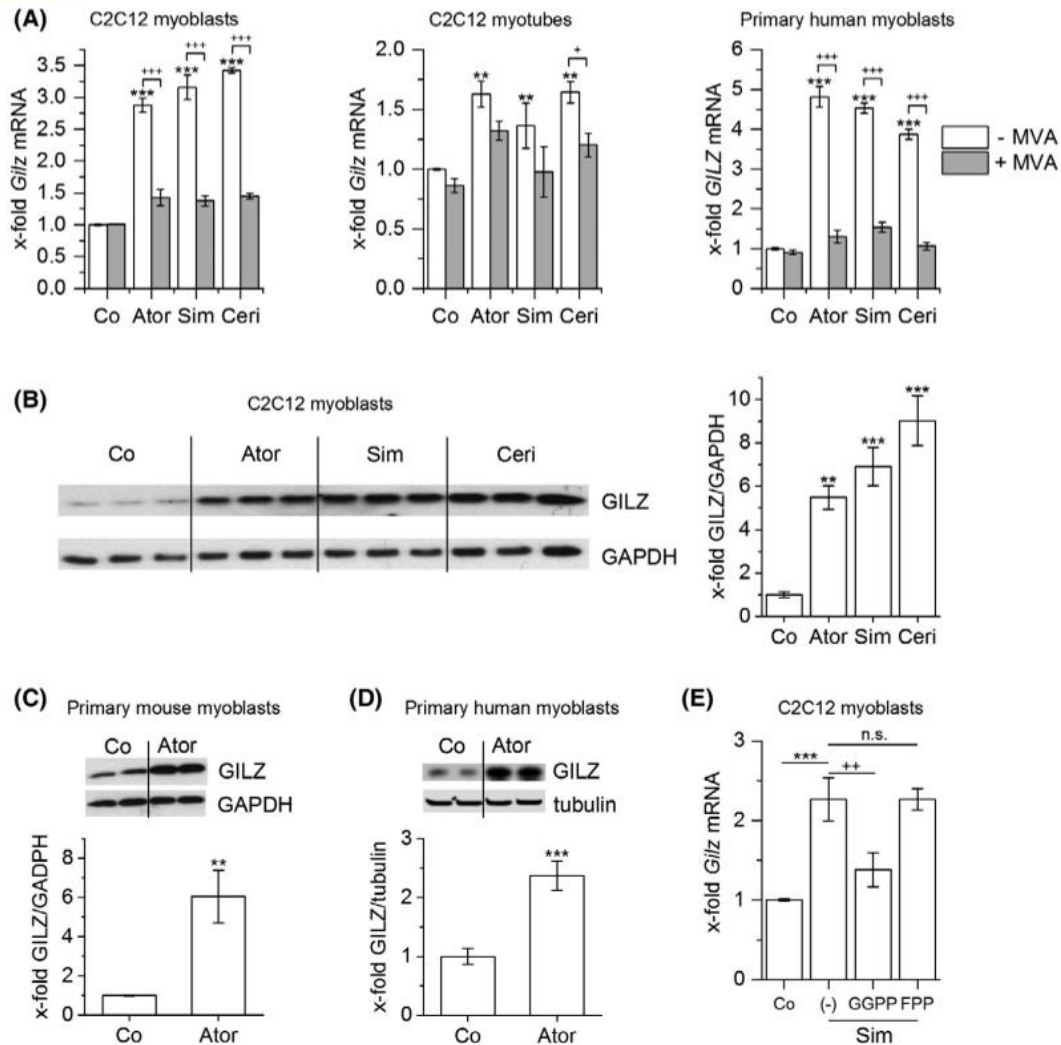


FIGURE 2 Effect of statin treatment at toxic concentrations on GILZ expression in muscle cells. A, C2C12 myoblasts, C2C12 72-h myotubes, or primary human skeletal muscle myoblasts were treated with 50 μ M statin (Ator, atorvastatin; Sim, simvastatin; Ceri, cerivastatin) in the absence or presence of mevalonate (MVA, 100 μ M) for 6 hours, and mRNA levels were determined by qPCR. *Gilz* expression in C2C12 samples was normalized to the housekeeping gene *Csnk2a2*, and *GILZ* expression in human samples was normalized to *RN18S5*. Data are presented as fold change of control. B-D, *GILZ* protein expression was determined in vehicle- or atorvastatin-treated C2C12 myoblasts (B), primary murine myoblasts (C), and primary human skeletal muscle myoblasts (D) by western blot. Representative blots and densitometric analyses are shown. For densitometric analysis, *GILZ* signal intensities were normalized to the housekeeping protein GAPDH (B, C) or tubulin (D). E, C2C12 myoblasts were treated with 50 μ M simvastatin in the absence or presence of GGPP and FPP (10 μ M) for 6 hours, and *Gilz* mRNA levels were measured. mRNA expression was normalized to the housekeeping gene (*Csnk2a2*) and is presented as fold change of control. Data show the mean of 2 (A, C2C12 data) or 3 (A, human myoblast data and B-E) independent experiments performed in replicates \pm SEM. ** P < .01, *** P < .001 relative to the corresponding control, ++ P < .01, +++ P < .001 relative to other treatments as indicated

(WT) and GILZ knockout (KO) mice, treated them with increasing doses of statins, and measured cell viability after 24 hours. Comparison of the dose-response curves obtained showed significant differences between genotypes: GILZ KO myoblasts were significantly less sensitive toward atorvastatin, simvastatin, and cerivastatin treatment than their WT counterparts (Figure 4A).

Due to the importance of the PI3K/Akt signaling pathway in statin-induced myotoxicity,^{40,42} we hypothesized that the resistance to cell death from GILZ KO myoblasts might be related to modulation of the Akt phosphorylation status.

Indeed, atorvastatin treatment induced dephosphorylation of Akt and activated the apoptotic pathway, as observed by cleaved caspase-3 detection, in WT myoblasts. On the other hand, Akt phosphorylation levels were restored to that of the control in statin-treated GILZ KO cells, and the active form of caspase-3 was undetectable (Figure 4B,C).

As an ex vivo model for the evaluation of statin myotoxicity, we used *flexor digitorum brevis* myofibers isolated from WT and KO animals. These short fibers can be isolated, dissociated, and cultured, representing a more mature system for evaluation of statin effects than cell culture systems, since myoblasts in

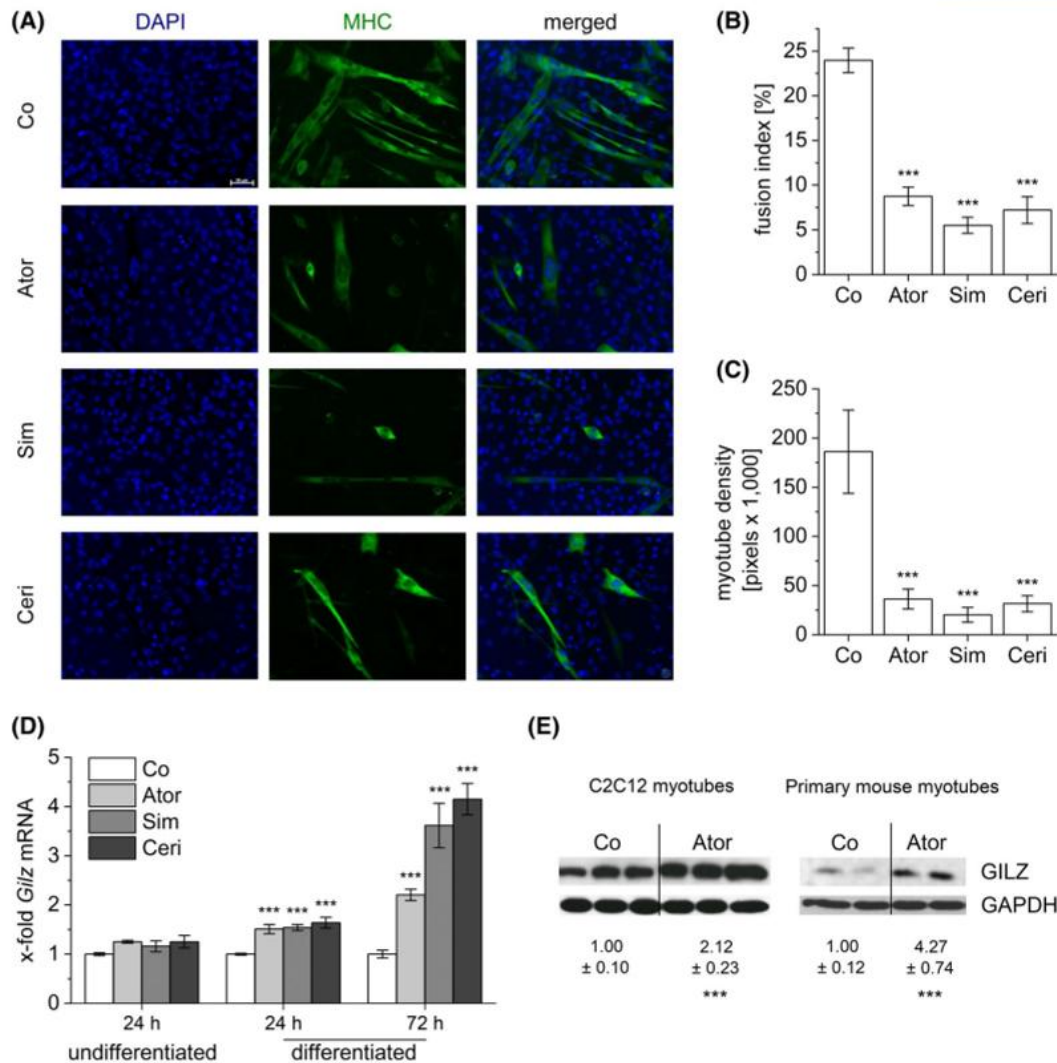


FIGURE 3 Effect of statins on GILZ expression during C2C12 differentiation. A-B, C2C12 were induced to differentiate for 6 days in the absence or presence of nontoxic concentrations of atorvastatin (5 μ M), simvastatin (1 μ M), and cerivastatin (0.1 μ M), and subjected to MHC IF. Co: vehicle-treated cells. A, Representative images are shown. Blue: DAPI, green: MHC, scale bar: 50 μ m. B, The degree of differentiation was quantified by measuring the fusion index in IF images. C, Myotube density in Jenner-Giemsa stained cells. D, *Gilz* expression was measured in nondifferentiated cells or cells differentiated for the indicated time points and normalized against the housekeeping gene (*Csnk2a2*). Data are presented as fold change of the corresponding vehicle-treated control (Co). E, GILZ protein levels measured in 72 h-C2C12 myotubes and primary murine myotubes treated with atorvastatin (5 μ M) during the course of myogenesis. Representative blots are shown. Data represent the means of three independent experiments performed in replicates \pm SEM. * P < .05, ** P < .01, *** P < .001 relative to the control

vitro can differentiate to myotubes but are unable to form fully differentiated myocytes and, therefore, do not exactly resemble the features of mature muscle.^{48,49} Treatment of FDB fibers from WT mice with atorvastatin, simvastatin, and cerivastatin started to induce vacuolation at 72 hours. After 5 days, the fibers were swollen, ruptured, and blebs appeared (Figure 5A and data not shown). Viability analysis using the trypan blue exclusion method after 5 days indicated that statins induced fiber death in a dose-dependent manner. Loss of GILZ prevented the morphological changes indicative of myotoxicity and made the fibers resistant toward statins: in KO fibers, there were no significant

differences in viability between the control and treatments at any of the concentrations evaluated (Figure 5A,B).

3.6 | GILZ contributes to statin-induced inhibition of myogenesis

To investigate the contribution of GILZ to statin-induced inhibition of myogenesis, we differentiated WT and GILZ KO myoblasts in the presence of statins and evaluated the expression of the MRF myogenin, which is required in cells committed

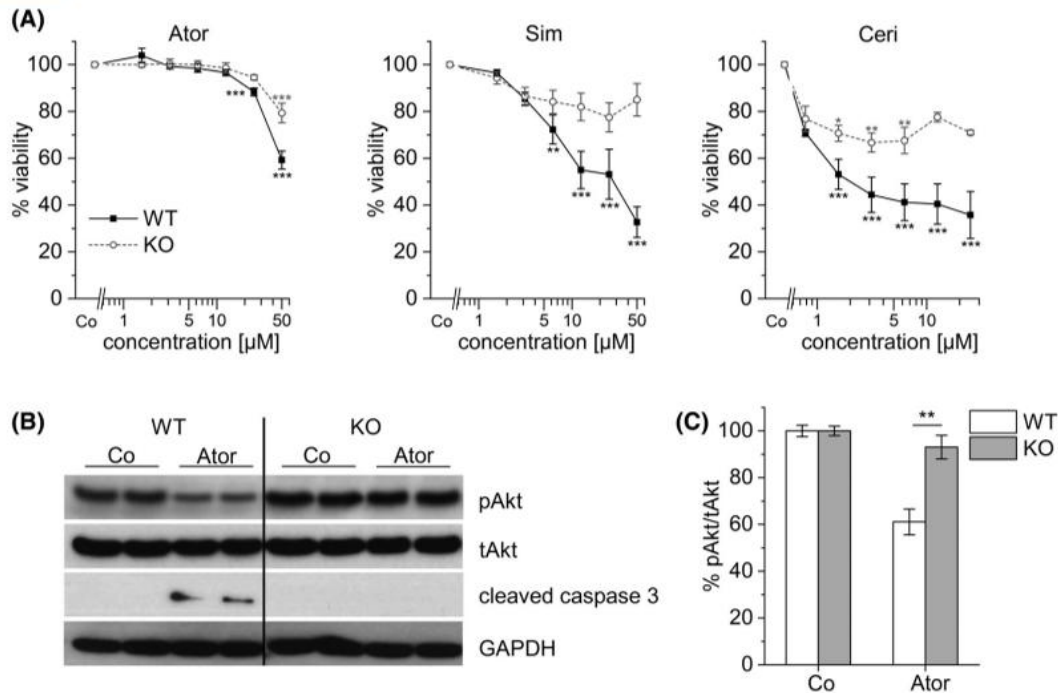


FIGURE 4 Effect of GILZ knockout on statin-induced myotoxicity. A, WT and GILZ KO primary murine myoblasts were treated with atorvastatin, simvastatin, or cerivastatin in increasing concentrations for 24 hours. Cell viability was measured via MTT assay and differences between curves were analyzed by two-way ANOVA [cell type main effect $F(1,124) = 10.06$, $P = .002$; $F(1,124) = 26.24$, $P < .0001$; and $F(1,116) = 24.18$, $P < .0001$, respectively, for each statin]. B, Myoblasts were treated with atorvastatin (50 µM) for 6 hours, and Akt phosphorylation and caspase-3 activation were measured by western blot. One representative blot is shown. C, The ratio of phosphorylated to total Akt was measured by densitometric analysis and normalized to the corresponding control. Data show the mean of at least three independent experiments performed in replicates \pm SEM. * $P < .05$, ** $P < .01$, *** $P < .001$ relative to the control

to the myogenic program for driving their fusion and terminal differentiation.⁴⁴ We observed a decrease in myogenin protein levels in WT primary murine myoblasts induced to differentiate for 72 hours in the presence of atorvastatin. By contrast, the expression of myogenin in atorvastatin-treated GILZ KO cells was restored to that of the control (Figure 6A).

To further analyze the role of GILZ in these effects, we generated C2C12 cell lines stably expressing scrambled or *Gilz* shRNA constructs by lentiviral transduction. The C2C12^{shGilz1} and C2C12^{shGilz2} cell lines showed a gene knockdown, whereas in the scrambled control cell line, C2C12^{scr}, *Gilz* expression was unaffected (Supplemental Figure 5A). Furthermore, statin-induced GILZ overexpression was inhibited in *Gilz* shRNA-expressing cells (Supplemental Figure 5B,C). We hypothesized that, as a result of restored myogenin expression, *Gilz* silencing should reinstate the ability of myoblasts to differentiate in the presence of statins. Noticeably, C2C12^{shGilz1} and C2C12^{shGilz2} cells displayed terminally differentiated myotubes already after 4 days in DM, whereas C2C12^{scr} cells were not fully differentiated yet (Figure 6B, left panels). GILZ knockdown, however, could only partially reverse the impairment in differentiation caused by statins: although Jenner-Giemsa staining showed myotube formation in the C2C12^{shGilz} lines

(Supplemental Figure 6), these myosin-expressing cells were not differentiated to the same extent as the respective controls. Nevertheless, fusion index analysis showed improvement in myotube formation from C2C12^{shGilz} cells compared to the C2C12^{scr} line (Figure 6C).

3.7 | FOXO3 mediates GILZ induction by statins in muscle

In the search for potential upstream regulators of GILZ expression after statin treatment in muscle, we focused on the Forkhead Box O3 (FOXO3) protein. FOXO3 is a direct phosphorylation target of Akt, and our observations in skeletal muscle tissue from FOXO3 KO mice, where *Gilz* expression levels were significantly lower than in WT animals, hinted toward FOXO3 as a transcriptional regulator of GILZ in this tissue (Figure 7A). Reporter gene assay showed that statins were able to induce FOXO3 transcriptional activity (Supplemental Figure 7) and, in fact, led to increased *Gilz* promoter-driven luciferase activity in C2C12 compared to the baseline. This indicates that statins elevate GILZ levels by activating its transcription (Figure 7B). Like in primary myoblasts, we observed that treatment of C2C12 myoblasts with statins led

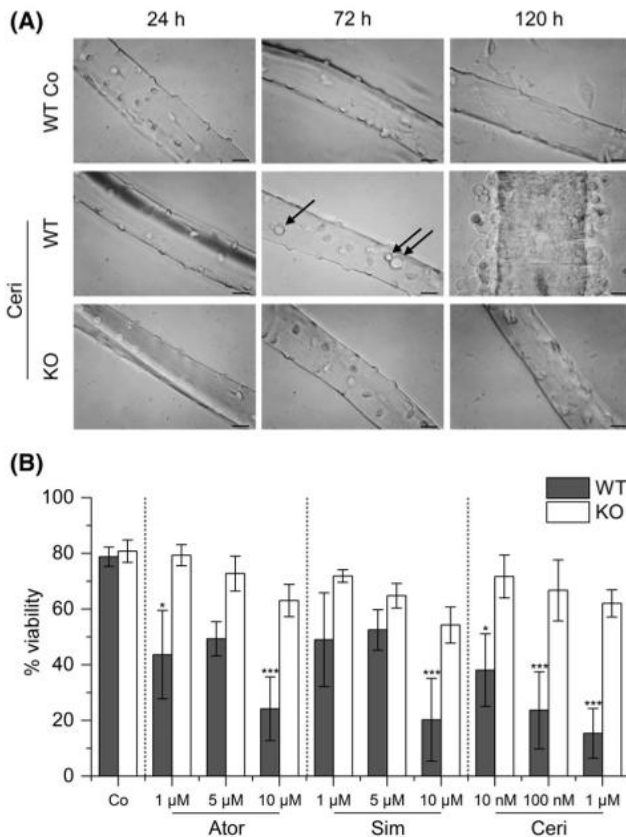


FIGURE 5 Effect of GILZ knockout on statin-induced FDB myofiber toxicity. WT and GILZ KO FDB myofibers were treated with cerivastatin (1 μM) for up to 120 hours and imaged for morphological analysis. A, Representative pictures are shown. Scale bar, 20 μm. B, Cell viability was measured after 120 hours of treatment, using the trypan blue exclusion method. Data show the mean of four independent experiments performed in replicates ± SEM. * $P < .05$, *** $P < .001$ relative to the corresponding control

to a decrease in Akt phosphorylation and, in line with this, to reduced levels of phosphorylated FOXO3 protein, that is, FOXO3 activation in parallel to GILZ induction (Figure 7C-E). Hence, we performed chromatin immunoprecipitation to evaluate whether FOXO3 activated *Gilz* expression in myoblasts by binding to the forkhead-responsive elements (FHRE) in its promoter following statin treatment. Indeed, we found an enrichment of sequences corresponding to three of the four FHREs presents in the *Gilz* promoter in immunoprecipitates from atorvastatin-treated myoblasts, indicating that GILZ induction in muscle follows dephosphorylation, nuclear translocation, and activation of FOXO3 (Figure 7F).

3.8 | Statins induce *Gilz* in zebrafish embryos, and deregulation of *Gilz* expression impairs somitogenesis

The zebrafish is a powerful and versatile in vivo model for the study of developmental and physiological processes, that

has been used for the elucidation of statin effects on muscle development⁵⁰ and homeostasis.^{41,51,52} Given that the zebrafish expresses a GILZ orthologue,⁵³ we chose this model to study the effects of statins on GILZ expression in vivo adhering to 3R rules to reduce animal experiments.

In line with our in vitro findings, treatment of zebrafish embryos at 20 hpf with statins at concentrations that have been described to cause major muscle damage³⁴ led to an up-regulation of *gilz* mRNA (Figure 8A). Moreover, statin treatment of embryos in the 2-4 cell stage for 24 hours resulted in disrupted muscle development in the tail of the embryos and a reduction of the frequency and dimension of muscle contractions, indicating an impaired muscle function (Figure 8B, Supplemental video). To characterize the effects of increased *gilz* expression in zebrafish muscle development, we performed myosin heavy chain IF and MyoD staining in *gilz* overexpressing and statin-treated embryos. Compared to control animals, we found an irregular MyoD expression and diffuse MHC staining with loss of septa in statin-treated embryos. Overexpression of *gilz* mimicked statin effects, suggesting that *gilz* mediated statin-induced muscle damage in this model (Figure 8C,D).

To investigate whether FOXO3b, the orthologue of mammalian FOXO3, was involved in *gilz* upregulation by statins, we knocked down *foxo3b* by morpholino injection.³⁵ *gilz* levels were reduced in *foxo3b* depleted embryos (Supplemental Figure 8). It was not possible to assess statin-induced muscle damage after morpholino-mediated knockdown of *foxo3b* because the embryos showed severe defects in axis formation, as previously reported by Xie et al³⁵ (Supplemental Figure 8B).

4 | DISCUSSION

More than 30 years after their introduction to the market, statins remain the cornerstone of the pharmacological management of hyperlipidemia and CVD prevention. In light of their importance and extended use, the understanding of the mechanisms underlying the onset of SAMS is of highest relevance.¹⁰ In the present study, we report a role for GILZ as a pivotal mediator of the myotoxic and antimyogenic effects of statins. We first demonstrate that treatment of murine myoblasts with different statins, at concentrations typical for in vitro studies on SAMS,^{41,43,54} induces GILZ expression. Since SAMS are a class effect and several of the mechanisms underlying muscle toxicity are directly related to the inhibition of HMG-CoA,^{47,55} we evaluated whether GILZ expression depended on this pathway as well. Indeed, we found GILZ induction to depend on mevalonate, and more specifically on geranylgeranylation.³⁴

Several molecular mechanisms of statin-induced myotoxicity have been proposed, describing their deleterious effects

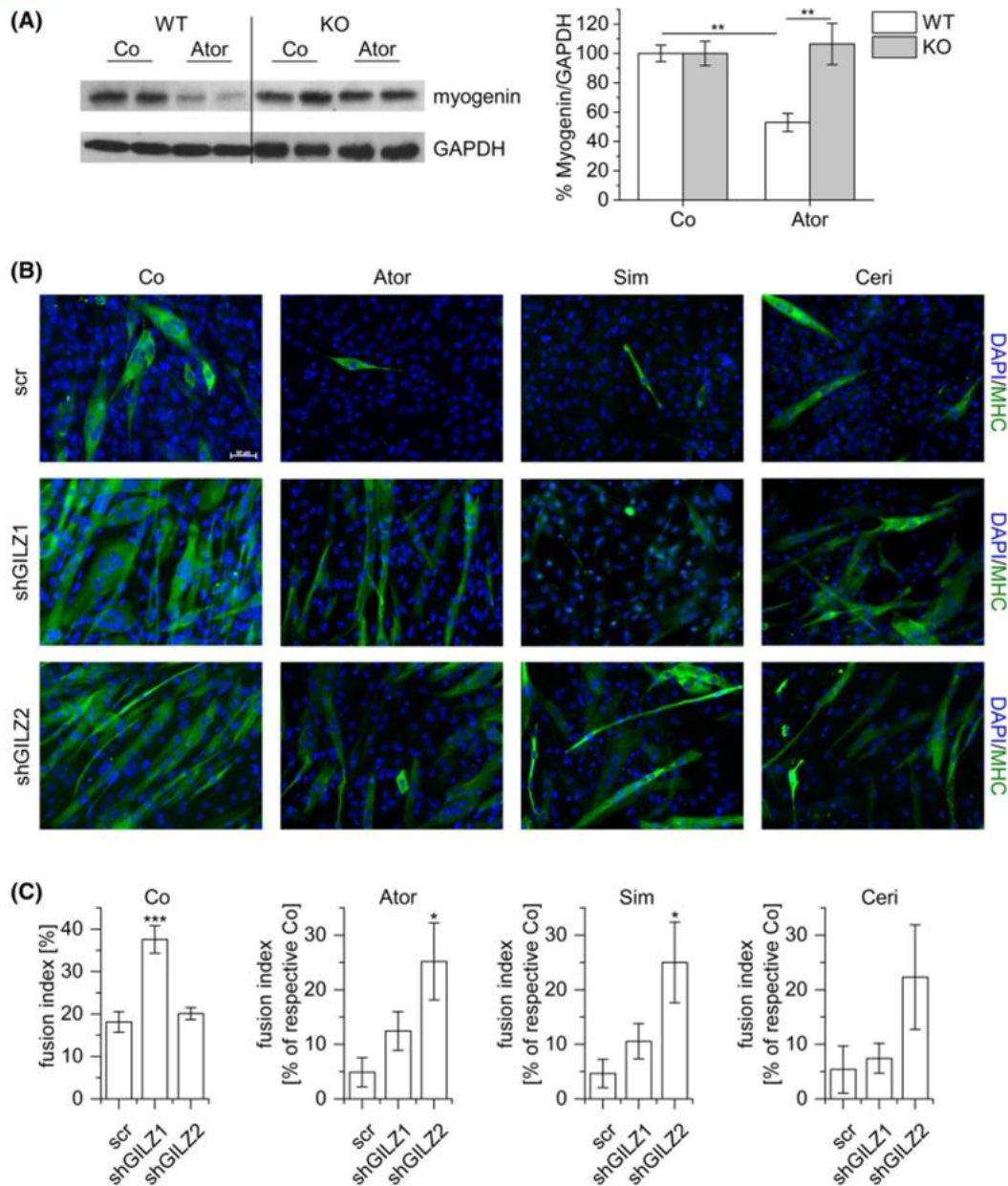


FIGURE 6 Effect of GILZ absence on statin-induced antimyogenic effects. A, Primary murine myoblasts from GILZ WT and KO animals were differentiated for 72 hours in the absence or presence of atorvastatin (5 μ M). Myogenin protein levels were measured by western blot. One representative blot and the densitometric analysis are shown. B-C, Scrambled (C2C12^{scr}) and C2C12^{shGILZ} cell lines were induced to differentiate for 4 days in the absence or presence of atorvastatin (5 μ M), simvastatin (1 μ M), and cerivastatin (0.1 μ M). Co: vehicle-treated cells. B, MHC IF. Blue: DAPI, green: MHC, scale bar: 50 μ m. Representative images are shown. C, The degrees of differentiation was quantified by measuring the fusion index. For statin-treated cells the fusion index is expressed as percentage of the corresponding vehicle-treated control. Data show the mean of at least three independent experiments performed in replicates \pm SEM. * P < .05, ** P < .01, *** P < .001 relative to the equally treated scr cells (C) or as indicated (A)

on mitochondrial function, calcium homeostasis, and cell survival in the myocyte.¹⁴ In our hands, statins caused Akt dephosphorylation and activation of the apoptotic cascade in undifferentiated myoblasts. This effect is in accordance with previous findings in cultured myotubes.^{42,56} Our observations suggest a crucial role for GILZ in mediating this action. First described in thymocytes as an antiapoptotic protein,¹⁵ GILZ can exert anti- or pro-apoptotic effects depending on the cell

type: GILZ has been shown to promote apoptosis by Mcl-1 downregulation in neutrophils⁵⁷ and by inhibition of the Akt/mTOR signaling pathway in myeloma cells.⁵⁸

There are discrepancies, however, regarding the mechanism by which statins induce cell death in cultured myoblasts/myotubes vs. mature fibers. For instance, statins trigger apoptosis in cultured cells, whereas mature skeletal muscles show necrotic features.⁴⁹ Hence, instead of using terminally

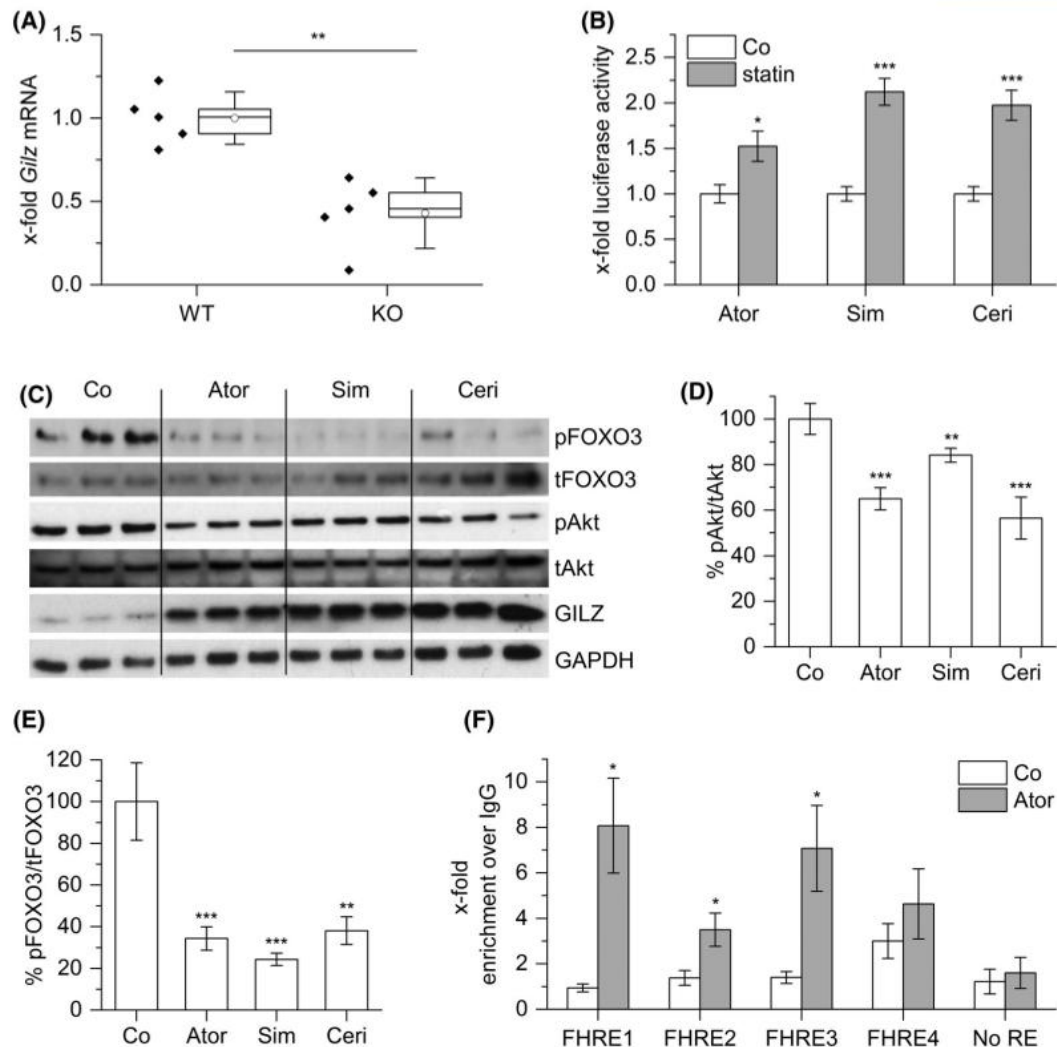


FIGURE 7 Involvement of FOXO3 in statin-induced GILZ expression. A, *Gilz* expression on skeletal muscle from WT and FOXO3 KO mice (n = 5). mRNA expression data normalized against the housekeeping gene (*Csnk2a2*) and is presented as fold change of WT in boxplots showing the 25-75th percentiles, mean (square), median (line), and SD (whiskers). B, Reporter gene assay in C2C12 myoblasts transfected with a *Gilz* promoter reporter plasmid and treated with vehicle (Co) or statins (50 μM) for 6 hours. Luciferase activity was normalized to the vehicle-treated control. C-E, Western blot analysis of statin-treated C2C12 cells (50 μM, 6 hours; Co: vehicle control). C, One representative blot is shown. D-E, Densitometric analysis. Values for vehicle-treated controls were set as 1. F, ChIP analysis was used to detect the binding of FOXO3 to the *Gilz* promoter region. Data are presented as fold enrichment over IgG. Data show the mean of at least three independent experiments performed in replicates ± SEM. **P* < .05, ***P* < .01, ****P* < .001 relative to the vehicle-treated control

differentiated cultured myotubes, we chose isolated FDB myofibers as an *ex vivo* model to evaluate the effects of the absence of GILZ in statin toxicity toward mature muscle. We noticed that treatment of murine FDB fibers with atorvastatin, simvastatin, and cerivastatin caused cell death with similar features as those previously described for fluvastatin-treated rat FDB fibers.⁵⁹ Furthermore, in accordance with our observations in proliferating myoblasts, GILZ was of crucial importance in mediating statin-induced fiber breakdown.

FOXO3 is a transcription factor involved in different aspects of muscle homeostasis, like regulation of mitochondrial metabolism, activation of protein breakdown *via* the ubiquitin-proteasome and autophagy pathways, and inhibition of muscle

precursor cell proliferation.⁶⁰ In statin-induced myopathy, reports have shown that FOXO3 activation results in expression of the muscle atrophy-related protein MAFbx/atrogin-1 and other genes implicated in muscle proteolysis *in vitro* and *in vivo*.^{40,41} Moreover, FOXO3 has been reported as a transcriptional regulator of GILZ in T cells, where it drives IL-2 withdrawal-induced GILZ expression.⁶¹ We found statin-induced GILZ expression in muscle to be FOXO3-dependent and, as mentioned above, GGPP dependent. These results are in accordance with previous studies that linked SAMS to reduced geranylgeranylation, but not farnesylation of different small GTPases like Rac1, Rap1, and Rab1.^{34,45,56,62} Our findings suggest that the inhibition of protein geranylgeranylation by statins downregulates the

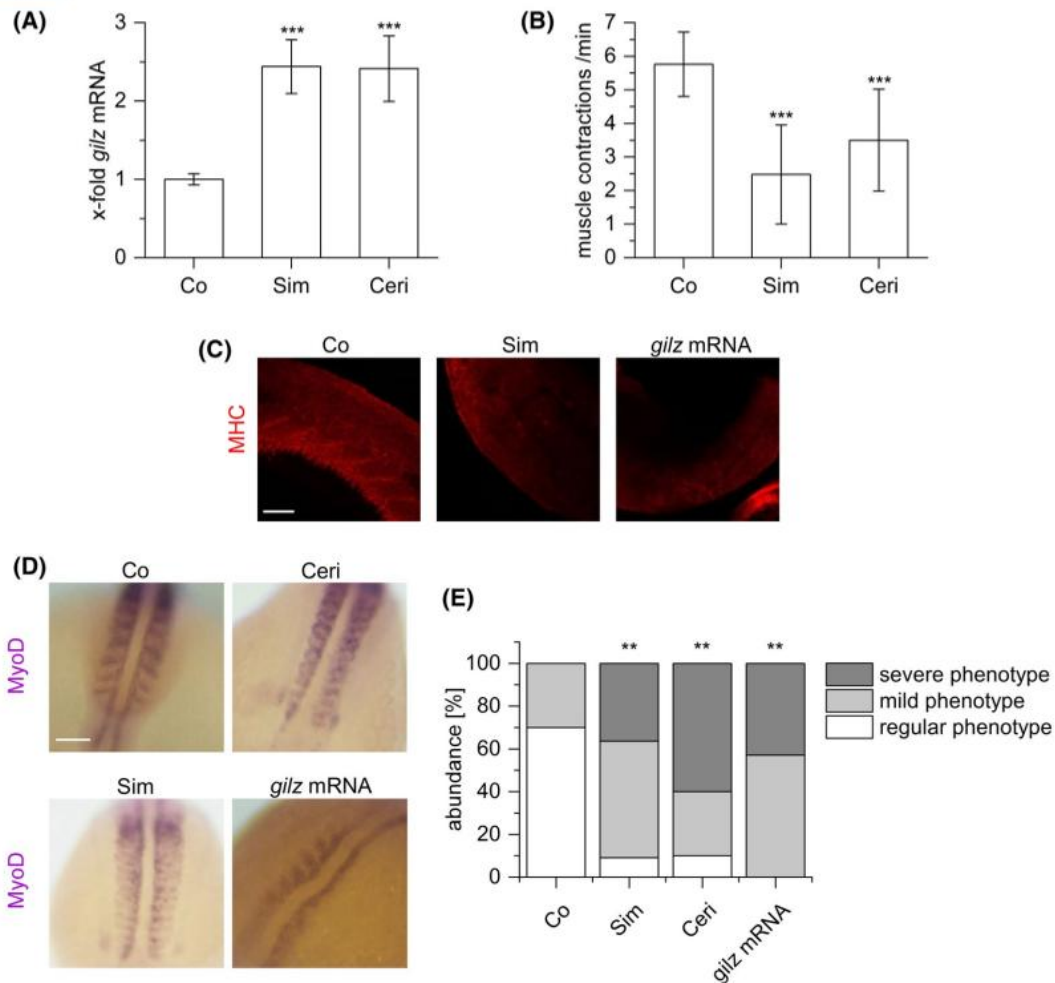


FIGURE 8 Effects of statins and GILZ on zebrafish muscle development. A, Zebrafish embryos at 20 hpf were treated with simvastatin lactone (1 μM) or cerivastatin (1 μM) for 12 hours. mRNA expression was normalized to the housekeeping gene (*actb2*) and is presented as fold change of control ± SEM (n = 3, duplicates). B, Zebrafish embryos at the 1-2 cell stage were treated with simvastatin lactone (1 μM) or cerivastatin (1 μM) for 24 hours, and muscle contractions per minute were counted (n ≥ 10) and are presented as means ± SEM. C-D, 1 ng statin or vehicle (Co) were injected into zebrafish embryos in the 1-2 cell stage. C, MHC IF of statin-treated and *gilz*-overexpressing 24 hpf embryos. Representative images are shown. A diffuse staining and a complete loss of the V-shaped somite pattern was observed in all simvastatin- or *gilz* mRNA-treated embryos (n ≥ 10 per group). Panels are side views. Red: MHC, scale bar: 50 μm. D, MyoD in situ hybridization of statin treated and *gilz*-overexpressing 16 hpf embryos shows a severely impaired MyoD expression when compared to control. Representative images are shown. Panels are dorsal views. Violet: MyoD, scale bar: 60 μm. E, Phenotypic scoring of MyoD-stained embryos (n = 7-10 per group). *P < .05, **P < .01, ***P < .001, relative to the control

Akt signaling pathway, leading to FOXO3-driven GILZ induction, which in turn further decreases Akt phosphorylation and promotes apoptosis of muscle cells.

The fact that GILZ is expressed in skeletal muscle, as observed by us and reported in earlier studies,¹⁶ might denote a role in muscle tissue homeostasis. Indeed, an earlier study showed that GILZ and its longer isoform, L-GILZ, modulate myogenesis in the absence of pharmacological intervention, and mediate glucocorticoid-induced inhibition of myogenesis by decreasing MyoD-mediated myogenin transcription, thus impairing myoblast fusion.²² For this reason, we investigated the role of GILZ in the antimyogenic effects of statins and found that the degree of GILZ induction during myogenesis

was correlated to the antimyogenic effect of the statin used. A previous study reported no differences in myogenin mRNA levels in simvastatin-treated C2C12.⁴⁵ We, however, found myogenin protein expression to be impaired in primary differentiating myoblasts treated with atorvastatin. Moreover, our results in GILZ KO myoblasts indicate that statin-induced GILZ expression, and the consequent myogenin transcriptional repression, is a mechanism by which this class of drugs impairs myogenesis.

GILZ silencing by shRNA caused the resulting C2C12^{shGilz} cell lines to differentiate considerably faster than the C2C12^{scr} control, even to a higher degree than observed for WT cells after terminal differentiation. This supports the importance

of GILZ itself as a modulator of myogenesis and corresponds to our observations in zebrafish embryos, where *gilz* overexpression severely impaired somitogenesis. Importantly, zebrafish embryos represent a frequently used *in vivo* model for the mechanistic study of SAMS.^{50-52,63} The regulatory role played by GILZ in zebrafish embryonic development is rather complex: the study that first described the presence of a GILZ orthologue in zebrafish showed that manipulation of *gilz* expression in this model, either *via* morpholino oligomer silencing or mRNA overexpression, causes significant defects in embryonic development, altering the dorsoventral patterning, segmentation, and brain development processes.⁵³ In rodents, however, GILZ-independent regulatory pathways are most likely involved in the modulation of skeletal muscle development, since GILZ KO mice do not exhibit altered muscle features (unpublished observations).

Even though myogenin expression was rescued in the absence of GILZ, we could not observe a complete recovery in myotube formation after statin treatment in C2C12^{shGilz} cells. This might be related to residual GILZ expression in the silenced cells, or to additional pathways that mediate the antimyogenic effects observed, such as the IGF-1/PI3K/Akt pathway.⁴⁶ Our observations indicate that GILZ is critical for statin-induced inhibition of myogenin, an MRF crucial for myoblast fusion and terminal differentiation.⁶⁴ Additional factors, however, may also contribute to the inhibition of muscle regeneration by statins.

Taken together, our data point toward GILZ as an essential mediator of the molecular mechanisms leading to statin-induced muscle damage and impairment of muscle regeneration. This study contributes to a better understanding of the molecular mechanisms underlying statin-induced myopathy, a necessary step toward the development of prevention strategies, and safer therapy approaches for a class of drugs that remains a pillar in the treatment of cardiovascular disease.

CONFLICT OF INTEREST

The authors have nothing to disclose.

AUTHORS CONTRIBUTIONS

J. Hoppstädter, J.V. Valbuena Perez, R. Linnenberger, C. Dahlem, A. Hecksteden, W.K.F. Tse, S. Bruscoli, and S. Flamini conducted experiments. J.V. Valbuena Perez, J. Hoppstädter, R. Linnenberger, T.M. Legroux, and C. Dahlem acquired and analyzed data. J.V. Valbuena Perez, J. Hoppstädter, A.K. Kiemer, and R. Linnenberger wrote the manuscript. A. Andreas, J. Herrmann, C. Herr, S. Bruscoli, and W.K.F. Tse supported the mouse and zebrafish experiments. S. Bruscoli, C. Riccardi, A.K. Kiemer, and J. Hoppstädter designed research studies. J. Herrmann, R. Müller, R. Bals, C. Riccardi, S. Bruscoli, A.K. Kiemer, A. Hecksteden, and

J. Hoppstädter supervised the experiments, and all authors revised the manuscript. AKK initiated the study.

REFERENCES

1. Grundy SM, Stone NJ, Bailey AL, et al. 2018 AHA/ACC/AACVPR/AAPA/ABC/ACPM/ADA/AGS/APhA/ASPC/NLA/PCNA guideline on the management of blood cholesterol: a report of the American College of Cardiology/American Heart Association task force on clinical practice guidelines. *Circulation*. 2019;139:e1082-e1143.
2. Catapano AL, Graham I, De Backer G, et al. 2016 ESC/EAS guidelines for the management of dyslipidaemias. *Eur Heart J*. 2016;37:2999-3058.
3. Sirtori CR. The pharmacology of statins. *Pharmacol Res*. 2014;88:3-11.
4. Ward NC, Watts GF, Eckel RH. Statin toxicity. *Circ Res*. 2019;124:328-350.
5. Vancheri F, Backlund L, Strender LE, Godman B, Wettermark B. Time trends in statin utilisation and coronary mortality in Western European countries. *BMJ Open*. 2016;6:e010500.
6. Salami JA, Warraich H, Valero-Elizondo J, et al. National trends in statin use and expenditures in the US adult population from 2002 to 2013: insights from the medical expenditure panel survey. *JAMA Cardiol*. 2017;2:56-65.
7. Nolte E, Newbould J, Conklin A. International variation in the usage of medicines: a review of the literature. *Rand Health Q*. 2011;1:4.
8. Taylor F, Huffman MD, Macedo AF, et al. Statins for the primary prevention of cardiovascular disease. *Cochrane Database Syst Rev*. 2013;CD004816.
9. Heller DJ, Coxson PG, Penko J, et al. Evaluating the impact and cost-effectiveness of statin use guidelines for primary prevention of coronary heart disease and stroke. *Circulation*. 2017;136:1087-1098.
10. Stroes ES, Thompson PD, Corsini A, et al. Statin-associated muscle symptoms: impact on statin therapy-European atherosclerosis society consensus panel statement on assessment, aetiology and management. *Eur Heart J*. 2015;36:1012-1022.
11. Mosshammer D, Schaeffeler E, Schwab M, Morike K. Mechanisms and assessment of statin-related muscular adverse effects. *Br J Clin Pharmacol*. 2014;78:454-466.
12. Laufs U, Filipiak KJ, Gouni-Berthold I, Catapano AL, Mandraffino G, Benlian P. Practical aspects in the management of statin-associated muscle symptoms (SAMS). *Atheroscler Suppl*. 2017;26:45-55.
13. Needham M, Mastaglia FL. Statin myotoxicity: a review of genetic susceptibility factors. *Neuromuscul Disord*. 2014;24:4-15.
14. du Souich P, Roederer G, Dufour R. Myotoxicity of statins: mechanism of action. *Pharmacol Ther*. 2017;175:1-16.
15. D'Adamo F, Zollo O, Moraca R, et al. A new dexamethasone-induced gene of the leucine zipper family protects T lymphocytes from TCR/CD3-activated cell death. *Immunity*. 1997;7:803-812.
16. Cannarile L, Zollo O, D'Adamo F, et al. Cloning, chromosomal assignment and tissue distribution of human GILZ, a glucocorticoid hormone-induced gene. *Cell Death Differ*. 2001;8:201-203.
17. Bereshchenko O, Migliorati G, Bruscoli S, Riccardi C. Glucocorticoid-induced leucine zipper: a novel anti-inflammatory molecule. *Front Pharmacol*. 2019;10:305.

18. Shi X, Shi W, Li Q, et al. A glucocorticoid-induced leucine zipper protein, GILZ, inhibits adipogenesis of mesenchymal cells. *EMBO Rep.* 2003;4:374-380.
19. Soundararajan R, Zhang TT, Wang J, Vandewalle A, Pearce D. A novel role for glucocorticoid-induced leucine zipper protein in epithelial sodium channel-mediated sodium transport. *J Biol Chem.* 2005;280:39970-39981.
20. Rashmi P, Colussi G, Ng M, Wu X, Kidwai A, Pearce D. Glucocorticoid-induced leucine zipper protein regulates sodium and potassium balance in the distal nephron. *Kidney Int.* 2017;91:1159-1177.
21. Bruscoli S, Velardi E, Di Sante M, et al. Long glucocorticoid-induced leucine zipper (L-GILZ) protein interacts with ras protein pathway and contributes to spermatogenesis control. *J Biol Chem.* 2012;287:1242-1251.
22. Bruscoli S, Donato V, Velardi E, et al. Glucocorticoid-induced leucine zipper (GILZ) and long GILZ inhibit myogenic differentiation and mediate anti-myogenic effects of glucocorticoids. *J Biol Chem.* 2010;285:10385-10396.
23. Keire P, Shearer A, Shefer G, Yablonka-Reuveni Z. Isolation and culture of skeletal muscle myofibers as a means to analyze satellite cells. *Methods Mol Biol.* 2013;946:431-468.
24. Park KH, Weisleder N, Zhou J, et al. Assessment of calcium sparks in intact skeletal muscle fibers. *J Vis Exp.* 2014;e50898.
25. Hoppstädter J, Hachenthal N, Valbuena-Perez JV, et al. Induction of glucocorticoid-induced leucine zipper (GILZ) contributes to anti-inflammatory effects of the natural product curcumin in macrophages. *J Biol Chem.* 2016;291:22949-22960.
26. Czepukojc B, Abuhaliema A, Bargash A, et al. *IGF2* mRNA binding protein 2 transgenic mice are more prone to develop a ductular reaction and to progress toward cirrhosis. *Front Med.* 2019;6:179.
27. Bruscoli S, Sorcini D, Flamini S, et al. Glucocorticoid-induced leucine zipper inhibits interferon-gamma production in B Cells and suppresses colitis in mice. *Front Immunol.* 2018;9:1720.
28. Hoppstädter J, Diesel B, Linnenberger R, et al. Amplified host defense by Toll-like receptor-mediated downregulation of the glucocorticoid-induced leucine zipper (GILZ) in macrophages. *Front Immunol.* 2019;9:3111.
29. Hoppstädter J, Dembek A, Linnenberger R, et al. Toll-like receptor 2 release by macrophages: an anti-inflammatory program induced by glucocorticoids and lipopolysaccharide. *Front Immunol.* 2019;10:1634.
30. Velica P, Bunce CM. A quick, simple and unbiased method to quantify C2C12 myogenic differentiation. *Muscle Nerve.* 2011;44:366-370.
31. Schindelin J, Arganda-Carreras I, Frise E, et al. Fiji: an open-source platform for biological-image analysis. *Nat Methods.* 2012;9:676-682.
32. Andres V, Walsh K. Myogenin expression, cell cycle withdrawal, and phenotypic differentiation are temporally separable events that precede cell fusion upon myogenesis. *J Cell Biol.* 1996;132:657-666.
33. Kimmel CB, Ballard WW, Kimmel SR, Ullmann B, Schilling TF. Stages of embryonic development of the zebrafish. *Dev Dyn.* 1995;203:253-310.
34. Cao P, Hanai J, Tanksale P, Imamura S, Sukhatme VP, Lecker SH. Statin-induced muscle damage and atrogen-1 induction is the result of a geranylgeranylation defect. *FASEB J.* 2009;23:2844-2854.
35. Xie XW, Liu JX, Hu B, Xiao W. Zebrafish foxo3b negatively regulates canonical Wnt signaling to affect early embryogenesis. *PLoS ONE.* 2011;6:e24469.
36. Brunet A, Bonni A, Zigmond MJ, et al. Akt promotes cell survival by phosphorylating and inhibiting a Forkhead transcription factor. *Cell.* 1999;96:857-868.
37. Moffat J, Grueneberg DA, Yang X, et al. A lentiviral RNAi library for human and mouse genes applied to an arrayed viral high-content screen. *Cell.* 2006;124:1283-1298.
38. Sarbassov DD, Guertin DA, Ali SM, Sabatini DM. Phosphorylation and regulation of Akt/PKB by the rictor-mTOR complex. *Science.* 2005;307:1098-1101.
39. Laaksonen R, Katajamaa M, Paiva H, et al. A systems biology strategy reveals biological pathways and plasma biomarker candidates for potentially toxic statin-induced changes in muscle. *PLoS ONE.* 2006;1:e97.
40. Mallinson JE, Constantin-Teodosiu D, Sidaway J, Westwood FR, Greenhaff PL. Blunted Akt/FOXO signalling and activation of genes controlling atrophy and fuel use in statin myopathy. *J Physiol.* 2009;587:219-230.
41. Hanai J, Cao P, Tanksale P, et al. The muscle-specific ubiquitin ligase atrogen-1/MAFbx mediates statin-induced muscle toxicity. *J Clin Invest.* 2007;117:3940-3951.
42. Bonifacio A, Sanvee GM, Bouitbir J, Krahenbuhl S. The AKT/mTOR signaling pathway plays a key role in statin-induced myotoxicity. *Biochim Biophys Acta.* 2015;1853:1841-1849.
43. Schirris TJ, Renkema GH, Ritschel T, et al. Statin-induced myopathy is associated with mitochondrial complex III inhibition. *Cell Metab.* 2015;22:399-407.
44. Bentzinger CF, Wang YX, Rudnicki MA. Building muscle: molecular regulation of myogenesis. *Cold Spring Harb Perspect Biol.* 2012;4:a008342.
45. Baba TT, Nemoto TK, Miyazaki T, Oida S. Simvastatin suppresses the differentiation of C2C12 myoblast cells via a Rac pathway. *J Muscle Res Cell Motil.* 2008;29:127-134.
46. Ogura T, Tanaka Y, Nakata T, Namikawa T, Kataoka H, Ohtsubo Y. Simvastatin reduces insulin-like growth factor-1 signaling in differentiating C2C12 mouse myoblast cells in an HMG-CoA reductase inhibition-independent manner. *J Toxicol Sci.* 2007;32:57-67.
47. Trapani L, Segatto M, La Rosa P, et al. 3-hydroxy 3-methylglutaryl coenzyme a reductase inhibition impairs muscle regeneration. *J Cell Biochem.* 2012;113:2057-2063.
48. Ravenscroft G, Nowak KJ, Jackaman C, et al. Dissociated flexor digitorum brevis myofiber culture system—a more mature muscle culture system. *Cell Motil Cytoskeleton.* 2007;64:727-738.
49. Sakamoto K, Kimura J. Mechanism of statin-induced rhabdomyolysis. *J Pharmacol Sci.* 2013;123:289-294.
50. Campos LM, Rios EA, Guapyassu L, et al. Alterations in zebrafish development induced by simvastatin: comprehensive morphological and physiological study, focusing on muscle. *Exp Biol Med (Maywood).* 2016;241:1950-1960.
51. Pasha R, Moon TW. Coenzyme Q10 protects against statin-induced myotoxicity in zebrafish larvae (Danio rerio). *Environ Toxicol Pharmacol.* 2017;52:150-160.
52. Huang SH, Hsiao CD, Lin DS, Chow CY, Chang CJ, Liau I. Imaging of zebrafish in vivo with second-harmonic generation reveals shortened sarcomeres associated with myopathy induced by statin. *PLoS ONE.* 2011;6:e24764.
53. Tse WK, Jiang YJ, Wong CK. Zebrafish transforming growth factor-beta-stimulated clone 22 domain 3 (TSC22D3) plays critical roles in Bmp-dependent dorsoventral patterning via two deubiquitylating enzymes Usp15 and Otud4. *Biochim Biophys Acta.* 2013;1830:4584-4593.

54. Bouitbir J, Charles AL, Echaniz-Laguna A, et al. Opposite effects of statins on mitochondria of cardiac and skeletal muscles: a 'mitohormesis' mechanism involving reactive oxygen species and PGC-1. *Eur Heart J*. 2012;33:1397-1407.
55. Osaki Y, Nakagawa Y, Miyahara S, et al. Skeletal muscle-specific HMG-CoA reductase knockout mice exhibit rhabdomyolysis: a model for statin-induced myopathy. *Biochem Biophys Res Commun*. 2015;466:536-540.
56. Johnson TE, Zhang X, Bleicher KB, et al. Statins induce apoptosis in rat and human myotube cultures by inhibiting protein geranylgeranylation but not ubiquinone. *Toxicol Appl Pharmacol*. 2004;200:237-250.
57. Espinasse MA, Pepin A, Virault-Rocroy P, et al. Glucocorticoid-induced leucine zipper is expressed in human neutrophils and promotes apoptosis through Mcl-1 down-regulation. *J Innate Immun*. 2016;8:81-96.
58. Joha S, Nagues AL, Hetuin D, et al. GILZ inhibits the mTORC2/AKT pathway in BCR-ABL(+) cells. *Oncogene*. 2012;31:1419-1430.
59. Sakamoto K, Wada I, Kimura J. Inhibition of Rab1 GTPase and endoplasmic reticulum-to-Golgi trafficking underlies statin's toxicity in rat skeletal myofibers. *J Pharmacol Exp Ther*. 2011;338:62-69.
60. Sanchez AM, Candau RB, Bernardi H. FoxO transcription factors: their roles in the maintenance of skeletal muscle homeostasis. *Cell Mol Life Sci*. 2014;71:1657-1671.
61. Asselin-Labat ML, Biola-Vidamment A, Kerbrat S, Lombes M, Bertoglio J, Pallardy M. FoxO3 mediates antagonistic effects of glucocorticoids and interleukin-2 on glucocorticoid-induced leucine zipper expression. *Mol Endocrinol*. 2005;19:1752-1764.
62. Sakamoto K, Honda T, Yokoya S, Waguri S, Kimura J. Rab-small GTPases are involved in fluvastatin and pravastatin-induced vacuolation in rat skeletal myofibers. *FASEB J*. 2007;21:4087-4094.
63. Campos LM, Rios EA, Midlej V, et al. Structural analysis of alterations in zebrafish muscle differentiation induced by simvastatin and their recovery with cholesterol. *J Histochem Cytochem*. 2015;63:427-437.
64. Asfour HA, Allouh MZ, Said RS. Myogenic regulatory factors: the orchestrators of myogenesis after 30 years of discovery. *Exp Biol Med (Maywood)*. 2018;243:118-128.

SUPPORTING INFORMATION

Additional supporting information may be found online in the Supporting Information section.

How to cite this article: Hoppstädter J, Valbuena Perez JV, Linnenberger R, et al. The glucocorticoid-induced leucine zipper mediates statin-induced muscle damage. *The FASEB Journal*. 2020;34:4684-4701. <https://doi.org/10.1096/fj.201902557RRR>

SUPPLEMENTAL DATA

The Glucocorticoid-Induced Leucine Zipper Mediates Statin-Induced Muscle Damage

Jessica Hoppstädter^{1,2}; Jenny Vanessa Valbuena Perez^{1*}; Rebecca Linnenberger¹; Charlotte Dahlem¹; Thierry M. Legroux¹, Anne Hecksteden³; William K. F. Tse⁴; Sara Flamini²; Anastasia Andreas⁵; Jennifer Herrmann⁵; Christian Herr⁶; Rolf Müller⁵; Tim Meyer³; Robert Bals⁶; Carlo Riccardi²; Stefano Bruscoli²; Alexandra K. Kiemer¹.*

¹*Department of Pharmacy, Pharmaceutical Biology, Saarland University, Campus C2 3, 66123 Saarbrücken, Germany*

²*Department of Medicine, Section of Pharmacology, University of Perugia, Piazzale Severi 1, S. Andrea delle Fratte, 06132 Perugia, Italy*

³*Institute of Sports and Preventive Medicine, Saarland University, Campus B8 2, 66123 Saarbrücken, Germany*

⁴*Center for Promotion of International Education and Research, Faculty of Agriculture, Kyushu University, 744 Motoooka Nishi-ku Fukuoka, 819-0395, Japan*

⁵*Department of Microbial Natural Products, Helmholtz Institute for Pharmaceutical Research Saarland (HIPS), Campus E8 1, 66123 Saarbrücken, Germany*

⁶*Department of Internal Medicine V—Pulmonology, Allergology and Critical Care Medicine, Saarland University, 66421 Homburg, Germany*

**Equal contribution*

Correspondence to:

Alexandra K. Kiemer, Ph.D.

Pharmaceutical Biology

Saarland University

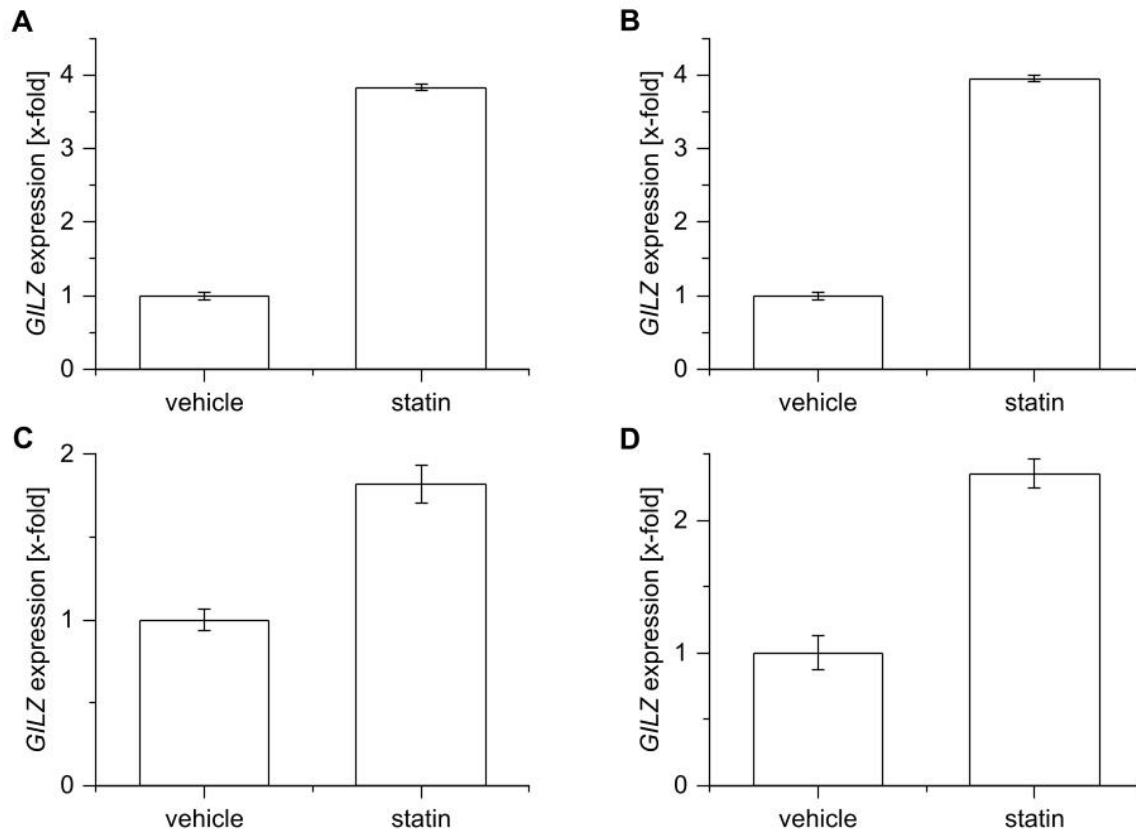
D-66123 Saarbrücken, Germany,

Tel: +49 681 302-57301

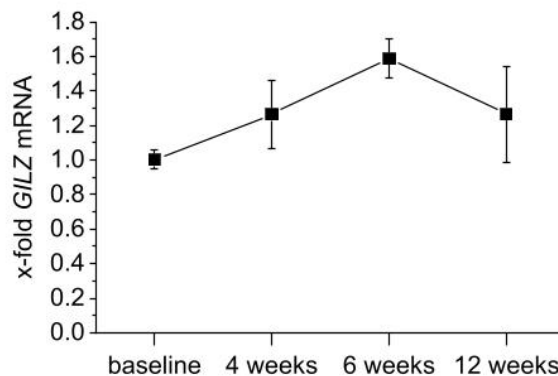
Fax: +49 681 302-57302

pharm.bio.kiemer@mx.uni-saarland.de

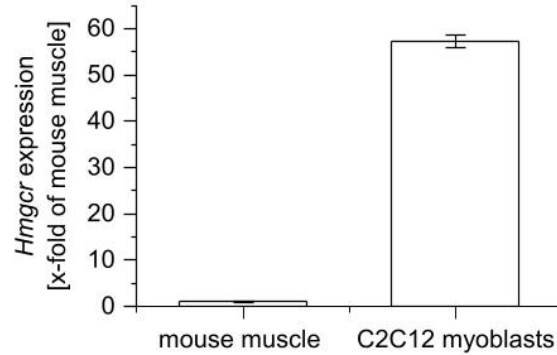
Supplemental Figures



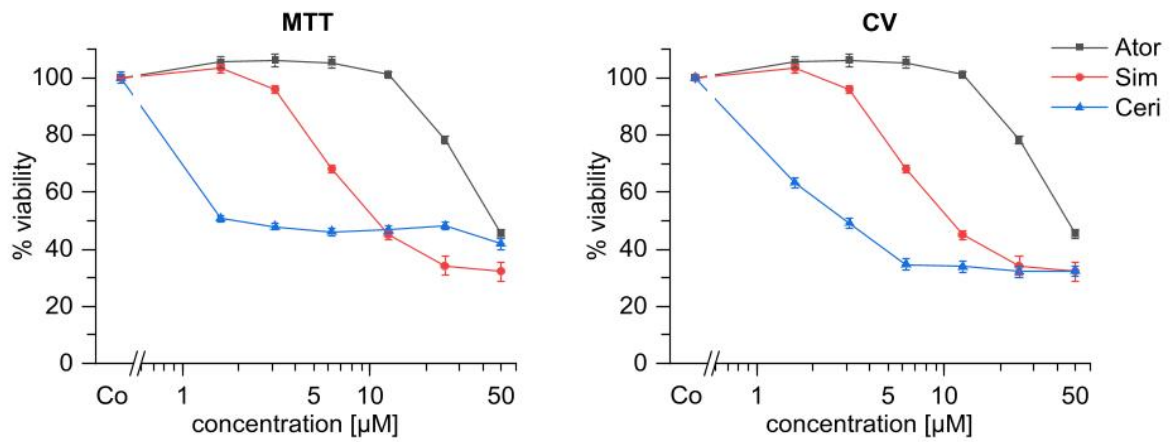
Supplemental figure 1. Analyses of Gene Expression Omnibus (GEO) datasets. A-D: *GILZ* expression after atorvastatin treatment (24 h, 10 μ M) in human microvascular endothelial cells (A) and pulmonary artery smooth muscle cells (B) (both GDS2987, n=3 for vehicle and treatment), after pitavastatin treatment (4 h, 1 μ M) in human umbilical vein endothelial cells (C) (GSE32547, n=9 for vehicle and treatment), and after simvastatin treatment (24 h, 10 μ M) human peripheral blood monocytes (D) (GSE4883, n=3 for vehicle and treatment).



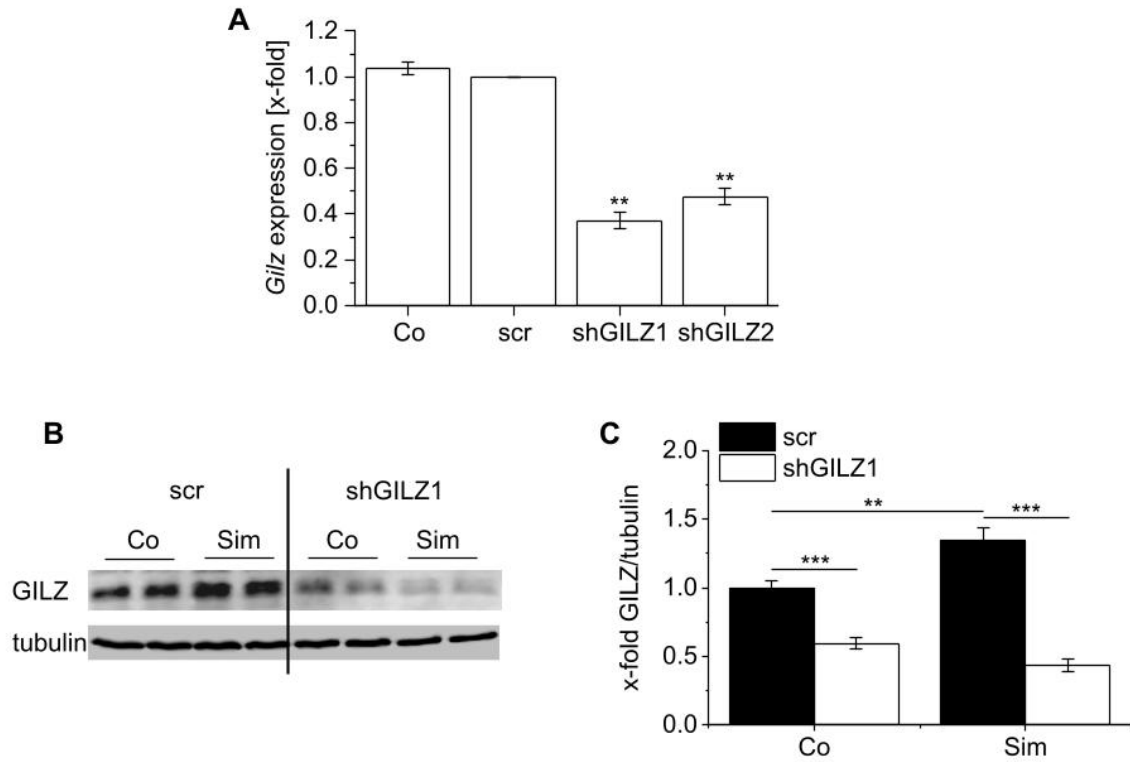
Supplemental figure 2. Effect of simvastatin on *GILZ* expression in human muscle in one hypercholesterolemic individual. mRNA expression was normalized to the housekeeping gene (*RNA18S5*) and is presented as fold change of baseline. Data show the mean of 2 biopsies at each time point (right and left leg) after 40 mg/d simvastatin treatment. RNA isolation was performed twice (except for muscle biopsies after 12 weeks of treatment), and qPCR measurements were performed in triplicates. Data show means \pm SEM.



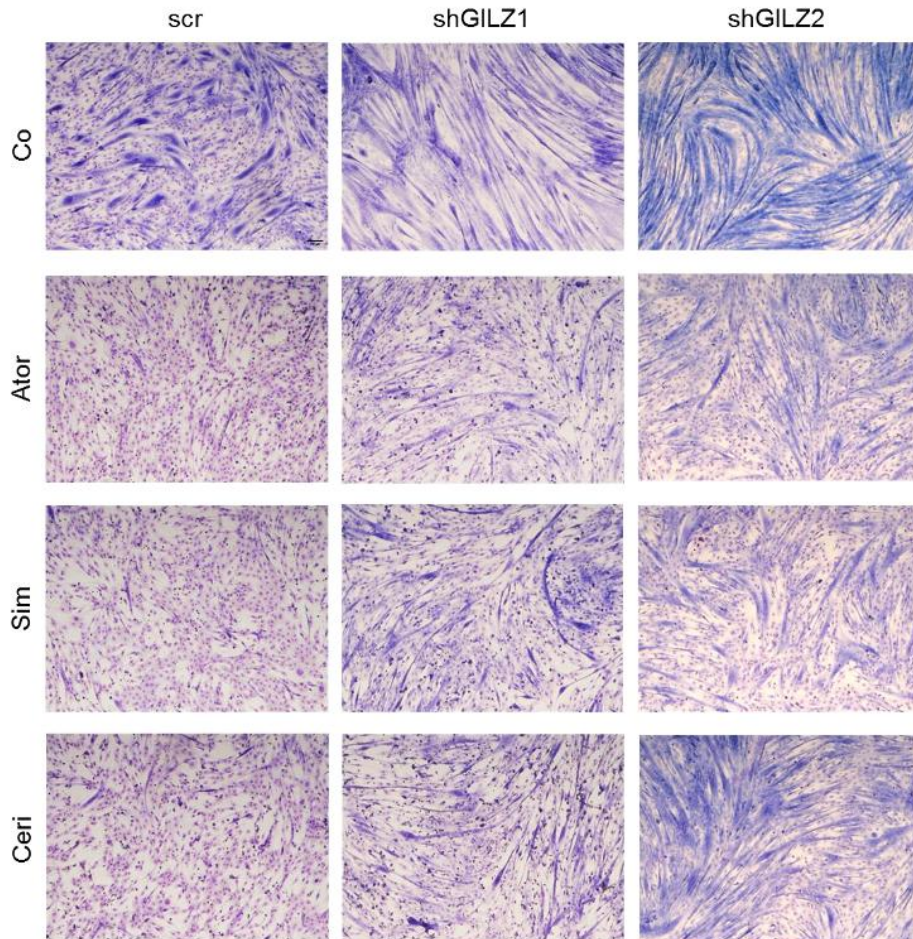
Supplemental figure 3. Baseline *Hmgcr* expression in murine muscle tissue and C2C12 myoblasts. *Hmgcr* mRNA expression was normalized to the housekeeping gene (*Ppia*) and is presented as fold of muscle tissue. Data show the mean of 3 independent experiments \pm SEM in C2C12 myoblasts and the mean \pm SEM of samples from 10 female C57/BL6 mice.



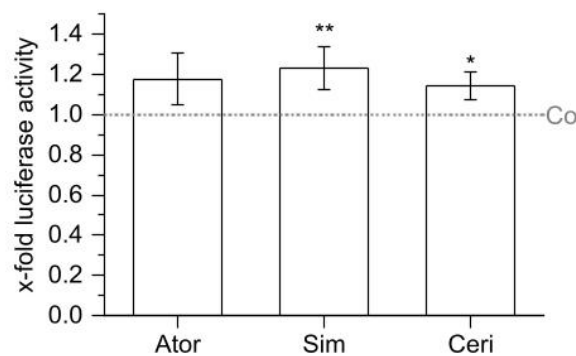
Supplemental figure 4. Effect of statins on C2C12 myoblast viability. C2C12 myoblasts were treated with atorvastatin (Ator), simvastatin (Sim), or cerivastatin (Ceri) at the indicated concentrations concentrations for 24 h. Cell viability was measured via MTT or crystal violet (CV) assay. Data show the mean of three independent experiments performed in replicates \pm SEM.



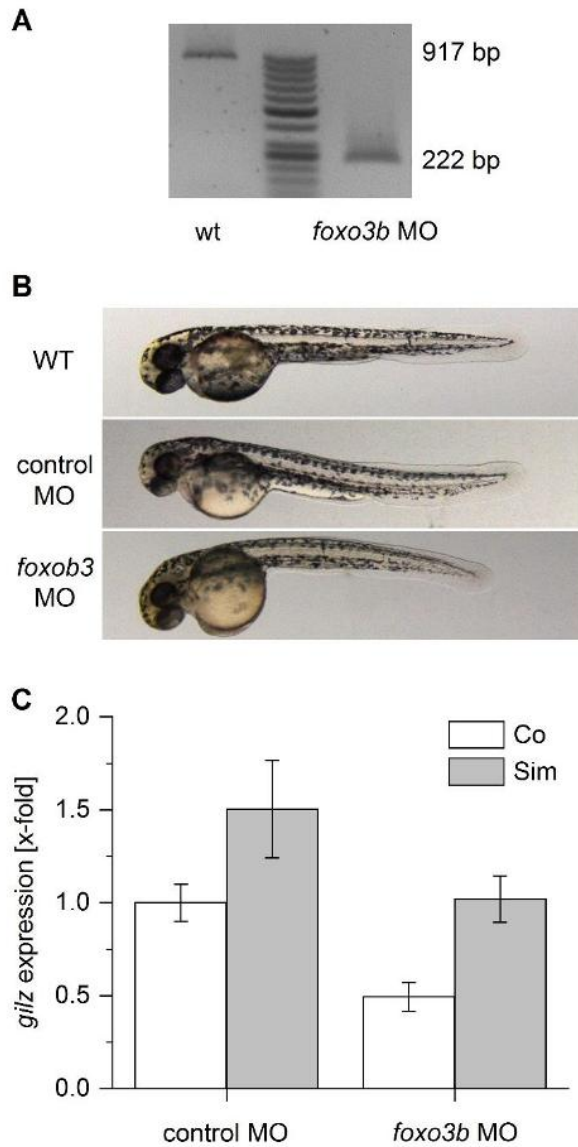
Supplemental figure 5. GILZ expression in stable C2C12^{shGILZ} cell lines. Scrambled control (C2C12^{scr}) and C2C12^{shGILZ} cell lines were generated by lentiviral transduction. A: *Gilz* mRNA expression was normalized to the housekeeping gene (*Csnk2a2*) and is presented as fold change of the non-transduced control (Co). Data show the mean of 3 independent experiments \pm SEM. ** $P < 0.01$ relative to scr cells. B, C: C2C12^{scr} and C2C12^{shGILZ1} were treated with simvastatin (50 μ M, 6 h) or vehicle (0.25% DMSO, Co), and GILZ expression was determined by Western blot using tubulin as a loading control. B: Representative blot. C: Densitometric analysis. GILZ values were normalized to tubulin and expressed as x-fold of vehicle-treated (Co) C2C12^{scr} (n = 3, duplicates). ** $P < 0.01$, *** $P < 0.001$.



Supplemental figure 6. Effect of GILZ absence on statin-induced anti-myogenic effects, as measured by Jenner-Giemsa staining. Scrambled ($C2C12^{scr}$) and $C2C12^{shGILZ}$ cell lines were induced to differentiate for 4 days in the absence or presence of atorvastatin (Ator, 5 μ M), cerivastatin (Ceri, 0.1 μ M), or simvastatin (Sim, 1 μ M), and subjected to Jenner-Giemsa staining. Representative images from one out of three experiments with similar outcome are shown. Scale bar, 100 μ m.



Supplemental figure 7. Reporter gene assay in C2C12 myoblasts transfected with a FoxO3 reporter plasmid. Cells were treated with 50 μ M statin or vehicle control (0.25% DMSO) for 6 h. Luciferase activity was measured and is presented as fold of control. Data show the mean of 4 independent experiments performed in replicates \pm SEM. * $P < 0.05$, ** $P < 0.01$ relative to the control.



Supplemental figure 8. Knockdown of *foxo3b* results in defects in body axis and reduced *gilz* expression in zebrafish embryos. Embryos were injected with 16 ng *foxo3b* or random control MO in the 1-2 cell stage. A: Validation of *foxo3b* splice-blocking MO effects. The *foxo3b* MO injection resulted in a truncated PCR product (222 bp), caused by the deletion of exon 2. B: Morphology of representative morphants 48 hpf. *foxo3b* morphants had a shorter body length. C: Morphants at 20 hpf were treated with 1 μ M simvastatin lactone (Sim) or vehicle control (Co) for 12 h. *Gilz* mRNA expression was normalized to the housekeeping gene (*actb2*) and is presented as fold change relative to vehicle-treated control MO. Data show the means \pm SEM of 3 samples pooled from 10-20 embryos per treatment group.

3.4. Statins and Bempedoic Acid: Different Actions of Cholesterol Inhibitors on Macrophage Activation

Int. J. Mol. Sci **2021**, doi: 10.3390/ijms222212480

R. Linnenberger conducted experiments and acquired data. R. Linnenberger and J. Hoppstädter analyzed data. S. Wrublewsky and E. Ampofo provided mice. R. Linnenberger, J. Hoppstädter, and A. K. Kiemer designed research studies and wrote the manuscript. A. K. Kiemer and J. Hoppstädter supervised and revised the manuscript. A. K. Kiemer initiated the study. All authors have read and agreed to the published version of the manuscript.

Rebecca Linnenberger planned, carried out, analyzed, and validated the work described in this publication. Lastly, she conceived, wrote parts of the manuscript, and submitted the manuscript.

© Linnenberger, Hoppstädter, Wrublewsky, Ampofo, Kiemer. This is an open-access article distributed under the terms of the Creative Commons Attribution Licence (CC BY).

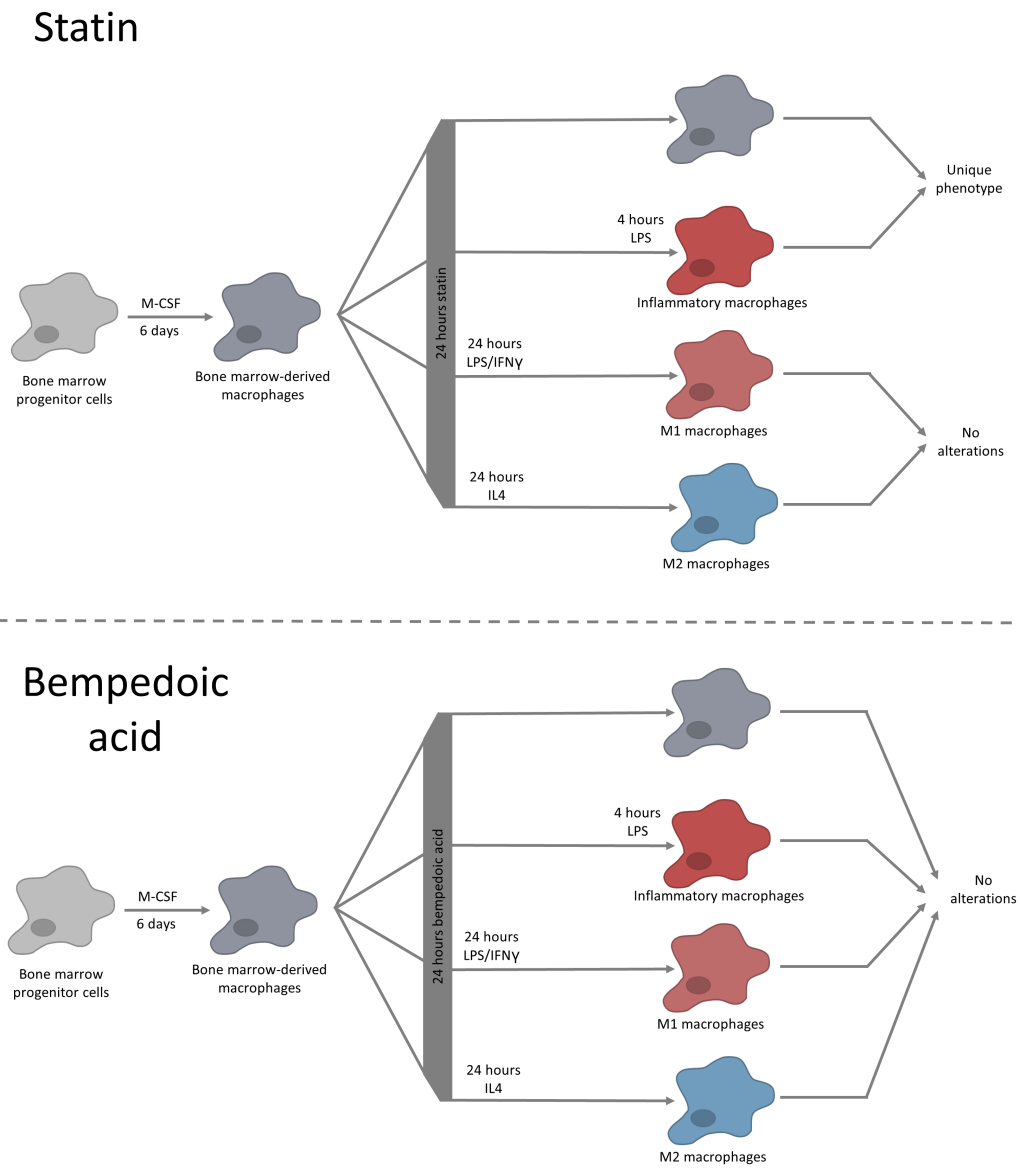




Figure 8: Graphical abstract of (Linnenberger et al., 2021).



Article

Statins and Bempedoic Acid: Different Actions of Cholesterol Inhibitors on Macrophage Activation

Rebecca Linnenberger ^{1,†}, Jessica Hoppstädter ^{1,†}, Selina Wrublewsky ², Emmanuel Ampofo ² 
and Alexandra K. Kiemer ^{1,*} 

¹ Department of Pharmacy, Pharmaceutical Biology, Saarland University, Campus C2.3, 66123 Saarbrücken, Germany; rebecca.linnenberger@uni-saarland.de (R.L.); j.hoppstaedter@mx.uni-saarland.de (J.H.)

² Institute of Clinical and Experimental Surgery, Saarland University, 66424 Homburg, Germany; selina.wrublewsky@uks.eu (S.W.); emmanuel.ampofo@uks.eu (E.A.)

* Correspondence: pharm.bio.kiemer@mx.uni-saarland.de

† These authors contributed equally to this work.



Citation: Linnenberger, R.; Hoppstädter, J.; Wrublewsky, S.; Ampofo, E.; Kiemer, A.K. Statins and Bempedoic Acid: Different Actions of Cholesterol Inhibitors on Macrophage Activation. *Int. J. Mol. Sci.* **2021**, *22*, 12480. <https://doi.org/10.3390/ijms222212480>

Academic Editor: Nadia Lampiasi

Received: 11 October 2021

Accepted: 16 November 2021

Published: 19 November 2021

Publisher's Note: MDPI stays neutral with regard to jurisdictional claims in published maps and institutional affiliations.



Copyright: © 2021 by the authors. Licensee MDPI, Basel, Switzerland. This article is an open access article distributed under the terms and conditions of the Creative Commons Attribution (CC BY) license (<https://creativecommons.org/licenses/by/4.0/>).

Abstract: Statins represent the most prescribed class of drugs for the treatment of hypercholesterolemia. Effects that go beyond lipid-lowering actions have been suggested to contribute to their beneficial pharmacological properties. Whether and how statins act on macrophages has been a matter of debate. In the present study, we aimed at characterizing the impact of statins on macrophage polarization and comparing these to the effects of bempedoic acid, a recently registered drug for the treatment of hypercholesterolemia, which has been suggested to have a similar beneficial profile but fewer side effects. Treatment of primary murine macrophages with two different statins, i.e., simvastatin and cerivastatin, impaired phagocytotic activity and, concurrently, enhanced pro-inflammatory responses upon short-term lipopolysaccharide challenge, as characterized by an induction of tumor necrosis factor (TNF), interleukin (IL) 1 β , and IL6. In contrast, no differences were observed under long-term inflammatory (M1) or anti-inflammatory (M2) conditions, and neither inducible NO synthase (iNOS) expression nor nitric oxide production was altered. Statin treatment led to extracellular-signal regulated kinase (ERK) activation, and the pro-inflammatory statin effects were abolished by ERK inhibition. Bempedoic acid only had a negligible impact on macrophage responses when compared with statins. Taken together, our data point toward an immunomodulatory effect of statins on macrophage polarization, which is absent upon bempedoic acid treatment.

Keywords: natural compounds; polarization; bone marrow-derived macrophages; LPS; phagocytosis; arginase; HMG-CoA reductase; inflammasome; GILZ; KLF2

1. Introduction

Mevastatin, exhibiting potent hypocholesterolemic activity, was isolated in 1976 from the fungus *Penicillium citrinum*. Shortly thereafter, two other statins, namely pravastatin and lovastatin, were discovered [1]. Whereas the semi-synthetic simvastatin solely differs in an alkyl moiety from lovastatin, synthetic statins, such as cerivastatin and atorvastatin, only have the pharmacophore in common with their ancestors [2]. Today, statins are the first-line treatment of cardiovascular diseases (CVDs), which represent the leading cause of death worldwide [3].

Due to hypercholesterolemia being one of the underlying conditions of atherosclerotic diseases, statin prescriptions have been rising within the last years, and statins are today the most prescribed class of drugs worldwide [4]. From natural compound-derived statins to new synthetic ones, the mode of action has remained the same: This class of drugs interferes with the rate-limiting step of cholesterol synthesis in the liver by competitively inhibiting hydroxy-methyl-glutaryl-coenzyme A (HMG-CoA) reductase, resulting in enhanced low-density lipoprotein (LDL) clearance from the circulation [5–7]. Besides their lipid-lowering

actions, statins exert pleiotropic effects, which might be due to the impaired synthesis of isoprenoids as intermediates of the mevalonate pathway. The reduced synthesis of prenylated proteins, such as Ras and Rho family small GTPases, results in altered cell signaling [8].

Clinical studies on atherosclerosis have shown that these pleiotropic effects are beneficial and linked them to antioxidant or anti-inflammatory effects and plaque stabilization [9,10]. Therefore, statins have been suggested for the treatment of respiratory conditions such as pneumonia and acute respiratory distress syndrome [11,12]. They have also been reported to be beneficial in different bacterial infections [13,14], and their benefits in the treatment of COVID-19 are currently under investigation [15]. Consistent clinical evidence for the benefits of statin use in a broader range of inflammatory conditions is lacking, which is why statins are still only approved for primary and secondary prevention of cardiovascular events.

It is, however, very much in doubt whether the statin-mediated inhibition of inflammation in the context of atherosclerosis is independent of its cholesterol-lowering actions since recently published studies suggested that statins may activate inflammatory pathways, and non-statin cholesterol-lowering drugs also have anti-inflammatory potential [16–24].

Macrophages have been postulated as one target cell type of statin actions. They represent a heterogeneous cell population that is characterized by high plasticity. Both exogenous and endogenous factors determine macrophage polarization, including, but not limited to, pathogen-associated molecular patterns, such as lipopolysaccharide (LPS), danger-associated molecular patterns, but also natural compounds [25–27]. They mediate their response towards pathogen- or danger-associated molecular patterns by the release of cytokines and small molecules.

Reports on whether and how statins interact with macrophages are conflicting, however. Both pro- and anti-inflammatory effects, which result from altered isoprenylation and activation of stress kinases, such as c-Jun N-terminal kinase (JNK) or extracellular signal-regulated kinase (ERK), have been described. In addition, statins have been suggested to affect the NOD- (nucleotide-binding oligomerization), LRR- (leucine-rich repeat), and pyrin domain-containing protein 3 (NLRP3) inflammasome and induce the expression of the transcription factor Krüppel-like factor 2 (KLF2), a potent inhibitor of metabolic inflammation [16,28–32].

The novel cholesterol-lowering agent bempedoic acid (ETC-1002) was recently approved for the treatment of hypercholesterolemia. This small synthetic prodrug is suggested to act only in hepatocytes. The compound requires a hepatocyte-specific enzyme, the very long-chain acyl-CoA synthetase-1 (gene name: *Slc27a2*), for transformation into its active form, ETC-1002-CoA, which then inhibits ATP-citrate lyase (gene name: *Acly*) upstream of HMG-CoA reductase [33,34]. Clinical studies revealed a reduction of LDL-cholesterol and total cholesterol, but not triglycerides, upon bempedoic acid administration [35].

The pharmacokinetic properties of bempedoic acid aim to prevent muscle-related side effects, which frequently occur under statin treatment. These adverse effects of statins have been associated with impaired mitochondrial function and disturbed calcium homeostasis within muscle cells [36]. Our previously published data also suggest an involvement of the glucocorticoid-induced leucine zipper (GILZ, gene name *Tsc22d3*), a protein formerly mainly known for its anti-inflammatory properties in leukocytes: GILZ was induced by statins in muscle cells and contributed to statin-mediated myotoxic and anti-myogenic effects [37].

In addition to its cholesterol-lowering activity, bempedoic acid treatment decreases high-sensitivity C-reactive protein serum levels, suggesting that the compound exhibits anti-inflammatory properties [35].

As both statins and bempedoic acid show anti-inflammatory activity in vivo, we hypothesized that both types of cholesterol-lowering agents might affect macrophage responses. The aim of the present study was to systematically test different aspects of macrophage activation upon statin and bempedoic acid treatment.

2. Results

2.1. Modulation of Inflammatory and Anti-Inflammatory Mediator Expression in Statin-Treated Macrophages

Potential effects of two statins, i.e., simvastatin (Sim, 2 μ M) and cerivastatin (Cer, 0.5 μ M), on macrophages were investigated at non-toxic concentrations (Supplementary Figures S1 and S2). These relatively high statin concentrations are in accordance with the literature [37,38] and were based on our observations of higher *Hmgcr* and *Acly* levels after statin treatment, as well as the known negative feedback regulation of HMG-CoA reductase in cell culture (Supplementary Figure S3) [39].

Nuclear factor 'kappa-light-chain-enhancer' of activated B-cells (NF- κ B) and activator protein 1 (AP-1) are the main transcription factors involved in macrophage inflammatory activation. Statin treatment of a macrophage reporter cell line activated NF- κ B/AP-1, and an additional short-term LPS challenge (4 h LPS) resulted in an even higher amplitude of inflammation (Figure 1A).

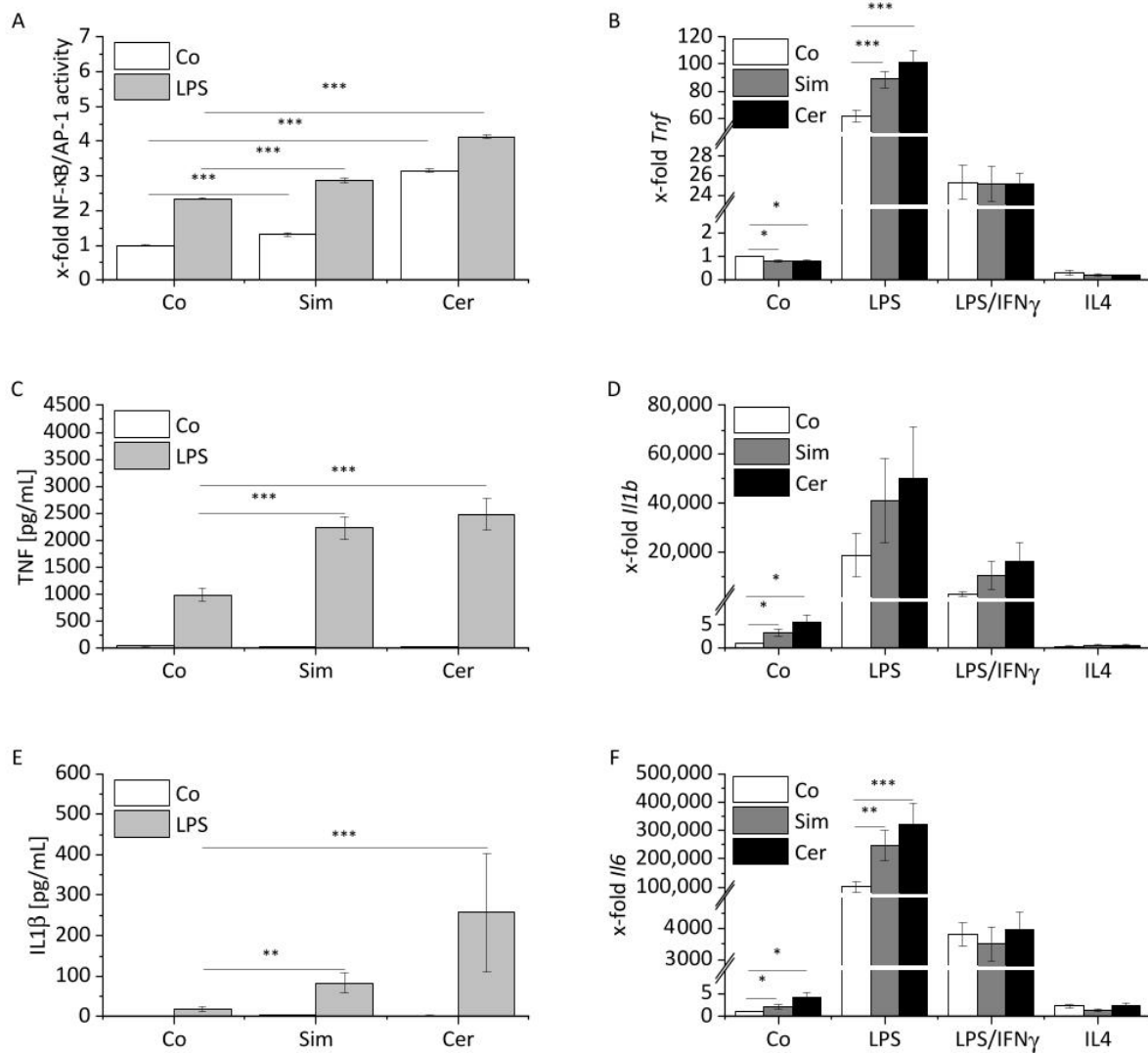


Figure 1. Cont.

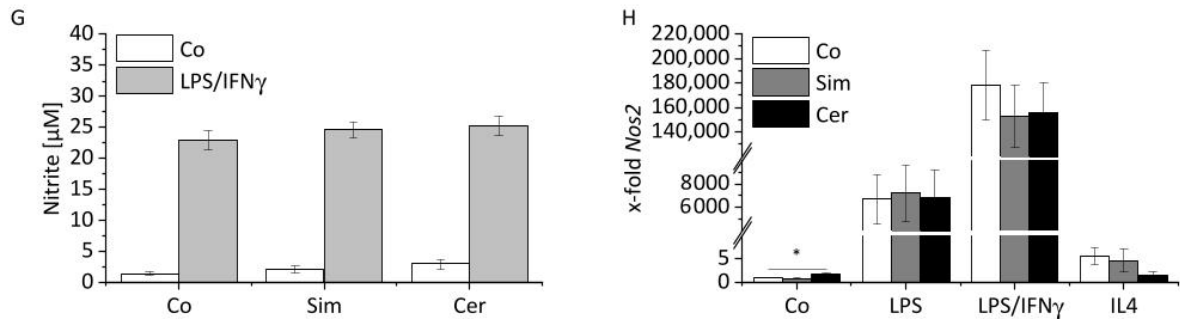


Figure 1. Effect of statin treatment on inflammatory macrophage activation. (A) RAW-BlueTM cells were treated with either simvastatin (Sim, 2 μ M) or cerivastatin (Cer, 1 μ M) for 24 h. Inflammatory activation was induced by treatment with LPS (100 ng/mL) for the final 4 h. NF- κ B/AP-1 activity was determined by secreted embryonic alkaline phosphatase (SEAP) detection. Co = solvent control ($n = 3$, triplicates). (B,D,F,H) *Tnf* (B), *Il1b* (D), *Il6* (F), and *Nos2* (H) mRNA expression in BMMs was determined by real-time RT-PCR, normalized to *Ppia*, and expressed as x-fold of Co. BMMs were stimulated for the last 4 h with LPS (100 ng/mL) or polarized towards M1 (LPS, 100 ng/mL; IFN γ , 20 ng/mL), or M2 (IL4, 20 ng/mL) in the presence or absence of Sim (2 μ M) or Cer (0.5 μ M) for 24 h. Co = solvent control ($n = 6$). (C,E) TNF (C) and IL1 β (E) were measured by bioassay. BMMs were treated for 24 h with either Sim (2 μ M) or Cer (0.5 μ M). Inflammatory activation was induced by treatment with LPS (100 ng/mL for IL1 β , 10 ng/mL for TNF) for the final 4 h. Co = solvent control ($n = 3$, duplicates for TNF, triplicates for IL1 β). (G) Nitrite production was measured by Griess assay. BMMs were treated for 24 h with either Sim (2 μ M) or Cer (0.5 μ M). Samples were stimulated for the final 20 h (LPS, 50 ng/mL; IFN γ , 20 ng/mL). Co = solvent control ($n = 3$, triplicates). A one-sample *t*-test followed by a Bonholm post hoc test was used for analyzing gene expression data of the control group. Means of more than two groups were compared by one-way ANOVA with Bonholm post hoc test (normal distribution). * $p < 0.05$, ** $p < 0.01$, and *** $p < 0.001$.

Primary bone marrow-derived macrophages (BMMs) were either treated with statins alone or in combination with different stimuli, namely a short-term inflammatory activation (4 h LPS), an M1 (24 h LPS/interferon-gamma (IFN γ)), or an M2 (24 h interleukin (IL) 4) treatment scheme. We then quantified the cytokines TNF and IL1 β , NO, and M1/M2-associated gene expression levels. Both statins amplified the LPS-induced production of TNF and IL1 β (Figure 1C,E). Moreover, statin treatment increased the levels of *Il6* mRNA in LPS-treated cells (Figure 1F). *Il1b* and *Il6* mRNA levels were above background levels upon treatment with either statin in the absence of LPS, while *Tnf* mRNA was decreased (Figure 1B,D,F, Supplementary Figure S4A–C). No modulatory effect of statins was observed under M1 conditions (Figure 1B,D,F). Statins did not influence NO release under inflammatory conditions, and only cerivastatin slightly affected *Nos2* mRNA (Figure 1G–H, Supplementary Figure S4D).

Next, we sought to examine whether statins exert modulatory effects on markers associated with anti-inflammatory actions. Statins significantly induced arginase-1 and GILZ (gene names: *Arg1*, *Tsc22d3*) under every tested condition (Figure 2A,B, Supplementary Figure S5A,B). While *Il10* and *Tgfb1* expression were hardly affected by statin treatment, *Mrc1* levels were decreased (Figure 2C–E, Supplementary Figure S5C,D). The transcription factor *Klf2* was induced by statins (Figure 2F, Supplementary Figure S5E,F). Its induction followed a similar pattern as observed for *Tsc22d3*, suggesting crosstalk between these anti-inflammatory mediators. This assumption was further supported by the observation that statin-induced *Klf2* expression was reduced in *Tsc22d3* knockout macrophages (Supplementary Figure S6).

In summary, these data point towards a unique statin-induced modulation of the macrophage phenotype regarding expression levels of M1/M2 markers after statin treatment. While the induction of M1-associated genes points towards a pro-inflammatory phenotype, an exacerbation of inflammatory responses may be limited by the selective induction of anti-inflammatory mediators.

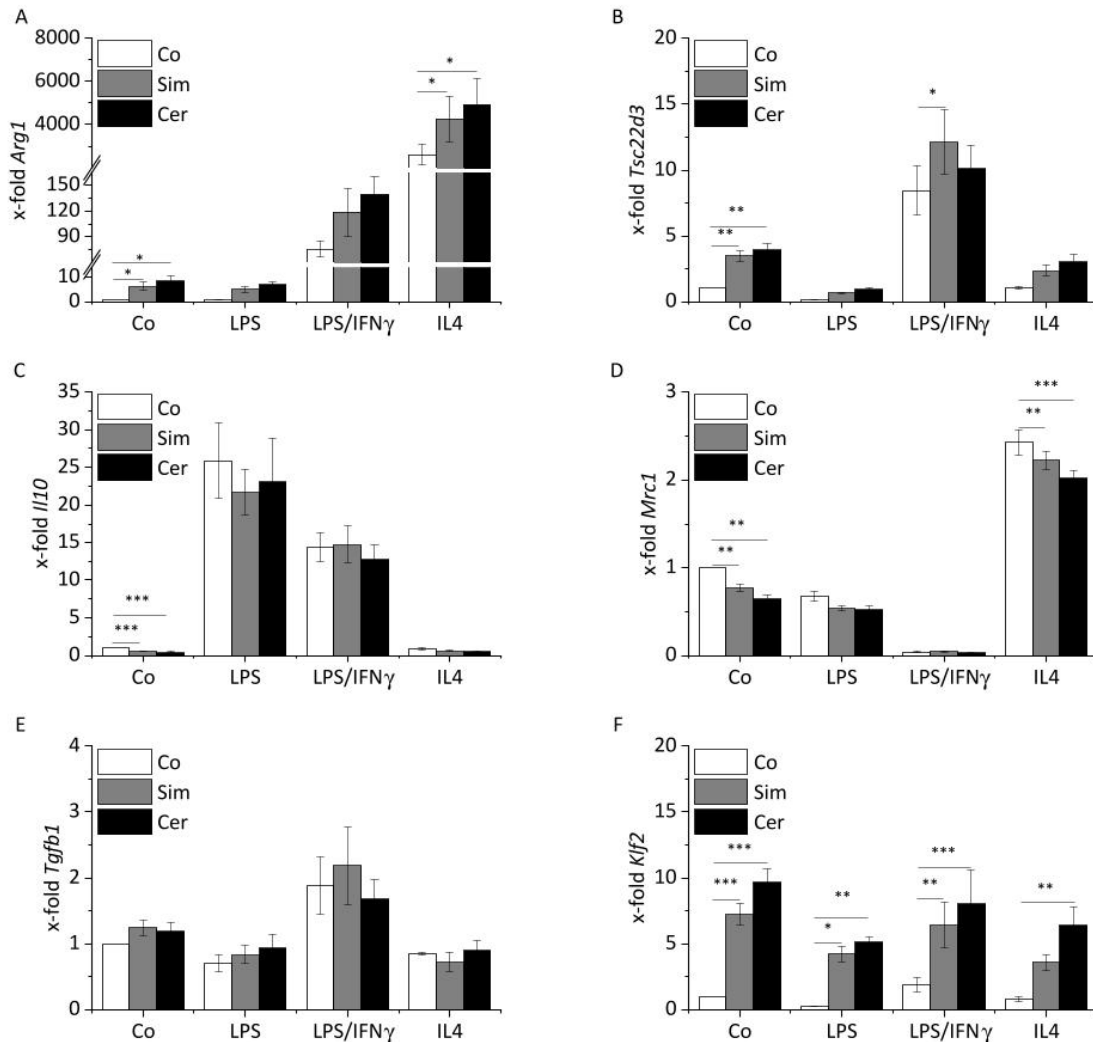


Figure 2. Effect of statin treatment on the anti-inflammatory response in macrophages. (A–D) *Arg1* (A), *Tsc22d3* (B), *Il10* (C), *Mrc1* (D), *Tgfb1* (E), and *Klf2* (F) mRNA expression in BMMs was determined by real-time RT-PCR, normalized to *Ppia*, and expressed as x-fold of Co. BMMs were stimulated for the last 4 h with LPS (100 ng/mL) or polarized towards M1 (LPS, 100 ng/mL; IFN γ , 20 ng/mL) or M2 (IL4, 20 ng/mL) in the presence or absence of simvastatin (Sim, 2 μ M) or cerivastatin (Cer, 0.5 μ M) for 24 h. Co = solvent control ($n = 6$). A one-sample *t*-test followed by a Bonholm post hoc test was used for analyzing the gene expression data of the control group. Means of more than two groups were compared by one-way ANOVA with a Bonholm post hoc test (normal distribution). * $p < 0.05$, ** $p < 0.01$, and *** $p < 0.001$.

2.2. Statins Modulate the Phagocytotic Activity of Macrophages

Phagocytosis represents one of the major macrophage functions, which has been shown to be altered in atherosclerosis [40]. Our data show a distinct reduction of phagocytotic activity by both simvastatin and cerivastatin when added to untreated cells or combined with short-term inflammatory activation (Figure 3A,B,G; 12 h time point; Supplementary Figures S7–S9: additional images). Both M1 and M2 polarization reduced the phagocytotic activity in a time-dependent manner (Figure 3C), as reported previously [41,42]. The presence of statins during polarization showed no additional effect (Figure 3D–F).

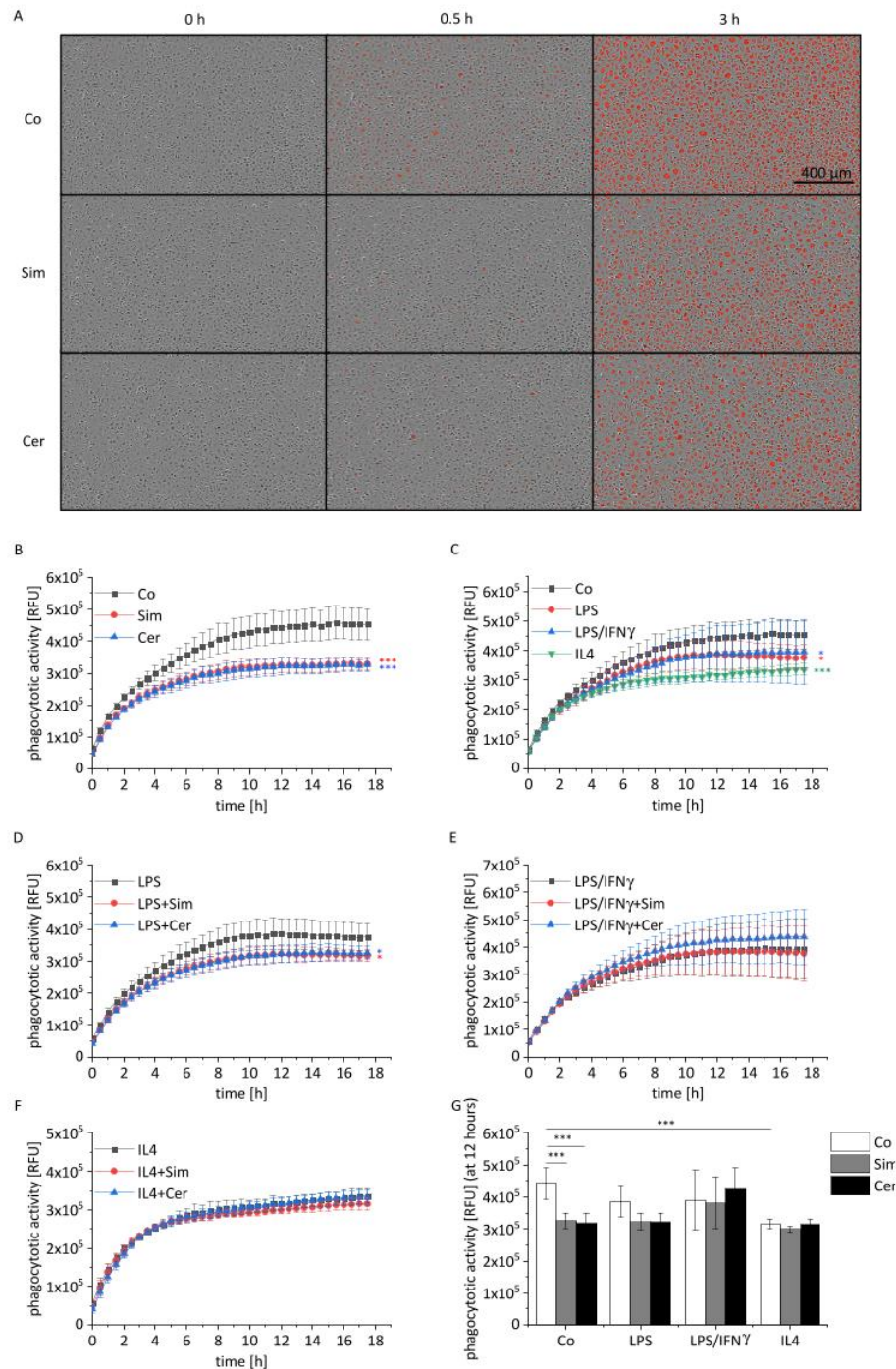


Figure 3. Effect of statin treatment on the phagocytotic activity of macrophages. (A–G) BMMs were stimulated for the last 4 h with LPS (100 ng/mL) or polarized towards M1 (LPS, 100 ng/mL; IFN γ , 20 ng/mL), or M2 (IL4, 20 ng/mL) in the presence or absence of simvastatin (Sim, 2 μ M) or cerivastatin (Cer, 0.5 μ M) for 24 h and monitored by an IncuCyte S3 system after addition of fluorogenic pHrodo[®] Red *S. aureus* bioparticles (5 μ g/well). Co = solvent control, RFU = relative fluorescence units. (A) Representative pictures at indicated time points are shown. (B–G) Quantification of phagocytotic activity expressed as mean red fluorescence intensity normalized to confluence ($n = 4$, duplicates). Statistical analysis was performed by two-way ANOVA with Bonholm post hoc test (B–F) or one-way ANOVA with Bonholm post hoc test (G). * $p < 0.05$, *** $p < 0.001$.

2.3. ERK Activation Contributes to Statin-Induced Inflammation

We then sought to elucidate the molecular mechanisms underlying statin-mediated modulation of the macrophage phenotype. It has been reported that macrophages produce cholesterol even in serum-containing media and that cholesterol biosynthesis can be reduced by statin treatment [43]. Macrophages can, however, quickly replenish cholesterol from the media if their cholesterol levels decline [44]. Thus, the total cellular cholesterol content is not necessarily affected when de novo synthesis is shut down. This reflects the in vivo situation, in which cholesterol can be scavenged from the surrounding environment, e.g., from the bloodstream, which is why we performed all assays in the presence of serum. To determine whether the cholesterol content indeed remains unchanged after statin treatment, we measured cellular cholesterol levels and found that they were not affected by statins (Figure 4A). Interestingly, we observed that the cellular cholesterol content was reduced by statins under low-serum conditions, i.e., under conditions that restrict cholesterol replenishment from the media (Supplementary Figure S10).

Since statins' pleiotropic effects have been described to be related to attenuated protein prenylation, we co-treated cells with mevalonate (MVA) as an intermediate of the mevalonate pathway. As shown in Figure 4B, the statin-mediated enhancement of LPS-induced NF- κ B/AP-1 activity was abolished by MVA priming during cerivastatin treatment, but not during simvastatin treatment, which may point towards distinct mechanisms or different kinetics. A similar effect was observed when farnesyl pyrophosphate (FPP) or geranylgeranyl pyrophosphate (GGPP) were added instead of MVA, suggesting that isoprenylation is required to induce cerivastatin-mediated downstream effects (Supplementary Figure S11). Interestingly, cerivastatin has been shown to reduce the expression of genes involved in the MVA pathway to a higher degree than simvastatin [45], implying that this pathway may be especially vulnerable to cerivastatin-mediated interference.

Statins have been shown to activate the NLRP3 inflammasome in BMMs [46]. To determine a potential involvement of the NLRP3 inflammasome in the statin-induced increase of IL1 β secretion, we used *Nlrp3* KO BMMs. The viability of statin-treated cells was not affected by *Nlrp3* knockout (Supplementary Figure S12). As shown in Figure 4C, IL1 β release was NLRP3 inflammasome-independent.

Gene expression data suggested an upregulation of *Tlr4*, which may contribute to the enhanced susceptibility to LPS of statin-treated cells. In contrast, the expression of neither *Nlrp3* nor *MyD88* or *Tlr2* was altered in the presence of statins (Figure 4D).

Since ERK represents an essential regulator in inflammatory macrophage activation [26,47], we hypothesized that ERK is involved in statin-mediated effects in macrophages. Statin treatment led to an enhanced ERK activation (Figure 4E,F). The addition of the MEK/ERK inhibitor PD98059 prior to statin treatment revealed that statin-induced activation in short-term LPS-treated cells was entirely abolished by the inhibitor (Figure 4G), suggesting ERK as a mediator of statin-facilitated inflammatory macrophage activation.

2.4. Bempedoic Acid Treatment Has Minimal Impact on the Phenotype of Macrophages

We then characterized the effect of bempedoic acid on macrophages at the highest concentration at which the solvent showed no effect and at which the compound was neither toxic in BMMs nor in RAW 264.7 cells (25 μ M, Supplementary Figures S1A and S2A).

The enzyme that converts the prodrug to its active form, i.e., *Slc27a2*, was barely expressed in BMMs, suggesting that potential effects of bempedoic acid on macrophages would be caused by the prodrug (Supplementary Figure S13A). This assumption was further supported by the observation that different types of human macrophages, i.e., monocyte-derived and alveolar macrophages, also expressed very low levels of *SLC27A2* (Supplementary Figure S13B).

In contrast to the pronounced effects of statins on macrophages, bempedoic acid treatment affected neither NF- κ B/AP-1 activity nor cytokine transcript levels, IL1 β secretion, or ERK activity (Figure 5A,B,D–F, Supplementary Figures S14 and S15). Only a minor increase of TNF protein levels was detectable in LPS-activated cells (Figure 5C).

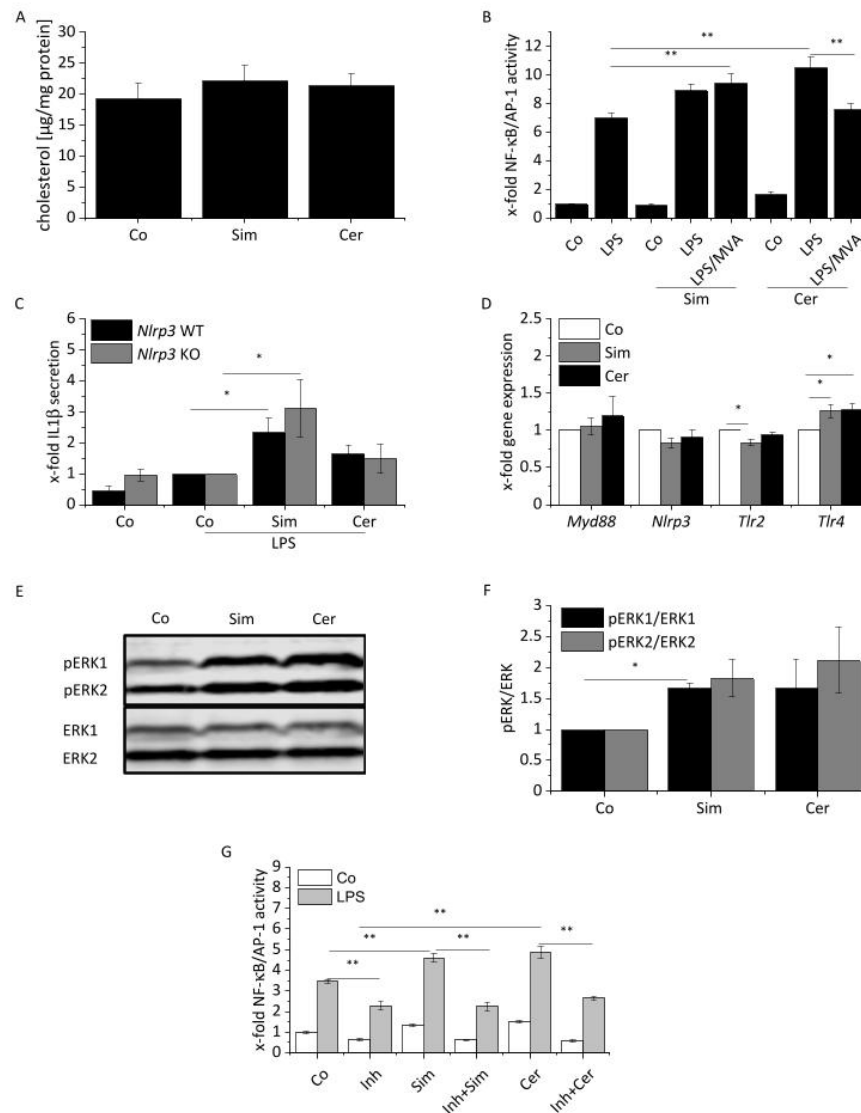


Figure 4. Statins affect different signaling pathways in macrophages. (A) Intracellular cholesterol levels. BMMs were either treated for 24 h with simvastatin (Sim, 2 μ M) or cerivastatin (Cer, 0.5 μ M). Co = solvent control ($n = 3$, triplicates). (B) RAW-BlueTM cells were treated for 24 h with either Sim (2 μ M) or Cer (1 μ M). Cells were co-treated with mevalonate (MVA, 100 μ M) where indicated. Inflammatory activation was induced by treatment with LPS (100 ng/mL) for the final 4 h. NF- κ B/AP-1 activity was determined by secreted embryonic alkaline phosphatase (SEAP) detection. Co = solvent control ($n = 3$, triplicates). (C) IL1 β was measured by bioassay. BMMs of *Nlrp3* WT and KO BMMs were treated for 24 h with either Sim (2 μ M) or Cer (0.5 μ M). Inflammatory activation was induced by treatment with LPS (100 ng/mL) for the final 4 h. Co = solvent control ($n = 4$ each WT and KO, quadruplicates). (D) mRNA expression of indicated genes were determined by real-time RT-PCR, normalized to *Ppia*, and expressed as x -fold of Co. BMMs were either treated for 24 h with Sim (2 μ M) or Cer (0.5 μ M). Co = solvent control ($n = 6$). (E,F) ERK phosphorylation was examined by Western Blot analysis. BMMs were treated with Sim (2 μ M) or Cer (0.5 μ M) for one hour. Co = solvent control. (E) One representative blot is shown. (F) Signal intensities were quantified and normalized to total ERK ($n = 3$). (G) RAW-BlueTM cells were pre-treated for 30 min with the ERK inhibitor PD98059 (Inh, 10 μ M). Cells were treated for 24 h with either Sim (2 μ M) or Cer (1 μ M). Inflammatory activation was induced by treatment with LPS (100 ng/mL) for the final 4 h. NF- κ B/AP-1 activity was determined by secreted embryonic alkaline phosphatase (SEAP) detection. Co = solvent control ($n = 3$, triplicates). One-sample t -test followed by Bonholm post hoc test was used for analyzing gene expression data of the control group and Western blot (D,F). Means of more than two groups were compared by one-way ANOVA with Bonholm post hoc test (normal distribution) (B,C,G). * $p < 0.05$, ** $p < 0.01$.

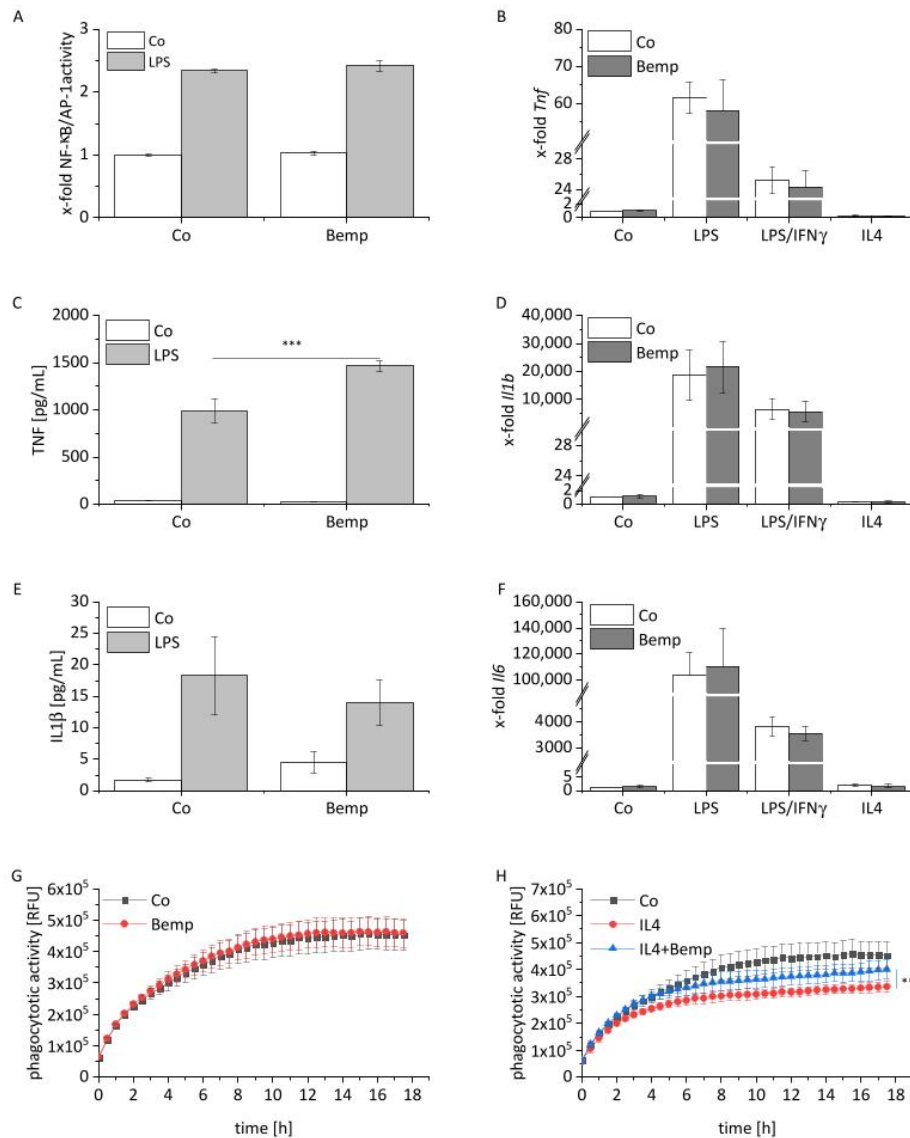


Figure 5. Effect of bempedoic acid treatment macrophages. (A) RAW-BlueTM cells were treated with bempedoic acid (Bemp, 25 μ M) for 24 h. Inflammatory activation was induced by treatment with LPS (100 ng/mL) for the final 4 h. NF- κ B/AP-1 activity was determined by secreted embryonic alkaline phosphatase (SEAP) detection. Co = solvent control ($n = 3$, triplicates). (B,D,F) *Tnf* (B), *Il1b* (D), and *Il6* (F), mRNA expression in BMMs was determined by real-time RT-PCR, normalized to *Ppia*, and expressed as x-fold of Co. BMMs were stimulated for the last 4 h with LPS (100 ng/mL) or polarized towards M1 (LPS, 100 ng/mL; IFN γ , 20 ng/mL) or M2 (IL4, 20 ng/mL) in the presence or absence of Bemp (25 μ M) for 24 h. Co = solvent control ($n = 6$). (C,E) TNF (C) and IL1 β (E) were measured by bioassay. BMMs were treated for 24 h with Bemp (25 μ M). Inflammatory activation was induced by treatment with LPS (100 ng/mL for IL1 β , 10 ng/mL for TNF) for the final 4 h. Co = solvent control ($n = 3$, duplicates for TNF, triplicates for IL1 β). (G,H) BMMs were treated for 24 h with Bemp (25 μ M) in the presence or absence of IL4 (20 ng/mL) and monitored by an IncuCyte S3 system after the addition of fluorogenic pHrodo[®] Red *S. aureus* bioparticles (5 μ g/well). Quantification of phagocytosis activity expressed as mean red fluorescence intensity normalized to confluence ($n = 4$, duplicates). RFU = relative fluorescence units. A one-sample t-test followed by a Bonholm post hoc test was used for analyzing gene expression data of the control group. Means of more than two groups were compared by one-way ANOVA with Bonholm post hoc test (normal distribution). Statistical analysis of phagocytosis activity was performed by two-way ANOVA with Bonholm post hoc test. *** $p < 0.001$.

The phagocytotic activity was not altered by bempedoic acid when cells were otherwise left untreated (Figure 5G). However, bempedoic acid was able to partially rescue the M2-associated decline in phagocytotic activity, while no effect of bempedoic acid was observed in cells under short-term inflammatory or M1 conditions (Figure 5H, Supplementary Figure S16).

3. Discussion

For decades, statins have been the gold standard for the treatment of CVD [48]. They have been suggested to exert pleiotropic effects beyond their cholesterol-lowering actions [2]. Previous publications reported pro- and anti-inflammatory responses in macrophages employing different models and treatment schemes [16,17,22,29,49–51]. Thus, we sought to investigate the influence of statins on macrophages during polarization and in short-term inflammation.

Our data showed that statins skew macrophages towards a unique mixed phenotype, both under otherwise unstimulated conditions and after short-term inflammatory activation, but not during M1/M2 polarization. The statin effects were characterized by enhanced inflammatory cytokine production but unaltered NO release. The enhanced cytokine release is in accordance with previously published studies investigating the influence of statins on inflammatory responses [17,50,52–54]. However, these studies differ regarding the investigated cell type, the treatment scheme, or the respective inflammatory stimulus. Kuijk et al. used a human monocytic cell line [52], Hohensinner et al. investigated atorvastatin effects [53], and Matsumoto et al. showed elevated TNF levels in RAW 264.7 cells [50]. Kiener et al. used a setup that was most similar to our short-term inflammation model, although human peripheral monocytes were used. In accordance with our results, their study showed elevated LPS-induced cytokine production in cells pre-treated with statins [17].

While we observed a distinct effect of statins on untreated or LPS-activated macrophages, statins did not affect transcript levels of *Tnf*, *Il1b*, and *Il6* when present during M1/M2 polarization. The study by Hohensinner et al. points toward the same direction, showing an unaltered macrophage polarization program after atorvastatin treatment in human macrophages, as suggested by unaltered levels of CD80, CD206, IL6, and IL10 [53].

Despite the induction of inflammatory cytokines, our findings do not show a clear inflammatory phenotype since we observed an unaltered NO release upon statin treatment. This observation might be linked to an increased expression of arginase, which represents a classical marker of M2 macrophages as it antagonizes NO production.

In fact, several studies showed anti-inflammatory effects of statins on monocyte and macrophage inflammatory responses, such as decreased iNOS in a macrophage cell line [38] and CRP-induced chemokine secretion in human monocytes [55], as well as decreased TNF levels in human monocytes ex vivo [56]. The latter can be explained by a 24 h LPS treatment scheme, which might have led to a relatively anti-inflammatory state termed endotoxin tolerance and therefore strongly differs from our experimental setup [55]. The lack of characterization of macrophage phenotypes, species-specific differences, or chemical properties of the used statins might also contribute to the differences to our results. Of note, many in vitro studies were conducted in serum-free media. This approach does not reflect physiologic conditions and may also heavily influence the macrophage phenotype [20,29,57].

There are discrepancies regarding the proposed mechanisms by which statins have been suggested to induce a pro- or anti-inflammatory response. On the one hand, physico-chemical interactions between statins and cell membranes have been described, resulting in impaired lipid rafts and membrane fluidity [58]. On the other hand, interactions between statins and cellular signaling pathways, either cholesterol-dependent or isoprenoid-dependent, have been suggested to cause downstream effects [59].

Our data demonstrate a clear activation of NF- κ B/AP-1, which represent central inflammatory transcription factors. This finding is in accordance with Healy et al., who showed an increase of NF- κ B activity after atorvastatin treatment in BMMs [22]. Interestingly, the study also showed that statins disrupted the complex between the small GTPase Rac1 and its negative regulator, the Rho guanine nucleotide dissociation inhibitor (RhoGDI), an interaction that is dependent on protein isoprenylation. This led to increased active Rac1 levels in monocytes and macrophages, which may be the cause of some of the pro-inflammatory statin effects in macrophages, including enhanced IL1 β secretion.

Similarly, Akula et al. showed that simvastatin facilitated IL1 β maturation and secretion in response to LPS [60]. This effect was reversible by GGPP addition, which restored GGase-I-mediated prenylation of Rac1. Thus, the authors speculated that the pro-inflammatory effects of statins may result from reduced Rac1 prenylation, which may also explain some of our findings.

Since Henriksbo et al. reported an NLRP3 inflammasome-dependent production of IL1 β by fluvastatin in BMMs, we aimed to reproduce their findings [46]. Our data do not support an NLRP3-dependent IL1 β release upon treatment of either simvastatin or cerivastatin, which, again, might be due to differences regarding the treatment scheme.

Stress kinases, such as ERK, play an important role in macrophage-mediated inflammation. We, therefore, investigated ERK activation after statin treatment and found that statins induce ERK phosphorylation. ERK activation was previously observed by Lee et al. after simvastatin treatment in RAW 264.7 cells in a time-dependent manner [61]. Thus, the activation of ERK might in part contribute to statin-induced inflammatory effects.

Phagocytosis is an essential aspect of macrophage host defense and plays a crucial role in all stages of atherogenesis, either by LDL clearance and foam cell formation or regarding plaque stability. Moreover, phagocytosis is pivotal for pathogen clearance in a wide range of infectious diseases [40]. We found that statins decreased the phagocytotic activity in otherwise unstimulated cells and under short-term inflammatory conditions. These findings are in accordance with published data for human macrophages [20], murine peritoneal macrophages, and human monocytes [62]. Interestingly, other experimental setups with in vivo and ex vivo murine peritoneal macrophages suggested an enhanced phagocytotic activity upon statin treatment, which might be related to differences regarding the macrophage origin or the phagocytosed material [63,64]. Mechanistically, statins may impair phagocytosis via reduced isoprenylation of members of the Rho family of small G-proteins, as shown in previous studies [65,66].

The recently registered drug bempedoic acid was known as ESP-55016 and ETC-1002 when it was first synthesized in 2004 [67]. Due to the prodrug properties of bempedoic acid, i.e., the fact that its pharmacologically active form is generated by a liver-specific enzyme, its action is supposed to be limited to hepatic cells. In fact, clinical trials show no muscle-related effects, which are associated with statin therapy as adverse effects [68]. Still, despite its supposed liver-specific action, bempedoic acid has been described to exhibit anti-inflammatory activities [69]. A previous study showed reduced TNF levels in human LPS-treated macrophages after treatment with 50–100 μ M bempedoic acid. The authors suggested a modulation of AMPK and MAPK pathways as the underlying mechanism [33]. The study also showed that macrophages did not convert the compound into its active form, implying that target-independent unspecific actions of the prodrug caused the observed effects.

While the *Slc27* gene family generally represents a family of fatty acid transporters [70], the protein encoded by *Slc27a2* also exhibits metabolic activity. This isozyme represents a member of the long-chain fatty-acid-coenzyme A ligase family, shows a preference for generating CoA derivatives of n-3 fatty acids [71], and is required to transform bempedoic acid into its active form [34]. We showed that different types of human macrophages express very low levels of *SLC27A2*, thereby supporting previous findings [33]. Furthermore, our data suggest that murine macrophages are also unable to transform the prodrug since *Slc27a2* was virtually not expressed in these cells.

In contrast to the study by Filippov et al. [33] we did not observe any effect of bempedoic acid for most readout parameters. This observation might be related to the fact that we used a lower concentration of 25 μM due to the toxicity of the compound itself (at $\geq 50 \mu\text{M}$ in RAW 264.7 cells) or the vehicle DMSO at the corresponding concentrations (at $\geq 0.5\%$ in BMMs). The maximal serum concentration of bempedoic acid in vivo averages out at 60–90 μM , but the compound shows a high degree of plasma protein binding ($>99\%$), which limits its activity [72,73]. Thus, less than 1 μM free bempedoic acid is available to affect immune cells in vivo, suggesting that a concentration of 25 μM should be sufficient to uncover potential effects in vitro.

Interestingly, the only clear effect of bempedoic acid was the rescue of the phagocytotic activity during its M2-associated decline. Since bempedoic acid is not converted into the ATP-citrate lyase-inhibitor bempedoic acid-CoA in macrophages [31], and macrophage cholesterol levels are not affected by bempedoic acid (Supplementary Figure S10), a cholesterol-dependent mechanism can be ruled out. One might speculate that this effect is due to the enhanced fatty acid oxidation in bempedoic acid-treated cells, which plays a more prominent role during M2 polarization compared to M1 [67,74,75]. As mentioned above, it has been shown that bempedoic acid in its prodrug form can activate AMPK [31], and AMPK activation may enhance phagocytosis [76]. Thus, AMPK activation may represent another pathway by which bempedoic acid modulates the phagocytotic capacity of M2 macrophages.

Modulation of macrophage phenotypes has been suggested as a novel strategy for the pharmacological treatment of atherosclerosis. Macrophages with different functional phenotypes are likely to play different roles in the pathogenesis and progression of atherosclerosis: M1 macrophages have been associated with initiating and sustaining inflammation, and M2 macrophages have been linked to inflammation resolution. In fact, M2 macrophages are particularly abundant in stable zones of the plaque and asymptomatic lesions. However, a broad spectrum of intermediate phenotypes has been identified in vivo studies. Different stimuli, such as various cytokines, lipids, senescent or apoptotic cells, and iron, can influence macrophage phenotypes in atherosclerotic lesions, thus generating a complex microenvironment that cannot be fully recapitulated in in vitro studies [77,78].

Our data suggest detrimental pro-inflammatory effects of statins on macrophages within the plaque, although another inflammatory trigger may be required. Indeed, it has been reported that full plaque regression upon treatment with cholesterol-lowering agents may be prevented if macrophage inflammation persists [78]. Our data show that an inflammatory activation might be fueled by statins, thus potentially limiting plaque regression. However, this issue might be outweighed by the beneficial effect of statins on other cell types, such as endothelial and smooth muscle cells, and the overall impact of reduced serum cholesterol levels [79].

In other contexts, statins may affect macrophages in a favorable manner due to their ability to induce KLF2: a recent study revealed that myeloid KLF2 reduces metabolic inflammation in peripheral and central tissues in a mouse model of obesity [32]. Thus, the impact of statin treatment on macrophages in vivo most likely depends on the degree of inflammation within the microenvironment.

Statins have been suggested as potential therapeutics for diseases beyond CVD, particularly inflammatory lung diseases and infectious diseases [11,12]. In our hands, statin treatment led to hyperinflammation under conditions that mimic acute inflammation, i.e., short-term LPS treatment. The decreased phagocytotic capacity in statin-treated cells implies that the clearance of pathogens in patients undergoing statin therapy may be reduced. Of note, phagocytosis can also contribute to disease progression if internalized bacteria are not completely killed, and the bactericidal capacity of macrophages is linked to a pro-inflammatory phenotype [80]. Thus, the pro-inflammatory state induced by statins may contribute to a better outcome in bacterial infections, which was previously observed for patients on statin therapy [13,14]. Bempedoic acid, on the other hand, had negligible effects on inflammation, but even enhanced phagocytosis, at least in M2 macrophages. Again,

the outcome of bempedoic acid treatment during a bacterial infection would depend on whether their bactericidal capacity is also altered. Thus, it would be interesting to examine the influence of bempedoic acid and statins on the bactericidal activity of macrophages in future studies.

Taken together, our data point towards a unique cholesterol-independent modulation of macrophage functions by statins, which is not exhibited by bempedoic acid. Furthermore, our data suggest that the anti-inflammatory properties that statins and bempedoic acid show in vivo are not related to their effects on macrophages but are more likely linked to systemic effects or effects on other cell types.

4. Materials and Methods

4.1. Reagents

Cell media (RPMI1640, #R0883; DMEM, #D6546), fetal calf serum (FCS, #F7524), penicillin/streptomycin (#P433), and glutamine (#G7513) were purchased from Sigma-Aldrich (St. Louis, MO, USA). PAN-FCS (#P040-37500) was purchased from PAN-Biotech (Aidenbach, Germany). ZeocinTM (#ant-zn-05), NormocinTM (#ant-nr-1) and HEK-BlueTM Selection (#hb-sel) were purchased from InvivoGen (San Diego, CA, USA). Anti-p44/42 (ERK1/2) mouse antibody (L34F12, #4696S) and anti-phospho-p44/42 MAPK (Thr202/Tyr204) rabbit mAbs (20G11, #4376S) were obtained from Cell Signaling Technology (Danvers, MA, USA). Anti-rabbit IRDye 680- and anti-mouse IRDye 800-conjugated secondary antibodies were from LI-COR Biosciences (#926-68071, #926-32210) (Lincoln, NE, USA). Ultrapure LPS from *E. coli* K12 (#tlrl-peklp) and QUANTI-BlueTM (#rep-qb) were purchased from InvivoGen (San Diego, CA, USA). MTT (#M5655), actinomycin D (#A9415), PD98059 (#P215), cerivastatin sodium salt hydrate (#SML0005), and (R)-Mevalonic acid lithium salt (#50838) were obtained from Sigma-Aldrich (St. Louis, MO, USA). Murine M-CSF (#130-101-704), IFN γ (#130-105-782), IL4 (#130-094-061), and IL1 β (#130-101-681) were obtained from Miltenyi Biotec (Bergisch Gladbach, Germany). Simvastatin sodium salt (#10010345) was purchased from Cayman Chemicals (Ann Arbor, MA, USA) and Bempedoic acid (#738606-46-7) was purchased from MedChemExpress (Monmouth Junction, NJ, USA). 5xHotFirePOI EvaGreen qPCR Mix (no Rox) (#08-25-00001) was purchased from Soli Biotdyne (Tartu, Estland). Rockland Blocking Buffer (#MB-070) was purchased from Biomol (Hamburg, Germany). pHrodoTM Red *S. aureus* BioparticlesTM Conjugate for Phagocytosis (#A10010) was purchased from Thermo Fisher Scientific (Waltham, MA, USA). Other chemicals were obtained from either Sigma-Aldrich (St. Louis, MO, USA) or Carl Roth (Karlsruhe, Germany) unless stated otherwise.

4.2. Cell Culture

RAW-BlueTM cells (InvivoGen, San Diego, CA, USA, #raw-sp) were grown in high glucose DMEM medium supplemented with 10% heat-inactivated FCS (30 min at 56 °C), 2 mM glutamine, 100 U/mL penicillin G, 100 μ g/mL streptomycin, 100 μ g/mL Normocin, and 200 μ g/mL Zeocin for selection.

HEK-BlueTM IL-1R cells (InvivoGen, San Diego, CA, USA, #hekb-il1r) were grown in high-glucose DMEM medium supplemented with 10% heat-inactivated FCS (30 min at 56 °C), 2 mM glutamine, 100 U/mL penicillin G, 100 μ g/mL streptomycin, 100 μ g/mL Normocin, and 1 \times HEK-BlueTM Selection.

L929 cells and RAW 264.7 cells (American Type Culture Collection) were cultivated in standard medium (RPMI 1640, 10% FCS, 100 U/mL penicillin G, 100 μ g/mL streptomycin, 2 mM glutamine). The cells were maintained at 37 °C in a humidified atmosphere of 5% CO₂.

BMMs were obtained from wild-type (WT) or *Nlrp3* knockout (KO) mice as described previously [47]. Femurs and tibias were flushed with standard medium (RPMI 1640, 10% PAN-FCS, 100 U/mL penicillin G, 100 μ g/mL streptomycin, 2 mM glutamine). After centrifugation (10 min, 200 \times g), erythrocytes were lysed by incubation in hypotonic buffer (155 mM NH₄Cl, 10 mM KHCO₃, 1 mM Na₂EDTA) for 3 min at 37 °C. Cells

were washed with PBS, resuspended in standard medium containing M-CSF (50 ng/mL, 30 mL per preparation), transferred into a 75 cm² culture flask, and cultured overnight. Fibroblast-like cells, mature mononuclear phagocytes, and other cells adhering to the flask were discarded [81]. Non-adherent cells were collected and cultured in a 150 cm² culture flask for another 5 to 6 d in M-CSF-containing medium. Differentiated cells were detached with Accutase[®] (Sigma-Aldrich, St. Louis, MO, USA #A6964), suspended in standard medium supplemented with 50 ng/mL M-CSF, and seeded into 96-well plates (7.5 × 10⁴ cells/well) for TNF and IL1 β measurements as well as MTT assays and 5.0 × 10⁴/well for phagocytosis and Griess assays or into 24-well plates (2.5 × 10⁵ cells/well) for RT-qPCR and Amplex[®] cholesterol kit (Thermo Fisher Scientific, Waltham, MA, USA, #A12216) and into 6-well plates (10⁶/well) for Western blot analysis. The solvent control was 0.25% DMSO. Higher DMSO concentrations were avoided due to toxicity issues (at 0.5%: viability reduced by 18.7 ± 3.4%, $p = 0.0004$, determined by MTT assay).

4.3. Mice

Mice were housed in a 12:12 h light–dark cycle with food and water ad libitum. For all experiments, C57B/6 mice of the same age were used. For the IL1 β bioassay, we used mice in which the entire coding sequence of *Nlrp3* was replaced with a Neo cassette (*Nlrp3* KO mice, The Jackson Laboratory, Bar Harbor, ME USA; #B6.129S6-*Nlrp3*^{tm1Bhk}/J). Genotyping was performed with 5x HOT FIREPol EvaGreen[®] qPCR Mix and a total volume of 20 μ L and primer sequences as follows: mutant forward 5'-TGCCTGCTCTTTACTGAAGG-3', wild type forward 5'-TCAGTTTCCTTGGCTACCAGA-3', and common reverse 5'-TTCCATTACAGTCACTCCAGATGT-3', as described by The Jackson Laboratory. B6.129P2-*Lyz2*^{tm1(cre)lfo}/J mice (The Jackson Laboratory) were crossed with C57B/6 mice bearing *LoxP* sites upstream and downstream of *Tsc22d3* exon 6 to obtain myeloid-specific *Gilz* knockout (KO) mice. Breeding and genotyping were performed as described previously [47].

4.4. Endotoxin Quantification

Simvastatin, cerivastatin, and bempedoic acid were tested for the absence of endotoxin using the endotoxin assay PyroGene[™] Assay (Lonza, Basel, Switzerland, #50-658U) according to the manufacturer's instructions. Its sensitivity ranges from 0.0005 to 5 EU/mL. Briefly, 100 μ L aliquots of samples diluted in endotoxin-free water and tested in the highest used concentration as well as standards were transferred to a microtiter plate. Each sample was measured in duplicate, and a standard curve was run alongside the samples. After 60 min incubation at 37 °C, fluorescence was measured using a fluorescence reader (Promega[™] GloMax[®] Plate Reader, Madison, WI, USA) at 415–445 nm emission and 365 nm excitation. Endotoxin levels of final compound concentrations were below those of cell culture media and sera.

4.5. Cytotoxicity Measurements

To ensure the use of non-toxic concentrations of all compounds, simvastatin, cerivastatin, bempedoic acid, PD98059, and mevalonate, the MTT colorimetric assay was performed as described previously (Supplementary Figures S1 and S2) [47]. Absorbance was measured at 560 nm using a microplate reader (Promega[™] GloMax[®] Plate Reader Madison, WI, USA). The cell viability obtained from at least three independent experiments performed in triplicate or sextuplicate was calculated relative to solvent controls.

4.6. Gene Expression in Human Macrophages

Publicly available RNA sequencing data sets (Gene Expression Omnibus (GEO) datasets GSE162669 and GSE162698) were analyzed to assess *HMGCR*, *ACLY*, and *SLC27A2* expression in human monocyte-derived macrophages and human alveolar macrophages, as detailed in [44].

4.7. RNA Isolation, Reverse Transcription, and Quantitative PCR (RT-qPCR)

Quantitative RT-PCR (qPCR) was performed as described previously [47]. Total RNA from cells was isolated using the High Pure RNA Isolation Kit (Roche, Basel, Switzerland, #11828665001), following the manufacturer's instructions. RNA was reverse transcribed using the High-Capacity cDNA Reverse Transcription Kit (Thermo Fisher Scientific, #4368813) in the presence of the RNase inhibitor RNaseOUT™ (Thermo Fisher Scientific, #10777019) following the manufacturer's instructions. qPCR was performed using the 5x HOT FIREPol EvaGreen® qPCR Mix and a total volume of 20 µL. The primer sequences for each transcript are detailed in Table 1. For each primer pair, an annealing temperature of 60 °C was used (except *Nlrp3* with 59 °C annealing temperature). The CFX96 touch™ Real-Time PCR detection system (Bio-Rad Laboratories, Hercules, CA, USA) was used to quantify gene expression. Data were analyzed with the comparative $\Delta\Delta C_t$ method. The housekeeping gene was chosen after evaluating the expression stability of at least three candidate genes under the experimental conditions, using the geNorm, NormFinder, and BestKeeper Software tools [82]. Absolute amounts of the transcript were normalized to the corresponding housekeeping genes.

Table 1. Primer sequences for RT-qPCR analyses.

Gene	Accession Number	Forward Primer Sequence 5'-3'	Reverse Primer Sequence 5'-3'
<i>Acly</i>	NM_134037.3	ATGCCCAAGGAAAGAGTGC	CTCGGAACACACGTAGTCA
<i>Arg1</i>	NM_007482.3	ACAAGACAGGGCTCCTTTCAG	GGCTTATGGTTACCCTCCCG
<i>Hmgcr</i>	NM_008255.2	ATCCAGGAGCGAACCAAGAGAG	CAGAAGCCCCAAGCACAAAC
<i>Il10</i>	NM_010548.2	GCCCAGAAATCAAGGAGCAT	GAAATCGATGACAGCGCCT
<i>Il6</i>	NM_031168.2	AAGAAATGATGGATGCTACAAACTG	GTACTCCAGAAGACCAGAGGAAATT
<i>Klf2</i>	NM_008452.2	CCTTGCACATGAAGCGACAC	ACTTGTCCGGCTCTGTCTTA
<i>Myd88</i>	NM_010851.3	TAAGTTGTGTGTGCCGACCG	CATGCGGCGACACCTTTTCT
<i>Nos2</i>	NM_010927.3	CTTCTGGACATTACGACCC	TACTCTGAGGGCTGACACAA
<i>Ppia</i>	NM_008907.1	GCGTCTCCTTCGAGCTGTTT	CACCTGGCACATGAATCCT
<i>Slc27a2</i>	NM_011978.2	AGCGGAGAGACCTCCTGATGAT	CAGAAGCCCCAACAAGCACAAAC
<i>Tlr2</i>	NM_011905.3	CACTGCCCGTAGATGAAGTC	TACCTCCGACAGTTCCAAGA
<i>Tlr4</i>	NM_021297.3	TCCCTGCATAGAGGTAGTTCC	TCAAGGGGTTGAAGCTCAGA
<i>Tnf</i>	NM_013693.2	CCATTCCTGAGTTCTGCAAAGG	AGGTAGGAAGGCCTGAGATCTTATC
<i>Tgfb1</i>	NM_011577.1	ACCCTGCCCCTATATTTGGA	CGGTTGTGTTGGTTGTAGAG
<i>Tsc22d3</i>	NM_010286.4	GCTGCTGAGAAGAACTCCCA	GAACCTTTCCAGTTGCTCGGG

4.8. Western Blot

Cells were lysed in lysis buffer (50 mM Tris-HCl, 1% (m/v) SDS, 10% (v/v) glycerol, 5% (v/v) 2-mercaptoethanol, 0.004% (m/v) bromphenol blue) supplemented with a protease inhibitor mix (cOmplete®; Roche Diagnostics, Basel, Switzerland, #04693124001) and stored at −80 °C until further use. After sonication, lysates were boiled for 5 min at 95 °C. Proteins were separated by SDS-PAGE on 12% gels using the Mini-Proteome Tetra Cell system (BioRad, Hercules, CA, USA) and transferred onto Immobilon FL-PVDF membranes (Millipore, Burlington, MA, USA, #IPFL00010) using the Tetra Blotting Module (BioRad). The membranes were blocked in Rockland blocking buffer for near-infrared Western Blotting for 1.5 h, incubated with primary antibody dilutions (1:1000 in Rockland blocking buffer) at 4 °C overnight and with IRDye 680 or IRDye 800 conjugated secondary antibodies (1:10,000 in Rockland blocking buffer) for 1.5 h at room temperature. Blots were scanned with an Odyssey Infrared Imaging System (LI-COR Bioscience, Lincoln, NE, USA), and relative protein amounts were determined using the Odyssey software.

4.9. Cytokine Quantification

Murine TNF was quantified by bioassay as previously described [83]. L929 cells were seeded at a density of 3×10^4 cells/well into a 96-well plate. After 24 h, the medium was replaced by 100 µL of actinomycin D solution (1 µg/mL in standard medium), and cells were incubated for 1 h at 37 °C. Subsequently, BMM supernatants (1:5 diluted, 100 µL total

volume/well) were added. Dilution series of recombinant murine TNF (100–2500 pg/mL) were run alongside the samples to generate a standard curve. The plates were incubated for an additional 24 h at 37 °C. The MTT assay was used to assess cell viability.

Murine IL1 β was quantified by bioassay. HEK-BlueTM IL-1R cells were seeded at a density of 5×10^4 cells/well with BMM supernatants (1:100 diluted, 20 μ L total volume/well) into a 96-well plate and incubated overnight at 37 °C. Dilution series of recombinant murine IL1 β (10^{-5} – 10^1 ng/mL) were run alongside the samples to generate a standard curve. The next day, supernatants were collected, and secreted embryonic alkaline phosphatase (SEAP) activity was determined using the QUANTI-BlueTM Solution according to the supplier's instructions. SEAP levels were determined at 600 nm with a microplate reader (PromegaTM GloMax[®]).

4.10. NF- κ B/AP-1 Reporter Cells

RAW-BlueTM cells (InvivoGen, San Diego, CA, USA, #raw-sp) expressing SEAP under the control of the IFN β minimal promoter fused to five NF- κ B and AP-1 binding sites were used to determine NF- κ B/AP-1 activity. Cells were seeded into 96-well plates (10^5 cells/well) and treated as indicated. After 24 h, supernatants were collected, and SEAP activity was determined using the QUANTI-BlueTM Solution according to the supplier's instructions. SEAP levels were determined at 600 nm with a microplate reader (PromegaTM GloMax[®]).

4.11. Griess Assay

BMMs were cultured in 96-well plates (5×10^5 cells/well) and treated as indicated. After 24 h, the concentration of nitrite was measured in the supernatants by Griess assay as previously described [84]. In brief, 90 μ L 1% sulfanilamide in 5% H₃PO₄ and 90 μ L 0.1% N-(1-naphthyl)ethylenediamine dihydrochloride in H₂O were added to 100 μ L of cell culture supernatant, followed by absorbance measurement at 560 nm using a PromegaTM GloMax[®] Plate Reader. A standard curve of sodium nitrite dissolved in medium was run alongside the samples.

4.12. Cholesterol Quantification

Intracellular cholesterol (free cholesterol and cholesteryl esters) was quantified with the Amplex[®] Red Cholesterol Assay Kit (Thermo Fisher Scientific, #A12216) according to the manufacturer's instructions with minor modifications as detailed in [44]. Briefly, BMMs were lysed in 200 μ L reaction buffer. A total of 50 μ L of a 1:5 dilution of the lysate in sample puffer were transferred into a 96-well plate and incubated with the Amplex[®] working solution. Each sample was measured in triplicate, and a standard curve was run alongside the samples. After 30 min incubation (37 °C, protected from light), fluorescence was measured using a plate reader (PromegaTM GloMax[®]) at 580–640 nm emission and 520 nm excitation. Total cellular protein concentrations used for data normalization were determined by Pierce BCA protein assay (Thermo Fisher Scientific, #23225) according to the manufacturer's instructions.

4.13. Phagocytotic Activity

BMMs were seeded into a 96-well plate (5×10^4 cells/well, 100 μ L) and treated as indicated. After 24 h treatment, 5 μ g pHrodoTM Red *S. aureus* BioparticlesTM Conjugate were added. Cells were imaged for 24 h in an IncuCyte S3 system. The phagocytotic activity was analyzed with the IncuCyte analysis software and expressed as mean red fluorescence intensity normalized to confluence.

4.14. Statistical Analysis

All experiments were performed at least three times. Data distribution was determined by the Shapiro–Wilk test. One-sample *t*-test followed by a Bonholm post hoc test was used for analyzing gene expression data of the control group and Western blot. Means

of more than two groups were compared by one-way ANOVA with a Bonholm post hoc test (normal distribution). Means of more than two groups that have been split into two independent variables were compared by two-way ANOVA with a Bonholm post hoc test. Statistical significance was set as * $p < 0.05$, ** $p < 0.01$, and *** $p < 0.001$ compared with controls or as indicated. Data analysis was performed using Origin software (OriginPro 2018b; OriginLab, Northampton, MA, USA).

Supplementary Materials: The following are available online at <https://www.mdpi.com/article/10.3390/ijms222212480/s1>.

Author Contributions: R.L. conducted experiments and acquired data. R.L. and J.H. analyzed data, S.W. and E.A. provided mice. R.L., J.H. and A.K.K. designed research studies and wrote the manuscript. A.K.K. and J.H. supervised and revised the manuscript. A.K.K. initiated the study. All authors have read and agreed to the published version of the manuscript.

Funding: This research was funded by the Deutsche Forschungsgemeinschaft (DFG, German Research Foundation), grant numbers KI 702/10-4 and 14-1. RL was supported by the Studienstiftung des deutschen Volkes. We acknowledge support by the DFG and Saarland University within the funding programme Open Access Publishing.

Institutional Review Board Statement: The use of murine BMMs was approved by the local animal welfare committee (Landesamt für Verbraucherschutz, Saarbrücken, Germany; AZ.: GB 3-2.4.2.2.-/2016 and AZ: 2.4.2.2.-06/2020) and was in accordance with the European Legislation on Protection of Animals (Guideline 2010/63/EU) and the NIH Guidelines for the Care and Use of Laboratory Animals (AZ: 39/3.5.2.1).

Data Availability Statement: Publicly available RNA sequencing data sets are accessible via the Gene Expression Omnibus (GEO) database (GSE162669 and GSE162698). Other datasets utilized in the present study are available from the corresponding author on reasonable request.

Acknowledgments: The authors thank Matti Müller and Lisa Flöck for excellent experimental support and Eva Dilly for animal care.

Conflicts of Interest: The authors declare no conflict of interest.

References

1. Endo, A.; Kuroda, M.; Tanzawa, K. Competitive inhibition of 3-hydroxy-3-methylglutaryl coenzyme A reductase by MI-236a and MI-236b fungal metabolites, having hypocholesterolemic activity. *FEBS Lett.* **1976**, *72*, 323–326. [CrossRef]
2. Murphy, C.; Deplazes, E.; Cranfield, C.G.; Garcia, A. The role of structure and biophysical properties in the pleiotropic effects of statins. *Int. J. Mol. Sci.* **2020**, *21*, 8745. [CrossRef] [PubMed]
3. World Health Organization. The Top 10 Causes of Death. Available online: <https://www.who.int/news-room/fact-sheets/detail/the-top-10-causes-of-death> (accessed on 5 June 2021).
4. ClinCalc DrugStats Database. The Top 300 of 2019. Available online: <https://clincalc.com/DrugStats/Top300Drugs.aspx> (accessed on 5 June 2021).
5. Sirtori, C.R. The pharmacology of statins. *Pharmacol. Res.* **2014**, *88*, 3–11. [CrossRef] [PubMed]
6. Igel, M.; Sudhop, T.; von Bergmann, K. Pharmacology of 3-hydroxy-3-methylglutaryl-coenzyme A reductase inhibitors (statins), including rosuvastatin and pitavastatin. *J. Clin. Pharmacol.* **2002**, *42*, 835–845. [CrossRef] [PubMed]
7. Istvan, E.S.; Deisenhofer, J. Structural mechanism for statin inhibition of HMG-CoA reductase. *Science* **2001**, *292*, 1160–1164. [CrossRef]
8. Palinski, W. New evidence for beneficial effects of statins unrelated to lipid lowering. *Arterioscler. Thromb. Vasc. Biol.* **2001**, *21*, 3–5. [CrossRef] [PubMed]
9. Oesterle, A.; Laufs, U.; Liao, J.K. Pleiotropic effects of statins on the cardiovascular system. *Circ. Res.* **2017**, *120*, 229–243. [CrossRef] [PubMed]
10. Blum, A.; Shamburek, R. The pleiotropic effects of statins on endothelial function, vascular inflammation, immunomodulation and thrombogenesis. *Atherosclerosis* **2009**, *203*, 325–330. [CrossRef] [PubMed]
11. McAuley, D.F.; Laffey, J.G.; O’Kane, C.M.; Perkins, G.D.; Mullan, B.; Trinder, T.J.; Johnston, P.; Hopkins, P.A.; Johnston, A.J.; McDowell, C.; et al. Simvastatin in the acute respiratory distress syndrome. *N. Engl. J. Med.* **2014**, *371*, 1695–1703. [CrossRef] [PubMed]
12. Grudzinska, F.S.; Dosanjh, D.P.S.; Parekh, D.; Dancer, R.C.A.; Patel, J.; Nightingale, P.; Walton, G.M.; Sapey, E.; Thickett, D.R. Statin therapy in patients with community-acquired pneumonia. *Clin. Med.* **2017**, *17*, 403–407. [CrossRef]

13. Nassaji, M.; Ghorbani, R.; Afshar, R.K. The Effect of Statins Use on the Risk and Outcome of Acute Bacterial Infections in Adult Patients. *J. Clin. Diagn. Res.* **2015**, *9*, OC09-12. [[CrossRef](#)] [[PubMed](#)]
14. Bjorkhem-Bergman, L.; Bergman, P.; Andersson, J.; Lindh, J.D. Statin treatment and mortality in bacterial infections—a systematic review and meta-analysis. *PLoS ONE* **2010**, *5*, e10702. [[CrossRef](#)]
15. Gupta, A.; Madhavan, M.V.; Poterucha, T.J.; DeFilippis, E.M.; Hennessey, J.A.; Redfors, B.; Eckhardt, C.; Bikdeli, B.; Platt, J.; Nalbandian, A.; et al. Association between antecedent statin use and decreased mortality in hospitalized patients with COVID-19. *Nat. Commun.* **2021**, *12*, 1325. [[CrossRef](#)] [[PubMed](#)]
16. Lindholm, M.W.; Nilsson, J. Simvastatin stimulates macrophage interleukin-1 β secretion through an isoprenylation-dependent mechanism. *Vascul. Pharmacol.* **2007**, *46*, 91–96. [[CrossRef](#)]
17. Kiener, P.A.; Davis, P.M.; Murray, J.L.; Youssef, S.; Rankin, B.M.; Kowala, M. Stimulation of inflammatory responses in vitro and in vivo by lipophilic HMG-CoA reductase inhibitors. *Int. Immunopharmacol.* **2001**, *1*, 105–118. [[CrossRef](#)]
18. Das, H.; Kumar, A.; Lin, Z.; Patino, W.D.; Hwang, P.M.; Feinberg, M.W.; Majumder, P.K.; Jain, M.K. Kruppel-like factor 2 (KLF2) regulates proinflammatory activation of monocytes. *Proc. Natl. Acad. Sci. USA* **2006**, *103*, 6653–6658. [[CrossRef](#)] [[PubMed](#)]
19. de Bont, N.; Netea, M.G.; Rovers, C.; Smilde, T.; Demacker, P.N.; van der Meer, J.W.; Stalenhoef, A.F. LPS-induced cytokine production and expression of LPS-receptors by peripheral blood mononuclear cells of patients with familial hypercholesterolemia and the effect of HMG-CoA reductase inhibitors. *Atherosclerosis* **1998**, *139*, 147–152. [[CrossRef](#)]
20. Benati, D.; Ferro, M.; Savino, M.T.; Olivieri, C.; Schiavo, E.; Nuccitelli, A.; Pasini, F.L.; Baldari, C.T. Opposite effects of simvastatin on the bactericidal and inflammatory response of macrophages to opsonized *S. aureus*. *J. Leukoc. Biol.* **2010**, *87*, 433–442. [[CrossRef](#)]
21. Churchward, M.A.; Todd, K.G. Statin treatment affects cytokine release and phagocytic activity in primary cultured microglia through two separate mechanisms. *Mol. Brain* **2014**, *7*, 85. [[CrossRef](#)]
22. Healy, A.; Berus, J.M.; Christensen, J.L.; Lee, C.; Mantounga, C.; Dong, W.; Watts, J.P., Jr.; Assali, M.; Ceneri, N.; Nilson, R.; et al. Statins disrupt macrophage Rac1 regulation leading to increased atherosclerotic plaque calcification. *Arterioscler. Thromb. Vasc. Biol.* **2020**, *40*, 714–732. [[CrossRef](#)] [[PubMed](#)]
23. Kamal, A.H.M.; Chakrabarty, J.K.; Udden, S.M.N.; Zaki, M.H.; Chowdhury, S.M. Inflammatory proteomic network analysis of statin-treated and lipopolysaccharide-activated macrophages. *Sci. Rep.* **2018**, *8*, 164. [[CrossRef](#)] [[PubMed](#)]
24. Hovland, A.; Retterstol, K.; Mollnes, T.E.; Halvorsen, B.; Aukrust, P.; Lappegaard, K.T. Anti-inflammatory effects of non-statin low-density lipoprotein cholesterol-lowering drugs: An unused potential? *Scand. Cardiovasc. J.* **2020**, *54*, 274–279. [[CrossRef](#)]
25. Leitinger, N.; Schulman, I.G. Phenotypic polarization of macrophages in atherosclerosis. *Arterioscler. Thromb. Vasc. Biol.* **2013**, *33*, 1120–1126. [[CrossRef](#)] [[PubMed](#)]
26. Hoppstädter, J.; Hachenthal, N.; Valbuena-Perez, J.V.; Lampe, S.; Astanina, K.; Kunze, M.M.; Bruscoli, S.; Riccardi, C.; Schmid, T.; Diesel, B.; et al. Induction of Glucocorticoid-induced Leucine Zipper (GILZ) Contributes to Anti-inflammatory Effects of the Natural Product Curcumin in Macrophages. *J. Biol. Chem.* **2016**, *291*, 22949–22960. [[CrossRef](#)]
27. Dahlem, C.; Siow, W.X.; Lopatniuk, M.; Tse, W.K.F.; Kessler, S.M.; Kirsch, S.H.; Hoppstädter, J.; Vollmar, A.M.; Müller, R.; Luzhetskyy, A.; et al. Thioholgamide A, a new anti-proliferative anti-tumor agent, modulates macrophage polarization and metabolism. *Cancers* **2020**, *12*, 1288. [[CrossRef](#)] [[PubMed](#)]
28. Koushki, K.; Shahbaz, S.K.; Mashayekhi, K.; Sadeghi, M.; Zayeri, Z.D.; Taba, M.Y.; Banach, M.; Al-Rasadi, K.; Johnston, T.P.; Sahebkar, A. Anti-inflammatory Action of Statins in Cardiovascular Disease: The Role of Inflammasome and Toll-Like Receptor Pathways. *Clin. Rev. Allerg. Immunol.* **2021**, *60*, 175–199. [[CrossRef](#)]
29. Tuomisto, T.T.; Lumivuori, H.; Kansanen, E.; Häkkinen, S.; Turunen, M.P.; van Thienen, J.V.; Horrevoets, A.J.; Levonen, A.; Ylä-Herttuala, S. Simvastatin has an anti-inflammatory effect on macrophages via upregulation of an atheroprotective transcription factor, Kruppel-like factor 2. *Cardiovasc. Res.* **2019**, *78*, 175–184. [[CrossRef](#)]
30. Liao, Y.H.; Lin, Y.C.; Tsao, S.T.; Lin, Y.C.; Yang, A.J.; Huang, C.T.; Huang, K.C.; Lin, W.W. HMG-CoA reductase inhibitors activate caspase-1 in human monocytes depending on ATP release and P2X7 activation. *J. Leukoc. Biol.* **2013**, *93*, 289–299. [[CrossRef](#)]
31. Chen, A.O.; Chen, Z.W.; Zhou, Y.; Wu, Y.; Xia, Y.; Lu, D.B.; Fan, M.K.; Li, S.; Chen, J.X.; Sun, A.J.; et al. Rosuvastatin protects against coronary microembolization-induced cardiac injury via inhibiting NLRP3 inflammasome activation. *Cell Death Dis.* **2021**, *12*, 78. [[CrossRef](#)]
32. Sweet, D.R.; Vasudevan, N.T.; Fan, L.; Booth, C.E.; Keerthy, K.S.; Liao, X.; Vinayachandran, V.; Takami, Y.; Tugal, D.; Sharma, N.; et al. Myeloid Kruppel-like factor 2 is a critical regulator of metabolic inflammation. *Nat. Commun.* **2020**, *11*, 5872. [[CrossRef](#)]
33. Filippov, S.; Pinkosky, S.L.; Lister, R.J.; Pawloski, C.; Hanselman, J.C.; Cramer, C.T.; Srivastava, R.A.K.; Hurley, T.R.; Bradshaw, C.D.; Spahr, M.A.; et al. ETC-1002 regulates immune response, leukocyte homing, and adipose tissue inflammation via LKB1-dependent activation of macrophage AMPK. *J. Lipid Res.* **2013**, *54*, 2095–2108. [[CrossRef](#)] [[PubMed](#)]
34. Pinkosky, S.L.; Newton, R.S.; Day, E.A.; Ford, R.J.; Lhotak, S.; Austin, R.C.; Birch, C.M.; Smith, B.K.; Filippov, S.; Groot, P.H.E.; et al. Liver-specific ATP-citrate lyase inhibition by bempedoic acid decreases LDL-C and attenuates atherosclerosis. *Nat. Commun.* **2016**, *7*, 13457. [[CrossRef](#)] [[PubMed](#)]
35. Jia, X.; Virani, S.S. CLEAR Serenity Trial: More Clarity for the Future of Bempedoic Acid in Patients Unable to Take Statins? *J. Am. Heart Assoc.* **2019**, *8*, e012352. [[CrossRef](#)] [[PubMed](#)]
36. Nikolic, D.; Banach, M.; Chianetta, R.; Luzzu, L.M.; Stoian, A.P.; Diaconu, C.C.; Citarrella, R.; Montalto, G.; Rizzo, M. An overview of statin-induced myopathy and perspectives for the future. *Expert Opin. Drug Saf.* **2020**, *19*, 601–615. [[CrossRef](#)]

37. Hoppstädter, J.; Valbuena Perez, J.V.; Linnenberger, R.; Dahlem, C.; Legroux, T.M.; Hecksteden, A.; Tse, W.K.F.; Flamini, S.; Andreas, A.; Herrmann, J.; et al. The glucocorticoid-induced leucine zipper mediates statin-induced muscle damage. *FASEB J.* **2020**, *34*, 4684–4701. [[CrossRef](#)]
38. Huang, K.C.; Chen, C.W.; Chen, J.C.; Lin, W.W. HMG-CoA reductase inhibitors inhibit inducible nitric oxide synthase gene expression in macrophages. *J. Biomed. Sci.* **2003**, *10*, 396–405. [[CrossRef](#)] [[PubMed](#)]
39. Brown, M.S.; Goldstein, J.L. Multivalent feedback regulation of HMG CoA reductase, a control mechanism coordinating isoprenoid synthesis and cell growth. *J. Lipid Res.* **1980**, *21*, 505–517. [[CrossRef](#)]
40. Schrijvers, D.M.; De Meyer, G.R.Y.; Herman, A.G.; Martinet, W. Phagocytosis in atherosclerosis: Molecular mechanisms and implications for plaque progression and stability. *Cardiovasc. Res.* **2007**, *73*, 470–480. [[CrossRef](#)]
41. Kapellos, T.S.; Taylor, L.; Lee, H.; Cowley, S.A.; James, W.S.; Iqbal, A.J.; Greaves, D.R. A novel real time imaging platform to quantify macrophage phagocytosis. *Biochem. Pharmacol.* **2016**, *116*, 107–119. [[CrossRef](#)]
42. Mendoza-Coronel, E.; Ortega, E. Macrophage Polarization Modulates FcγR- and CD13-Mediated Phagocytosis and Reactive Oxygen Species Production, Independently of Receptor Membrane Expression. *Front. Immunol.* **2017**, *8*, 303. [[CrossRef](#)]
43. Keidar, S.; Aviram, M.; Maor, I.; Oiknine, J.; Brook, J.G. Pravastatin inhibits cellular cholesterol synthesis and increases low density lipoprotein receptor activity in macrophages: In vitro and in vivo studies. *Br. J. Clin. Pharmacol.* **1994**, *38*, 513–519. [[CrossRef](#)]
44. Hoppstädter, J.; Dembek, A.; Horing, M.; Schymik, H.S.; Dahlem, C.; Sultan, A.; Wirth, N.; Al-Fityan, S.; Diesel, B.; Gasparoni, G.; et al. Dysregulation of cholesterol homeostasis in human lung cancer tissue and tumour-associated macrophages. *EBioMedicine* **2021**, *72*, 103578. [[CrossRef](#)]
45. Rimpelova, S.; Kolar, M.; Strnad, H.; Ruml, T.; Vitek, L.; Gbelcova, H. Comparison of Transcriptomic Profiles of MiaPaCa-2 Pancreatic Cancer Cells Treated with Different Statins. *Molecules* **2021**, *26*, 3528. [[CrossRef](#)]
46. Henriksbo, B.D.; Lau, T.C.; Cavallari, J.F.; Denou, E.; Chi, W.; Lally, J.S.; Crane, J.D.; Duggan, B.M.; Foley, K.P.; Fullerton, M.D.; et al. Fluvastatin causes NLRP3 inflammasome-mediated adipose insulin resistance. *Diabetes* **2014**, *63*, 3742–3747. [[CrossRef](#)]
47. Hoppstädter, J.; Kessler, S.M.; Bruscoli, S.; Huwer, H.; Riccardi, C.; Kiemer, A.K. Glucocorticoid-induced leucine zipper: A critical factor in macrophage endotoxin tolerance. *J. Immunol.* **2015**, *194*, 6057–6067. [[CrossRef](#)]
48. Stewart, J.; Addy, K.; Campbell, S.; Wilkinson, P. Primary prevention of cardiovascular disease: Updated review of contemporary guidance and literature. *JRSM Cardiovasc. Dis.* **2020**, *9*, 2048004020949326. [[CrossRef](#)] [[PubMed](#)]
49. Loppnow, H.; Buerke, M.; Schlitt, A.; Muller-Werdan, U.; Werdan, K. Anti-inflammatory effect of statins in an atherosclerosis-related coculture model. *FASEB J.* **2011**, *25*, 638.3. [[CrossRef](#)]
50. Matsumoto, M.; Einhaus, D.; Gold, E.S.; Aderem, A. Simvastatin augments lipopolysaccharide-induced proinflammatory responses in macrophages by differential regulation of the c-Fos and c-Jun transcription factors. *J. Immunol.* **2004**, *172*, 7377–7384. [[CrossRef](#)] [[PubMed](#)]
51. Giroux, L.M.; Davignon, J.; Naruszewicz, M. Simvastatin inhibits the oxidation of low-density lipoproteins by activated human monocyte-derived macrophages. *Biochim. Biophys. Acta* **1993**, *1165*, 335–338. [[CrossRef](#)]
52. Kuijk, L.M.; Mandey, S.H.; Schellens, I.; Waterham, H.R.; Rijkers, G.T.; Coffey, P.J.; Frenkel, J. Statin synergizes with LPS to induce IL-1β release by THP-1 cells through activation of caspase-1. *Mol. Immunol.* **2008**, *45*, 2158–2165. [[CrossRef](#)]
53. Hohensinner, P.J.; Baumgartner, J.; Ebenbauer, B.; Thaler, B.; Fischer, M.B.; Huber, K.; Speidl, W.S.; Wojta, J. Statin treatment reduces matrix degradation capacity of proinflammatory polarized macrophages. *Vascul. Pharmacol.* **2018**, *110*, 49–54. [[CrossRef](#)] [[PubMed](#)]
54. Fu, H.; Alabdullah, M.; Grossmann, J.; Spieler, F.; Abdosh, R.; Lutz, V.; Kalies, K.; Knopp, K.; Rieckmann, M.; Koch, S.; et al. The differential statin effect on cytokine production of monocytes or macrophages is mediated by differential geranylgeranylation-dependent Rac1 activation. *Cell Death Dis.* **2019**, *10*, 880. [[CrossRef](#)] [[PubMed](#)]
55. Methé, H.; Kim, J.O.; Kofler, S.; Nabauer, M.; Weis, M. Statins decrease toll-like receptor 4 expression and downstream signaling in human CD14+ monocytes. *Arterioscler. Thromb. Vasc. Biol.* **2005**, *25*, 1439–1445. [[CrossRef](#)]
56. Montecucco, F.; Burger, F.; Pelli, G.; Poku, N.K.; Berlier, C.; Steffens, S.; Mach, F. Statins inhibit C-reactive protein-induced chemokine secretion, ICAM-1 upregulation and chemotaxis in adherent human monocytes. *Rheumatology* **2009**, *48*, 233–242. [[CrossRef](#)]
57. Williams, M.R.; Cauvi, D.M.; Rivera, I.; Hawisher, D.; De Maio, A. Changes in macrophage function modulated by the lipid environment. *Innate Immun.* **2016**, *22*, 141–151. [[CrossRef](#)] [[PubMed](#)]
58. Redondo-Morata, L.; Sanford, R.L.; Andersen, O.S.; Scheuring, S. Effect of statins on the nanomechanical properties of supported lipid bilayers. *Biophys. J.* **2016**, *111*, 363–372. [[CrossRef](#)] [[PubMed](#)]
59. Bu, D.X.; Griffin, G.; Lichtman, A.H. Mechanisms for the anti-inflammatory effects of statins. *Curr. Opin. Lipidol.* **2011**, *22*, 165–170. [[CrossRef](#)]
60. Akula, M.K.; Ibrahim, M.X.; Ivarsson, E.G.; Khan, O.M.; Kumar, I.T.; Erlandsson, M.; Karlsson, C.; Xu, X.; Brisslert, M.; Brakebusch, C.; et al. Protein prenylation restrains innate immunity by inhibiting Rac1 effector interactions. *Nat. Commun.* **2019**, *10*, 3975. [[CrossRef](#)]
61. Lee, D.K.; Park, E.J.; Kim, E.K.; Jin, J.; Kim, J.S.; Shin, I.J.; Kim, B.Y.; Lee, H.; Kim, D.E. Atorvastatin and simvastatin, but not pravastatin, up-regulate LPS-induced MMP-9 expression in macrophages by regulating phosphorylation of ERK and CREB. *Cell. Physiol. Biochem.* **2012**, *30*, 499–511. [[CrossRef](#)]

62. Loike, J.D.; Shabtai, D.Y.; Neuhut, R.; Malitzky, S.; Lu, E.; Husemann, J.; Goldberg, I.J.; Silverstein, S.C. Statin inhibition of Fc receptor-mediated phagocytosis by macrophages is modulated by cell activation and cholesterol. *Arterioscler. Thromb. Vasc. Biol.* **2004**, *24*, 2051–2056. [[CrossRef](#)]
63. Djaldetti, M.; Salman, H.; Bergman, M.; Bessler, H. Effect of pravastatin, simvastatin and atorvastatin on the phagocytic activity of mouse peritoneal macrophages. *Exp. Mol. Pathol.* **2006**, *80*, 160–164. [[CrossRef](#)]
64. Tanaka, N.; Abe-Dohmae, S.; Iwamoto, N.; Fitzgerald, M.L.; Yokoyama, S. HMG-CoA reductase inhibitors enhance phagocytosis by upregulating ATP-binding cassette transporter A7. *Atherosclerosis* **2011**, *217*, 407–414. [[CrossRef](#)] [[PubMed](#)]
65. Cordle, A.; Koenigsnecht-Talboo, J.; Wilkinson, B.; Limpert, A.; Landreth, G. Mechanisms of statin-mediated inhibition of small G-protein function. *J. Biol. Chem.* **2005**, *280*, 34202–34209. [[CrossRef](#)] [[PubMed](#)]
66. Mao, Y.; Finnemann, S.C. Regulation of phagocytosis by Rho GTPases. *Small GTPases* **2015**, *6*, 89–99. [[CrossRef](#)]
67. Cramer, C.T.; Goetz, B.; Hopson, K.L.M.; Fici, G.J.; Ackermann, R.M.; Brown, S.C.; Bisgaier, C.L.; Rajeswaran, W.G.; Oniciu, D.C.; Pape, M.E. Effects of a novel dual lipid synthesis inhibitor and its potential utility in treating dyslipidemia and metabolic syndrome. *J. Lipid Res.* **2004**, *45*, 1289–1301. [[CrossRef](#)]
68. Laufs, U.; Banach, M.; Mancini, G.B.J.; Gaudet, D.; Bloedon, L.T.; Sterling, L.R.; Kelly, S.; Stroes, E.S.G. Efficacy and safety of bempedoic acid in patients with hypercholesterolemia and statin intolerance. *J. Am. Heart Assoc.* **2019**, *8*, e011662. [[CrossRef](#)]
69. Bays, H.E.; Banach, M.; Catapano, A.L.; Duell, P.B.; Gotto, A.M., Jr.; Laufs, U.; Leiter, L.A.; Mancini, G.B.J.; Ray, K.K.; Bloedon, L.T.; et al. Bempedoic acid safety analysis: Pooled data from four phase 3 clinical trials. *J. Clin. Lipidol.* **2020**, *14*, 649–659. [[CrossRef](#)] [[PubMed](#)]
70. Anderson, C.M.; Stahl, A. SLC27 fatty acid transport proteins. *Mol. Asp. Med.* **2013**, *34*, 516–528. [[CrossRef](#)] [[PubMed](#)]
71. Melton, E.M.; Cerny, R.L.; Watkins, P.A.; DiRusso, C.C.; Black, P.N. Human fatty acid transport protein 2a/very long chain acyl-CoA synthetase 1 (FATP2a/Acsvl1) has a preference in mediating the channeling of exogenous n-3 fatty acids into phosphatidylinositol. *J. Biol. Chem.* **2011**, *286*, 30670–30679. [[CrossRef](#)]
72. Ballantyne, C.M.; Bays, H.; Catapano, A.L.; Goldberg, A.; Ray, K.K.; Saseen, J.J. Role of Bempedoic Acid in Clinical Practice. *Cardiovasc. Drugs Ther.* **2021**, *35*, 853–864. [[CrossRef](#)] [[PubMed](#)]
73. Amore, B.M.; Cramer, C.T.; MacDougall, D.E.; Sasiela, W.J.; Emery, M.G. Absence of effect of steady state bempedoic acid on cardiac repolarization: Results of a thorough QT/QTc study in healthy volunteers. *Clin. Transl. Sci.* **2021**, *00*, 1–10. [[CrossRef](#)] [[PubMed](#)]
74. Castoldi, A.; Monteiro, L.B.; Bakker, N.V.; Sanin, D.E.; Rana, N.; Corrado, M.; Cameron, A.M.; Hassler, F.; Matsushita, M.; Caputa, G.; et al. Triacylglycerol synthesis enhances macrophage inflammatory function. *Nat. Commun.* **2020**, *11*, 4107. [[CrossRef](#)] [[PubMed](#)]
75. Chandra, P.; He, L.; Zimmerman, M.; Yang, G.Z.; Koster, S.; Ouimet, M.; Wang, H.; Moore, K.J.; Dartois, V.; Schilling, J.D.; et al. Inhibition of fatty acid oxidation promotes macrophage control of mycobacterium tuberculosis. *Mbio* **2020**, *11*, e01139-20. [[CrossRef](#)] [[PubMed](#)]
76. Bae, H.B.; Zmijewski, J.W.; Deshane, J.S.; Tadie, J.M.; Chaplin, D.D.; Takashima, S.; Abraham, E. AMP-activated protein kinase enhances the phagocytic ability of macrophages and neutrophils. *FASEB J.* **2011**, *25*, 4358–4368. [[CrossRef](#)]
77. Chinetti-Gbaguidi, G.; Colin, S.; Staels, B. Macrophage subsets in atherosclerosis. *Nat. Rev. Cardiol.* **2015**, *12*, 10–17. [[CrossRef](#)]
78. Barrett, T.J. Macrophages in Atherosclerosis Regression. *Arterioscler. Thromb. Vasc. Biol.* **2020**, *40*, 20–33. [[CrossRef](#)]
79. Liberale, L.; Carbone, F.; Montecucco, F.; Sahebkar, A. Statins reduce vascular inflammation in atherogenesis: A review of underlying molecular mechanisms. *Int. J. Biochem. Cell Biol.* **2020**, *122*, 105735. [[CrossRef](#)]
80. Benoit, M.; Desnues, B.; Mege, J.L. Macrophage polarization in bacterial infections. *J. Immunol.* **2008**, *181*, 3733–3739. [[CrossRef](#)]
81. Stanley, E.R. Murine bone marrow-derived macrophages. *Methods Mol. Biol.* **1997**, *75*, 301–304. [[CrossRef](#)] [[PubMed](#)]
82. Czepukojc, B.; Abuhaliema, A.; Barghash, A.; Tierling, S.; Nass, N.; Simon, Y.; Korb, C.; Cadenas, C.; van Hul, N.; Sachinidis, A.; et al. IGF2 mRNA binding protein 2 transgenic mice are more prone to develop a ductular reaction and to progress toward cirrhosis. *Front. Med.* **2019**, *6*, 179. [[CrossRef](#)]
83. Kiemer, A.K.; Müller, C.M.; Vollmar, A.M. Inhibition of LPS-induced nitric oxide and TNF-alpha production by alpha-lipoic acid in rat Kupffer cells and in RAW 264.7 murine macrophages. *Immunol. Cell Biol.* **2002**, *80*, 550–557. [[CrossRef](#)] [[PubMed](#)]
84. Hoppstädter, J.; Diesel, B.; Linnenberger, R.; Hachenthal, N.; Flamini, S.; Minet, M.; Leidinger, P.; Backes, C.; Grässer, F.; Meese, E.; et al. Amplified Host Defense by Toll-Like Receptor-Mediated Downregulation of the Glucocorticoid-Induced Leucine Zipper (GILZ) in Macrophages. *Front. Immunol.* **2019**, *9*, 3111. [[CrossRef](#)] [[PubMed](#)]



Linnenberger et al., 2021

Supplementary Materials

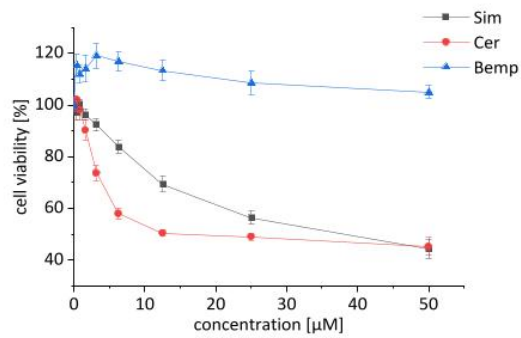


Figure S1. Cytotoxicity of statins and bempedoic acid. BMMs were treated with simvastatin (Sim), cerivastatin (Cer), or bempedoic acid (Bemp) at the indicated concentrations for 24 hours and viability was normalized to the respective DMSO control (Co). Cell viability was measured by MTT ($n = 3$, sixtuplicates).

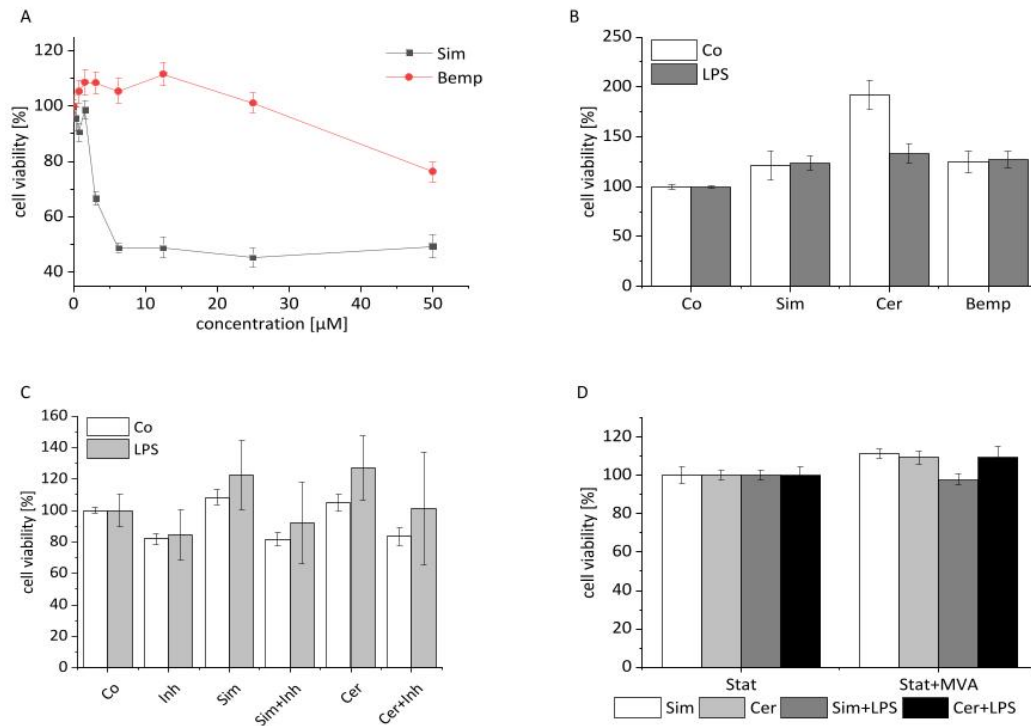


Figure S2. Cytotoxicity of compounds. A. RAW 264.7 cells were treated with simvastatin (Sim), or bempedoic acid (Bemp) at the indicated concentrations for 24 hours and viability was normalized to the respective DMSO control (Co). Cell viability was measured by MTT ($n = 3$, sextuplicates). B. RAW-Blue™ cells were stimulated for the last 4 hours with LPS (100 ng/mL) in the presence or absence of simvastatin (Sim, 2 μM), cerivastatin (Cer, 1 μM), or bempedoic acid (Bemp, 25 μM) for 24 hours and viability was normalized to the respective DMSO control. Cell viability was measured by MTT. Co = solvent control ($n = 3$, triplicates). C. RAW-Blue™ cells were treated with simvastatin (Sim, 2 μM) or cerivastatin (Cer, 1 μM) in the presence or absence of PD98059 (Inh, 10 μM) for 24 h and in the presence or absence of LPS (100 ng/mL) for 4 hours. Cell viability was measured by MTT. Co = solvent control ($n = 3$, triplicates). D. RAW-Blue™ cells were treated with the statins (Stat) simvastatin (Sim, 2 μM) or cerivastatin (Cer, 1 μM) in the presence or absence of mevalonate (MVA, 100 μM) for 24 h and in the presence or absence of LPS (100 ng/mL) for 4 hours. Cell viability was measured by MTT. Co = solvent control ($n = 3$, triplicates).

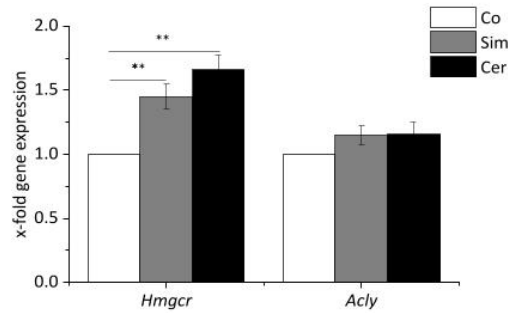


Figure S3. Expression of genes associated with cholesterol synthesis. *Hmgcr* and *Acly* mRNA expression in BMMs were determined by real-time RT-PCR, normalized to *Ppia*, and expressed as x-fold of Co. BMMs were either treated for 24 hours with simvastatin (Sim, 2 μ M) or cerivastatin (Cer, 0.5 μ M). Co = solvent control. Statistical analysis was performed by one-sample *t*-test followed by Bonholm post hoc test ($n = 6$). ** $p < 0.01$.

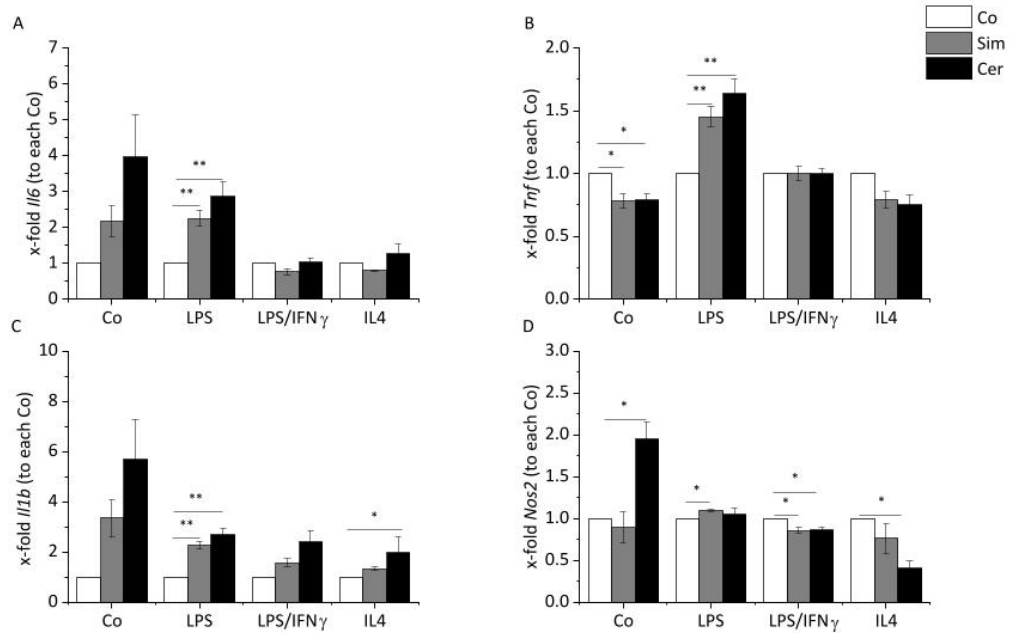


Figure S4. Effect of statin treatment on the inflammatory response in macrophages. A-D. *Il6* (A), *Tnf* (B), *Il1b* (C), and *Nos2* (D) mRNA expression in BMMs were determined by real-time RT-PCR, normalized to *Ppia*, and expressed as x-fold of the respective Co. BMMs were stimulated for the last 4 hours with LPS (100 ng/mL) or polarized towards M1 (LPS, 100 ng/mL; IFN γ , 20 ng/mL), or M2 (IL4, 20 ng/mL), in the presence or absence of simvastatin (Sim, 2 μ M) or cerivastatin (Cer, 0.5 μ M) for 24 hours. Co = solvent control. Statistical analysis was performed by one-sample *t*-test followed by Bonholm post hoc test for data of the control group. Means of more than two groups were compared by one-way ANOVA with Bonholm post hoc test (normal distribution) ($n = 6$). * $p < 0.05$, ** $p < 0.01$.

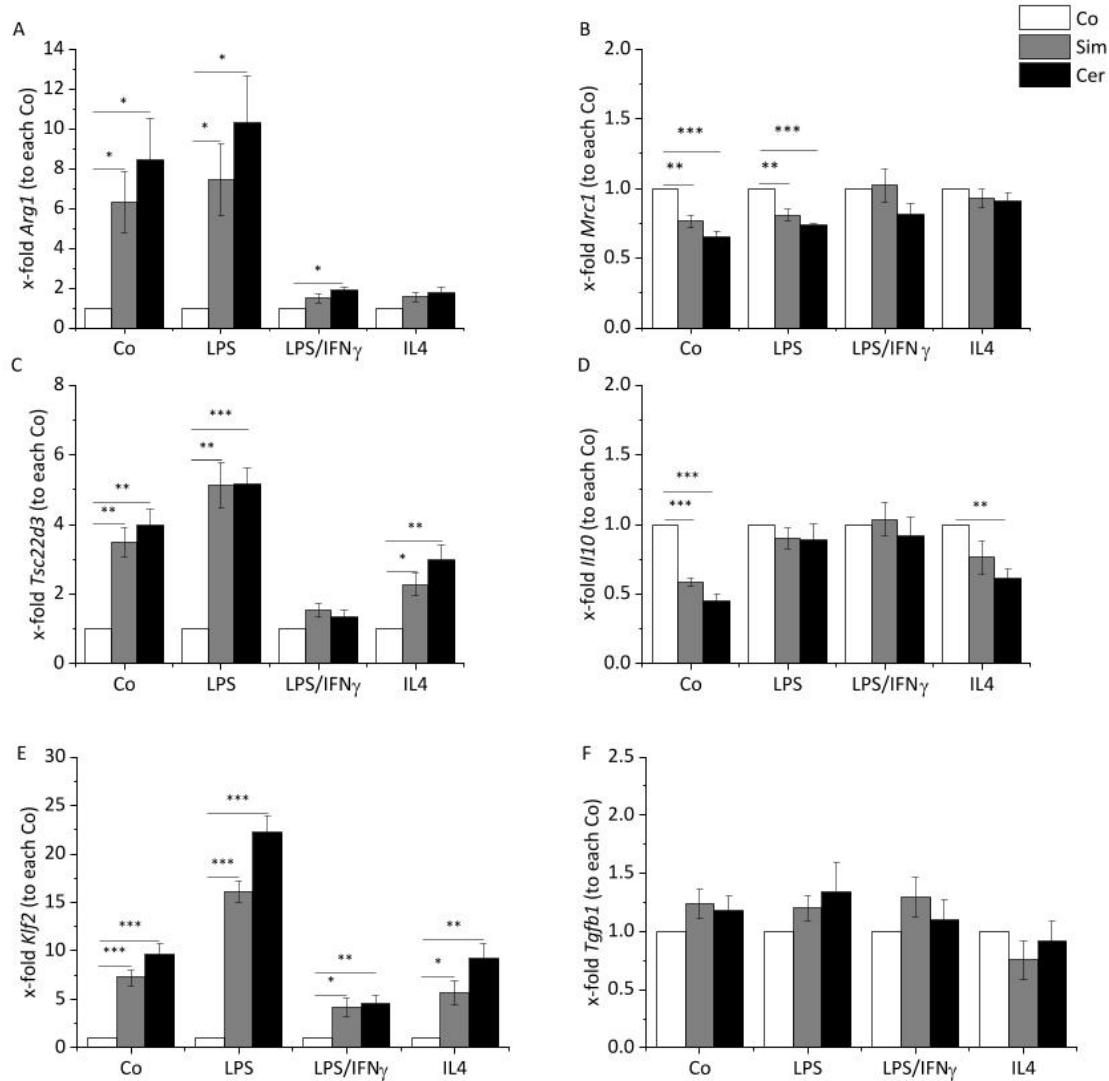


Figure S5. Effect of statin treatment on the anti-inflammatory response in macrophages. A-F. *Arg1* (A), *Mrc1* (B), *Tsc22d3* (C), *Il10* (D), *Tgfb1* (E), and *Klf2* (F) mRNA expression levels in BMMs were determined by real-time RT-PCR, normalized to *Ppia*, and expressed as x-fold of the respective Co. BMMs were stimulated for the last 4 hours with LPS (100 ng/mL) or polarized towards M1 (LPS, 100 ng/mL; IFN γ , 20 ng/mL), or M2 (IL4, 20 ng/mL) in the presence or absence of simvastatin (Sim, 2 μ M) or cerivastatin (Cer, 0.5 μ M) for 24 hours. Co = solvent control. Statistical analysis was performed by one-sample *t*-test followed by Bonholm post hoc test for data of the control group. Means of more than two groups were compared by one-way ANOVA with Bonholm post hoc test (normal distribution) ($n = 6$). * $p < 0.05$, ** $p < 0.01$, and *** $p < 0.001$.

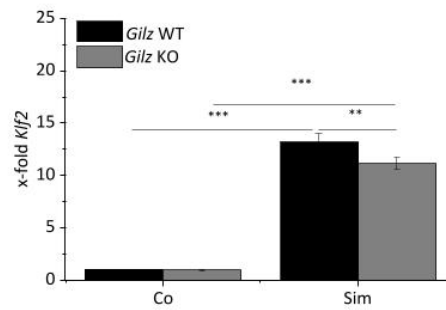


Figure S6. *Klf2* mRNA expression. *Klf2* mRNA expression in BMMs was determined by real-time RT-PCR, normalized to *Ppia*, and expressed as x-fold of Co. BMMs of *Gilz* WT and KO BMMs were treated for 24 hours with simvastatin (Sim, 2 μ M). Co = solvent control. Statistical analysis was performed by one-way ANOVA with Bonholm post hoc test (normal distribution) ($n = 4$, triplicates). ** $p < 0.01$, *** $p < 0.001$.

Control

Phase contrast

Red fluorescence

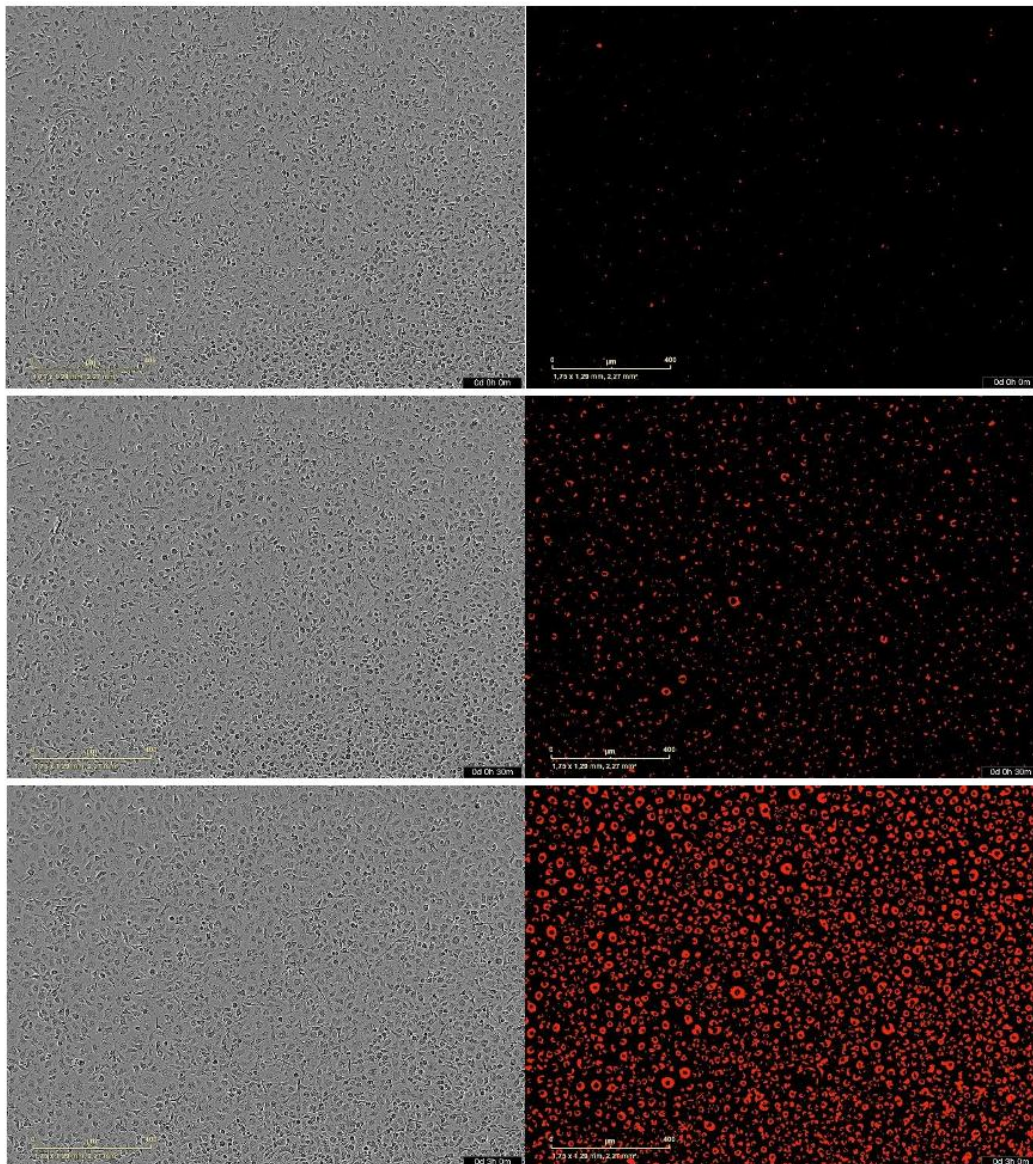


Figure S7. Images shown in Figure 3A (Control) as an overlay are shown as phase contrast and red fluorescence only.

Simvastatin

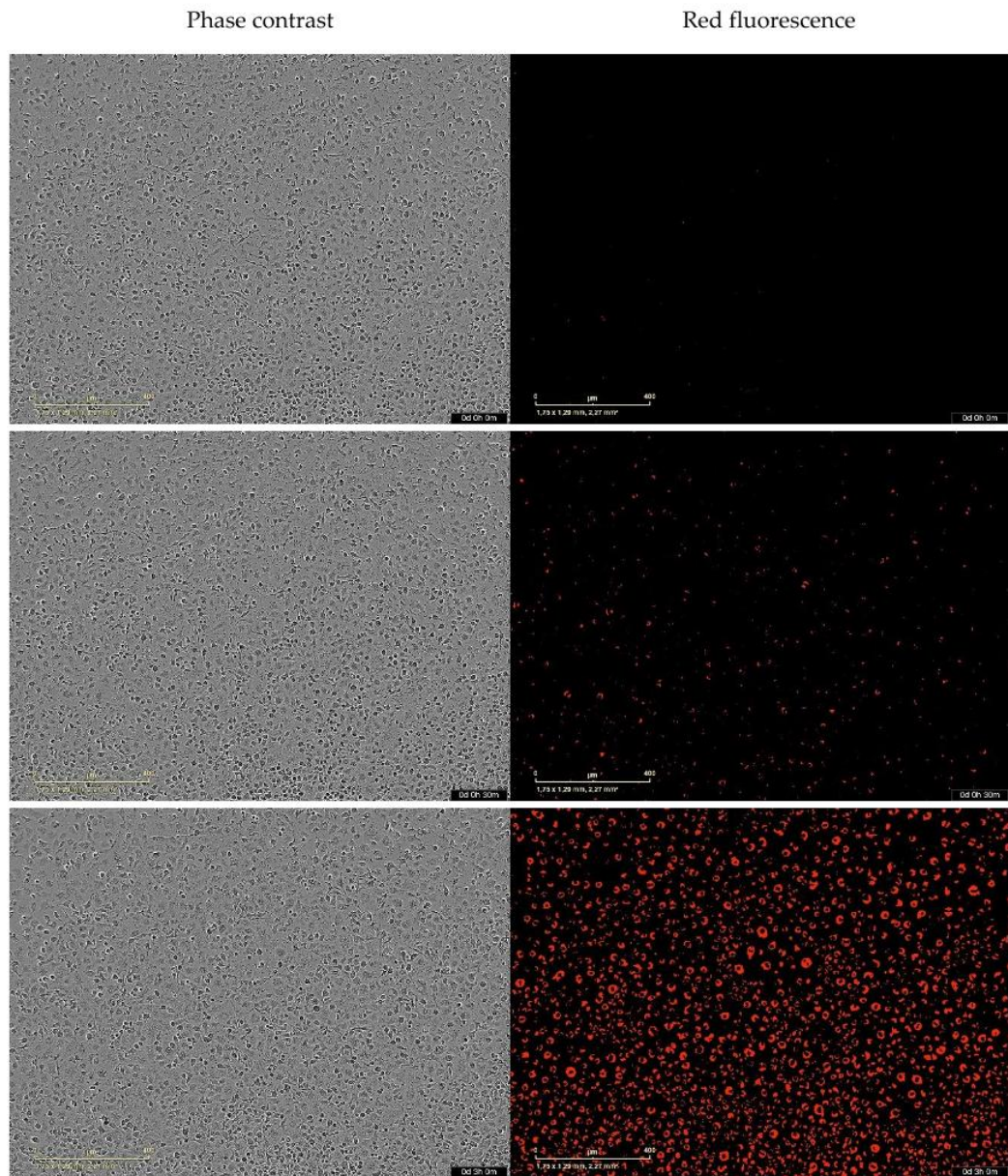


Figure S8. Images shown in Figure 3A (Sim) as an overlay are shown as phase contrast and red fluorescence only.

Cerivastatin

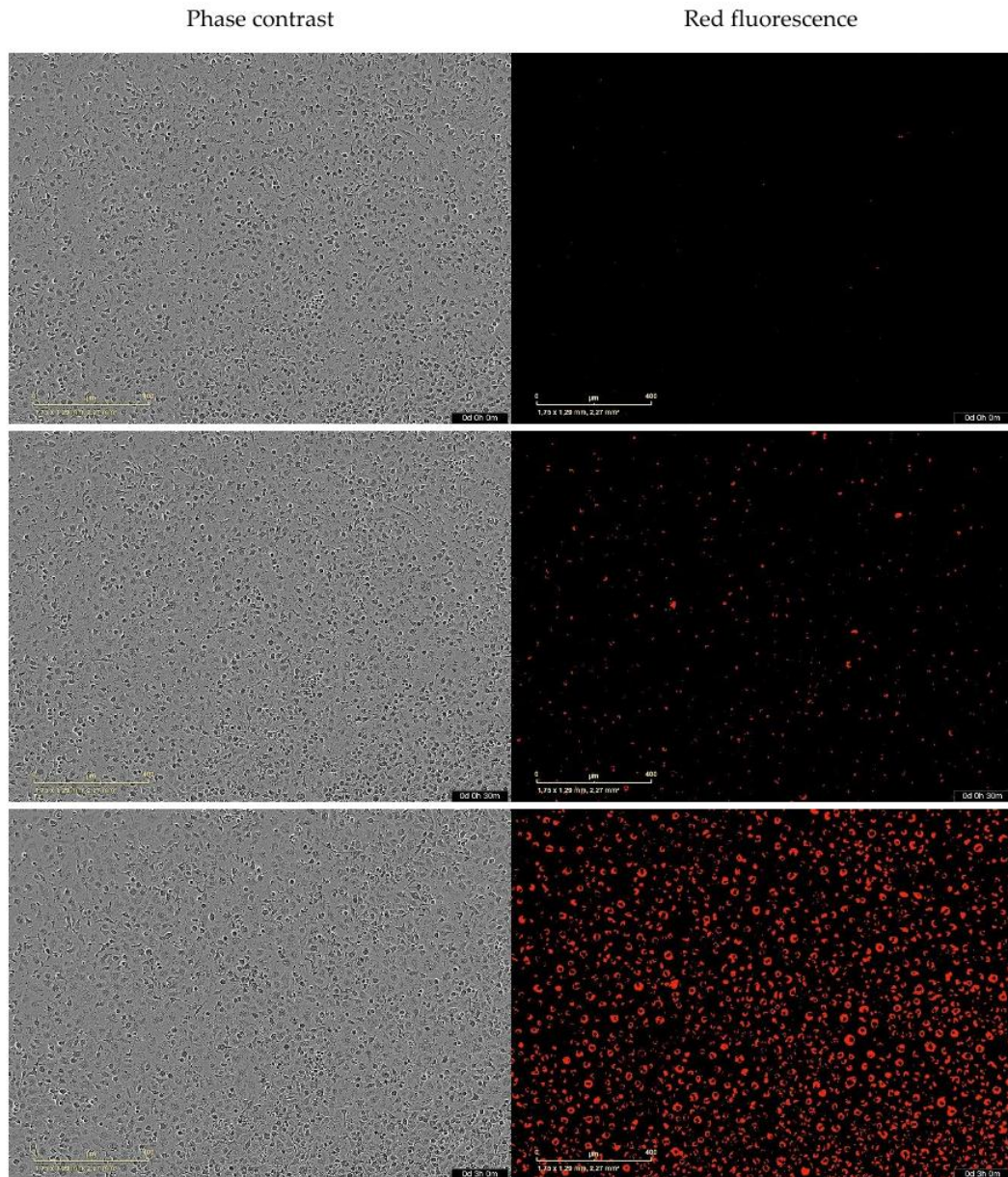


Figure S9. Images shown in Figure 3A (Cer) as an overlay are shown as phase contrast and red fluorescence only.

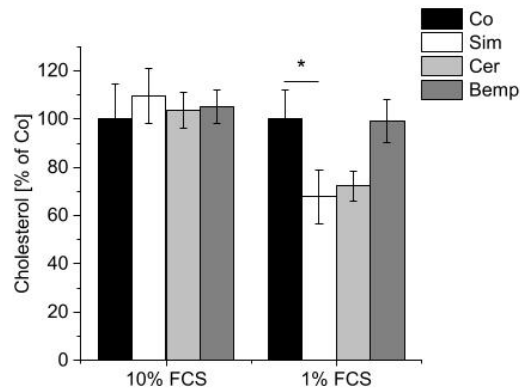


Figure S10. Cellular cholesterol content of statin-treated macrophages under standard and serum-starving conditions. BMMs were either kept in standard medium (10% FCS) or medium containing only 1% FCS and treated for 24 hours with simvastatin (Sim, 2 μ M), cerivastatin (Cer, 0.5 μ M), or bempedoic acid (25 μ M). Intracellular cholesterol levels were assessed using the Amplex assay ($n = 2$, triplicates). Co = solvent control. Statistical analysis was performed by one-way ANOVA with Bonholm post hoc test (normal distribution). * $p < 0.05$.

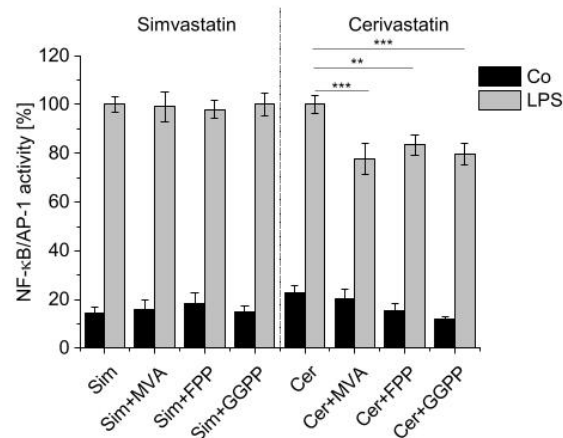


Figure S11. Intermediates of the mevalonate pathway inhibit NF- κ B/AP-1-activity in cerivastatin-treated macrophages. RAW-BlueTM cells were treated for 24 hours with either Sim (2 μ M) or Cer (1 μ M). Cells were co-treated with mevalonate (MVA, 100 μ M), farnesyl pyrophosphate (FPP, 10 μ M), or geranylgeranyl pyrophosphate (GGPP, 10 μ M) where indicated. Inflammatory activation was induced by treatment with LPS (100 ng/mL) for the final 4 hours. NF- κ B/AP-1 activity was determined by secreted embryonic alkaline phosphatase (SEAP) detection. Co = solvent control ($n = 4$, triplicates). Statistical analysis was performed by one-way ANOVA with Bonholm post hoc test (normal distribution); ** $p < 0.01$, *** $p < 0.001$.

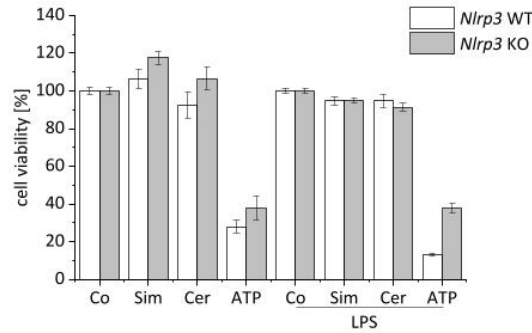


Figure S12. Cytotoxicity of statins in *Nlrp3* WT and KO BMMs. BMMs were treated with simvastatin (Sim, 2 μ M), cerivastatin (Cer, 0.5 μ M), or ATP as positive control (3 mM, 30 min). Inflammatory activation was induced by treatment with LPS (100 ng/mL) for the final 4 hours. Cell viability was measured by MTT. Co = solvent control ($n = 4$, quadruplicates).

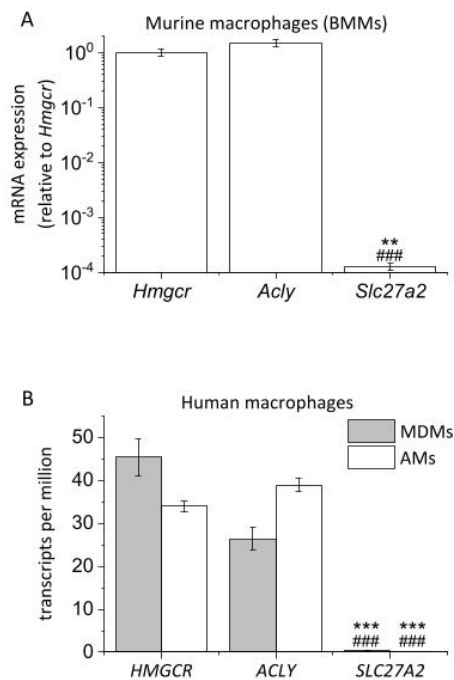


Figure S13. Expression of HMG-CoA reductase (*Hmgcr* / *HMGCR*), ATP-citrate lyase (*Acly* / *ACLY*), and very-long-chain acyl-CoA synthetase-1 (*Slc27a2* / *SLC27A2*) in murine and human macrophages. (A) Gene expression levels in BMMs were determined by real-time RT-PCR, normalized to *Ppia*, and expressed as x-fold of *Hmgcr* ($n = 3$). (B) Gene expression in human monocyte-derived macrophages (MDMs) and alveolar macrophages (AMs) according to Gene Expression Omnibus (GEO) datasets GSE162669 and GSE162698 ($n = 3$). Statistical analysis was performed by one-way ANOVA with Bonholm post hoc test (normal distribution); ** $p < 0.01$, *** $p < 0.001$ vs. *Hmgcr* / *HMGCR*; ### $p < 0.001$ vs. *Acly* / *ACLY*.

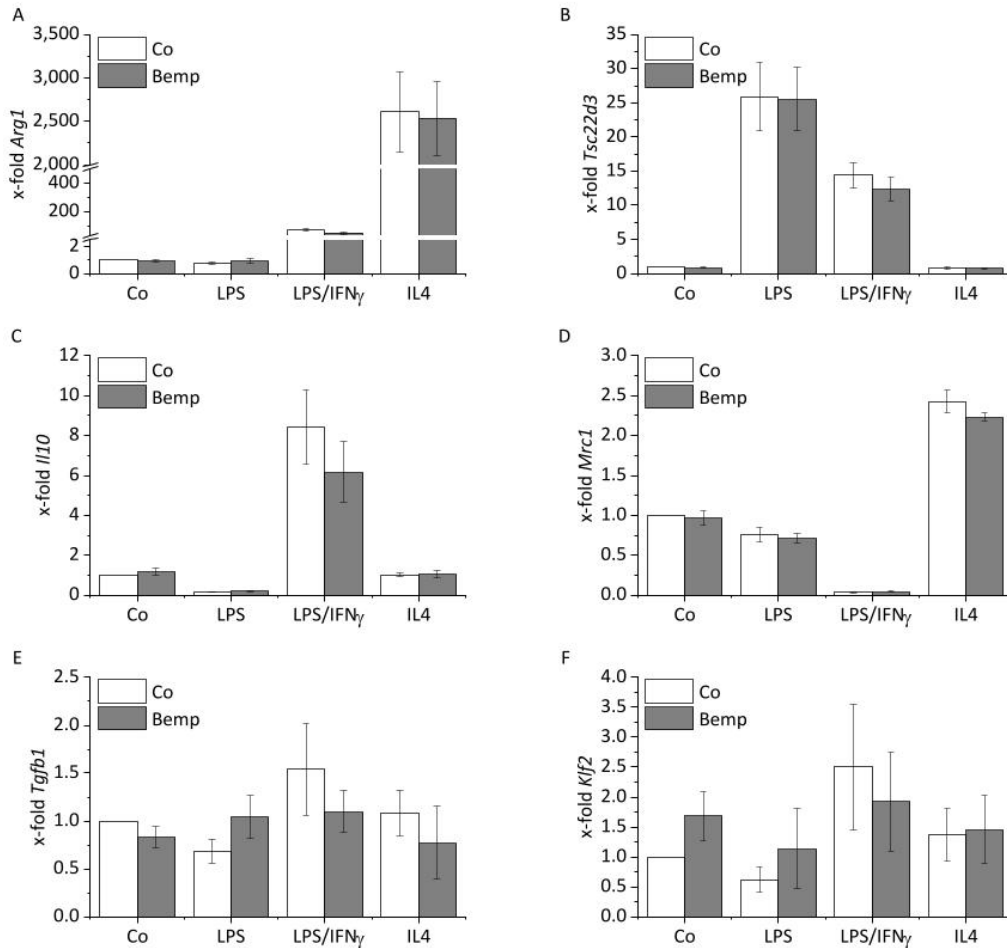


Figure S14. Effect of bempedoic acid treatment on the anti-inflammatory response in macrophages. A-F. *Arg1* (A), *Tsc22d3* (B), *Il10* (C), *Mrc1* (D), *Tgfb1* (E), and *Klf2* (F) mRNA expression in BMMs were determined by real-time RT-PCR, normalized to *Ppia*, and expressed as x-fold of Co. BMMs were stimulated for the last 4 hours with LPS (100 ng/mL) or polarized towards M1 (LPS, 100 ng/mL; IFN γ , 20 ng/mL), or M2 (IL4, 20 ng/mL) in the presence or absence of Bemp (bempedoic acid, 25 μ M) for 24 hours. Co = solvent control ($n = 6$). One-sample *t*-test followed by Bonholm post hoc test was used for analyzing gene expression data of the control group. Means of more than two groups were compared by one-way ANOVA with Bonholm post hoc test (normal distribution).

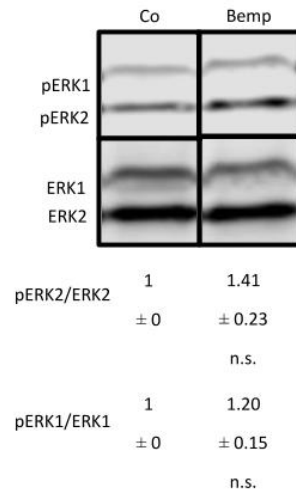


Figure S15. Bempedoic acid does not affect ERK signaling. ERK phosphorylation was examined by Western Blot analysis. BMMs were treated with bempedoic acid (Bemp, 25 μ M) for one hour. One representative blot is shown. Signal intensities were quantified and normalized to total ERK and expressed as mean \pm SEM. Co = solvent control. Statistical analysis was performed by one-sample *t*-test followed by Bonholm post hoc test. n.s. = not significant ($n = 3$).

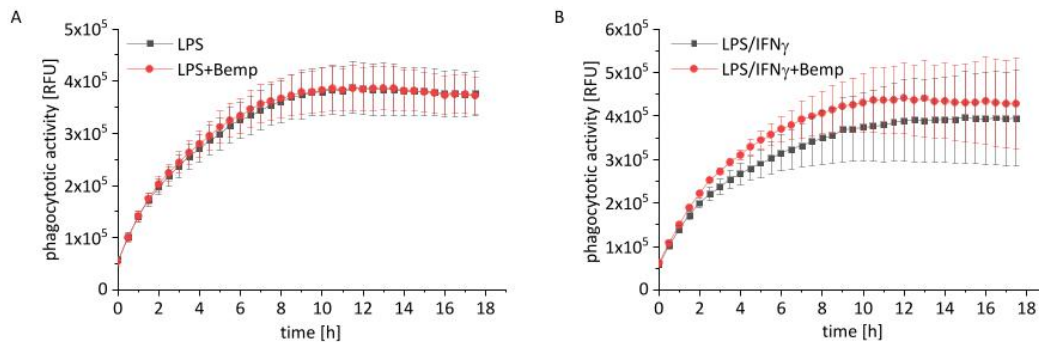


Figure S16. Effect of bempedoic acid treatment on the phagocytotic activity of macrophages. A-B. BMMs were stimulated for the last 4 hours with LPS (100 ng/mL) or polarized towards M1 (LPS, 100 ng/mL; IFN γ , 20 ng/mL) in the presence or absence of bempedoic acid (Bemp, 25 μ M) for 24 hours and monitored by an IncuCyte S3 system after addition of fluorogenic pHrodo® Red *S. aureus* bioparticles (5 μ g/well). Co = solvent control, RFU = relative fluorescence units. Statistical analysis was performed by two-way ANOVA with Bonholm post hoc test ($n = 4$, duplicates).

4. Summary and Conclusion

Generally, GILZ exerts different effects, such as inhibiting the expression of cell adhesive molecules in endothelial cells, tolerogenic effects in dendritic cells, and modulation of Th17 immune response but also mimics many anti-inflammatory effects of glucocorticoids in diseases such as arthritis, inflammatory bowel disease, and systemic lupus erythematosus (Jones et al., 2016; Luz-Crawford et al., 2015; Nataraja et al., 2021). Of note, this is also in accordance with the data that GILZ promotes an M2-like phenotype during macrophage polarization (Vago et al., 2020). In *in vivo* models GILZ cured colitis and facilitated the resolution of LPS-induced inflammation and a synthetic GILZ analog suppressed autoimmune encephalopathy (reviewed by (Bereshchenko et al., 2019)). Those data are indicating that GILZ protein and its analogs have therapeutic effects and are non-toxic to cells and rodents.

The regulation of GILZ is complex and addresses diverse mechanisms, such as transcriptional and post-transcriptional mechanisms, GC's general negative feedback loop, and epigenetic effects (Bruscoli et al., 2010; Hahn et al., 2014; Hoppstädter et al., 2015, 2016). In accordance with our data, He et al. identified the precursor of miR-hsa-222 as a GILZ regulator which was able to downregulate GILZ in epithelial cells, whereas our data showed macrophage activation via repression of GILZ protein expression, which was facilitated by several miRNAs at once, including miR-222 (He et al., 2020). In general, macrophage activation by GILZ downregulation helps the immune response to clear pathogens but might also be detrimental to the host by an excessive inflammatory response. Our data reveal, that the state of low-grade inflammation during inflammaging is characterized by reduced GILZ levels.

Regarding GILZ signaling pathways it is known that GILZ cross talks with MAPK pathway by binding Raf or Ras proteins and forkhead family transcription factors are involved in the PI3K/Akt pathway of homeostasis of immune cells (Ayroldi et al., 2002, 2012; Hoppstädter et al., 2015). It has been shown that GILZ inhibits FoxO3 activity and is part of the PI3K/Akt-FoxO3 signaling pathways in myeloid and lymphoid cell

lines by the nuclear exclusion of FOXO3 (Latré de Laté et al., 2010). Our data identified FOXO3 as a potential GILZ upstream regulator in muscle cells and its involvement in macrophages by binding to the GILZ promotor region. Previous data described the involvement of FOXO3 in muscle homeostasis and GILZ in the anti-myogenic effects of dexamethasone (Bruscoli et al., 2010). Our data supported this finding by determining GILZ as an important mediator of statin-induced muscle damage linking this effect to Akt deactivation and FOXO3 activation.

Beyond their lipid-lowering actions, statins and bempedoic acid are described in the literature to have anti-inflammatory effects. Clinical data showed a decrease in CRP after statin treatment and attenuation in immune-associated conditions (reviewed by (Diamantis et al., 2017)). To date, conflicting data from statins in cell culture and animal experiments using statins have been published. Our report showed for the first time a systematic experimental setup for the determination of statins' effect on macrophages *in vitro* depending on macrophages' microenvironment. The data highlight an inflammatory effect of statins on short-term activated macrophages characterized by increased NF- κ B activity in contrast to bempedoic acid. However, we neither observed any inflammatory nor anti-inflammatory effect of statins on macrophages after polarization towards the M1 or M2 phenotype. However, we clearly show that statins exhibit rather an immunomodulatory effect on macrophages than an anti-inflammatory or inflammatory effect which was later reviewed by Sheridan et al. (Sheridan et al., 2022).

In conclusion, the data presented in this work contribute to a better understanding of GILZ regulation and the underlying mechanisms elucidating the detrimental and beneficial effects of GILZ as a potential therapeutic agent. Further, we identified mechanistic aspects of statins' pleiotropic effects including underlying molecular mechanisms which represent an aspect of tailored statin therapy.

5. References

Adamson, S., & Leitinger, N. (2011). Phenotypic modulation of macrophages in response to plaque lipids. *Current Opinion in Lipidology*, Volume 22, Page 335–342.

Aikawa, M., Rabkin, E., Sugiyama, S., Voglic, S. J., Fukumoto, Y., Furukawa, Y., Shiomi, M., Schoen, F. J., & Libby, P. (2001). An HMG-CoA Reductase Inhibitor, Cerivastatin, Suppresses Growth of Macrophages Expressing Matrix Metalloproteinases and Tissue Factor In Vivo and In Vitro. *Circulation*, Volume 103, Page 276–283.

Ardura, J. A., Rackov, G., Izquierdo, E., Alonso, V., Gortazar, A. R., & Escribese, M. M. (2019). Targeting Macrophages: Friends or Foes in Disease? *Frontiers in Pharmacology*, Volume 10, Article 1255.

Asselin-Labat, M.-L., David, M., Biola-Vidamment, A., Lecoecuche, D., Zennaro, M.-C., Bertoglio, J., & Pallardy, M. (2004). GILZ, a new target for the transcription factor FoxO3, protects T lymphocytes from interleukin-2 withdrawal-induced apoptosis. *Blood*, Volume 104, Page 215–223.

Ayroldi, E., Cannarile, L., Migliorati, G., Nocentini, G., Delfino, D. V., & Riccardi, C. (2012). Mechanisms of the anti-inflammatory effects of glucocorticoids: Genomic and nongenomic interference with MAPK signaling pathways. *The FASEB Journal*, Volume 26, Page 4805–4820.

Ayroldi, E., Macchiarulo, A., & Riccardi, C. (2014). Targeting glucocorticoid side effects: Selective glucocorticoid receptor modulator or glucocorticoid-induced leucine zipper? A perspective. *The FASEB Journal*, Volume 28, Page 5055–5070.

Ayroldi, E., Zollo, O., Macchiarulo, A., Di Marco, B., Marchetti, C., & Riccardi, C. (2002). Glucocorticoid-induced leucine zipper inhibits the Raf-extracellular signal-regulated kinase pathway by binding to Raf-1. *Molecular Cell Biology*, Volume 22(22), Page 7929–7941.

Baardman, J., Verberk, S. G. S., van der Velden, S., Gijbels, M. J. J., van Roomen, C. P. P. A., Sluimer, J. C., Broos, J. Y., Griffith, G. R., Prange, K. H. M., van Weeghel, M., Lakbir, S., Molenaar, D., Meinster, E., Neele, A. E., Kooij, G., de Vries, H. E., Lutgens, E., Wellen, K. E., de Winther, M. P. J., & Van den Bossche, J. (2020). Macrophage ATP citrate lyase deficiency stabilizes atherosclerotic plaques. *Nature Communications*, Volume 11, Article 6296.

Barrett, T. J. (2020). Macrophages in Atherosclerosis Regression. *Arteriosclerosis, Thrombosis, and Vascular Biology*, Volume 40, Page 20–33.

Baylis, D., Bartlett, D. B., Patel, H. P., & Roberts, H. C. (2013). Understanding how we age: Insights into inflammaging. *Longevity & Healthspan*, Volume 2, Article 8.

Bellavance, M.-A., & Rivest, S. (2014). The HPA - Immune Axis and the Immunomodulatory Actions of Glucocorticoids in the Brain. *Frontiers in Immunology*, Volume 5, Article 136.

Bentzon, J. F., Otsuka, F., Virmani, R., & Falk, E. (2014). Mechanisms of Plaque Formation and Rupture. *Circulation Research*, Volume 114, Page 1852–1866.

Bereshchenko, O., Migliorati, G., Bruscoli, S., & Riccardi, C. (2019). Glucocorticoid-Induced Leucine Zipper: A Novel Anti-inflammatory Molecule. *Frontiers in Pharmacology*, Volume 10, Article

308.

Beuscher, H. U., Günther, C., & Röllinghoff, M. (1990). IL-1 beta is secreted by activated murine macrophages as biologically inactive precursor. *Journal of Immunology*, Volume 14, Page 2179–2183.

Biswas, S. K., Chittechath, M., Shalova, I. N., & Lim, J.-Y. (2012). Macrophage polarization and plasticity in health and disease. *Immunologic Research*, Volume 53, Page 11–24.

Bouzeyen, R., Haoues, M., Barbouche, M.-R., Singh, R., & Essafi, M. (2019). FOXO3 Transcription Factor Regulates IL-10 Expression in Mycobacteria-Infected Macrophages, Tuning Their Polarization and the Subsequent Adaptive Immune Response. *Frontiers in Immunology*, Volume 10, Article 2922.

Brubaker, S. W., Bonham, K. S., Zanoni, I., & Kagan, J. C. (2015). Innate immune pattern recognition: A cell biological perspective. *Annual Review of Immunology*, Volume 33, Page 257–290.

Bruscoli, S., Donato, V., Velardi, E., Di Sante, M., Migliorati, G., Donato, R., & Riccardi, C. (2010). Glucocorticoid-induced leucine zipper (GILZ) and long GILZ inhibit myogenic differentiation and mediate anti-myogenic effects of glucocorticoids. *The Journal of Biological Chemistry*, Volume 285, Page 10385–10396.

Cannarile, L., Zollo, O., D'Adamio, F., Ayroldi, E., Marchetti, C., Tabilio, A., Bruscoli, S., & Riccardi, C. (2001). Cloning, chromosomal assignment and tissue distribution of human GILZ, a glucocorticoid hormone-induced gene. *Cell Death & Differentiation*, Volume 8, Page 201–203.

Chinenov, Y., Coppo, M., Gupte, R., Sacta, M. A., & Rogatsky, I. (2014). Glucocorticoid receptor coordinates transcription factor-dominated regulatory network in macrophages. *BMC Genomics*, Volume 15, Article 656.

Colin, S., Chinetti-Gbaguidi, G., & Staels, B. (2014). Macrophage phenotypes in atherosclerosis. *Immunological Reviews*, Volume 262, Page 153–166.

Coutinho, A. E., & Chapman, K. E. (2011). The anti-inflammatory and immunosuppressive effects of glucocorticoids, recent developments and mechanistic insights. *Molecular and Cellular Endocrinology*, Volume 335, Page 2–13.

Czepukojc, B., Abuhaliema, A., Bargash, A., Tierling, S., Naß, N., Simon, Y., Körbel, C., Cadenas, C., van Hul, N., Sachinidis, A., Hengstler, J. G., Helms, V., Laschke, M. W., Walter, J., Haybaeck, J., Leclercq, I., Kiemer, A. K., & Kessler, S. M. (2019). IGF2 mRNA Binding Protein 2 Transgenic Mice Are More Prone to Develop a Ductular Reaction and to Progress Toward Cirrhosis. *Frontiers in Medicine*, Volume 6, Article 179.

D'Adamio, F., Zollo, O., Moraca, R., Ayroldi, E., Bruscoli, S., Bartoli, A., Cannarile, L., Migliorati, G., & Riccardi, C. (1997). A new dexamethasone-induced gene of the leucine zipper family protects T lymphocytes from TCR/CD3-activated cell death. *Immunity*, Volume 7, Page 803–812.

Diamantis, E., Kyriakos, G., Quiles-Sanchez, L. V., Farmaki, P., & Troupis, T. (2017). The Anti-Inflammatory Effects of Statins on Coronary Artery Disease: An Updated Review of the Literature. *Current Cardiology Reviews*, Volume 13, Page 209-216.

Draper, N., & Stewart, P. M. (2005). 11 β -Hydroxysteroid dehydrogenase and the pre-receptor regulation of corticosteroid hormone action. *Journal of Endocrinology*, 186(2), 251–271. <https://doi.org/10.1677/joe.1.06019>

Endo, A., Kuroda, M., & Tanzawa, K. (1976). Competitive inhibition of 3-hydroxy-3-methylglutaryl coenzyme A reductase by MI-236a and MI-236b fungal metabolites, having hypocholesterolemic activity. *FEBS Letters*, Volume 72, Page 323–326.

Filippov, S., Pinkosky, S. L., Lister, R. J., Pawloski, C., Hanselman, J. C., Cramer, C. T., Srivastava, R. A. K., Hurley, T. R., Bradshaw, C. D., Spahr, M. A., & Newton, R. S. (2013). ETC-1002 regulates immune response, leukocyte homing, and adipose tissue inflammation via LKB1-dependent activation of macrophage AMPK. *Journal of Lipid Research*, Volume 54, Volume 2095–2108.

Filippov, S., Pinkosky, S. L., & Newton, R. S. (2014). LDL-cholesterol reduction in patients with hypercholesterolemia by modulation of adenosine triphosphate-citrate lyase and adenosine monophosphate-activated protein kinase. *Current Opinion in Lipidology*, Volume 25, Page 309–315.

Franceschi, C., Bonafe, M., Valensin, S., Olivieri, F., De Luca, M., Ottaviani, E., & De Benedictis, G. (2000). Inflamm-aging. An evolutionary perspective on immunosenescence. *Annals of the New York Academy of Sciences*, Volume 908, Page 244–254.

Fujiwara, N., & Kobayashi, K. (2005). Macrophages in Inflammation. *Current Drug Target - Inflammation & Allergy*, Volume 4, Page 281–286.

Fukumoto, Y., Libby, P., Rabkin, E., Hill, C. C., Enomoto, M., Hirouchi, Y., Shiomi, M., & Aikawa, M. (2001). Statins Alter Smooth Muscle Cell Accumulation and Collagen Content in Established Atheroma of Watanabe Heritable Hyperlipidemic Rabbits. *Circulation*, Volume 103, Page 993–999.

Fulop, T., Dupuis, G., Baehl, S., Le Page, A., Bourgade, K., Frost, E., Witkowski, J. M., Pawelec, G., Larbi, A., & Cunnane, S. (2016). From inflamm-aging to immune-paralysis: A slippery slope during aging for immune-adaptation. *Biogerontology*, Volume 17, Page 47–157.

Gay, N. J., & Keith, F. J. (1991). Drosophila Toll and IL-1 receptor. *Nature*, Volume 351, Page 355–356.

Genedani, S., Filaferro, M., Carone, C., Ostan, R., Bucci, L., Cevenini, E., Franceschi, C., & Monti, D. (2008). Influence of f-MLP, ACTH and CRH on in vitro Chemotaxis of Monocytes from Centenarians. *Neuroimmunomodulation*, Volume 15, Page 285–289.

Gisterå, A., & Hansson, G. K. (2017). The immunology of atherosclerosis. *Nature Reviews Nephrology*, Volume 13, Page 368–380.

Goldstein, J. L., & Brown, M. S. (1990). Regulation of the mevalonate pathway. *Nature*, Volume 343, Page 425–430.

Grundy, S. M., Stone, N. J., Bailey, A. L., Beam, C., Birtcher, K. K., Blumenthal, R. S., Braun, L. T., de Ferranti, S., Faiella-Tommasino, J., Forman, D. E., Goldberg, R., Heidenreich, P. A., Hlatky, M. A., Jones, D. W., Lloyd-Jones, D., Lopez-Pajares, N., Ndumele, C. E., Orringer, C. E., Peralta, C. A., Saseen, J. J., Smith, S. C., Sperling, L., Virani, S. S. & Yeboah, J. (2019). 2018 AHA/ACC/AACVPR/AAPA/ABC/ACPM/ADA/AGS/APhA/ASPC/NLA/PCNA Guideline on the Management of Blood Cholesterol: A Report of the American College of Cardiology/American Heart Association Task Force on Clinical Practice Guidelines. *Circulation*, Volume 139(25), Page e1082–e1143.

Hahn, R. T., Hoppstädter, J., Hirschfelder, K., Hachenthal, N., Diesel, B., Kessler, S. M., Huwer, H., & Kiemer, A. K. (2014). Downregulation of the glucocorticoid-induced leucine zipper (GILZ) promotes vascular inflammation. *Atherosclerosis*, Volume 234, Page 391–400.

Hayflick, L., & Moorhead, P. S. (1961). The serial cultivation of human diploid cell strains.

Experimental Cell Research, Volume 25, Page 585–621.

He, N., Liu, L., Ding, J., Sun, Y., Xing, H., & Wang, S. (2020). MiR-222-3p ameliorates glucocorticoid-induced inhibition of airway epithelial cell repair through down-regulating GILZ expression. *Journal of Receptors and Signal Transduction*, Volume 40, Page 301–312.

Healy, A., Berus, J. M., Christensen, J. L., Lee, C., Mantsounga, C., Dong, W., Watts, J. P., Jr., Assali, M., Ceneri, N., Nilson, R., Neverson, J., Wu, W. C., Choudhary, G., & Morrison, A. R. (2020). Statins Disrupt Macrophage Rac1 Regulation Leading to Increased Atherosclerotic Plaque Calcification. *Arteriosclerosis, Thrombosis, and Vascular Biology*, Volume 40, Page 714–732.

Honigberg, M. C., & Natarajan, P. (2019). Bempedoic Acid for Lowering LDL Cholesterol. *Journal of the American Medical Association*, Volume 322, Article 1769.

Hoppstädter, J., Kessler, S. M., Bruscoli, S., Huwer, H., Riccardi, C., & Kiemer, A. K. (2015). Glucocorticoid-induced leucine zipper: A critical factor in macrophage endotoxin tolerance. *Journal of Immunology*, Volume 194, Page 6057–6067.

Hoppstädter, J., & Kiemer, A. K. (2015). Glucocorticoid-induced leucine zipper (GILZ) in immuno suppression: Master regulator or bystander? *Oncotarget*, Volume 6, Article 6197.

Hoppstädter, J., Hachenthal, N., Valbuena-Perez, J.V., Lampe, S., Astanina, K., Kunze, M. M., Bruscoli, S., Riccardi, C., Schmid, T., Diesel, B. & Kiemer, A. K. (2016). Induction of Glucocorticoid-induced leucine zipper (GILZ) Contributes to Anti-Inflammatory Effects of the Natural Product Curcumin in Macrophages. *Journal of Biological Chemistry*, Volume 291, Page 22949–22960.

Hsu, M., Muchova, L., Morioka, I., Wong, R. J., Schröder, H., & Stevenson, D. K. (2006). Tissue-specific effects of statins on the expression of heme oxygenase-1 in vivo. *Biochemical and Biophysical Research Communications*, Volume 343, Page 738–744.

<https://clincalc.com/DrugStats/Top300Drugs.aspx>. (2021).

<https://www.who.int/news-room/fact-sheets/detail/the-top-10-causes-of-death>. (2021).

Ikeda, U., & Shimada, K. (1999). Statins and monocytes. *The Lancet*, Volume 353, Article 2070.

Italiani, P., & Boraschi, D. (2014). From Monocytes to M1/M2 Macrophages: Phenotypical vs. Functional Differentiation. *Frontiers in Immunology*, Volume 5, Article 514.

Jinnouchi, H., Guo, L., Sakamoto, A., Torii, S., Sato, Y., Cornelissen, A., Kuntz, S., Paek, K. H., Fernandez, R., Fuller, D., Gadhoke, N., Surve, D., Romero, M., Kolodgie, F. D., Virmani, R., & Finn, A. V. (2020). Diversity of macrophage phenotypes and responses in atherosclerosis. *Cellular and Molecular Life Sciences*, Volume 77, Page 1919–1932.

Jones, S. A., Toh, A. E. J., Odobasic, D., Oudin, M.-A. V., Cheng, Q., Lee, J. P. W., White, S. J., Russ, B. E., Infantino, S., Light, A., Tarlinton, D. M., Harris, J., & Morand, E. F. (2016). Glucocorticoid-induced leucine zipper (GILZ) inhibits B cell activation in systemic lupus erythematosus. *Annals of the Rheumatic Diseases*, Volume 75, Page 739–747.

K. V. Anderson, Bokla, L., & Nüsslein-Volhard, C. (1985). Establishment of Dorsal-Ventral Polarity in the Drosophila Embryo: The Induction of Polarity by the Toll Gene Product. *Cell*, Volume 42, Page 791–798.

Kobayashi, M., Chisaki, I., Narumi, K., Hidaka, K., Kagawa, T., Itagaki, S., Hirano, T., & Iseki, K.

(2008). Association between risk of myopathy and cholesterol-lowering effect: A comparison of all statins. *Life Sciences*, Volume 82, Page 969–975.

Kuilman, T., Michaloglou, C., Mooi, W. J., & Peeper, D. S. (2010). The essence of senescence. *Genes & Development*, Volume 24, Page 2463–2479.

Kuipers, H. F., Biesta, P. J., Groothuis, T. A., Neefjes, J. J., Mommaas, A. M., & van den Elsen, P. J. (2005). Statins affect cell-surface expression of major histocompatibility complex class II molecules by disrupting cholesterol-containing microdomains. *Human Immunology*, Volume 66, Page 653–665.

Latré de Laté, P., Pépin, A., Assaf-Vandecasteele, H., Espinasse, C., Nicolas, V., Asselin-Labat, M.-L., Bertoglio, J., Pallardy, M., & Biola-Vidamment, A. (2010). Glucocorticoid-induced Leucine Zipper (GILZ) Promotes the Nuclear Exclusion of FOXO3 in a Crm1-dependent Manner. *Journal of Biological Chemistry*, Volume 285, Page 5594–5605.

Laufs, U., Ballantyne, C. M., Banach, M., Bays, H., Catapano, A. L., Duell, P. B., Goldberg, A. C., Gotto, A. M., Leiter, L. A., Ray, K. K., Bloedon, L. T., MacDougall, D., Zhang, Y., & Mancini, G. B. J. (2022). Efficacy and safety of bempedoic acid in patients not receiving statins in phase 3 clinical trials. *Journal of Clinical Lipidology*, Volume 16, Page 286-297.

Laufs, U., Endres, M., Custodis, F., Gertz, K., Nickenig, G., Liao, J. K., & Böhm, M. (2000). Suppression of endothelial nitric oxide production after withdrawal of statin treatment is mediated by negative feedback regulation of rho GTPase gene transcription. *Circulation*, Volume 102, Page 3104–3110.

Lavin, Y., Mortha, A., Rahman, A., & Merad, M. (2015). Regulation of macrophage development and function in peripheral tissues. *Nature Reviews Immunology*, Volume 15, Page 731–744.

Leifer, C. A., & Medvedev, A. E. (2016). Molecular mechanisms of regulation of Toll-like receptor signaling. *Journal of Leukocyte Biology*, Volume 100, Page 927–941.

Leitinger, N., & Schulman, I. G. (2013). Phenotypic polarization of macrophages in atherosclerosis. *Arteriosclerosis, Thrombosis, and Vascular Biology*, Volume 33, Page 1120–1126.

Liao, J. K. (2002). Isoprenoids as mediators of the biological effects of statins. *Journal of Clinical Investigation*, Volume 110, Page 285–288.

Liao, J. K. & Laufs, U. (2005). Pleiotropic Effects of Statins. *Annual Review of Pharmacology and Toxicology*, Volume 45, Page 89–118.

Linnenberger, R., Hoppstädter, J., Wrublewsky, S., Ampofo, E., & Kiemer, A. K. (2021). Statins and Bempedoic Acid: Different Actions of Cholesterol Inhibitors on Macrophage Activation. *International Journal of Molecular Sciences*, Volume 22, Article 12480.

Lopez-Otin, C., Blasco, M. A., Partridge, L., Serrano, M., & Kroemer, G. (2013). The hallmarks of aging. *Cell*, Volume 153, Page 1194–1217.

Luz-Crawford, P., Tejedor, G., Mausset-Bonnefont, A. L., Beaulieu, E., Morand, E. F., Jorgensen, C., Noël, D., & Djouad, F. (2015). Glucocorticoid-Induced Leucine Zipper Governs the Therapeutic Potential of Mesenchymal Stem Cells by Inducing a Switch From Pathogenic to Regulatory Th17 Cells in a Mouse Model of Collagen-Induced Arthritis. *Arthritis & Rheumatology*, Volume 67, Page 1514–1524.

Macedo, A. F., Taylor, F. C., Casas, J. P., Adler, A., Prieto-Merino, D., & Ebrahim, S. (2014).

Unintended effects of statins from observational studies in the general population: Systematic review and meta-analysis. *BMC Medicine*, Volume 12, Page 51.

Mach, F., Baigent, C., Catapano, A. L., Koskinas, K. C., Casula, M., Badimon, L., Chapman, M. J., De Backer, G. G., Delgado, V., Ference, B. A., Graham, I. M., Halliday, A., Landmesser, U., Mihaylova, B., Pedersen, T. R., Riccardi, G., Richter, D. J., Sabatine, M. S., Taskinen, M.-R., Tokgozoglu, L & Wiklund, O. (2020). 2019 ESC/EAS Guidelines for the management of dyslipidaemias: Lipid modification to reduce cardiovascular risk. *European Heart Journal*, Volume 41, Page 111–188.

Metchnikoff, E. (1883). Untersuchungen ueber die mesodermalen Phagocyten einiger Wirbeltiere. *Biologisches Centralblatt*, 3:560-5.

Minciullo, P. L., Catalano, A., Mandraffino, G., Casciaro, M., Crucitti, A., Maltese, G., Morabito, N., Lasco, A., Gangemi, S., & Basile, G. (2016). Inflammaging and Anti-Inflammaging: The Role of Cytokines in Extreme Longevity. *Archivum Immunologiae et Therapiae Experimentalis*, Volume 64, Page 111–126.

Mittelstadt, P. R., & Ashwell, J. D. (2001). Inhibition of AP-1 by the glucocorticoid-inducible protein GILZ. *Journal of Biological Chemistry*, Volume 276, Page 29603–29610.

Monti, D., Ostan, R., Borelli, V., Castellani, G., & Franceschi, C. (2017). Inflammaging and human longevity in the omics era. *Mechanisms of Ageing and Development*, Volume 165, Page 129–138.

Moore, K. J., Sheedy, F. J., & Fisher, E. A. (2013). Macrophages in atherosclerosis: A dynamic balance. *Nature Reviews Immunology*, Volume 13, Page 709–721.

Moyer, C. F., Sajuthi, D., Tulli, H., & Williams, J. K. (1991). *Synthesis of IL-1 Alpha and IL-1 Beta by Arterial Cells in Atherosclerosis*. Volume 138, Page 951–960.

Murphy, C., Deplazes, E., Cranfield, C. G., & Garcia, A. (2020). The role of structure and biophysical properties in the pleiotropic effects of statins. *International Journal of Molecular Sciences*, Volume 21, 22, Article 8745.

Nataraja, C., Dankers, W., Flynn, J., Lee, J. P. W., Zhu, W., Vincent, F. B., Gearing, L. J., Ooi, J., Pervin, M., Cristofaro, M. A., Sherlock, R., Hasnat, M. A., Harris, J., Morand, E. F., & Jones, S. A. (2021). GILZ Regulates the Expression of Pro-Inflammatory Cytokines and Protects Against End-Organ Damage in a Model of Lupus. *Frontiers in Immunology*, Volume 12, Article 652800.

Nguyen, H., Akamnonu, I., & Yang, T. (2021). Bempedoic Acid: A cholesterol lowering agent with a novel mechanism of action. *Expert Review of Clinical Pharmacology*, Volume 14, Page 545–551.

Nicholls, S. J., Ballantyne, C. M., Barter, P. J., Chapman, M. J., Erbel, R. M., Libby, P., Raichlen, J. S., Uno, K., Borgman, M., Wolski, K., & Nissen, S. E. (2011). Effect of Two Intensive Statin Regimens on Progression of Coronary Disease. *New England Journal of Medicine*, Volume 365, Page 2078–2087.

Nohria, A., Prsic, A., Liu, P.-Y., Okamoto, R., Creager, M. A., Selwyn, A., Liao, J. K., & Ganz, P. (2009). Statins inhibit Rho kinase activity in patients with atherosclerosis. *Atherosclerosis*, Volume 205, Page 517–521.

Olivieri, F., Prattichizzo, F., Grillari, J., & Balistreri, C. R. (2018). Cellular Senescence and Inflammaging in Age-Related Diseases. *Mediators of Inflammation*, Volume 2018, Page 1–6.

Parmar, K. M., Nambudiri, V., Dai, G., Larman, H. B., Gimbrone, M. A., & García-Cardeña, G.

(2005). Statins Exert Endothelial Atheroprotective Effects via the KLF2 Transcription Factor. *Journal of Biological Chemistry*, Volume 280, Page 26714–26719.

Pinkosky, S. L., Newton, R. S., Day, E. A., Ford, R. J., Lhotak, S., Austin, R. C., Birch, C. M., Smith, B. K., Filippov, S., Groot, P. H. E., Steinberg, G. R., & Lalwani, N. D. (2016). Liver-specific ATP-citrate lyase inhibition by bempedoic acid decreases LDL-C and attenuates atherosclerosis. *Nature Communication*, Volume 7, Article 13457.

Preston, G. C., Feijoo-Carnero, C., Schurch, N., Cowling, V. H., & Cantrell, D. A. (2013). The Impact of KLF2 Modulation on the Transcriptional Program and Function of CD8 T Cells. *PLoS ONE*, Volume 8(10), Article 77537.

Reichardt, S. D., Amouret, A., Muzzi, C., Vettorazzi, S., Tuckermann, J. P., Lühder, F., & Reichardt, H. M. (2021). The Role of Glucocorticoids in Inflammatory Diseases. *Cells*, Volume 10, Page 2921.

Ronchetti, S., Migliorati, G., & Riccardi, C. (2015). GILZ as a Mediator of the Anti-Inflammatory Effects of Glucocorticoids. *Frontiers in Endocrinology*, Volume 6, Page 170.

Russell, D. G., Huang, L., & VanderVen, B. C. (2019). Immunometabolism at the interface between macrophages and pathogens. *Nature Reviews Immunology*, Volume 19, Page 291–304.

Samsoundar, J. P., Burke, A. C., Sutherland, B. G., Telford, D. E., Sawyez, C. G., Edwards, J. Y., Pinkosky, S. L., Newton, R. S., & Huff, M. W. (2017). Prevention of diet-induced metabolic dysregulation, inflammation, and atherosclerosis in *Ldlr*($-/-$) mice by treatment with the ATP-citrate lyase inhibitor bempedoic acid. *Arteriosclerosis, Thrombosis, and Vascular Biology*, Volume 37, Page 647–656.

Sanchez, A. M., Candau, R. B., & Bernardi, H. (2014). FoxO transcription factors: Their roles in the maintenance of skeletal muscle homeostasis. *Celular and Molecular Life Sciences*, Volume 71, Page 1657–1671.

Sheridan, A., Wheeler-Jones, C. P. D., & Gage, M. C. (2022). The Immunomodulatory Effects of Statins on Macrophages. *Immunology*, Volume 2, Page 317–343.

Sirtori, C. R. (2014). The pharmacology of statins. *Pharmacological Research*, Volume 88, Page 3–11.

Sirtori, C. R., Mombelli, G., Triolo, M., & Laaksonen, R. (2012). Clinical response to statins: Mechanism(s) of variable activity and adverse effects. *Annals of Medicine*, Volume 44, Page 419–432.

Solinas, G., Germano, G., Mantovani, A., & Allavena, P. (2009). Tumor-associated macrophages (TAM) as major players of the cancer-related inflammation. *Journal of Leukocyte Biology*, Volume 86, Page 1065–1073.

Soundararajan, R., Wang, J., Melters, D., & Pearce, D. (2007). Differential Activities of Glucocorticoid-induced Leucine Zipper Protein Isoforms. *Journal of Biological Chemistry*, Volume 282, Page 36303–36313.

Stahn, C., & Buttgerit, F. (2008). Genomic and nongenomic effects of glucocorticoids. *Nature Clinical Practice Rheumatology*, Volume 4, Page 525–533.

Strehl, C., Ehlers, L., Gaber, T., & Buttgerit, F. (2019). Glucocorticoids—All-Rounders Tackling the Versatile Players of the Immune System. *Frontiers in Immunology*, Volume 10, Article 1744.

Stroes, E. S., Thompson, P. D., Corsini, A., Vladutiu, G. D., Raal, F. J., Ray, K. K., Roden, M., Stein, E., Tokgozoglu, L., Nordestgaard, B. G., Bruckert, E., De Backer, G., Krauss, R. M., Laufs, U., Santos, R. D., Hegele, R. A., Hovingh, G. K., Leiter, L. A., Mach, F., März W., Newman, C. B., Wiklund, O., Jacobson, T. A., Catapano, A. L., Chapman, M. J. & Ginsberg, H. N., European Atherosclerosis Society Consensus Panel (2015). Statin-associated muscle symptoms: Impact on statin therapy-European Atherosclerosis Society Consensus Panel Statement on Assessment, Aetiology and Management. *European Heart Journal*, Volume 36, Page 1012–1022.

Tapp, Z. M., Godbout, J. P., & Kokiko-Cochran, O. N. (2019). A Tilted Axis: Maladaptive Inflammation and HPA Axis Dysfunction Contribute to Consequences of TBI. *Frontiers in Neurology*, Volume 10, Page 345.

Taylor, F., Huffman, M. D., Macedo, A. F., Moore, T. H., Burke, M., Davey Smith, G., Ward, K., & Ebrahim, S. (2013). Statins for the primary prevention of cardiovascular disease. *Cochrane Database Systematic Reviews*.

Toth, P. P., Granowitz, C., Hull, M., Anderson, A., & Philip, S. (2019). Long-term statin persistence is poor among high-risk patients with dyslipidemia: A real-world administrative claims analysis. *Lipids in Health and Disease*, Volume 18, Page 175.

Tuomisto, T. T., Lumivuori, H., Kansanen, E., Häkkinen, S., Turunen, M. P., van Thienen, J. V., Horrevoets, A. J., Levenon, A., & Ylä-Herttuala, S. (2019). Simvastatin has an anti-inflammatory effect on macrophages via upregulation of an atheroprotective transcription factor, Kruppel-like factor 2. *Cardiovascular Research*, Volume 78, Page 175–184.

Tynan, S. H., Lundeen, S. G., & Allan, G. F. (2004). Cell type-specific bidirectional regulation of the glucocorticoid-induced leucine zipper (GILZ) gene by estrogen. *The Journal of Steroid Biochemistry and Molecular Biology*, Volume 91, Page 225–239.

Vago, J. P., Galvão, I., Negreiros-Lima, G. L., Teixeira, L. C. R., Lima, K. M., Sugimoto, M. A., Moreira, I. Z., Jones, S. A., Lang, T., Riccardi, C., Teixeira, M. M., Harris, J., Morand, E. F., & Sousa, L. P. (2020). Glucocorticoid-induced leucine zipper modulates macrophage polarization and apoptotic cell clearance. *Pharmacological Research*, Volume 158, Article 104842.

Vallejo, J., Cochain, C., Zerneck, A., & Ley, K. (2021). Heterogeneity of immune cells in human atherosclerosis revealed by scRNA-Seq. *Cardiovascular Research*, Volume 117, Page 2537-2543.

Van Aelst, L., & D'Souza-Schorey, C. (1997). Rho GTPases and signaling networks. *Genes & Development*, Volume 11, Page 2295–2322.

van Furth, R. & Cohn, Z. A. (1968). The origin and kinetics of mononuclear phagocytes. *Journal of Experimental Medicine*, Volume 128, Page 415–435.

Vinci, P., Panizon, E., Tosoni, L. M., Cerrato, C., Pellicori, F., Mearelli, F., Biasinutto, C., Fiotti, N., Di Girolamo, F. G., & Biolo, G. (2021). Statin-Associated Myopathy: Emphasis on Mechanisms and Targeted Therapy. *International Journal of Molecular Sciences*, Volume 22, Article 11687.

Ward, N. C., Watts, G. F., & Eckel, R. H. (2019). Statin Toxicity: Mechanistic Insights and Clinical Implications. *Circulation Research*, Volume 124, Page 328–350.

Wassmann, S., Laufs, U., Bäumer, A. T., Müller, K., Ahlbory, K., Linz, W., Itter, G., Rösen, R., Böhm, M., & Nickenig, G. (2001). HMG-CoA Reductase Inhibitors Improve Endothelial Dysfunction in Normocholesterolemic Hypertension via Reduced Production of Reactive Oxygen Species. *Hypertension*, Volume 37, Page 1450–1457.

Wilke, R. A., Moore, J. H., & Burmester, J. K. (2005). Relative impact of CYP3A genotype and concomitant medication on the severity of atorvastatin-induced muscle damage. *Pharmacogenetics and Genomics*, Volume 15, Page 415–421.

Willemsen, L., & Winther, M. P. (2020). Macrophage subsets in atherosclerosis as defined by single-cell technologies. *The Journal of Pathology*, Volume 250, Page 705–714.

Yang, N., Caratti, G., Ince, L. M., Poolman, T. M., Trebble, P. J., Holt, C. M., Ray, D. W., & Matthews, L. C. (2014). Serum cholesterol selectively regulates glucocorticoid sensitivity through activation of JNK. *Journal of Endocrinology*, Volume 223, Page 155–166.

Yarbro, J. R., Emmons, R. S., & Pence, B. D. (2020). Macrophage Immunometabolism and Inflammation: Roles of Mitochondrial Dysfunction, Cellular Senescence, CD38, and NAD. *Immunometabolism*, Volume 2.

Yu, D., & Liao, J. K. (2022). Emerging views of statin pleiotropy and cholesterol lowering. *Cardiovascular Research*, Volume 118, Page 413–423.

Zhang, C., Yang, M., & Ericsson, A. C. (2021). Function of Macrophages in Disease: Current Understanding on Molecular Mechanisms. *Frontiers in Immunology*, Volume 12, Article 620510.

Appendix

General Methods

Reagents

Cell media (RPMI1640, #R088), fetal calf serum (FCS, #F7524), penicillin/streptomycin (#P433), simvastatin-lactone (#S6196) and glutamine (#G7513) were purchased from Sigma-Aldrich (St. Louis, MO, USA). PAN-FCS (#P040-37500) was purchased from PAN-Biotech (Aidenbach, Germany). (R)-Mevalonic acid lithium salt (#50838), atorvastatin calcium salt trihydrate (#PZ001), geranylgeranyl transferase inhibitor (GGTI)-2133 (#G5294), and farnesyl transferase inhibitor (FTI)-277 trifluoroacetate salt (#F9803) were obtained from Sigma-Aldrich (St. Louis, MO, USA). Simvastatin sodium salt (#10010345), farnesyl pyrophosphate ammonium salt (#Cay63250), and geranylgeranyl pyrophosphate (#Cay63330) were purchased from Cayman Chemicals (Ann Arbor, MA, USA). 5xHotFirePol EvaGreen qPCR Mix (no Rox) (#08-25-00001) was purchased from Solis Biodyne (Tartu, Estland). Other chemicals were obtained from either Sigma-Aldrich (St. Louis, MO, USA) or Carl Roth (Karlsruhe, Germany) unless stated otherwise. Statin stocks were prepared in DMSO.

Cell Culture

RAW 264.7 cells (American Type Culture Collection) were cultivated in standard medium (RPMI 1640, 10% FCS, 100 U/mL penicillin G, 100 µg/mL streptomycin, 2 mM glutamine). The cells were maintained at 37 °C in a humidified atmosphere of 5% CO₂.

BMMs were obtained from wild-type (WT) or *Foxo3* knockout (KO) mice. Femurs and tibias were flushed with standard medium (RPMI 1640, 10% PAN-FCS, 100 U/mL penicillin G, 100 µg/mL streptomycin, 2 mM glutamine). After centrifugation (10 min,

200× g), erythrocytes were lysed by incubation in hypotonic buffer (155 mM NH₄Cl, 10 mM KHCO₃, 1 mM Na₂EDTA) for 3 min at 37 °C. Cells were washed with PBS, resuspended in a standard medium containing M-CSF (50 ng/mL, 30 mL per preparation), transferred into a 75 cm² culture flask, and cultured overnight. Fibroblast-like cells, mature mononuclear phagocytes, and other cells adhering to the flask were discarded. Non-adherent cells were collected and cultured in a 150 cm² culture flask for another 5 to 6 days in a M-CSF-containing medium. Differentiated cells were detached with Accutase (Sigma-Aldrich, St. Louis, MO, USA #A6964), suspended in a standard medium supplemented with 50 ng/mL M-CSF, and seeded into 12-well plates (5 × 10⁵ cells/well) for RT-qPCR. The solvent control was 0.005% DMSO.

Mice

Mice were housed in a 12:12 h light-dark cycle with food and water *ad libitum*. For all experiments, C57B/6 mice of the age of 12-16 weeks were used (according to Tierversuchsnummer 06/2018). For the RT-qPCR, we used mice in which the first coding exon, was flanked by a loxP-frt-neo-frt cassette in intron 1 and a loxP site (*Foxo3* KO mice, The Jackson Laboratory, Bar Harbor, ME USA; #024668 *Foxo3*^{tm1Rdp/J}).

To elucidate the effect of simvastatin *in vivo* female C57B/6 mice at the age of 12-16 weeks were randomly divided into two groups (*n* = 10). One group was administered orally 10 mg/kg body weight simvastatin (lactone) by oral gavage using 0.5% methylcellulose/0.025% tween 20 as a vehicle. The sham group received the vehicle as control. Mice were sacrificed after 24 h and aorta, heart, kidney, liver, lung, muscle, peripheral blood leukocytes, and spleen were excised. The organs were flash-frozen in liquid nitrogen and stored at - 80°C for further analysis.

Cytotoxicity Measurement

For the 3-(4,5-dimethylthiazol-2-yl)-2,5-diphenyltetrazolium bromide (MTT) reduction assay, RAW 264.7 cells, C2C12 myoblasts, and BMMs were seeded into 96-

well plates at a density of 10^5 cells/well for RAW 264.7 cells and BMMs, and 10^4 cells/well for C2C12 myoblasts, adhered overnight, and treated with increasing concentrations of the test compound for 24 hours. Cells incubated with DMSO solvent in its maximum concentration (0.5%) served as the negative control. At the end of the treatment, C2C12 myoblasts were treated for three hours, RAW 264.7 cells for 25 minutes, and BMMs for one hour with MTT solution (0.5 mg/mL in medium) and lysed with DMSO. Absorbance was measured at 560 nm using a microplate reader Glomax Discover multiplate reader (Promega, Madison, WI, USA).

RNA Isolation, Reverse Transcription, and Quantitative PCR (RT-qPCR)

RNA was isolated either by Directzol[®] RNA Mini-Prep Plus (ZymoResearch, Irvine, CA, USA, #R2072), by QIAzol Lysis Reagent (Qiagen, Hilden, Germany, #79306), or by using the High Pure RNA Isolation Kit (Roche, Basel, Switzerland, #11828665001), following the manufacturers' instructions. RNA was reverse transcribed using the High-Capacity cDNA Reverse Transcription Kit (Thermo Fisher Scientific, #4368813) in the presence of the RNase inhibitor RNaseOUT[™] (Thermo Fisher Scientific, #10777019) following the manufacturer's instructions. qPCR was performed using the 5x HOT FIREPol EvaGreen[®] qPCR Mix and a total volume of 20 μ L. The primer sequences for each transcript are detailed in Table 1.

For each primer pair, an annealing temperature of 60 °C was used. The CFX96 touch[™] Real-Time PCR detection system (Bio-Rad Laboratories, Hercules, CA, USA) was used to quantify gene expression. Data were analyzed by normalization to the mentioned housekeeping gene. The housekeeping gene was chosen after evaluating the expression stability of at least three candidate genes under the experimental conditions, using the geNorm, NormFinder, and BestKeeper Software tools.

Gene	Accession Number	Forward Primer Sequence 5'-3'	Reverse Primer Sequence 5'-3'
<i>Hmox</i>	NM_010442.2	CACATCCAAGCCGAGAATGC	AGGAAGCCATCACCAGCTTAAA
<i>Klf2</i>	NM_008452.2	CCTTGCACATGAAGCGACAC	ACTTGTCCGGCTCTGTCCTA
<i>Ppia</i>	NM_008907.1	GCGTCTCCTTCGAGCTGTTT	CACCCTGGCACATGAATCCT
<i>Tsc22d3</i>	NM_010286.4	GCTGCTTGAGAAGAACTCCCA	GAACCTTTCCAGTTGCTCGGG

Table 1: Primer sequences of used primers for RT-qPCR.

Luciferase Assay

The proximal *Gilz* promoter (a fragment located between -1938 bp upstream and +206 bp downstream of the transcription start site) was a gift and cloned into the pGL3 luciferase reporter vector (Promega, Madison, WI, USA) using KpnI and SmaI according to the manufacturer's instructions. The FOXO3 reporter vector (FHRE-Luc) was a gift from Michael Greenberg (Addgene plasmid #1789). The pHRG-TK vector (Promega, Madison, WI, USA) provided constitutive expression of Renilla luciferase and served as an internal control value, to which expression of the firefly luciferase reporter gene was normalized. RAW 264.7 cells were seeded at a density of 10^5 cells/well into 96-well plates, co-transfected in a 1:1 ratio with the luciferase vector and the respective reporter vector using the Lipofectamine 3000 reagent (Thermo Fisher Scientific, Waltham, MA, USA) for 24 hours, treated as indicated, and the lysate was harvested by the addition of 1x passive lysis buffer (Promega, Madison, WI, USA). Luciferase activity was determined in the lysate by the addition of firefly luciferase substrate (470 μ M D-luciferin, 530 μ M ATP, 270 μ M coenzyme A, 33 μ M DTT, 20 μ M Tricine, 2.67 μ M MgSO₄, 1.07 μ M MgCO₃, and 0.1 μ M EDTA, pH 7.8) or renilla substrate solution (0.1 M NaCl, 25 mM Tris HCl pH 7.5, 1 mM CaCl₂, and 0.9 μ M

coelenterazine) followed by luminescence measurement using the Glomax Discover multiplate reader (Promega, Madison, WI, USA).

Introduction

GILZ is known to exert an anti-inflammatory effect in macrophages and endothelial cells and regulate macrophages' endotoxin tolerance (Hahn et al., 2014; Hoppstädter et al., 2015). This data is supported by the exacerbation of inflammation in the absence of GILZ in a MyD88-dependent and -independent manner (Hoppstädter et al., 2015).

To date, the literature shows controverse results regarding potential anti-inflammatory effects of statins. The analyses of GEO dataset GSE 4883 in human macrophages showed a *Gilz* and *Klf2* induction in parallel after statin treatment (Tuomisto et al., 2019). Similar to GILZ, KLF2 is known to mediate anti-inflammatory and vasoprotective effects (Parmar et al., 2005). Further, it is known that besides statins, also glucocorticoids induce *Klf2*. Interestingly *Klf2* and *Gilz* are in the same GR cluster (Chinenov et al., 2014) and Preston et al. showed elevated GILZ levels after KLF2 overexpression in T cells, suggesting an interaction of both proteins (Preston et al., 2013). Thus, we were interested in the anti-inflammatory effects of statins on GILZ and KLF2 expression in macrophages.

Results

Effect of Bempedoic Acid on Cell Viability and *Gilz* expression

To evaluate the toxicity of bempedoic acid on myoblasts and macrophages RAW 264.7 cells, C2C12 myoblasts, and BMMs were treated with increasing concentrations of bempedoic acid. The effect was determined *via* MTT assay at 24 hours. Similar to the findings of statins (see manuscript in chapter 3.3 “The Glucocorticoid-Induced Leucine Zipper (GILZ) Mediates Statin-Induced Muscle Damage” and in chapter 3.4 “Statins and Bempedoic Acid: Different Actions of Cholesterol Inhibitors on Macrophage Activation”) bempedoic acid had the most toxic effect on C2C12 myoblasts compared to macrophages RAW 264.7 cells and BMMs (Figure S1 A). For this reason, the lowest non-toxic concentration was used to determine the effect of bempedoic acid on *Gilz* expression in myoblasts and macrophages at 24 hours. Bempedoic acid neither induced *Gilz* in myoblasts nor in macrophages in a significant manner (Figure S1 B).

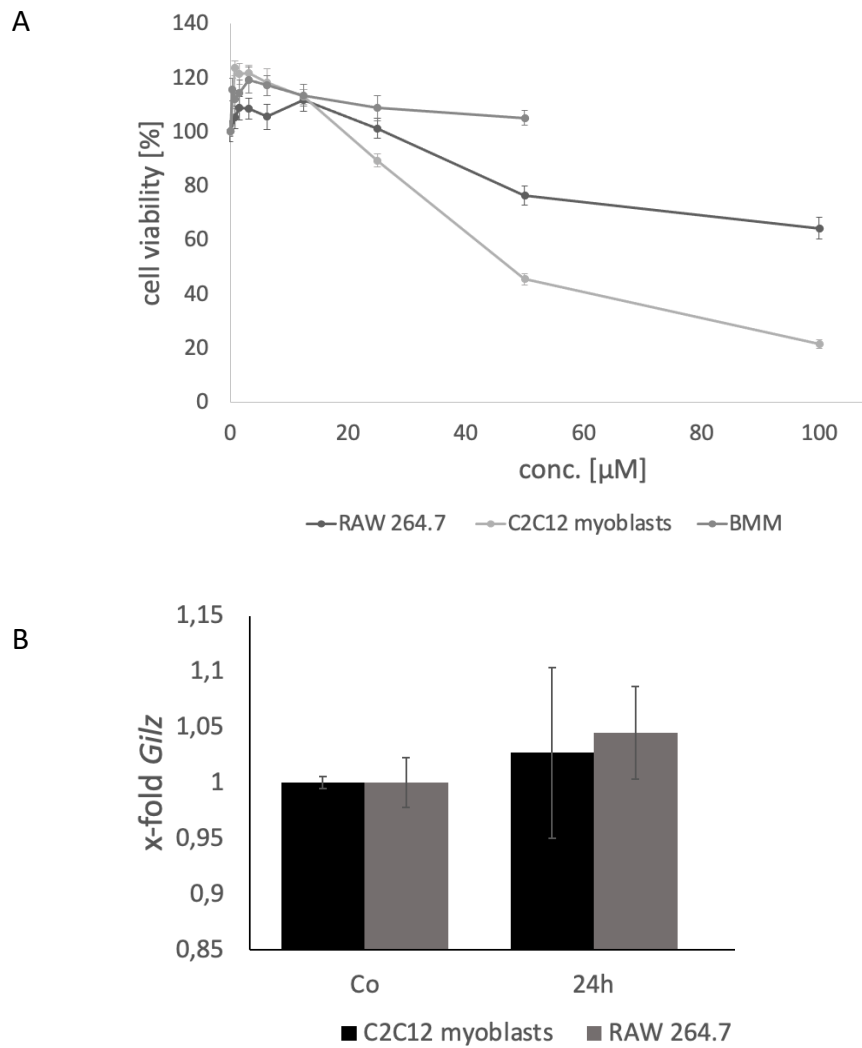


Figure S1: Cell viability of different cells treated with bempedoic acid and *Gilz* expression. (A) RAW 264.7, C2C12 myoblasts, and BMMs were treated with increasing concentrations of bempedoic acid and cell viability was determined *via* MTT assay. Data show the mean of three independent experiments performed in sixtuplicates \pm SEM. (B) C2C12 myoblasts were treated for 24 hours with 12.5 μM bempedoic acid, RAW 264.7 cells for 24 hours with 25 μM bempedoic acid, and respective DMSO control (Co). *Gilz* mRNA levels were measured. mRNA expression was normalized to the housekeeping gene (*Ppia*) and is presented as fold change of control. Data show the mean of 2 independent experiments performed in replicates \pm SEM.

Involvement of the Mevalonte Pathway in Simvastatin-Induced *Gilz* and *Klf2* Expression

Treatment of macrophages with simvastatin revealed an induction of *Gilz* and *Klf2* mRNA levels. Since the inhibition of HMG-CoA by statins not only affects the cholesterol synthesis, but also other biosynthetic pathways such as protein prenylation. To evaluate whether isoprenoid intermediates can reverse *Gilz* or *Klf2* induction either mevalonate, farnesylpyrophosphate, or geranylgeranylpyrophosphate were added to the medium. Co-treatment with all different mediators could reverse the respective induction of *Gilz* and *Klf2* suggesting cholesterol-dependent and -independent pathways in macrophages (Figure S2 A) but in contrast to myoblasts (see manuscript in chapter 3.3 “The Glucocorticoid-Induced Leucine Zipper (GILZ) Mediates Statin-Induced Muscle Damage”). To gain further insights into effects on the prenylation pathways specific transferase inhibitors of either FPP or GGPP were added to the medium to mimic the effect of simvastatin on *Gilz* and *Klf2* expression. Treatment of RAW 264.7 cells with 10 μ M FTI and GGTI mimicked *Gilz* induction, while had no effect on *Klf2* expression (Figure S2 B).

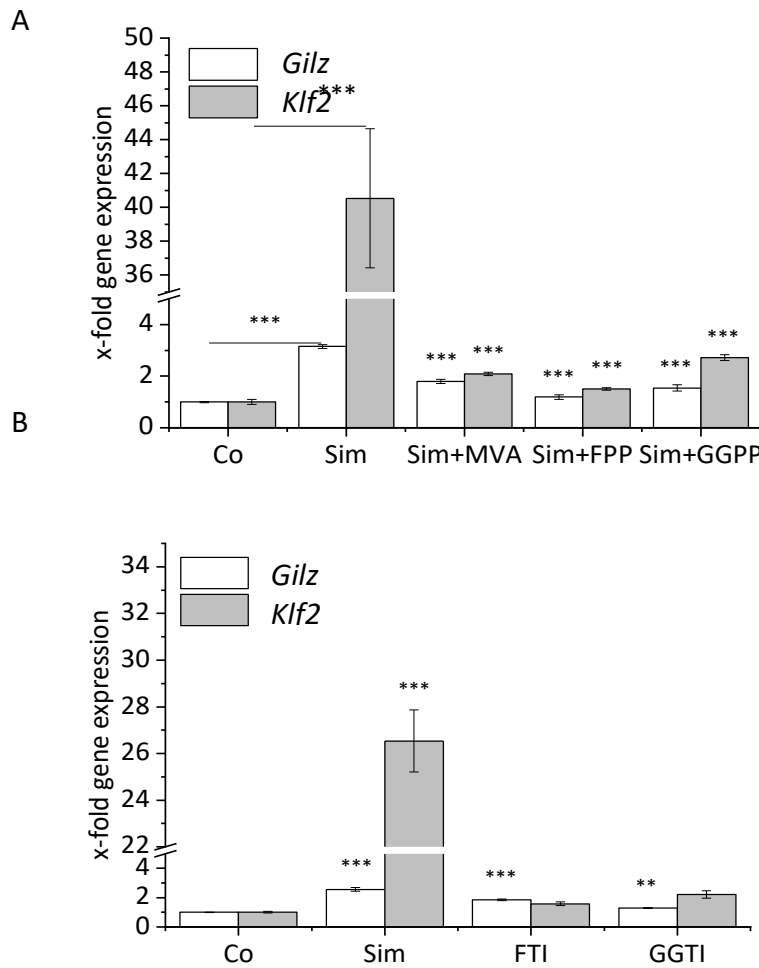


Figure S2: Involvement of the mevalonate pathway in simvastatin-induced *Gilz* expression. (A) RAW 264.7 cells were treated with vehicle (Co) or simvastatin (2 μ M Sim) and co-treated with either mevalonate (100 μ M MVA), farnesylpyrophosphate (10 μ M FPP) or geranylgeranylpyrophosphate (10 μ M GGPP) for 24 hours. (B) RAW 264.7 cells were treated either with simvastatin (2 μ M Sim), farnesyltransferase inhibitor (10 μ M FTI), or geranylgeranyltransferase inhibitor (10 μ M GGTI) for 24 hours. Data show the mean of three independent experiments performed in six replicates \pm SEM and normalized to the respective control. Statistical analysis was performed as one-way ANOVA with Bonholm posthoc in comparison to the control (indicated by line and asterisks) or in comparison to simvastatin treatment (just asterisks) in (A) and in comparison to control in (B). ** $p < 0.01$, *** $p < 0.001$.

Involvement of FOXO3 in Simvastatin-Induced *Gilz* Expression

FoxO3 is described as a transcription factor of muscle homeostasis (Sanchez et al., 2014). Statin-induced *Gilz* expression was mediated by FOXO3 activation in C2C12 myoblasts (see manuscript in chapter 3.3 “The Glucocorticoid-Induced Leucine Zipper (GILZ) Mediates Statin-Induced Muscle Damage”). Thus, we supposed FoxO3 as an upstream regulator of *Gilz* induction in macrophages and treated BMMs with either control or simvastatin for 24 hours. In FoxO3 KO animals simvastatin-induced *Gilz* upregulation was significantly lower than in der WT counterparts identifying FoxO3 partially as an upstream regulator of *Gilz* (Figure S3).

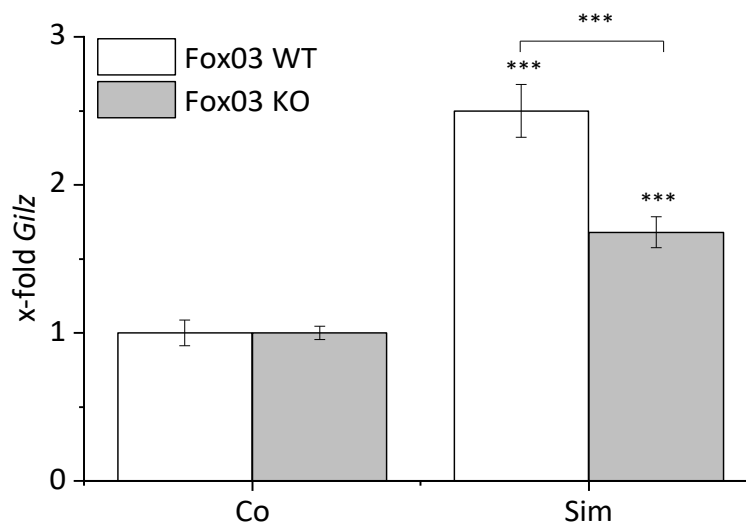


Figure S3: **Involvement of FoxO3 in simvastatin-induced *Gilz* expression.** BMM cells of either wildtype (WT) or **FoxO3** knockout (KO) animals were treated with vehicle (Co) or simvastatin (2 μ M Sim) for 24 hours. Data show the mean of three independent experiments performed in sixtuplicates \pm SEM normalized to the respective control. Statistical analysis was performed as one-way ANOVA with Bonholm posthoc. *** $p < 0.001$.

Involvement of *Gilz* Promoter Region in Statin-Induced *Gilz* Expression

To determine the *Gilz* promoter region which is involved in statin-induced *Gilz* expression we transfected RAW 264.7 cells by either GILZ or by forkhead responsive element (FHRE) promoter following statin-treatment. Results of the reporter gene assay showed that FHRE is involved in simvastatin-induced *Gilz* expression in macrophages (Figure S4). In contrast, the effect could not be confirmed in atorvastatin-treated cells.

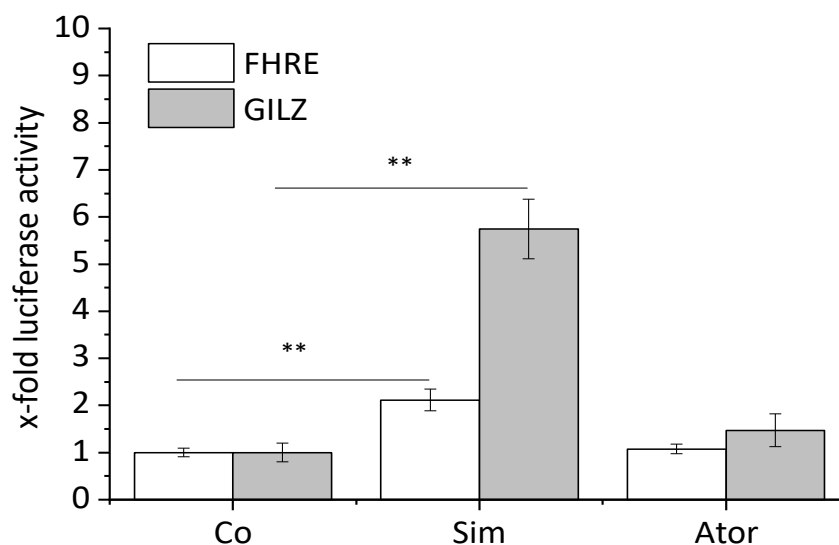


Figure S4: ***Gilz* promoter (and FHRE promoter as a part of the GILZ promoter) region is involved in simvastatin-induced *Gilz* expression.** Reporter gene assay in RAW 264.7 cells transfected with either GILZ or FHRE promoter reporter plasmid and treated with either vehicle (Co) or statin (2 μ M simvastatin = Sim; 5 μ M atorvastatin = Ator) for 24 hours. Luciferase activity was normalized to the vehicle-treated control. Data show the mean of three independent experiments performed in sixtuplicates +/- SEM. Statistical analysis was performed as Mann-Whitney test. ** p < 0.01.

Effect of Simvastatin on *Gilz* and *Hmox* Expression *in vivo*

Heme oxygenase-1 (HO-1) is supposed to mediate anti-inflammatory actions and is induced by statins in various tissues *in vivo* and might mediate statins' pleiotropic effects (Hsu et al., 2006). Thus, we treated mice with simvastatin by oral gavage, harvested respective tissues, and measured mRNA levels of *Gilz* and *Hmox*. Data showed no differences in *Gilz* and *Hmox* levels after simvastatin treatment compared to their vehicle-treated counterparts in heart, kidney, liver, lung, muscle, and PBLs. Slightly increased *Hmox* levels were observed in spleen and significantly decreased *Gilz* levels were observed in heart tissue (Figure S5).

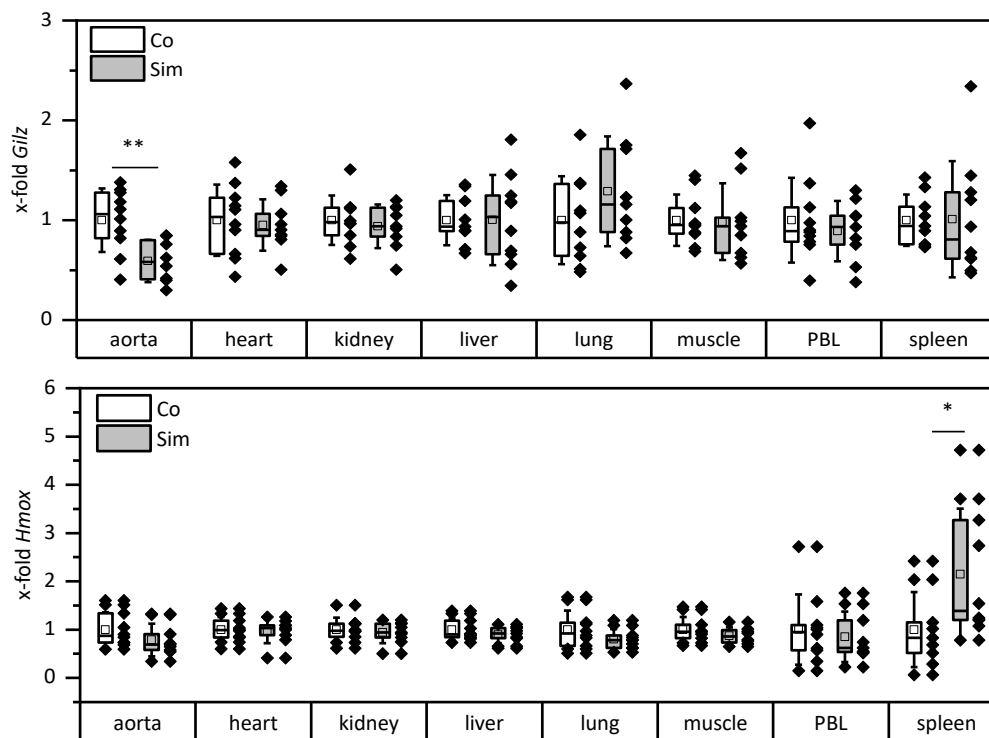


Figure S5: **Effect of simvastatin treatment *in vivo*.** Mice were administered orally 10 mg/kg body weight simvastatin (Sim) or vehicle (Co) by oral gavage. After 24 h, mice were sacrificed and transcript levels of *Gilz* (A) (gene name: *Tsc22d3*) and *Hmox* (B) (gene name: *Hmox1*) were measured and quantified by normalization to the housekeeping gene *Csnk2a2*. Co = 0.5% methylcellulose/0.025% tween 20 vehicle. Data show the mean of $n = 10$ (each group) measured in triplicates \pm SEM. Statistical analysis was performed as one sample t-test of untreated vs. treated sample for each organ. * $p < 0.05$, ** $p < 0.01$.

Discussion

Statins have a sufficient risk-safety profile and are effective cholesterol-lowering agents in the therapy of CVDs. Besides their lipid-lowering actions, they exert SAMS as well as desired pleiotropic effects. Due to the huge importance in reducing CVD morbidity and mortality rates, they have become indispensable therapeutics. Understanding the molecular mechanisms behind pleiotropic effects is of interest to improve their therapeutical profile and tailoring their application. The recently registered bempedoic acid addresses the same metabolic pathway as statins, however, without myotoxic effects. The first clinical reports show anti-inflammatory actions; thus, one might speculate that bempedoic acid exerts similar pleiotropic interactions. In the present studies, we identified GILZ as a statin-induced mediator in muscle cells *in vitro*, *ex vivo*, and *in vivo* as well as in macrophages *in vitro*, but not *in vivo* (see manuscript in chapter 3.3 “The Glucocorticoid-Induced Leucine Zipper (GILZ) Mediates Statin-Induced Muscle Damage” and in chapter 3.4 “Statins and Bempedoic Acid: Different Actions of Cholesterol Inhibitors on Macrophage Activation” and Figure S5). Of note, bempedoic acid was not capable to induce *Gilz* in any of the investigated cell models (Figure S1).

Our data pointed towards different underlying molecular mechanisms regarding the affected isoprenylated proteins, namely on GGPP in the muscle, and FPP and GGPP in macrophages (see manuscript in chapter 3.3 “The Glucocorticoid-Induced Leucine Zipper (GILZ) Mediates Statin-Induced Muscle Damage” and Figure S2). In accordance with literature and data published in muscle cell experiments, simvastatin-induced upregulation of *Gilz* is partially dependent on FoxO3 as indicated by an abolished *Gilz* upregulation in *FoxO3* KO animals in contrast to their WT counterparts (see manuscript in chapter 3.3 “The Glucocorticoid-Induced Leucine Zipper (GILZ) Mediates Statin-Induced Muscle Damage” and Figure S3). The involvement of the forkhead responsive element (FHRE) as part of the *Gilz* promoter and its respective binding partner FoxO3 -involved in muscle as well as innate immune homeostasis- could be identified as part of the statin-induced *Gilz*-upregulation (Figure S3 and S4) (Asselin-

Labat et al., 2004; Bouzeyen et al., 2019; Sanchez et al., 2014). Of note, potential upstream regulation of *Gilz* might be due to simvastatin-induced GC transactivation (Yang et al., 2014). We could identify the involvement of the Akt pathway in the statin-induced GILZ-induction and its myogenic impairment in muscle development and myotoxicity and ERK activation after statin-treatment in macrophages (see manuscript in chapter 3.3 “The Glucocorticoid-Induced Leucine Zipper (GILZ) Mediates Statin-Induced Muscle Damage” and in chapter 3.4 “Statins and Bempedoic Acid: Different Actions of Cholesterol Inhibitors on Macrophage Activation”). However, potential downstream effectors of GILZ in its anti-inflammatory context could not be identified and, thus, remain to be investigated.